University of Évora
ARCHMAT
(ERASMUS MUNDUS MASTER IN ARCHaeological MATerials Science)

Mestrado em Arqueologia e Ambiente : Ciencia dos Materiais Arqueologicos

Rock paintings and microorganisms – a new insight on Escoural cave

Guilhem Mauran m34312

Ana Teresa Caldeira, Universidade de Évora
António Candeias, Universidade de Évora
Nicola Schiavon, Universidade de Évora

Évora, September 2016

Cofinanciado por:

This page intentionally left blank

Rock paintings and microorganisms – a new insight on Escoural cave

Infrared reflectography of charcoal drawings of horses' heads in Escoural cave.
©Sonia Costa, Hercules Lab., Universidade de Evora, Evora, Portugal.

ARCHMAT 2014-2016

Guilhem MAURAN m34312

Table of contents

Table of figures

Table of tables

Table of appendixes

Table of abbreviations

Abbreviation	Definition
A	Absorbance
ATP	Adenosine Triphosphate
B.P.	Before Present
CH	Cultural Heritage
DNA	Deoxyribonucleic acid
EPS	Extra Polymeric Substance
HPLC	High Performance Liquid Chromatography
IR	Infrared
MTT	3-(4,5-dimethylthiazol-2-yl)-2,5-diphenyltetrazolium bromide
NGS	Next Generation Sequencing
PB	Presto Blue® Thermo Fisher Scientific
SEM-EDS	Scanning Electron Microscopy – Energy Dispersive Spectroscopy
UV	Ultra-violet
XRD	X-ray Diffraction
XRF	X-ray Flourescence

Acknowledgements

This work was funded by “HIT3CH - HERCULES Interface for Technology Transfer and Teaming in Cultural Heritage”, Ref: ALT20-03-0246-FEDER-000004, co-funded by the Regional Development European Fund through ALENTEJO 2020 (Programa Operacional Regional do Alentejo).

As this work was made possible by an ARCHMAT Erasmus Mundus scholarship under the FPA agreement 0238-2013 between Education, Audiovisual and Culture Executive Agency (EACEA) agency of the EU and the University of Évora, I wish to thank the EACEA for the economic support through the Erasmus Mundus Scholarship FPA.

I would also like to thank my thesis’ supervisor Pr. A.T. Caldeira of the Chemistry department at Universidade de Evora (Portugal), and co-supervisors Pr. A. Candeias and Pr. N. Schiavon of the HERCULES laboratory at Universidade de Evora (Portugal). They were of great help whenever I had a question about my research or writing, always finding some time to help me carrying out my work.

I would like to especially thank Pr. Caldeira, Pr. Candeais, and C.S. Silva for the opportunity they gave me to work on cave art and more precisely the very unique site of the cave of Escoural (Alentejo, Portugal). I am also extremely grateful to them for including me to the article published in July 2016 in National Geographic Portugal.

I would also like to express my entire gratitude to Tania Rosado, Catia Salvador and Marina Gonzalez. The three of them helped me to carry out my research and provided useful advices for writing the present thesis. I especially want to thank Marina Gonzalez for her help and advices concerning the microbial contamination’s assessment. I then would like to thank Tania Rosado and Catia Salvador for their help and remarks concerning the microbial isolation.

I am entirely grateful to Tania Rosado for her help with the Raman analyses and SEM observations of the different samples from the cave. Moonmilk and Palaeolithic habits of Escoural Cave have revealed a lot of their mysteries thanks to her help and remarks.

I would also like to thank all the professors, researchers and technicians who were involved in this master thesis for their help, time, expertise and advices: Ricardo Vieira, Nuno, Pr. J. Mirao, C.S. Silva, Dona Lena and Dona Esperanza. I would like to especially acknowledge Ana Cardoso for the preparation embedded samples and their analyses with micro-infrared, Sonia Costa for the photographs and the infrared reflectographs she performed. I would like to also thank Antonio Luis Campos for the pictures of the cave and microbial cultures he provided.

I am also grateful to Tania Rosado of the HERCULES laboratory at Universidade de Evora and Jessica Delavoipière as second readers of this thesis, and I am gratefully indebted to them for their time and very valuable comments on this thesis.

Finally, I would like to express my gratitude to all my colleagues and friends whom help to make this thesis a wonderful experience.

Part I Escoural and Upper Palaeolithic cave art

Sampling of the red horse's panel, Escoural Cave (Alentejo, Portugal), © A.L. Campos

Chapter 1. Cave art: the rise of art?

A. Cave art: a phenomenon through space and time

Parietal art occurred on a broad geographical region covering the vast majority of the continents and a large temporal span ranging from the Upper Palaeolithic to nowadays. Its extensive occurrence in various places on the different continents interrogates on its function or meaning. Although they both will remain mysterious for the prehistoric representations, studying the artwork provides valuable information on the communities who performed them. The main issue is to define with as much precision as possible to what refers the expression "cave art".

i. Cave art: the semantic issue

At first glance, the semantic meaning of the term mentioned just above seems clear, and it feels not necessary to clarify it. Though, trying to distinguish the four distinct and used expressions appears more complex. Indeed, researchers tend to employ "prehistoric art", "rock art", "parietal art" and "cave art" as analogues one to another with no consideration of their distinct meaning. Other expressions such as "mural art" or "primitive art" were sometimes used in early publications but will not be mentioned here since they are now disused in the field of this present work. All of them offer slight distinctions, and this is why it is important to clarify their different meaning. As all of them include the term "art", the issue of whether the artworks considered should be interpreted as a part of "art" or not is developed in Part I Chapter 1. B p.6, once the proper terms to use in this work are correctly defined.

"Prehistoric art" is of course rather general since it corresponds to all artefacts from the Palaeolithic to the end of the Protohistoric times in all geographic locations (Huyghe, 1962). It includes the vast majority of the artworks which are mentioned by the three other expressions, but not all of them since it limits itself to prehistoric times. It also refers to other artworks such as carved bones, although they are not part of any of the other three terms, and will not be evoked in this work.

Instead “rock art” points out to any works on or of stone such as geoglyphs, petroforms, petroglyphs, engravings and pictographs (Abadía, 2006; Huyghe, 1962). Consequently, the Australian Aboriginal artworks still performed nowadays in some rock shelters should be mentioned as “rock art” although it is not part of “prehistoric art”.

Of higher interest for the present work, the archaeological term “parietal art” refers exclusively to any artworks performed on cave walls or large stone blocks (Abadía, 2006; Leroi-Gourhan, 1982). Naturally, all parietal art belongs to rock art, but the opposite is not true. Both do not refer to any temporal specificity, and therefore are rather general.

Finally, the term “cave art” refers to the numerous artworks found inside cavities all over the world (Huyghe, 1962; Leroi-Gourhan, 1982), though it is most of the time used to refer specifically to parietal art of the Upper Palaeolithic (40 000 – 14 000 BP) found in European caves and shelters (Abadía, 2006). It includes various techniques, among them, paintings and engravings correspond to the vast majority of “cave art” artworks, but sculptures and models also fall into this category. It is the term that will be preferred in this thesis.

This brief clarification should help the reader to follow the present thesis better. It also exemplifies one of the main issues of cave art’s studies: semantic. Too many times the four terms defined above are confused and used as synonyms of each other without any considerations of their actual meaning.

Since the topic of this work corresponds to the only Portuguese cave art’s site, the following paragraphs mainly focus on the European Upper Palaeolithic, taking the most common, though restrictive, definition of “cave art”.

ii. Historical context

European cave art is often mentioned as being the oldest trace of art in the world. Although these artworks are among the earliest vestiges of the emergence of a symbolic expression in the world, its artistic character is subject to debate, Part I Chapter 1. B p.6, and older relics have been found in other regions of the world. Indeed, the oldest symbolic artefact discovered was excavated in Blombos Cave (Heidelberg, South Africa). It corresponds to a polished and engraved hematite block dated back to 75 000 BP (Henshilwood et al., 2009), making European cave art a rather recent phenomenon.

Although European parietal art is not the oldest of the world, historical and economic reasons explain the extent of the studies performed on it compared to other ones such as San and Aboriginal rock art.

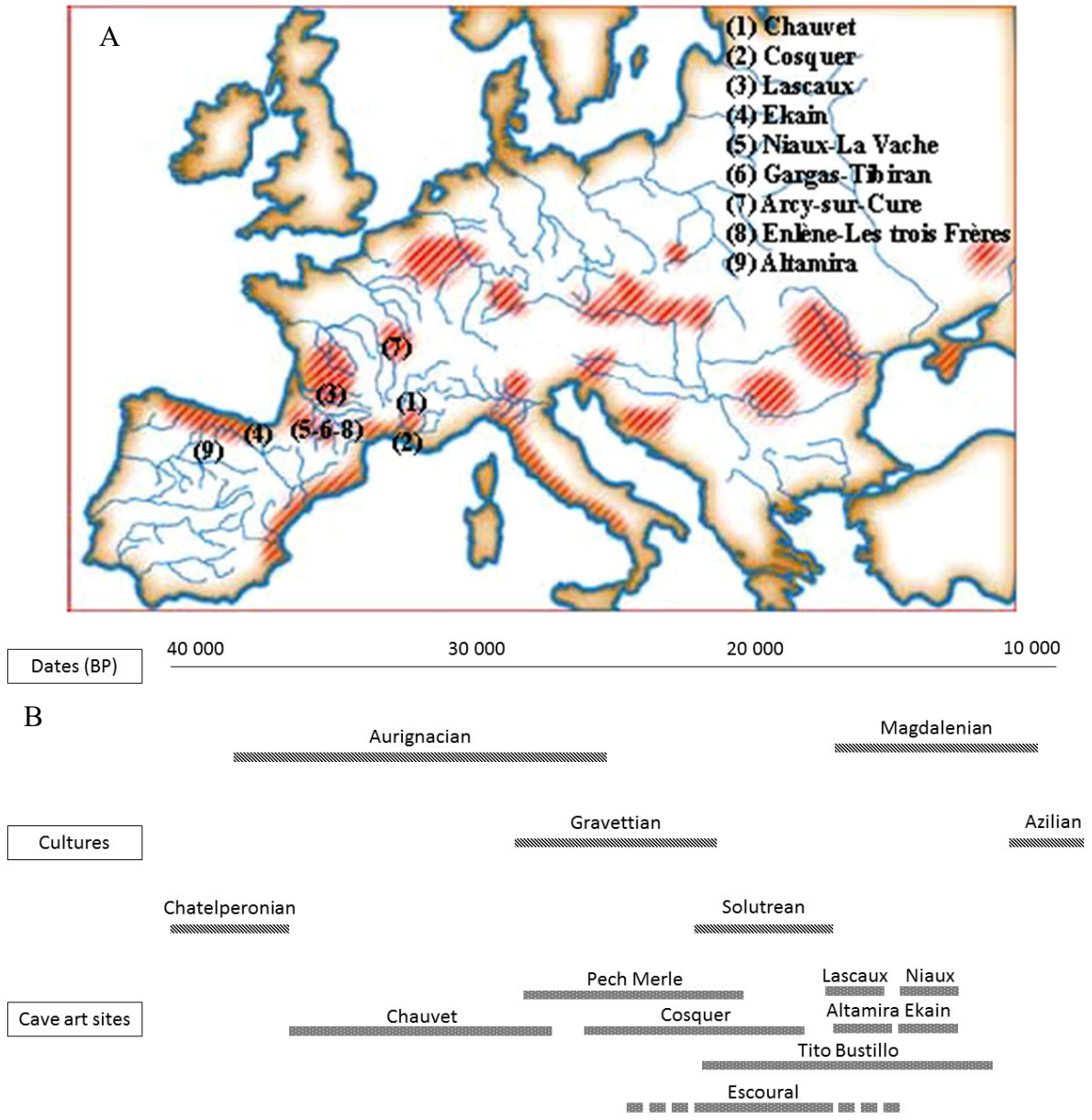

Figure 1: Geographical and chronological context of Western Europe parietal art. A: Geographical distribution of cave art in western Europe with the location of the most important caves mentioned in this work, red areas correspond to areas with settlements' evidences (Chalmin et al. 2003). B: Chronology of the Upper Palaeolithic Cultures and the traces they left all over Europe.

European parietal art dates back to the Upper Palaeolithic (40 000 – 14 000 BP) and lies in a vast geographical region which goes from England to Russia and Portugal including Germany, Romania, Italy, France and Spain. Despite its large geographic span, the vast majority of the sites gathers in the last two countries, and more accurately in the French-Cantabrian region

hosting some of the most notable sites such as Lascaux (Dordogne, France), Altamira (Cantabria, Spain) and Tito Bustillo (Asturias, Spain).

Various cultures established in Europe during the Upper Palaeolithic and with them distinct phenomena and styles spread over the continent. The earliest culture, known to have performed cave art, is the Aurignacian (40 000 – 28 000 BP) with the site of Chauvet (Ardèche, France). The impressive techniques and skills the communities used to perform the artworks found inside the cave testify of an incredible art mastery, which led J. Clottes to see it as an accomplishment of a nowadays lost tradition (Clottes, 2008a; Clottes and Arnold, 2001).

The Gravettian culture (28 000 – 22 000 BP) later replaced the Aurignacian one. The Gravettian presents some few specificities in the artistic, or at least symbolic, field with the apparition of the negative hands in various sites: Gargas (Vaucluse, France), Cosquer (Bouches-du-Rhône, France) and El Castillo (Cantabria, Spain); and the significant development of the "Venus" statues all over Europe.

Then the Solutrean culture (22 000 – 17 000 BP) appeared. Crucial in cave art's development, the Solutrean culture seems to have a limited spread in space to France, and Spain with some possible presence in Portugal. They left numerous rock art sites among which the most famous one: Lascaux (Dordogne, France); and possibly the one investigated in this work: Escoural (Alentejo, Portugal).

The Magdalenian (17 000 – 11 000 BP) constitute the latest European culture of the Upper Palaeolithic. It corresponds to a significant rise of the mobile artworks and a wide diversification of the techniques used to perform parietal art with: sculptures in Cap-Blanc (Dordogne, France) and Roc-aux-Sorciers (Vienne, France); drawings in Niaux (Ariège, France) and Portel (Ariège, France); polychrome paintings in Altamira (Cantabria, Spain), Ekain (Guipúzcoa, Spain); models in the Tuc-d'Audoubert (Ariège, France); and engravings in the Trois-Frères (Ariège, France).
Both the large space and time span tend to wonder on the importance of those artworks for the communities who performed them. Was "cave art" art? A way of expression? A process to contact spirits? Why did the Palaeolithic decide to realise those figures in caves?

B. Symbolism

i. Art or symbol?

For long, the exploration of the underground was thought to be exclusively limited to modern humans, but the recent dating of the annular anthropic stalagmites' structures of the cave of Bruniquel (France) dated back to 176 500 (± 2 100) BP (Jaubert et al., 2016), showed that even early Neanderthals started to exploit those locations before the arrival of modern humans in Europe. Beyond changing all the notions of culture among prehistoric populations, those structures raise the question of their importance and use by the Palaeolithic populations. Together with cave art, and to a lesser extent rock art in general, these structures remain mysterious about it, and many theories were developed to understand the reason that pushed early humans to brave the danger of the underground. Pioneers were often confronted with the semantic issues of "cave art" phenomenon.

By naming it "cave art" archaeologists assumed that those ancestral representations had an artistic value, without questioning the practices and the possible other functions they might have had. However, art is a complex phenomenon, and fierce debates took place to know if cave art should be referred as an art.

"L'art résulte de la projection, sur le monde qui entoure l'homme, d'une image mentale forte qui colore la réalité, avant de prendre forme et de la transfigurer ou de la recréer dans la matière."[1]

J. Clottes (Clottes, 2008a, p. 11)

As written by the French Prehistorian J. Clottes, art reveals a theoretical capacity of abstraction during which humans use their imagination to interpret and transform the world surrounding them. Major sites such as Lascaux and Altamira highlight the very high technical skills of the

[1] Art results in the projection, in the world surrounding mankind, of a strong mental picture which colours reality, before taking form and transfiguring or recreating it in a specific material. (Translation G. Mauran)

Palaeolithic with the use of complex pictorial technique such as anamorphosis[2] to accurately represent animals despite the walls' shape. However, the vast majority of cave art sites present a much simpler style allowing to question their definition as "art". Despite, they might not have any artistic value, cave art's symbolic importance is incontestable. The animals painted and engraved, the negative and positive hands, the symbols found in the various caves carry in them or their realisation a symbolic meaning that pushed the Palaeolithic to perform them inside of cavities. Therefore, the term "art" can be used to refer the inherent symbolic meaning of the artworks but also the skills and techniques that Palaeolithic had to use to execute them. These figures are even seen as one of the earliest phenomena that paved the way for the development of writing. Although it will never be understood, numerous attempts have been carried out to understand it and the societies who performed them better.

ii. Cave art's interpretations

Since the recognition of cave art at the beginning of the 20th century, archaeologists have tried to give a sense, a particular value to the representations they discovered in secluded galleries of numerous cavities from all over the world.

The earliest theory about cave art considers it as an "art for art" and was developed during the end of the 19th century and the beginning of the 20th century, while cave art's recognition was a fierce debate among Prehistorians. The father of this theory, Gabriel de Mortillet, considered that the Magdalenian populations were fundamentally artistic, and therefore, they realised paintings and engravings in a quest to reach the Beautiful (De Mortillet, 1883). The theory did not survive long since it was in complete contradiction with the location where the representations were found. Indeed, in a quest about the Beautiful for the Beautiful, art would be exposed to all, not hidden in dark places, remote and hardly accessed places such as caves. The theory rapidly disappeared after the recognition of Altamira's authenticity, leaving Salomon Reichnach's totemism developed itself.

[2] Technique consisting in a willing distortion of a representation, requiring the viewer to be in a specific location to reconstruct the distorted image.

S. Reichnach's theory is now well developed in ethnology and relies on a tight correlation between a community and a particular species, animal or vegetal (Reichnach, 1900). Due to the precise bound between the two, the humans' population develops a cult implying the worship of the species to which the community felt linked to, known as the totem. The theory failed to explain the little diversity of the representations found in most caves and the existence of some figures of injured animals, leading to it to its end. Although it cannot explain the whole phenomenon, it is still thought that totemism, together with later theories, could be at the origin of some representations found in cave art (Clottes, 2008a).

While the two previous hypotheses did not last long, the idea developed by Henri Breuil and Henri Bégouen, two French prehistorians, lasted longer. According to them, the paintings were part of a magic process performed to help the tribes and communities to obtain a better hunt. Therefore, the representations are not vital in themselves; it is the act of tracing them which imports, explaining why, in some cases, they were not fully finished. The choice to perform them in caves is then seen as the result of the idea that they are unique locations binding unnatural forces and humans. However, the theory does not correspond to the consumption's leftovers of the Palaeolithic populations. The species identified from the bones discovered on archaeological sites do not match with the species represented in cave art.

André Leroi-Gourhan then developed a structuralist approach to interpret the artworks contained in a cave. According to his theory, each cavity has a particular organisation which could be understood thanks to statistics. Although large parts of this theory are no longer used, the techniques evoked by A. Leroi-Gourhan to study the artworks' corpus in a cave are still employed nowadays.

Recently, J. Clottes and D. Lewis-Williams developed a new theory that was badly received by most of their colleagues. Their theory, the shamanism, rests on the idea that some people from Palaeolithic tribes were seen as capable of travelling from the human world to the spirits one. By entering caves and going underground, those people were entering the world of the spirits. There, spirits would communicate with them through various means. The shamans would then be able to contact the spirit through art, by painting what they could see in the cave, what the spirits would reveal to them. During their explorations of the underground, those populations

gave shadows and geomorphological formations the shape of particular animals impersonating some very specific characteristics. Palaeolithic communities who performed parietal art were largely influenced by their environment, as it can be induced from the diversity of the animals found in caves. The very unique case of Cosquer (France) highlights it with numerous aquatic figures in a cave which was very close to the sea and which is nowadays partially underwater (Clottes et al., 2005). Although this theory was poorly received, recent studies of Australian and African rock art tend to reinforce it

As seen in this brief overview of the distinct interpretations that were made about parietal art, understanding the reasons why the Palaeolithic performed artwork in caves is arduous. Archaeologists agree that it will never be fully understood, but through the study of the corpus, the materials used to perform the artwork it is possible to comprehend better the communities who realised them. It should help to get a better knowledge of the development of art and culture but also for some archaeologists of the early developments of writing throughout the world (Aujoulat, 2004) despite the lack of repetition and syntax of cave paintings.

C. Realisation

Since their discoveries, parietal art was extensively studied. Therefore, a lot is known about the realisation of cave paintings and engravings throughout space and time.

This part tries to present a brief overview of the material and techniques used to perform cave art, further details of the coloured material used will be provided in Part II Chapter 1 p.38. As the present work focuses on Escoural's paintings the following pages focus on paintings' accomplishment.

i. The support

Limestone constitutes the usual support encountered in Western Europe and more precisely in the large French-Spanish region, over 95% of the registered sites have a limestone's support (Brunet and Vouvé, 1996). Nevertheless, throughout the world other host rock have been

registered: granitic in Australia (Flood, 1999), Namibia and South Africa, sandstone in Algeria (Soleilhavoup, 1986) and few sites in France such as Croc-Marin (Brunet and Vouvé, 1996). One of the aims of the analyses of the substrate is to provide a better understanding of the distribution of the paintings, to understand the Palaeolithic choices of a panel rather than another one to perform their representations and their conservation throughout time.

ii. Pictorial techniques

The characterisation of the material is only one of the numerous aspects allowing to investigate the technical skills of the Palaeolithic, another possible way is through the analysis of the pictorial techniques, how the pigments were applied on the walls' surface. These analyses are usually performed through macrophotography to identify traces left by the Palaeolithic.

The range of the techniques used by the Palaeolithic was wide, even in the early period of the Aurignacian, who performed Chauvet's artwork (Clottes and Arnold, 2001). Five different steps can be identified during the realisation of cave paintings. Not all of them are always present, reflecting the communities or individuals' knowledge and skills.
The earliest step consists in collecting the coloured material from various outcrops before their preparation to obtain pigments. Since these two steps are only reachable with microscopic observations, they are further developed in the next subpart dealing with the pigments' manufacture and the Palaeolithic's palette. The next three steps consisting in choosing and preparing the support, planning the drawing and finally applying the pigments on the wall, are developed in the following paragraphs.

The choice and sometimes the preparation of the panel hosting the painting were primordial. They often determined the techniques and skills the Palaeolithic had to deploy to perform their representation (Aujoulat, 2004). While the Palaeolithic adapted to the environment they discovered and had to use anamorphosis to accomplish their realisations in Lascaux, in some other sites, they decided to alter and adjust the walls to what they wanted to prepare the support before drawing on it. These preparations, Figure 2, provided a relatively flat and smooth surface clear of most anterior traces, such as bears' claws in Chauvet (Ardèche, France)(Clottes and Arnold, 2001), previous exploitation of cave's speleothems such as

moonmilk in Cosquer (Bouches-du-Rhône, France)(Clottes et al., 2005) or even previous representations (Clottes, 2008a; Clottes and Arnold, 2001).
Such preparations often consisted in scratching the walls with flints or smoothing the surface with the hand according to the hardness of the support, as seen in Figure 2. They often left very specific traces, such as fingerprints or hand shapes (Clottes et al., 2005), giving no doubt on the way the surfaces were prepared.

Once the host rock's surface had been processed, Palaeolithic could either perform a sketch or directly apply the pigments. Relatively rare traces of drawings' preparation were found either directly on clay soils in Niaux (Ariège, France), Montespan (Haute-Garonne, France) and Fontanet (Ariège, France)(Clottes, 2008b), or on the panel hosting the painting as a light discontinuous engraving performed before the application of the pigments, as it was found on the Black Frieze of Pech-Merle (Quercy,France) (Lorblanchet, 2010).

The last and most accessible step consists in applying the pigment to the surface of the wall. The methods employed were numerous, probably depending on the group or individual who performed the paintings. Pigments could be applied dry, without any filler as pigment's powder or pencil, or wet, with the addition of water and clay to obtain a paste easy to apply on the surface of the walls. Figure 2 illustrates few of the Palaeolithic techniques through their characteristics features identified with macrophotography (Clottes and Arnold, 2001; Delluc et al., 1983; Lorblanchet, 2010; Menu et al., 1993).

iii. Pigments' preparation

Among the five steps previously evoked, two deal with pigments' preparation: coloured materials' collection, or in the case of charcoal and bone black of the material to burn, and their manufacture to obtain the desired pigment.
In this work "pigment" refers to the coloured layer of the painting and the preparations used to perform the painting, while "coloured material" only evokes the original material, such as wood, bone or the metal oxides, before its processing. Due to these definitions, charcoal will be either referred to as a pigment, as the pictorial layer, or a coloured material.

Figure 2: Prehistoric pictorial techniques. A: Example of support preparation's traces on the lower left corner with the presence of engravings to highlight the painting (Chauvet)(Clottes and Arnold, 2001). B: Parallel ridges left by a brush with red pigments (Chauvet).(Clottes and Arnold, 2001) C: Digital imprint's traces tending to prove the use of finger to smooth the pigment's surface (Chauvet).(Clottes and Arnold, 2001) D: Speckled aspect of the spitted wet pigment with no stencil (Pech-Merle)(Lorblanchet, 2010). E: Black and yellow horse heads performed with probably hand-stencils (Lascaux)(Aujoulat, 2004).

The first step - the collection of the raw materials - was highly dependent on the site in which the paintings were performed. Indeed, the resources found inside the cave and at its vicinity often provided the coloured materials necessary to perform cave paintings. Some caves, such as Chauvet (Clottes and Arnold, 2001) and Cosquer (Clottes et al., 2005), contained ochre that the Palaeolithic exploited to prepare their paintings pots. If the cave did not provide sufficient proper material, nearby local outcrops were most of the time exploited. Studies on the black manganese oxides' paintings of Lascaux traced their origin to local outcrops thanks to their barium's concentration (Chalmin et al., 2004, 2003).

After their collection, coloured materials could be used directly, or it could be prepared by various processing methods implying crushing and mixing it with a filler such as clay and water (Clottes et al., 1990a; Couraud, 1991). By studying the composition of the clay present in the pictorial layer, and comparing it to local natural ones it is possible to determine if the mixture is of anthropic origin (Chalmin et al., 2003; d'Errico et al., 2016; Dayet et al., 2014; Hughes and Solomon, 2000; Menu et al., 1993; Moyo et al., 2016; Román et al., 2015; Tsatskin and Gendler, 2016; Vignaud et al., 2006), to identify the way the coloured material was ground (Chalmin et al., 2003; Hughes and Solomon, 2000; Vignaud et al., 2006) and if heat treatments have been applied or not (Chalmin et al., 2004; Garate et al., 2004; Jezequel et al., 2011).

The colours' palette of the Palaeolithic is rather small, only five colours have been registered in cave art: red, black, yellow, white and purple. Among those, red and black are the most common ones and are the usual colours spotted in the French-Cantabrian region. In this same area, rare cases of yellow (Lascaux) and purple pigments are known (Aujoulat, 2004). Their scarce use and their low visibility often lead the archaeologists to suppose these colours to be used for more mystical purposes than the red and black ones (Geneste et al., 2008). Part II Chapter 1 p.40 presents an overview of the red and black pigments known to have been used in cave art.

Nowadays, prehistoric colours suffer greatly from various alterations, which lead to severe aesthetical damages covering small colours' disruption to complete fading of the paintings due to their biodegradation and weathering.

Chapter 2. Cave art alteration

A. Cultural Heritage biodegradation

Despite their relative good conservation, cave paintings and walls are not immune to decay, also known as degradation. Although artefacts' decay involves numerous parameters, it is possible to reduce them to two dominant factors: weathering, and biodegradation. Weathering consists in materials' irreversible breakdown due to the direct contact with its surroundings. Humidity, temperature, ventilation, pollution are a few aspects that play a major role in weathering. They usually compete against one another, leading to unique environmental conditions. These, together with the substrate's properties, constitute extremely specialised ecological niches which favour the development of microbes, such as bacteria, fungi, algae, and cyanobacteria.

These microorganisms participate in the decay of the artefact they colonise. Their metabolic activities induce the production of compounds such as salts or acids altering the material. This deterioration's process is known as biodegradation.

i. Biodegradation

As defined by G. Ranalli, E. Zanardini and C. Sorlini (Ranalli et al., 2009), biodegradation corresponds to "any material's alteration involving a direct or an indirect action from any living organisms", called biodeteriogens. It is usually seen as a secondary process, following an initial deterioration due to weathering (Griffin et al., 1991).

Numerous organisms play a role in Cultural Heritage's biodegradation; the crucial ones are microorganisms such as bacteria, fungi, algae, and lichens. By their diversity and versatility, they can colonise, contaminate and alter all substrates (Warscheid and Braams, 2000). They thence induce a large variety of alterations from superficial and reversible to more problematic ones impacting the structure and complete integrity of the material which hosts them. They can, for example, induce cracks during their growth, or form degradation products setting up coloured

patinas (Garcia-Vallès et al., 1997), or dissolve the host-rock. Many of the deterioration compounds they produce can also directly alter the material with which they are in contact, making the microorganisms influence on the materials' decay more complex, leading to a broad range of biodegradation processes split into different categories.

Moreover, independently from the reason they occur, alterations are usually separated into two major groups: the aesthetic damages and the physicochemical ones. A few authors prefer to separate the physical/mechanical deterioration from the chemical (Ranalli et al., 2009). Although the degradations' processes are different, they both lead to severe structural damages of the artefact. It is why, here, they are considered to be only one sort of alterations. Typically, high-coloured spots – red, pink, purple, blue, green, white – reveal aesthetic deteriorations, implying a biocontamination of the artefact, the formation of degradation products on the surface of the material or a major alteration of the compound constituting the artefact considered (Nugari et al., 2009; Strzelczyk, 2004). Physicochemical damages cover a large panel of modifications as cracks, oxidation, solubilisation, and precipitation; all of them change the structure of the material itself.

In a nutshell, the aesthetical modifications of materials only alter their aspects, possibly leading to misreading, misinterpretation, or even complete loss of pieces of art, while physical and chemical alterations weaken their structure and can lead to its entire destruction.

Fungi are considered as the most harmful microbial organisms colonising artworks. Their occurrence on mural paintings and mortars usually result in aesthetic and structural damages, stains and biofilms formation, cracking and detachment of fragments (Capodicasa et al., 2010; Pepe et al., 2010). Fungi colonise almost all materials due to their relatively easy spreading, thanks to arthropods transport and their sporulation. Their activity extensively damages the substrate they contaminate by producing acids weakening the support and their mechanical actions through their hyphae's growth into the material.

Other entities such as cyanobacteria and algae also contaminate mortars and mural paintings (Altenburgera et al., 1996; Ariño and Saiz-Jimenez, 1996; Cappitelli et al., 2009; Kusumi et al., 2013; Tran et al., 2012). Such species have been pointed to promote deterioration of low light intensity environments, and, more precisely cause pink discolouration in indoor environments (Cappitelli et al., 2009). However, other organisms can produce pigmented compounds such as

carotenoids, widely distributed colourful dyes harvesting energy and protecting the microbes against oxidative damages, and induce irreversible staining and chromatic alterations (Aksu and Eren, 2005; Davies, 2009; Polo et al., 2010; Sandmann et al., 1999; Tinoi et al., 2005).

Though microorganisms are usually damageable for CH, in few cases they are of prime importance in its conservation. Some studies proved they can be used to remove degradation products, such as black gypsum crusts on marbles of the Cathedral of Milan (Italy) (Cappitelli et al., 2007), or to protect material's surface from damageable colonisation, such as *Myxoccocus Xanthus*' usage to develop a protective calcium carbonate coating for limestones (Rodriguez-Navarro et al., 2003). Of higher concern, the systemic removal of biofilms and microorganisms can lead to higher damages than leaving the initial microbiota colonising the artefact studied, such effects are of crucial importance for cave art conservation as exemplified by the case of Lascaux Cave and the recent *Fusarium* contamination crisis in 2000. As it will be further developed, Part I Chapter 2.B p.22-23, Lascaux cave suffered from severe biological contamination crises, due to the lack of knowledge of karstic environments and consequently a poor conservation strategy. During the recent crisis, new intruders resistant to biocide and close to industrial aeration microbes, such as the fungi *Fusarium*, replaced the indigenous communities (Bastian et al., 2009b). Besides their biocide resistance, the recent fungi contaminants started to contaminate the pigments area, threatening the paintings. The new conservation strategy allowed to save the artwork without removing the fungi, which would have allowed other species to develop such it was the case for *Fusarium*.
Therefore, it is of prime importance to identify the different microorganisms contaminating CH and their influence on its preservation to develop the best conservative actions.

A complete study of the decay of CH's materials should be interdisciplinary with the combination of materials and microbiological characterisation techniques (Herrera and Videla, 2009; Rosado et al., 2015). Such studies require to analyse the altered and, if they still exist, non-altered parts of the artefact. The structure, the elemental and mineral composition of the different part of the artefact must be fully understood. It is also necessary to identify and characterise as much as possible the predominant microorganisms contaminating the material. All the pieces of information collected during the previously mentioned analysis should finally

be correlated to interpret the role of the microorganisms in the decay of the artefact studied and to understand the extent of the artefact's degradations.

ii. Biofilm and microorganisms

Micro-ecosystems colonising materials constitute rather complex and highly-environment-dependant structures referred to as biofilm or patina. Since 1990, numerous researchers studied these layers' development and microbiology (Tarragona, Cave) (Garcia-Vallès et al., 1997). Appearance and growth of biofilms are the primary causes of heritage materials' microbial deterioration. These arrangements usually correspond to thin layers assembled by the aggregation of different communities of microorganisms, interacting among themselves. The various microbial populations are embedded in Extracellular Polymeric Substance (EPS), a matrix produced by the microorganisms themselves. Such layers have a very high structural heterogeneity, where the pH, the oxygen and nutrient amounts vary inside the biofilm leading to an extremely rich diversity of the population hosted, complicating the identification of the different microbes involved. Moreover, enhancing this difficulty to understand the involvement of the various microorganisms in the biodegradation, distinct species have various influences on the different alterations' processes (Capodicasa et al., 2010; Pepe et al., 2010).

Biofilms constitute very specific systems since their structure and composition depend on the evolutions of microbiota present in it and the local environmental conditions. Usually, prime coloniser species, besides from altering the substrate, dispense nutrients consumed by other species to develop on the same support. This process permits entities not suited for specific nutrient-low environments to grow thanks to a cooperative growth with better-suited microbes, who provide enough nutrients for the first ones to survive and grow. A prime example of this could be the biocontamination of stone artefacts by autotrophic, carbon-self-producing, and heterotrophic, carbon-environment-dependant, organisms (Warscheid and Braams, 2000). Thanks to their metabolism, autotrophic microbes constitute the pioneer of the microbiota. Their self-sufficiency for procurement of carbon, favours their growing on poor-nutrient substrates. Through the oxidation of reduced sulphur, they produced sulphuric acid, which reacts with calcium carbonate generating gypsum. Calcium sulphate thence migrates to the surface of the stone, whence it crystallises as a crust, later falling, exposing deeper layers

of the substrate, and causing severe damages. Meanwhile, the pioneer entities increase, through various processes such as their metabolic activity or the death of individuals among their population, the amount of organic carbon present at the surface of the stone. This supply of nutrients provides an opportunity for heterotrophic microbes to colonise the material, leading to the development of associative microbial contamination on the surface of the stone. Further colonisation and growth lead to the formation of a biofilm, favouring the development of another species.

Since biofilms correspond to the aggregation of organisms, they tend to present a common growth pattern. Their development on the surface of an artefact can be divided into four essential steps: contamination, attachment, maturation and dispersion. During the contamination phase, microorganisms reach the substrate through diverse transport process from dissemination by arthropods or by wind transport of spores. Once they reach a surface, the organisms start to develop if they have the requirements for their growth. As they grow, they form large colonies and produce the EPS, which protects them and ensures their survival. During this step of attachment to the material, the biofilm appears, and the microorganisms present in it start to diversify. The biofilm thence experiences numerous maturation phases, during which different generations of microorganisms grow inside the polymeric matrix. Finally, the biofilm collapses and turns into a reservoir for microbial dissemination by dispersing surviving colonies and spores.

Due to the previously mentioned specificities of biofilms, they usually constitute very specific layers with interconnection between different species and inorganic materials. These networks lead to the formation of peculiar geomorphological structures of high interest for numerous fields. A large extent of caves' speleothems, such as moonmilk, are thought to be the result of a calcification of biofilms. Due to their unique structure, the layers entrap calcium, which leads to the calcification of the microorganisms or their entrapment into calcified layers resulting in a substantial reduction of the microbial activity. Such theories are not yet entirely proved due to the difficulty to detect and identify the microbial species involved in such biofilms. Recent developments of cultivation-independent microbial identification allowed to suppose a bacterial origin of the moonmilk, future studies should permit to understand better the role of the microorganisms and their biofilm in the formation of such speleothems.

As previously mentioned, though arduous, the identification of the microorganisms contaminating culturally valuable objects is crucial to determine their degradation extent. Due to the difficulty to identify the microorganisms in natural biofilms, microbiologists developed numerous techniques to classify and study them in their laboratory.

iii. Identification of the microbial colonies

As mentioned previously, understanding the biodegradations' process requires the identification of the microbial diversity contaminating CH artefacts.

Commonly, techniques to characterise and identify the communities colonising a sample rest on culture-dependent techniques, consisting of the six following steps: inoculation, incubation, isolation, inspection, information gathering and identification. During the inoculation, different media allow the growth of distinct microbes, depending on their metabolism and nutrient requirements. The various colonies can thence be isolated and distinguished according to their microscopic appearance and reactions to biochemical tests, determining the nutrient requirements, the way of energy's production, and the presence of particular enzymes. Although none of the characteristics mentioned corresponds by itself to a specific trait of a sole species, they complement each other and together permit the identification of the microorganisms to the genus and species level.

However, these methods, relying on culture on nutrient-rich media, solely detect less than 1 % of the existing microbial communities. The vast majority of the microbes cannot grow on media usually used because such experiments miss a few of the conditions required for their growth. For instance, reproduction of the same circumstances of growth of microbes involved in a biofilm arrangement is arduous, since as mentioned previously, these systems mainly rely on a cooperative development of the communities responsible for the appearance of those structures. If one of the entities misses, then the whole system misses a crucial element of its development and a broad range of species cannot develop. This issue is highly strengthened in the case of cave microbiology since some species adapted to oligotrophic environment and media present too high nutrients content to permit them to grow in a viable way. It is why culture-dependent methods need to be complemented by culture-independent techniques.

These last methods rely on the unicity of the microorganisms' nucleic acids sequences, allowing their detection and differentiation through the direct analysis of their DNA (Portillo and Gonzalez, 2009). Since they do not require isolation of the different microorganisms, these techniques present major advantages and were extensively used to identify the genetic diversity of natural communities in CH artefacts (Gurtner et al., 2000; Rölleke et al., 1996). These tests are sometimes very specific and can by themselves identify a microbial species.
Both culture-dependent and culture-independent tests complete each other; together they provide a full picture of the microbial diversity contaminating the sample studied. Final identification of the microbial populations rests on the comparison of the results obtained with characteristics of known organisms.

B. Cave art microbiology

i. Hypogean environment

As seen in Part I Chapter 1, cave art is crucial due to its specificities in time but also to its very specific locations in hypogean environments. Subterranean environments encompass a tremendous number of distinct cavities and potholes, sharing the essential property of having a partial or complete absence of sunlight. This broad definition includes numerous different spaces, among them, caves only constitute a negligible proportion of these habitats. The size of those ecosystems usually permit to divide them into two distinct groups: large cavities, large enough to admit a human being (White, 1988), and small ones referred to as interstitial habitats. The following sections focus more on the case of caves, as defined by Culver and Pipan (Culver and Pipan, 2009), as broad apertures in solid rock presenting some areas entirely deprived of natural light. This definition permits to exclude features such as rock-shelters, exhibiting divergent characteristics.

Subterranean environments include natural and artificial, anthropogenic cavities, such as catacombs, crypts and other underground structures. As they share many similarities, the facts presented here from both natural and artificial underground environments all apply to the specific case of caves.

Subterranean sites present distinct areas according to the photon flux in each of them: entrances, twilight zones, and dark zone. Entrances constitute unique boundaries with the outside world. They receive the greatest amount of natural light and experience the highest climatic variations. Therefore, they present features closer to the outside world than the ones encountered in the dark zones. Twilight zones, located near the entrances receive some natural light during some particular time of the day. Since they correspond to a buffer zone between entrances and dark areas, they present common characteristics with both of them. They are areas where phototrophic and autotrophic communities have the highest possibility to interact one with another. Finally, dark zones are found in the most remote parts of the subterranean environments, they receive no natural light and have very low climatic variations.

As it can be seen with the entrances' instance, hypogean sites do not constitute entirely closed systems. They interact with its surroundings: karstic massif, soil, hydrosphere, and atmosphere. Their specific locations inside the vadose zone, the area located at the interface between the atmosphere-pedosphere and the water table, induce very specific characteristics, highly dependent on its geomorphology.

All subterranean spaces' dark and twilight zones have a considerably reduced amplitude of variation of the environmental parameters such as temperature and humidity when compared to those of the surface. Nevertheless, it does not prevent them from having a climatological annual cycle, it rather confers them very specific conditions throughout the entire year, Appendix 1. Naturally, temperatures' variations embody the best this yearly cycle. Several environmental studies showed that the amplitude of variations of the temperatures registered in subterranean sites, usually represent up to 2% of the surface's changes of temperatures (Cigna, 2002). It explains why for so long references considered hypogean environments as stable and environmentally constant systems (Culver and Pipan, 2009). However, the temperature is far from being the only parameter changing, besides it, air flows, water levels, humidity, and the amount of organic matter brought into the underground environments greatly variate over time and from places to places. Indeed, subterranean sites constitute complex environments in constant interaction with its surroundings. Therefore, to fully understand the climate, ecology, and microbiology of a hypogean environment, it is of prime importance to analyse its characteristics according to the one of the hydrosphere, geosphere, and atmosphere nearby. Doing so provide the keys to the understanding of the disparities but

also similarities of the various underground environments, allowing a better understanding of the biofilm and their requirements, already known to be distinct from the ones of open-air sites.

A major issue encountered when studying prehistoric pigments resides in the fact that they constitute traces of ancestral artwork, which have suffered weathering and biodegradation.

ii. Cave art alteration

The issue of cave art alteration, therefore also of rock art's microbiology, was initiated by Philippe Renault in 1953 and his large-scale research studies focused on how the condition of walls in the endokarst could support cave art. It became of prior importance with the appearance of the green and white diseases in Lascaux Cave (Dordogne, France) and Altamira (Cantabria, Spain) in the 1960's. The caves were then closed, and several studies were carried out on the alteration and preservation of cave art. Their conclusions lead to major facts: caves' preservation implies to maintain as much as possible the site in its discovery's situation and to restrict its access to visitors (Vouvé, 1987). Indeed, the introduction of light and a large number of visitors inside the cavities weakened the substrate by respiration pitting the ceilings and favouring the development of invasive fungi, through their dissemination all over the cave by the visitors and the modification of the climatic conditions allowing their development.

However, caves alterations are also natural, occurring without any anthropogenic interventions. Some researches were carried out on the chemical and physical processes responsible for the evolution of caves walls (Aujoulat, 2002; Lorblanchet et al., 1973; Renault, 1983). They paved the way for current studies dealing with conservation problems. Numerous studies on a large panel of preservation issues were performed since then : quantification of the wall-corrosion induced by visitors (Sánchez-Moral et al., 1999), characterisation of specific alteration or deposits altering the artworks (Cañaveras et al., 2001; Cuezva et al., 2009; Sánchez-Moral et al., 1999) and the microbiology of cave containing artworks (Cañaveras et al., 2001, 1999, Cuezva et al., 2012, 2009, Sanchez-Moral et al., 2012, 2003).

Among the microbial studies, Lascaux Cave plays a crucial role due to the numerous biological crises it suffered. The invasion of the alga *Bracteacoccus minor* in 1963 (Lefèvre, 1974) was the first microorganism outbreak threatening the artwork and was later followed by the fungus *Fusarium solani* in 2001 (Dupont et al., 2007). Although recent the *Fusarium* invasion was not the last biological crisis the cave experienced, more recently, in 2010 black stains produced by the fungus *Ochroconis lascauxensis* (Pedro Maria Martin-Sanchez et al., 2012) put the paintings in jeopardy again (Bastian et al., 2010, 2009a, 2009b). Since then numerous studies have been carried out to understand better the microbiology and origin of the outbreak and colonisation of Lascaux Cave.

As in the case of Lascaux Cave, the biodegradation and microbiology of caves containing cave art raise several issues on the propagation and dissemination of microbial species in different areas of the cave. Fauna and meio-fauna living in these environments play a crucial role in the spread of the microorganisms. Besides from carrying some spores and microorganisms all over the surfaces they touch, they also provide organic nutrients through their faeces and death. As reviewed by Jurado (Jurado et al., 2008), numerous entomogenous fungi found in karst grow thanks to the death of other organisms such as frogs or trychopter. Among the meiofauna, the arthropods play a significant role since they can usually occupy any surfaces of the cavity and propagate microorganisms such as the fungi in all the interstitial cracks. Another crucial fact is the exchanges with the surfaces through the karstic system. Significant changes at the surface can induce a tremendous shift in the microbial population of the surface, who will then migrate to the cave through different processes, according to the porosity and extent of the karstic system. Several studies revealed the outbreak of uncommon species in karstic environments, due to the extensive use of fertiliser and biocide just above the caves studied (Arroyo et al., 1997).

Microbial influence on cave goes beyond the direct alteration of the paintings since microbes are thought to be at the origin of some speleothems growing next and sometimes over cave paintings as it is the casein Altamira (Cañaveras et al., 2006, 2001, 1999 ; Sanchez-Moral et al., 2012), Tito Bustillo (Cañaveras et al., 2001), Lascaux (Berrouet, 2009), Les Combarelles, Gargas (Berrouet, 2009). Cosquer's cave even revealed that Palaeolithic exploited it quite intensively (Clottes et al., 2005). In all these caves, moonmilk can be found either just next to some paintings or engravings or form a small film covering it and making the artworks disappear.

iii. Hypogean microbial metabolism

Most of hypogean microbial populations present some particularities. Indeed, the fundamental source of energy, light constitutes, does not appear at all in such ecosystems. Therefore, the bulk of the suited surface species, dominantly phototrophic, cannot colonise those habitats. Chemoautotrophy, relying on the use of chemical bonds' energy, appears as a crucial source for many microbes present in caves' dark zone. During a chemoautotrophic process, the organism turns the energy of chemical bonds into biological molecules, such as adenosine triphosphate (ATP), allowing it to store energy. An instance of this can be the biologically mediated oxidation of hydrogen sulphide to sulphuric acid.

$$H_2S + 2O_2 \rightarrow SO_4^{2-} + 2H^+ \quad (1)$$

The bacterium *Thiobacillus thioparus* collects the energy released by the reaction (1) to produce ATP for its metabolic activity (Vlasceanu et al., 1997). This somewhat simple example is rather rare but illustrates well the process of chemoautotrophy.

Other sources of energy favoured the development of hypogean biota and microbiota. All of those alternatives constitute external nutrients sources since they bring organic compound into the cavity (Culver and Pipan, 2009). Among them, percolating water plays a fundamental role in the hypogean ecosystem, since it usually corresponds to the dominant organic compounds' way of supply. Indeed, it carries with it dissolved organic matter made of suspended organic matter, microbes and invertebrates, favouring the development of karstic biota by both providing nutrients and favouring the habitat's colonisation. Another crucial source of food for the ecosystem is brought by animals, such as bats and meiofauna, moving in and out of the cavities. Numerous other sources play a role in the organisms' development inside caves, the vast majority does not influence the growth of terrestrial karstic species tremendously.

As mentioned previously, entrances constitute very specific areas in interactions between the outside world and the rest of the cavity. Therefore, their microbiology presents unique specificities such as the development of many species of algae and cyanobacteria specialised to low light conditions (Mulec, 2008). Studies revealed that under low photon flux, such as in

the case of caves' entrances, particular species of cyanobacteria and green algae increase their production of accessory pigments.

Inside dark zones, numerous species adapt to the environment, though they usually cannot be cultured in the laboratory. Ubiquitous organisms in those areas comprise bacteria, cyanobacteria, and fungi. As mentioned in Part I Chapter 2.A, they develop biofilms, helping other microorganisms to develop by producing nutrients and specific environmental conditions favourable for the development of less oligotrophic microbes (Engel, 2012).

In the last decade, numerous studies focused on the microbiology of subterranean CH: catacombs, caves, and crypts are usually the most analysed sites. As previously said, few can be told about the microbiology of such sites, due to their high diversity and their distinct climatic and ecological conditions, each of these sites is unique and present some unique microbial features.

Nevertheless, researchers considered that fungi predominate the microbial life in the hypogean environment, and more strongly in a non-touristic cave. The introduction of light in such locations substantially alter the natural diversity and bacteria and cyanobacteria phylogenetic groups tend to prolifer a lot even with the very low amount of light. Under those conditions, they usually induce black, grey, green and white spots colouration of the walls.

C. Karstic climate and cave art's weathering

Although they are not exposed to outdoors climatic variations, cave paintings also suffer from the "weathering" phenomenon. Such degradations mainly occur due to relatively high climatic variations such as temperature, humidity, and carbon dioxide content, which are enhanced once they are opened to the public. Numerous projects focused on monitoring cave climate to understand their very specific conditions and improve the conservation of the mural paintings that can be found inside of them. Although some of them are still in progress, they demonstrated that cave had very specific climate that should not be disturb to better preserve the artworks contained in it (Cañaveras et al., 2001; Cigna, 2002; Northup and Lavoie, 2001).

Contrary to what was thought initially, caves do not constitute a closed homogeneous system with constant temperature and humidity. According to the location of the room in the karstic system, it presents specific climatic conditions. The distance to the entry, but also the thickness of the soil above it strongly influence the local climate of each room of a cave. Caves also have day-to-day as well as yearly climatic cycles. The following paragraphs briefly present these two climatic cycles and their influence on the alteration of the wall and possible artwork.

i. Day to day cycle

Daily climatic cycles of caves correspond to the variations the outside environment encounters between day and night periods. The amplitude of the variations of this cycle depends heavily on the geomorphology and deepness of the cave. Indeed, the deeper the cave, the smaller the climatic variations thanks to the attenuation role of the soils. The soil lying above the cave acts as an insulating, therefore as its layer increases, the insulation is more efficient and the climatic variations decrease.

Naturally, it also is highly dependent on the regional climate, since areas with low climatic variations between day and night present lower amplitude variations than the ones with high ones.

In the case of Portugal, the climatic conditions correspond to relatively high variations between night and day periods. Therefore, temperature, relative humidity and carbon dioxide concentration cannot strictly be seen as stable over 24 hours, especially during spring and autumn.

ii. Yearly cycle

Microenvironmental parameters at the entrance of caves are clearly conditioned by the external climate. However, inside the caves, air temperatures are more homogeneous throughout the year. Condensation periods correspond to periods when air temperature inside the cave is warmer than the temperature of the host rock. Those periods usually vary from one year to another according to the precipitations and atmospheric humidity.

Air circulation in Western Europe caves tends to present a similar pattern. During summer, the temperature outside the cave is warmer than inside; the cave behaves like a cold trap: air circulation is low, the CO_2 accumulates. During winter, the air temperature inside the cave is warmer than outside. The cold dense air enters the cave replacing the hot air. It leads to convective exchanges between the inside and the outside of the cave. The cold, dry air entering the cave rapidly warms up, and its humidity rises to 100%. In this way, ventilation is important and thereby avoids the accumulation of CO_2 in the cave. The exchanges between the inside and the outside of caves are the most important during spring and autumn when the temperature differences are the most important. During the day the air is warmer outside than inside, so the cave behaves like a cold trap and there is no exchange with the exterior, CO_2 accumulates in the cave, whereas at night, the air temperature is warmer inside the cave. As in winter, it implies convective exchanges between the inside and the outside. These variations exemplify the climatic parameters cycles which the caves are subject.

Numerous factors play a crucial role in cave art conservation, only a few of them were developed in the previous paragraph. Although they present different cycle, the principle stays similar and can lead to some important walls' degradation.

iii. Influences of the cycles on the walls' degradation

By comparing the air and rock temperatures in a same location, it is possible to determine if condensation or evaporation phenomena can occur on the wall's surface without needing the measure of the humidity in all places. When the air temperature is higher than the rock one, condensation can occur, while on the opposite when it is lower than the rock one, evaporation can occur on and in the walls of the cave. While condensation can lead to the dissolution of the substrate and alter the wall and rock art's support, evaporation can result in the development of calcite layer over the wall's surface. Cycles of condensation followed by evaporation periods are extremely harmful to the conservation of cave art. Dissolution of the support, the painting and the precipitation of calcite over the representations are characteristic of such conditions, leading to their complete disappearance.

Another major issue is due to the air velocity inside the cave. Indeed, the morphology of the karstic system determines very specific conditions inside the cave, leading to a normal and relatively stable air flow (also subject to seasonal changes). Variations in the air flow play a major role on the condensation/evaporation cycles occurring on the surface of caves' walls. Although other phenomena can alter caves' walls' surfaces and the artworks it can host, the evaporation/condensation cycle is the easiest and most important one to understand the importance of weathering's phenomena on cave art's preservation.

Chapter 3. Escoural an Iberian "marginal" cave

A. Context and specificities of Escoural

The cave of Escoural, lies near Santiago do Escoural, in the municipality of Montemor-o-Novo, Alentejo (Portugal). It is a natural hypogean cavity located to the following UTM geographic coordinates: M-575250, P-266700, Altitude-370 meters.

It has an important chronological sequence ranging from the Middle Palaeolithic up until the Early Chalcolithic. Essential humans' occupations date back to the Upper Palaeolithic during which populations painted and engraved symbols, and to the Neolithic when inhabitants turned the cave into a collective burial. The region implemented high monitoring and visits' regulations of the site under the recommendations of French (Malaurent et al., 2004) and Spanish (Barquin, 2013) research teams, to ensure the preservation of this exceptional heritage.

i. Description of the cave

Alentejo's region corresponds to a Hercynian region made of granitic outcrops in a Cambrian metamorphic context between the two major Portuguese hydrological basins of the Tejo and the Sado (Lotze, 1945). The municipality of Montemor-o-novo lies on the "Formation of the Serra de Monfurado", Cambrian geological formation with, contrary to the bulk of Alentejo's region, limestones allowing the development of karstic systems.

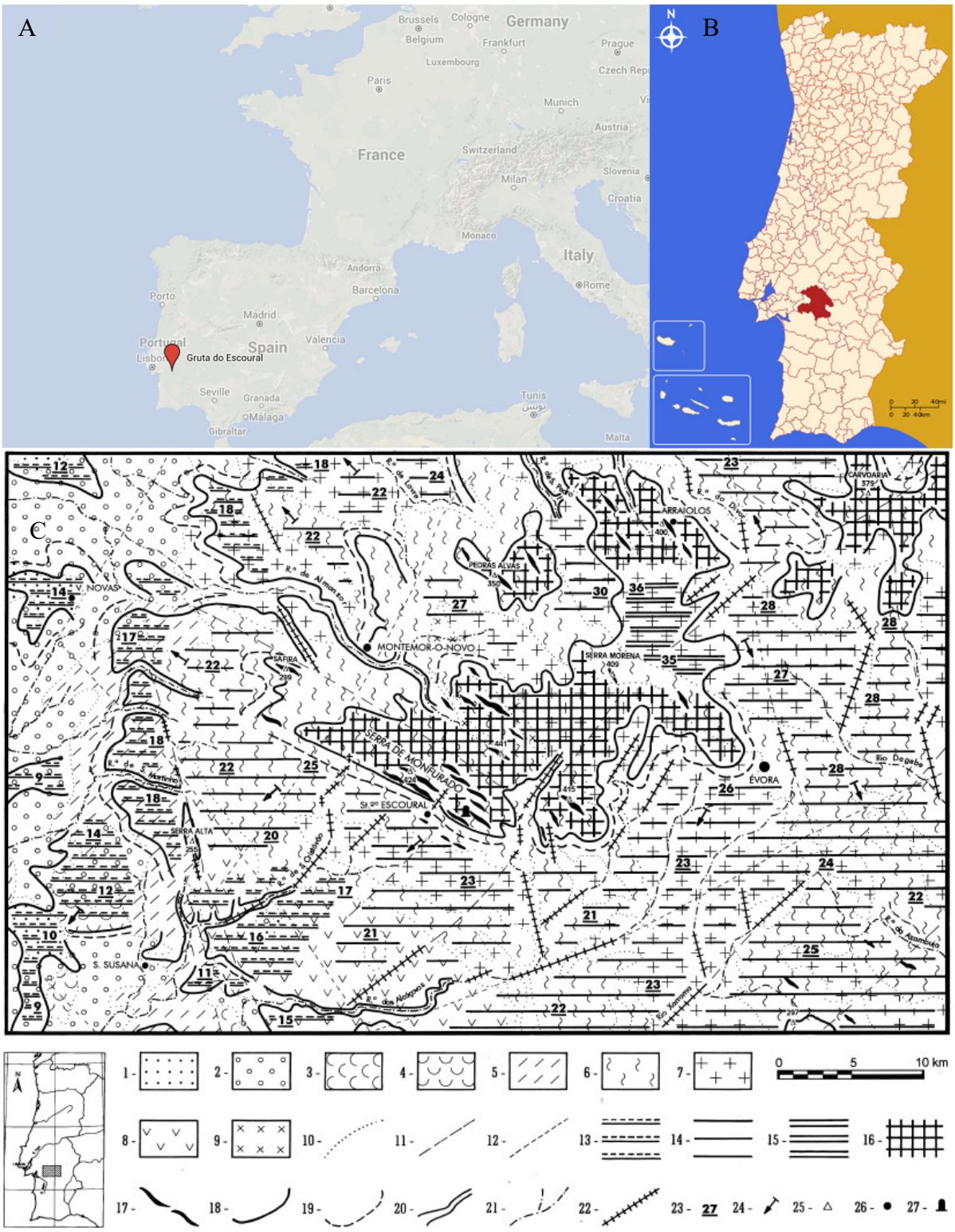

Figure 3: Location and geological context of the cave of Escoural. A. A and B: Location of the cave of Escoural. C: Geological context (from Araujo 1995).1: Pliocene (detritic rocks), 2: Miocene (detritic rocks), 3: Continental carbonate facies (sandstone, schist and carbonaceous material), 4: Marine carbonate facies (schist and metavolcanic),5: Devonian (schist and limestone), 6: Precambrian metamorphic series (gneiss, marble, quartz, schist), 7: Granitic rocks, 8: Quartz from Beja's massif, 9: Gabros, 10: Stratigraphic limit, 11: Lineament, 12: Rift, 13-15: Applanation levels, 26: Localities, 27: Escoural Cave

Escoural's limestones insert themselves between metamorphic stones composed of schist, mica-schist, amphibole schist, volcanic residues and gneiss (Araujo et al., 1995; Carvalhosa, 1989; Vegas, 1968). They result from the Cambrian hydrothermalism during which hot water springs flew inside basaltic lava.
The carbonate precipitates from Escoural thence recrystallized into marble during a regional metamorphic phase.

The cave lies under a hill which culminates to 372 meters above the sea level, with the nowadays entrance to the cave at 358 meters above the sea level (Malaurent et al., 2004). The cave counts several rooms, galleries and underground passages. Nowadays, the cave can be divided into three main areas: the entrance, the room 1 and the remote galleries of the cave, Appendix 1.

The cave had initially one entrance located in its southern part, in the nowadays most remote galleries. However, it was closed possibly willingly after the Neolithic used it as a burial. This entrance is still nowadays closed, and nowadays leads directly to the most important of the cavity: the room 1. It was initially a remote area, from which numerous galleries could be reached and where most of the parietal art was performed.

ii. Discovery and recognition

The cave was discovered in April 1963 during quarrying works, an extracting-marble-block explosion revealed the existence of a cavity on the quarry site. After entering the cave and discovering soils covered with human remains, worker rapidly ran away from the site. Professor Farinha dos Santos closed the access to the public and first studied the cave by excavating the Neolithic tombs found inside and observing some red and black prehistorical paintings (dos Santos, 1964). Farinha dos Santos only observed and referenced nine representations, but he quickly attributed the prehistorical paintings to be part of the French-Cantabrian culture and more precisely Aurignacio-Perigordian style (dos Santos, 1964; Vaultier et al., 1965). His attribution rested on the stylistic comparison of the representations found in Escoural with those found in other caves of the French-Cantabrian region, such as Cougnac, Pech-Merle (Quercy, France) and Nerja (Spain). Prehistorians, more precisely, cave art specialists such as

the Abbey Glory (Vaultier et al., 1965), rapidly confirmed the authenticity of the paintings thanks to their style and the calcite layer overlapping them and obstructing their observation. Despite its recognition as prehistoric traces, archaeologists debated, and still debate, on the attribution of the artwork, Part I Chapter 3.C p.32.

Although the artworks present in the cave reveal some alteration signals, it was rapidly and is still considered as one of the most important discoveries for cave art since it is the westernmost European example of such art. However, its location is not its only singularity, the cave of Escoural shows several characteristics of "marginal" caves, as defined by R. Pigeaud in 2002 (Pigeaud, 2002). According to him, marginal caves have a higher number of unique characteristics than the others, they all share a common characteristic: being restricted in areas with almost no other example of cave art. In the case of Escoural, the other features of marginal cave rely on the theme of the artwork, resting mostly on geometric figures and horses, the techniques used and some aesthetic aspects, both due to the engravings' infilling used to provide the sensation of volume to the different engraved horses' heads.

B. Climatic conditions and conservation state of the cave

Climatic studies performed on the cave of Escoural (Barquin, 2013; Malaurent et al., 2004) revealed that the daily temperatures' variations are as predicted higher in summer than in winter. Seasonal variations from one year to another also appear to be similarly higher in summer than in winter. All the rooms are subject to rock temperatures variations of around 2°C for the most constant conditions. These show a good correlation with the air temperature of each gallery.

Due to the relative high variations of the temperatures registered in the cave, the relative humidity also encounters significant daily variations (high (>95%) at the end of the night and low (70 to 95 %) at the end of the afternoon)(Malaurent et al., 2004). During rainy periods, the relative humidity inside the cave quickly saturates to 100 %.

The right wall of the room 1 and some of the most remote galleries appear to lack evaporation/condensation cycles and are always in evaporation conditions, Appendix 1. No wall

seems to be always in condensation conditions. On walls presenting evaporation/condensation cycles, the period from May to October is extremely favourable to condensation. Following their studies Malaurent et al. (Malaurent et al., 2004) concluded that the fast variations of the humidity on the walls' surfaces are strongly connected to the evaporation/condensation cycles occurring on the walls' surfaces. They pointed out the fact that the calcite layer development, and therefore the cave paintings' degradation, is mainly due to those surfaces' weathering.

C. The occupations' sequence of the cave

i. Human occupation phases of the cave

The cave of Escoural constitutes an exclusive testimony of Alentejo's earliest human' inhabitancy. It is with the site of Monte da Fainha, 50 km away from Escoural, the only trace left by Solutrean or earlier cultures in this region of Portugal (Silva, 2011). Therefore, it appears as a particular site providing a scarce, though crucial, view of hunter-gatherers' culture.
Moreover, prehistoric people occupied the cave of Escoural over a broad time lapse, making nowadays one of the only site in Portugal with such a chronological sequence ranging from Middle Palaeolithic to Early Chalcolithic.

Palaeolithic

The first occupation of the cave dates back to the Middle Palaeolithic (50 000 B.P.) when *Homo neanderthalensis* still survived in the Iberian Peninsula. The few artefacts found in the cave, in majority quartz tools associated with extinct animals' remains, and their location, near the original entrance, though not considered *in situ*, do not permit to conclude on the function of the cave for those communities. Theories support the idea of a seasonal usage by Middle Palaeolithic community.

During the Upper Palaeolithic (37 000 - 10 000 B.P.), Homo sapiens extensively handled Escoural's cave's walls. The large room located at the innermost section of the cavern still hosts many pieces of evidence of their passing. In the case of Escoural, the scarcity of artefacts from

this period discovered on the site tends to point out sporadic humans' incursions, coherent with the interpretations' theories developed in Part I Chapter 1.B, p. 7-8.

The attribution of the representations' realisation appears to be rather arduous since the vast majority of the symbols present in the cave are common to the different cultures of the European Upper Palaeolithic. Since no dating of the paintings nor of the calcite layers covering them has been performed yet, attribution relies on artwork's distribution, structure and style. Gomez differentiated the engravings into two phases according to their stylistic arrangement: the first one being concomitant to the paintings, such as the ox heads, and later ones representing other animals and geometrical figures. According to Leroi-Gouhran's chronology, he attributed the first phase to the style II (27 000 - 20 000 B.P.) and the second one to the style III (20 000 - 15 000 B.P.) (Araujo et al., 1995; dos Santos, 1964). Those dates leaded archaeologists to confirm the attribution made by F. dos Santos the cave art of Escoural to the Solutrean culture (24 000 - 20 000 B.P.), although Gravettian culture (31 000 - 24 000 B.P.) might have performed the earliest illustrations and Magdalenian later ones (Araujo et al., 1995; Silva, 2011).

Neolithic

After these intensive exploitations of the walls, it seems that communities only sporadically visited the cave during the Early Neolithic. Scarce Cardial ceramic remains located near the original entrance tend to highlight sporadic visits during the Early Neolithic and a complete desertion of the site by the Middle Neolithic communities (Araujo et al., 1995; Silva, 2011).

The Upper Neolithic corresponded to a major occupation phase as it was turned into a collective burial, where they deposited corpses at the surface of the cavity together with ceramic jars, polished axes and bone tools. Distribution of the bodies points out the existence of an organisation of the funerary space. Indeed, populations must probably have packed group of skeletons into the different natural niches, once bodies lost their soft tissues. The ceramics correspond to the typical vessel of the megalithic culture of the region (Araujo et al., 1995; Vaultier et al., 1965).

Since then

The cave was closed during the Early Chalcolithic by local populations, it remained isolated from the outside world since its closure up to its discovery in 1963. Since then, numerous excavations and studies were carried out in the cave to understand better the site and its importance for the early Iberian communities of the Palaeolithic and Neolithic. Apart from the work performed by F. dos Santos, an important study was conducted by a belgo-lusitanian team to discover the initial entrance's location (Araujo et al., 1995).

Other studies permitted to analyse the climatic variations and impact on the cave and the preservation of its precious artwork.
Dating the distinct calcite layers covering and hosting the paintings and engravings are included in a European project and should be performed in the coming years (Silva, 2011).

So far, no real analysis was carried out on the pigments, and no study focused on the microbial communities thriving inside the cave.

ii. The parietal art's corpus

So far around 100 figures were observed and recorded inside the cave of Escoural. Engravings represent the majority of this artwork and can be distinguished into two distinct phases of realisation. Paintings represent around 30 distinct figures made of red and black pigments.

The painted representations, as the engraved ones can be differentiated into three types: the animalistic, the geometric and the unidentified ones. The animalistic include representations of horses, bovines and bovid's heads and bodies. Geometric figures include a large variety of shape and therefore seem to correspond to numerous distinct symbols such as dots, roof-shaped symbols and different lines. The unidentified figures could be either greatly altered, or only initially partially performed, or complete but not recognisable by us nowadays. Figure 3 presents the distribution of the distinct representations spotted by the Belgo-Lusitanian team inside the cave. One red painting was added to the parietal corpus described by M. Lejeune. It

is the right red ox head discovered in 2011 in the upper part of the left (North) wall of the gallery 6.

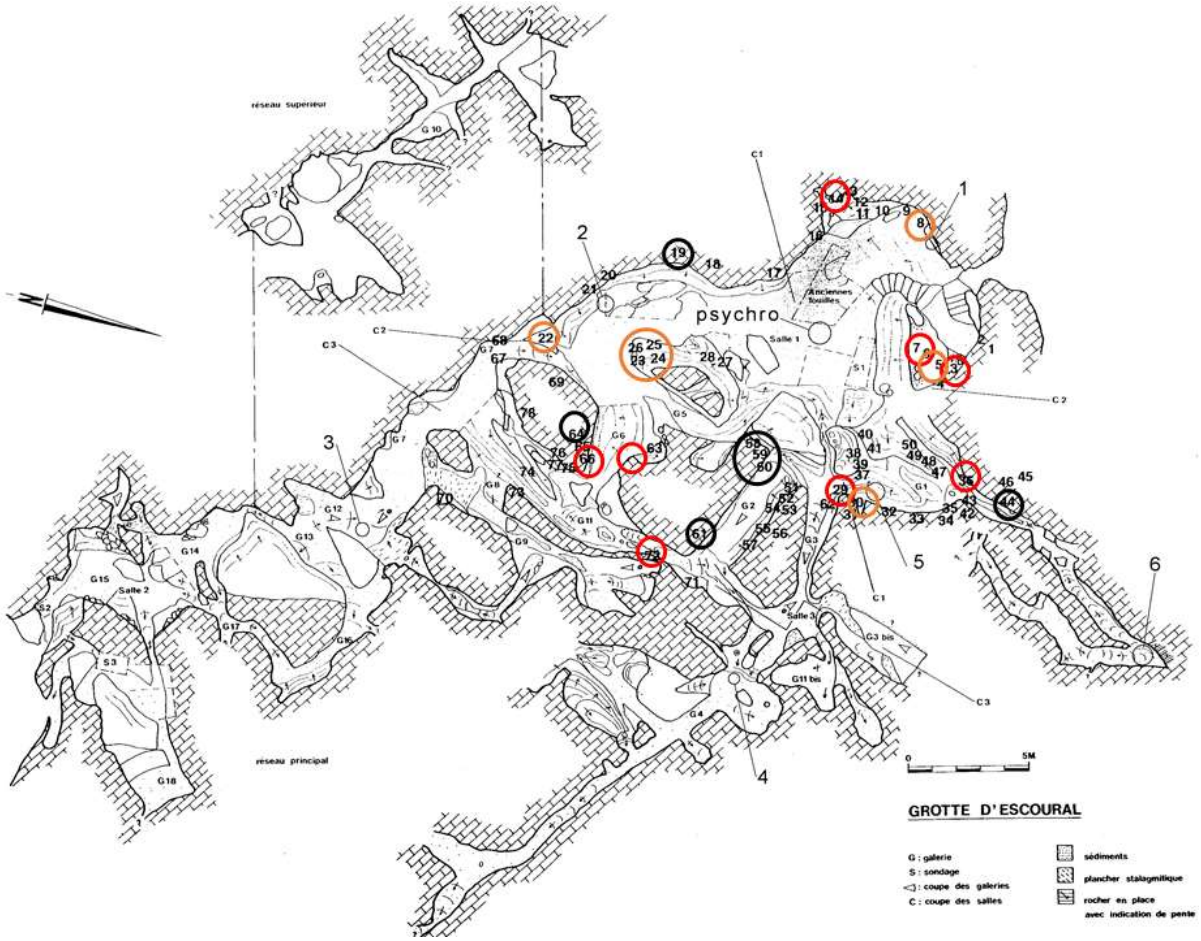

Figure 4: The parietal art's corpus of Escoural. Location of the engravings, and red and black paintings/drawings inside the cave of Escoural. Red: red paintings/drawings, Black: black representations, Orange: red and black figures. Engravings correspond to the number not circled. Adapted from Araujo et al. 1995.

The Palaeolithic parietal corpus of Escoural presents some very specific features which make it, together with its location, a "marginal" cave, as defined by Pigeaud (Pigeaud, 2002). The large number of geometric symbols present in the cave corresponds to a unique specificity, the morphology of the horse heads with rather small ears, the technique used to perform the engravings by performing infilling through the use of parallel engravings to figure shade and volumes (Pigeaud, 2002). All of these constitute specificities, making Escoural's cave unique and original in Western European cave art.

As with all of the other geographically isolated caves, the main question is to understand if those caves are original because isolated or the opposite. It leads to the question of the homogeneity of the cultures which performed cave art throughout Europe.

Study of the pictorial techniques and material used to perform the paintings found in Escoural should help to understand better the originality and uniqueness of this archaeological site. It is also important to comprehend the different factors that could have alter the representations to be able to determine if the traces left today can be considered as representative of the original parietal corpus.

Both aspects should provide key understanding of the cave and more generally of “marginal” caves, though only minor works have been performed on both aspects evoked just before.

The present work aims at filling this important gap by bringing a new understanding of the pigments and microbial diversity of the cave and its influence on the formation of secondary minerals. To do so, samples of the cave were studied between March and August 2016.

Part II The parietal art's analyses

The hybrid's panel, Escoural Cave (Alentejo, Portugal), © G. Mauran

Chapter 1. Prehistoric palette

As seen in Part I Chapter 1. C p.11, the prehistoric palette was rather limited, though the main colours that were red and black were obtained through various means. The following part presents a short overview of the red and black coloured materials registered as being used by the Palaeolithic.

Archaeologists did not consider of great help the early studies of the cave art's pigments used in Font-de-Gaume (Dordogne, France)(Moissan, 1902), La Mouthe (Dordogne, France) (Moissan, 1903) and Niaux (Ariège, France) (Cartailhac and Breuil, 1908). However, they are at the origin of the theory of the use of charcoal, iron and manganese oxides as prehistoric pigments, paving the way for further in-depth analyses.

A. Red pigments

Red paintings were often performed through the use of hematite (Fe_2O_3) with or without anthropic mixing with clay or some natural red ochres rich in iron. Different shades of red were obtained by the various proportions of hematite and clay, but also by the admixture of some other compound such as the yellow goethite, providing a lighter red tending toward orange, or charcoal providing a darker red. By studying the composition of the pigments, the size of the particles it contains, it is possible to distinguish the natural and anthropic mixtures and the distinct painting pot used on a same site.

Hematite, a mineral of chemical formula α-Fe_2O_3, is the most stable iron oxides due to its rhombohedral crystalline structure. Due to its stability, it is the most abundant iron oxide found on Earth's surface. It has an important hiding power and can be discovered in a wide range of shade, though the black-grey crystals, forming a blood red powder, are the most commonly found.

Hematite can also be produced by heating goethite, an iron hydroxide of chemical formula FeO-OH. The dehydration is irreversible and can be performed in several ways (Pomies et al., 1998;

Salomon, 2009; Šubrt et al., 2000). Since the reaction is topotactic, the hematite produced through the heat-treatment presents a different structure than the one found naturally. Indeed, it keeps the acicular arrangement of the goethite, differing from the natural crystals. This property was extensively studied, and literature about the topic is abundant.

Ochres also have a broad range of shades going from dark brown to light yellow and bright red (Dayet et al., 2014 ; Moyo et al., 2016 ; Román et al., 2015 ; Tsatskin and Gendler, 2016). In this work, ochre refers to the geological earth naturally composed of clay and a mineral pigment giving its colouration (Román et al., 2015; Tsatskin and Gendler, 2016). Their colour is due to their composition, according to the minerals present in it: an ochre will tend to be reddish (hematite) or yellowish (goethite). Distinguishing an anthropic mixture of hematite and clay with a natural ochre requires studying the natural ochre present near the cave.

B. Black pigments

Three main different kinds of black pigments have been identified as being used by Palaeolithic: charcoal, bone black and manganese oxides

Charcoal corresponds to the most common black pigment found in cave paintings. Their identification often relies on the elimination of the other black pigments through the absence of manganese and phosphorus in their composition (Chalmin et al., 2002 ; Clottes et al., 1990a ; Couraud, 1991 ; Pigeaud et al., 2010). In some rare cases, SEM observations of the pigments samples even permitted to go further and allowed a rough identification of the wood used to produce charcoal. Indeed, in the case of the black Frieze of Pech-Merle, Lorblanchet et al. could identify the charcoal as being a *Juniperus* (Lorblanchet, 2010). Those scarce identifications provided very rough ideas of the climate at the time of their realisation.

Although charcoal is thought to be the main black pigment used by the Palaeolithic, it is important to have in mind that most studies identified its presence through the absence of characteristic features from other pigments. It is crucial to have this in mind since more and more cave paintings pigments' analyses are performed through the use *in situ* of XRF and Raman. However, the detection of phosphorus thanks to portable XRF requires specific

conditions that are not always respected. Similarly, Raman spectroscopy normally distinguishes charcoal from bone black thanks to the 961 cm^{-1} phosphate peak. A recent study performed by Coccato et al. (Coccato et al., 2015) revealed that this peak is not always detected by Raman analyses, and its absence should not be used as an appropriate criterion to distinguish charcoal from bone black. Having this in mind, it is then not surprising to realise that bone black is known to be used in cave paintings, though no study has been found clearly identifying it on a specific cave painting. Only one study reporting the use of burnt reindeer antler in Lascaux (Dordogne, France) has been found (Chadefaux et al., 2008). A couple of publications mention it as a pigment used during the Upper Palaeolithic thanks to archaeological traces found on soils in the cave of Arcy-sur-Cure and the Abri Pateaud (Jaubert, 2008).

The last major type of black pigments used by the Palaeolithic are manganese oxides. Although they were discovered in numerous sites, only a few studies focused on the composition and processing of manganese oxides as black pigments (Chalmin et al., 2006, 2004, 2003, 2002). They are present in various minerals, around 20 distinct natural ones are known, with different chemical composition, oxidation degree of Mn (II, III, IV or mixed) and crystalline structure. Those distinct manganese oxides are split into two main families: the ones without any cation, the manganite family, and the ones with any cations, the cryptomelane family. Table 1 presents a brief overview of the manganese oxides identified in prehistoric paintings, their respective composition, crystalline structure and family.

Table 1: Manganese oxides recorded as Palaeolithic black pigments.

Manganese oxide	*Composition*	*Structure*	*Site*	*Publication*
		Manganite family		
Manganite	MnOOH	Monoclinic, pseudo-orthorhombic	Gargas	Chalmin et al. 2006
Pyrolusite	MnO_2	Tetragonal	Lascaux	Vouvé et al. 1992
Bixbyite	Mn_2O_3	Isometric	Les Merveilles	Smith et al. 1999
Groutite	MnOOH	Orthorhombic	Ekain	Chalmin et al. 2006
		Cryptomelane family		
Cryptomelane	$(K, Ba)Mn_8O_{16}\cdot xH_2O$	Monoclinic	Lascaux	Chalmin et al. 2004
Romanechite	$Ba_2Mn_5O_{10}\cdot xH_2O$	Monoclinic, prismatic	Lascaux	Vouvé et al. 1992
Hollandite	$BaMn_8O_{16}\cdot xH_2O$	Monoclinic	Lascaux	Chalmin et al. 2004
Todorokite	$(Ba, Ca,K, Na)Mn_6O_{12}\cdot xH_2O$	Monoclinic	Combe Saunière, Lascaux	Chalmin et al. 2004, Chalmin et al. 2006

Although both families naturally occur and can be encountered in clays, quartz, calcite and iron oxides, they have different thermogeochemical stabilities. While manganite (MnOOH) is typical from low-temperature hydrothermal veins, cryptomelane is more characteristic of high-temperature metamorphism. These properties provide some crucial clues to understand the preparation of the pigments. Indeed, in the cave of Ekain, manganese-based black pigments show the coexistence of manganite together with cryptomelane. Due to the different thermo-stability of the two oxides, their mixture is most likely due to an anthropic action. It is thought that they are proving the fact that Palaeolithic crushed and mixed different manganese ores (Chalmin et al., 2006), highlighting a very specific manufacture.

Similarly, to the red pigments made of hematite, the manganese oxides could also have been heated. Due to the distinct thermo-stability of the manganese oxides, the mineral phases provide a first insight on the thermal history of the pigment. Chalmin et al. focused on this issue and provided a procedure to investigate the heat treatment of manganese-based black pigments (Chalmin et al., 2004).

C. Preparation

So far, the present work did not clearly distinguish drawings from paintings, though a major difference exists in the coloured materials and pigments used for these two techniques. Indeed, artwork should be referred to as a painting only if the Palaeolithic modified the raw coloured material used to perform it, else the term of drawing should be preferred (Menu and Walter, 1996).

At this point, it is also necessary to introduce another concept: the pigments manufacturing recipe. This notion refers to “all the different gestures and steps used by the Prehistoric to produce a coloured material, referred to as pigment, with specific, reproducible mechanical and aesthetical characteristics” (Menu and Walter, 1996). These gestures include collecting the coloured material, crushing, heating and mixing it with other compounds, a lot of them were previously evoked in Part I Chapter 1.C p.11. As the heating procedure and its influence on the

different pigments have already been evoked in the previous paragraphs, the following part only focuses on the mixture of the prepared coloured material with other material.

As defined above the pigments manufacturing recipe corresponds to a cultural characteristic of a community. By identifying the different recipes used in a cave, it is possible to determine cultural differences or specificities. In Gargas, the different negative red hands were performed with numerous distinct mixtures that could only indicate a long chronological sequence of use of the wall to carry out these artworks (Clot et al., 1995).

Paintings prepared by the Palaeolithic consisted of mixtures of at least two, and possibly three compounds: the coloured material, a filler and a binder. While coloured materials have been briefly detailed in the above sections, Part II Chapter 1 A and B, p.38-41, fillers and binders have to be mentioned here.

Binders consisted in a wide variety of materials: organic ones such as oil and animal fat, but also calcium-rich water found inside the cave. The use of binders is mostly recorded for Magdalenian periods. As traces are scarce, and research on this topic are still incomplete, not much can be said about it except that organic compounds such as animal and vegetal fats could have been used with this purpose.

The filler plays a crucial role in the mechanical properties of the painting since it is the compound which is providing the pigments with their rheological properties. In Ariège (France), three main kinds of fillers have been identified: potassic feldspar, potassic feldspar with biotite and talc. While talc, identified by SEM-EDS by the association of Si-Mg without Al, was only identified on two paintings and might have been an accidental result, the other two fillers identified are present in numerous paintings. Potassic feldspars are recognisable thanks to their ovoid shape and the association of Si-Al-K, while biotites are lamellar and characterised by the presence of Si-Al-K-Mg and Fe ((Clottes et al., 1990a)). Gypsum is also known to have been used as an extender ((Clottes et al., 1990b)) without altering the colour of the material coloured with which it was mixed. Numerous studies refer the use of clay as a filler in different caves such as Lascaux (Chalmin et al., 2003; Vignaud et al., 2006), Arenaza (Garate et al., 2004), and Ekain (Chalmin et al., 2002).

In some rare cases, crushed bones were added to red paintings as it was the case at Arcy-sur-Cure (Baffier et al., 1999). In other sites apatite or hydrated calcium phosphates were pulverised and added to the preparation of various paintings as in Ekain (Basque country, Spain), Arenaza (Basque country, Spain) and Lascaux (Dordogne, France). These calcium phosphates are possibly due to the use of bone tools during the manufacture of the pigments used to perform those representations (Chalmin et al., 2002, Garate et al., 2004, Pomiés et al., 1999).

Further studies should be performed to understand better the manufacturing recipes of prehistoric pigments and the possible existence of an operational chain. Improving the knowledge about pigments preparation should shed light on crucial cultural aspects of the Palaeolithic communities and understand the organisation and chronology of the parietal corpus in a cave and its regional context.

Chapter 2. Methods

A. Material

Imaging techniques coupled with non-invasive *in situ* analyses and studies of micro-samples collected in different parts of the cave were carried out, to study the parietal art of Escoural. The sampling procedure was performed with a scalpel on the paintings with great care to ensure no disruption of conservation and understanding of the artwork. Sixteen pigments' samples were collected, eight red and eight black, from six different panels, located in four different parts of the cave, Appendix 2 and 3.

Micro-samples were then divided into distinct aliquots to perform the following analyses: FTIR, Raman spectroscopy, SEM observations of embedded polished cross-sections and XRD.

i. Black pigments

The eight black pigments, detailed in Table 5 and Appendix 2 Table 1, were collected from eight different panels located in the room 1, the gallery 1, the gallery 2 and the gallery 6 as depicted in Appendix 2 Figure 1. Three samples (GdE A, E1 and E8) are found next (GdE A) or in direct contact with red pigments (E1 and E8).

The black representations present in the cave of Escoural present different state of conservation some having suffered from dissolution caused by water leaking on the walls of the cave and others from the deposition of calcite over them.

ii. Red pigments

The eight red pigments, detailed in Table 6 and Appendix 3 Table 1, were collected from eight different panels located in the room 1, the gallery 1, the gallery 11 and the gallery 6 as depicted in Appendix 3 Figure 1. Three (GdE B, E2 and E7) of them are found next (GdE B and E7) or in direct connection with black pigments (E2). In this last case, the red covers a thin layer of calcite partially covering a black drawing of a right horse's back legs. It leads to consider the following chronology: realisation of the black lines, formation of a calcite layer and realisation of the red line. This specific sequence might be testifying of a process of graphic narration appropriation, during which a population decides to reuse a drawing performed by earlier communities and change its meaning by adding some new lines. Although narrative appropriation has been documented in Levantine rock art, only one site is known to host figures with recognised narrative appropriation through the use of different colour (López-Montalvo et al., 2014). It could also be due to the technique used to performed the representation and the preparation of the pictorial surface.

The red representations of Escoural Cave present a broad diversity of the state of conservation ranging from almost not altered to highly degraded due to water leaking on the surface of the wall hosting the painting/drawing, leading also to a wide variety of reds.

B. Methods

i. *In situ* analysis

X-ray fluorescence spectrometry

Portable Energy Dispersive X-Ray Fluorescence (EDXRF) spectrometers have recently been used and tested to determine the elemental composition of rock art pigments (Beck et al., 2014a, 2014b, 2013; de SANOIT et al., 2005; Nuevo et al., 2012; Olivares et al., 2013; Roldán et al., 2013, 2010). Although improvements are still needed to improve the signal to noise ratio, it often provides enough to understand the coloured material used to perform the paintings.
In situ elemental analyses were carried out on some of the most accessible paintings using a handheld energy-dispersive X-ray fluorescence (EDXRF) spectrometer TRACER III/IV SD (Bruker, Germany). The instrument has a Rhodium source of excitation, allowing to reach until 40 keV. Time of measure was set to 30 s to ensure proper collection of the signal. The paintings on which it was tested were all sampled to allow comparison between the *in situ* XRF results with the micro-sampling analyses of the pigments.

Visible observations and macrophotography

Visible light images allow for a general look at the painting, an idea of the artist's technique, and the overall condition of the work. The images were acquired with a NIKON D3100 camera and a FUJIFILM X-A1 camera. The set-up consisted of the camera facing the cave's wall while two light sources were pointed at it, at 45º each. The visible light images were acquired with two halogen lamps. All visible light pictures were then analysed with the software DStretch (ImageJ, Jon Harman) to understand the artwork present in the cave of Escoural. The DStretch software was developed to analyse rock art figures in open air site[3]. It permits to enhance the contrast between the artwork and the host rock by modifying the colour space of the pictures analysed.

[3] See: http://www.dstretch.com/ (consulted on 26/07/2015)

Macrophotography was performed to assess the state of conservation of the paintings on a microscopic scale but also to the techniques used by the Palaeolithic to perform this ancestral artwork. Observations were performed with a Dino-Lite Digital microscope AM7115MZT (Dino-Lite 5MP Edge AM7115MZT, Dino-Lite). Six representations were scrutinized with the handheld digital Dino-Lite microscope: 2 reds and 4 blacks. Appendix 4 presents the figures observed, their location in the cave and the conclusions of the *in situ* observations.

The FUJIFILM X-A1 camera was also used to perform macrophotography of the paintings, drawings and engravings. It was then used with two macro extension tubes (MCEX-16 and MCEX -11), with a focal of 200 mm.

Infrared reflectography

Infrared imaging rests on the analysis of the light reflected by a subject illuminated with Vis-IR radiations (400 to 1800 nm). As infrared radiations are highly penetrative and calcite is transparent to them, sketches and old drawings covered by other layers can be seen in the resulting images. IR photography, combined with visible imaging, can give some important information on the kind of cracks, those originating in the pictorial surface or from the ground, present in the painting's layers making it a technique of great importance for diagnostic studies. The images were acquired with an OSIRIS camera equipped with an InGaAs detector. The IR images were acquired with the same set-up than for the visible light images, with the addition of a visible light filter.

ii. Micro-samples analyses

Samples were collected with a sterile scalpel by scratching the paintings with great care to collect as little pigment as necessary without damaging the artwork's lecture. Each sample was collected with a new blade to ensure the non-contamination of the pigments and then stored in sterile tubes. The location of each sample was precisely documented through various photographs taken during the sampling procedure.

Samples were then observed with a stereomicroscope to ensure the presence of pigment on the sample collected and to divide each sample into several sub-samples. One aliquot of each

sample was embedded in methacrylate resin to perform Raman and SEM-EDX analyses of the cross sections. Another aliquot was used to perform FTIR, XRD analyses with uncoated SEM observations of the pigment layer.

Infrared microscopy

Infrared transmission spectra of the samples were recorded with a Fourier transform infrared spectrometer (Bruker Tensor 27; Ettlingen, Germany) coupled with a microscope (Hyperion 3000) and a Mercury Cadmium Telluride (MCT) detector, allowing distinct acquisitions in various areas of the samples. The IR absorption spectra were performed with the OPUS 7.2 (Copyright© Bruker Optik GmbH 2012) software, in the Mid-Infrared region of 4,000 to 600 cm^{-1}. Each spectrum results from the accumulation of 64 scans with a spectral resolution of 4 cm^{-1}. Samples' analyses were performed with an x15 objective and a diamond compression microcell (EX'Press 1.6 mm).

Scanning electron microscopy

Stratigraphic cuts of the micro-samples were prepared in epoxy resin, observed and analysed in a Hitachi S-3700 N SEM (Tokyo, Japan) coupled with a Bruker XFlash 5010 EDX spectrometer (Berlin, Germany) at an accelerating voltage of 20 kV in a variable pressure mode at a 40 Pa partial pressure. Microanalyses were performed through point analysis and two-dimensional mapping.

Raman microscopy

Raman spectrometry was used to complete the Scanning electron microscopy analysis and permit full identification of the pigments used by the prehistoric artists. Measurements were performed on cross sections embedded in resin and on samples without any preparation by Raman microspectrometry using an HORIBA Xplora Raman microscope (Tokyo, Japan), with capacity increased to one hundred times, and a charge coupled device detector. Analyses were carried out with two different lasers of 638 and 785 nm with a 1-50 % filter to avoid samples' destruction. The spectra were acquired in scanning mode after 5 to 20 scans with an acquisition

of 10-20 s and spectral resolution of 5 cm^{-1}. Calibration was performed with a silica standard and ensured with powders of pigments standards of cadmium yellow, chromium oxide and ultramarine blue. The colour camera allowed the observation of the working area, and data were collected with the software package OPUS 7.2. The identification of the mineral phases was based on comparison of the spectra and characteristic peaks found in the literature.
Analyses were carried out with the 638 nm laser for black pigments with low power (less than 10 mW) and with the 785 nm laser for red pigments with special attention to avoid samples' burning. Great care was given to specific regions, 150-800 cm^{-1} for black pigments and 100-1400 cm^{-1} for red pigments, to ensure the proper detection of the Raman signals of the minerals present in the pigments' preparation.

X-ray micro-diffraction

XRD measurements were carried out either on an X-ray microdifractometer Bruker D8 Discover equipped with a Cu source, a Lynxeye linear detector and operating for 3° to 75° with step of 0.05°/s. The X-ray diffraction patterns were analysed with the software provided by Bruker: DIFFRAC.EVA. Only six samples presented enough pigment to perform the micro-XRD analyses, among them two were black (GdE 7 and E8) and four were red (GdE 11, E2, E7 and E13).

Chapter 3. Results and discussion

A. Observation of the drawings and paintings of Escoural

A brief description of the various representations and of their interpretations is presented in Appendix 5. As no study had ever been performed on the pigments and pictorial layer of Escoural's representations, it was decided to investigate both of them to understand the diversity of the occupation phases and its influence on the variability of techniques and materials used by the Palaeolithic communities.

Observations made on the site precised a bit more the corpus thanks to a better understanding of the figures and their relative chronology. Indeed, due to the small calcite layer covering most

of the representations found inside the cave, it is not always easy to analyse and interpret the various paintings, drawings and engravings found in Escoural. Thanks to the Infrared reflectography for the black representations, and the use of the DStretch software for the other representations, it was possible to revise the corpus of the representations found inside the cave of Escoural.

Table 2 presents an overview of the distinct figures that were better characterized thanks to the use of infrared reflectography and modification of the colour space of the visible light pictures. As the interpretation performed thanks to these methods is tedious, Table 3 only includes the representations for which the new interpretations are confirmed thanks to the different methods. Further observations made with those techniques and not entirely confirmed results are presented in Appendix 5.

As the representation 59 illustrates the possibilities and limits of the imaging techniques, the following paragraphs detail its interpretation and possible chronology. It is located at the entrance of the gallery 2 on its right wall (South), Figure 4. It was described and registered by M. Lejeune as seen in Figure 5.A. She recorded it as "the shape of an unidentifiable animal orientated to the right. For M. Lejeune the animal exhibits a rectangular head, a rounded muzzle, a massive neck, a short and stocky body and fragile legs oriented in various directions"[4] (Araujo et al., 1995).

Infrared and false-colours visible light pictures revealed the representation 59 to be more complex than what M. Lejeune thought. Indeed, the nowadays visible drawing is the result of numerous anthropic artworks. Thanks to the pictures realized during this thesis, it was possible to identify, as it can be seen in Figures 5.B and 5.C, not one animal but at least three horses' drawings, and three uncomplete or unidentified animals, performed on each other. To this, it is necessary to add the engravings, that were not clearly identified due to the absence of skimming light, due to the morphology of the panel hosting those representations. The different stylistic features of the distinct horse's heads tend to indicate that they were all performed by distinct individuals, most probably at various phase of occupation of the cavity.

[4] Translation from French : G. Mauran

The first drawing unit performed on the panel of panel 59 corresponds to an animal, interpreted as an ox, presented in orange in Figure 5.C. Since the head and the body do not present the same characteristics in infrared, it is possible that this ox is in reality made of two unidentified representations, or that later population reused two previous drawings in a well-known process of narrative appropriation (López-Montalvo et al., 2014). Experiences with thermal imaging performed after the work of the present thesis, did not permit to improve the understanding of the figure. Development of techniques such as terahertz should permit to increase the reading of such panels.

Later populations drew on top of it several horses, starting with 59.C, which is nowadays visible thanks to its body and front leg, its head being largely covered by a thick layer of calcite, but still perceptible in some parts, Figures 5.C and 5.E.
Another drawing was then performed on the top of 59.C, it consisted in a right horse head with possibly the figuration of some parts of the mane through the use of small black lines on the dorsal part of its neck.

A smaller horse was then performed on top of 59.A, this horse evidenced in red in Figure 5.C, is clearly visible with the Infrared and presents a head with mane, and front leg. This representation also presents one unique feature in Escoural: the presence of an asperity of the wall figuring the eye of the horse. Although the question of the intentional or accidental nature of this asperity to present an eye is naturally disputable. However, numerous similar artworks have been registered in other caves (Clottes, 2008a). In all those cases, the answer to the previously mentioned debate was not provided, though they were all interpreted as deliberate signs of a choice of the support by the Palaeolithic communities who performed cave art connected to them.

At least two other representations were spotted. They are depicted in blue and purple in Figure 5.D. Although it is thought that the figure 59.D represents a horse, the drawing does not present enough morphological characteristics to ensure this interpretation. Furthermore, some of the attribution of the lines detected could be in reality to other representations. It is why, further investigations should be carried out to complete the present interpretations. Some lines

spotted but not directly connected to any of the representations were depicted in white in Figure 5.D.

Table 2: Figures better understood thanks to imaging techniques.

Old reference	*New reference*	*Localisation*	*Anthropic*	*Colour*	*Category*	*Previous interpretation*	*New interpretation*
19	19.A*	S 1 (East)	Yes	B	D	Horse (G)	Horse (G)?
	19.B*		Yes	B	D		Horse (TD)?
	19.C*		Yes	B	D		Horse (TD)?
	19.D*		?	B	D		Horse (J)?
23	23.A*	S 1 (North)	Yes	B	D	Hybrid (D)	Hybrid (D)
	23.B*		Yes	B	D		Horse (TG)
	23.C*		Yes	B	D		Animal (G)
	23.D*		Yes	B	D		Cheval (TD)
30	30.A	G 1 (West)	Yes	B	D	Horse (JG)	Horse (JG)
	30.B		Yes	B	D	Unidentified	Horse (G)
	30.C		Yes	B	D	NR **	Unidentified
	30.D		Yes	R	P		Ox (TD)
	30.E		Yes	R	P	Unidentified	Horse (TG)
44	44	G 1 (East)	Yes	B	P	Horse	Horse (TD)
58	58.A	G 2 (South)	Yes	B	D	Animal	Horse (TD)
	58.B		Yes	B	D		Unidentified
	58.C		Yes	R	P	NR	G (P)?
59	59.A	G 2 (South)	Yes	B	D	Unidentified animal	Horse (TD)
	59.B		Yes	B	D		Horse (D)
	59.C		Yes	B	D		Horse (D)
	59.D		Yes	B	D		Horse (D)
	59.E		Yes	B	D		Ox?
	59.F		Yes	B	D		Animal
72	72.A	G 11 (West)	Yes	R	D?	Horse (TD)?	Horse (TD)
	72.B		Yes	B	?	NR	Horse (TD)?
NR	79	G 6 (North)	Yes	R	P	NR	Ox (TG)

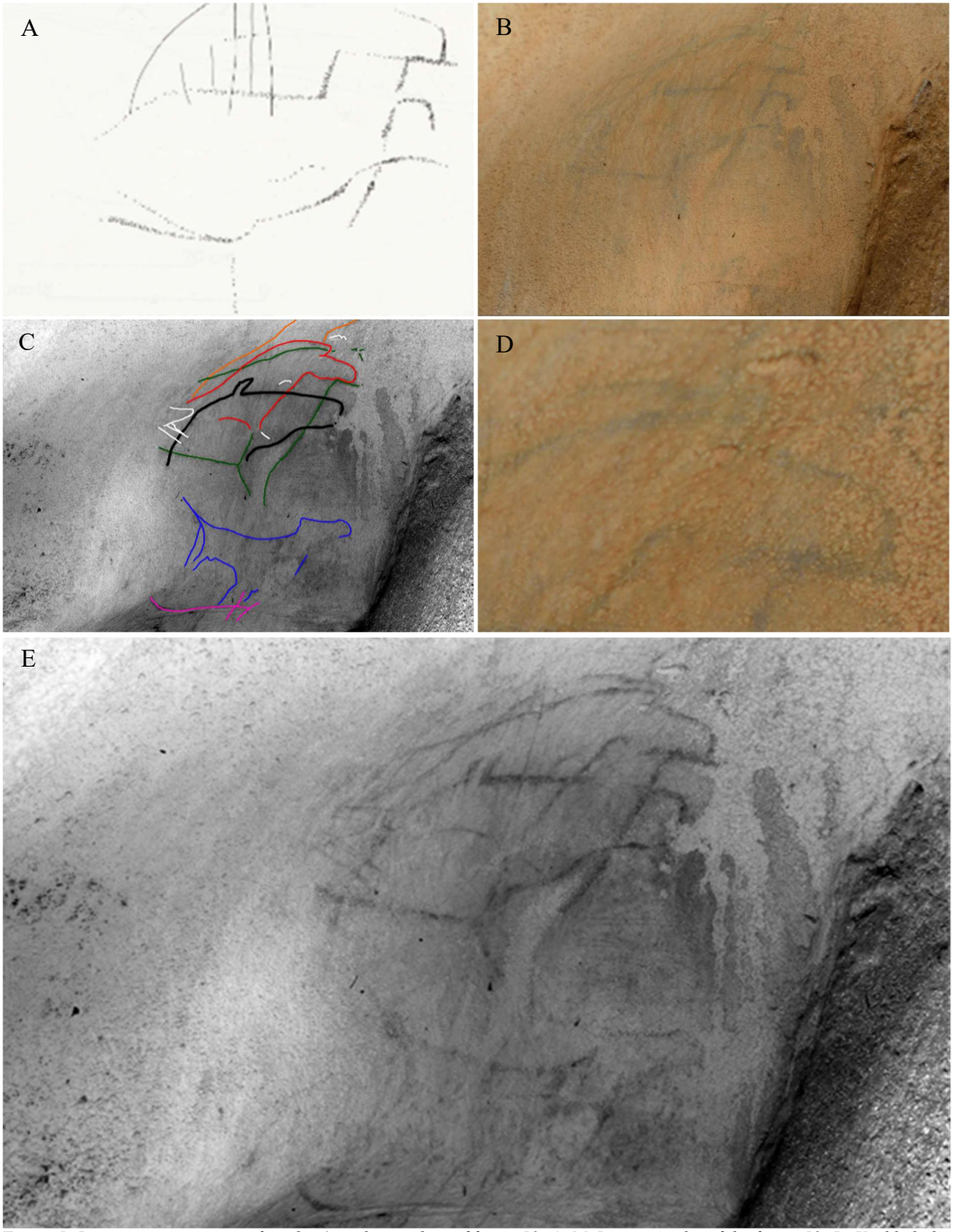

Figure 5: Imaging improvement of reading's understanding of figure 59. A: M. Lejeune's plot of the figure 59; B: Visible light picture of the figure 59, ©Sonia Costa, C: Interpretation of the black drawings constituting figure 59: black figure 59.A, red figure 59.B, green figure 59.C, blue figure 59.D, orange figure 59.E, purple figure 59.F, white: unidentified traces; D: Close-up of horse 59.B with the asperity of the wall figuring the eye of the horse.59. E: Infrared reflectography of the figure 59, ©Sonia Costa.

During the observation and the processing of the pictures of figure 58, located just above figure 59, a red spot connected to a red drip was spotted. Although it was impossible to interpret this red trace, it explained the presence of hematite particles on the sample of the black pigments taken from figure 59. Further should be done, to understand the role of the degradation in the spread of the red painting, since it could either due by the application of a wet pigment which leaked on other representations or the weathering of a red painting.

The detailed case exemplified the detection possibilities of infrared and Dstretch images. It is important to note that both should be complementing each other, since they provide complementary images on the presence of red and black pigments. Further observations and analyses of pictures of "blank" panels – without any apparent representations – of the cave of Escoural, especially in its non-visited part might provide more new figures further altered, and therefore less visible.

B. Pictorial techniques

Macro-photography was carried out to understand the techniques used to apply the pigments on the walls of the cave. Due to the conservation's state of the paintings and drawings, most of which are fading besides a layer of calcite, the observations failed at comprehending the pictorial techniques used to perform some of the figures found inside the cavity.

Observations performed with the digital microscope were at a too high magnification, due to the digital microscope range of magnification, to correctly interpret the pictorial techniques. They mostly provided a good insight on the state of preservation of the pictorial layer and the extent of the calcite layer covering the representations, Figure 6.A. It also provided some insights on the composition of the material used to perform the different representations, Figure 6.B, confirming the representativeness of the micro-samples analysed to characterise the pigments used by the Palaeolithic.

The macro-observations performed with the two distinct cameras provided a better insight on the pictorial techniques used to perform the various figures found in Escoural Cave. Table 4 sums up the observations and conclusions about it.

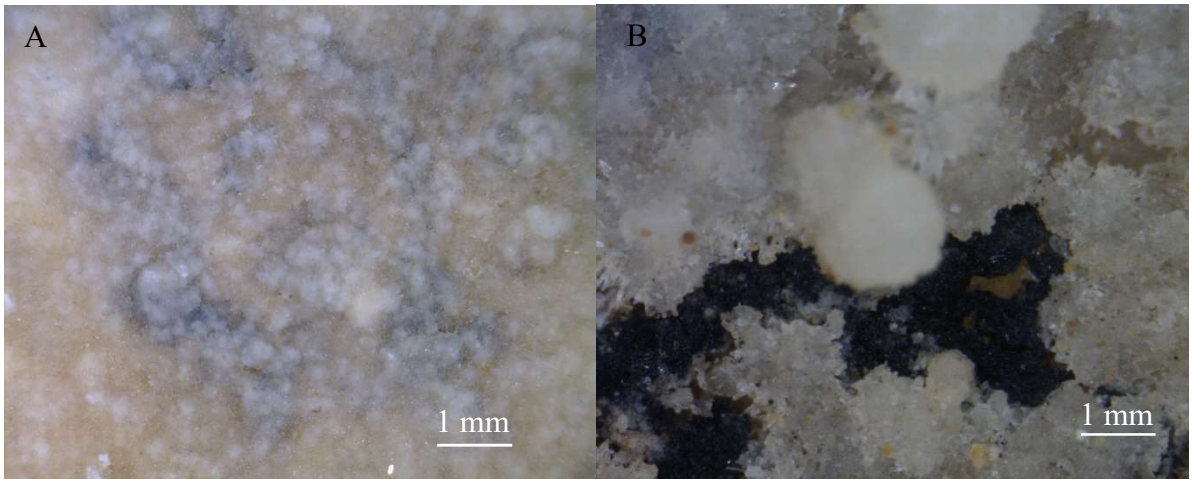

Figure 6: Observations performed with the digital microscope. A: Observation of figure 22 fading behind a non-homogeneous calcite layer. B: Observation of the figure 22 evidencing the presence of charcoal particles and some minerals in the pictorial layer.

As reported in Table 3 and depicted by Figure 7, four distinct techniques have been identified: the charcoal drawing, the painting performed with the finger, the painting realized with an ochre crayon, and the painting performed with a thin pencil.

The last technique mentioned is relatively easy to detect and was observed on only one painting: figure 61, Appendix 5. The particularity, at the scale of Escoural Cave, of the technique used to perform the figure is coherent with the unique pictorial material used. Indeed, the figure 61 is the only figure inside the cavity to be performed with manganese oxides, Part II Chapter 3.C p.58-64. The thin thickness of the line - less than 5 mm -, the presence of tiny ridges not imputable to the substrate, Figure 7.A, and the relatively homogenous aspect of the line support the idea of the use of a thin pencil to perform these black traces (Aujoulat, 2004; Clottes and Arnold, 2001; Lorblanchet, 2010). In some parts of the figure 61, the figure presents thicker lines of approximately 5 mm. The diffused aspect and some of the pattern seen in those diffused black area evidence a step of finger smoothing of the painting, Figure 7.B (Clottes and Arnold, 2001).

*Table 3: Pictorial techniques used to perform Escoural's parietal art. * The characterisation of the techniques is relevant for only some traces of the figure considered. Legend: C: charcoal drawing, F: finger painting, O: ochre paste painting, S: pencil painting with irregular smoothing.*

Figure	*Location*	*Colour*	*Pictorial layer*	*Specific features*	*Category*
19	Room 1	black	Superficial and heterogeneous	Both engraved and coloured	Drawing (H)
*22**	Room 1	red	Covered by calcite	Not observed	?
		black	Superficial and heterogeneous	Both engraved and coloured	Drawing (H)
*24-28**	Room 1	red	Homogenized	Finger shape and ridges	Painting (F)
		black	Superficial and heterogeneous	Both engraved and coloured	Drawing (H)
29	Gallery 1	red	Irregular lines' thickness	Ridges	Painting (O)
		black	Presence of black particle	Not enough pigment	?
30	Gallery 1	red	Irregular lines' thickness	Ridges	Painting (O)
		black	Superficial and heterogeneous	Superficial and similar size	Drawing (L)
36	Gallery 1	red	Paste texture	No specific	Painting (O)
		black	Presence of black particle	Charcoal particles	Drawing?
44	Gallery 1	black	Irregular line, homogenized	Finger shape and ridges	Painting (F)
58-60	Gallery 2	black	Superficial and heterogeneous	Both engraved and coloured	Drawing (H)
61	Gallery 2	black	Thin smoothed lines	Ridges and smooth aspect	Painting (S)
72	Gallery 6	red	Irregular lines' thickness	Ridges	Painting (O)

Although these techniques present some similarities, they slightly differ, since the final aesthetic differ between a smoothed and non-smoothed painting. As the two were observed in different spots of the figure 61, it tends to point out that the panel hosts not only one representation but several as it was demonstrated for the figure 59 in Part II Chapter 3.A p. 47-48.

Despite all the efforts deployed to evidence and comprehend the distinct representations composing the figure 61, it was not possible to provide a better interpretation than the presence of unidentified lines possibly attributable to some herbivores. The last assessment could be made by comparison with the figure 59. Indeed, it seems that the visible parts of the

two figures present some slight similarities. If to be confirmed, the figure 61 would probably represent a composition of heads and entire animals of small dimensions.

Similarly, the only black painting performed with a finger corresponds to the only representations performed with only bone black. Indeed, the observations of the figure 44 revealed the presence of ridges not imputable to the host rock, a regular thickness of the lines, and the presence of what looks like finger shape, though no fingerprint was observed, Figure 7.C. All the previous features tend to point out the use of finger to paint the right black horse. Other representations were possibly performed with finger such as red traces reported as being part of figure 28, Appendix 5. These traces do not form an identifiable shape, though the scarce traces left have the shape and size of finger imprints on the cave's wall, Figure 7.F. The issue in the interpretation of these red traces resides in the large alteration of the red representations of the figure 28. As for figure 61, it is thought that what was recorded as being one figure is in reality the vestiges of many distinct paintings of animals and anthropic imprints.

The charcoal drawings could be differentiated into two sub-categories according to the engraved character of the figures or not. When the pigments were found on a line that seemed to also be engraved, Figure 7.E, the charcoal drawing was performed with a "high" pressure, while if the charcoal particles seemed to remain superficial, Figure 7.D, it was realised with a low pressure (Clottes et al., 2005; Clottes and Arnold, 2001; Delluc et al., 1983; Lorblanchet, 2010). As detailed in Part II Chapter 3.C p.58-64, the two charcoal drawings groups defined here correlate well with those defined with the charcoals particles' sizes, tending to point out the existence of two distinct habits connected with charcoal drawings.

The last group corresponds to the ochres representation. Although ochre could be used directly to perform a red drawing, most of the representations found in the cave present a composition which seems to indicate the existence of a manufacturing step with the presence of feldspar, biotite and apatite, as detailed in Part II Chapter 3.C p.64-69. Therefore, despite they were performed with ochre, they are considered to be ochre painting. Depending on the ochre used, the state of conservation and the relative humidity near the red painting, the aspect of the pictorial layers differs greatly from one to another, Figure 7.G and 7.H.

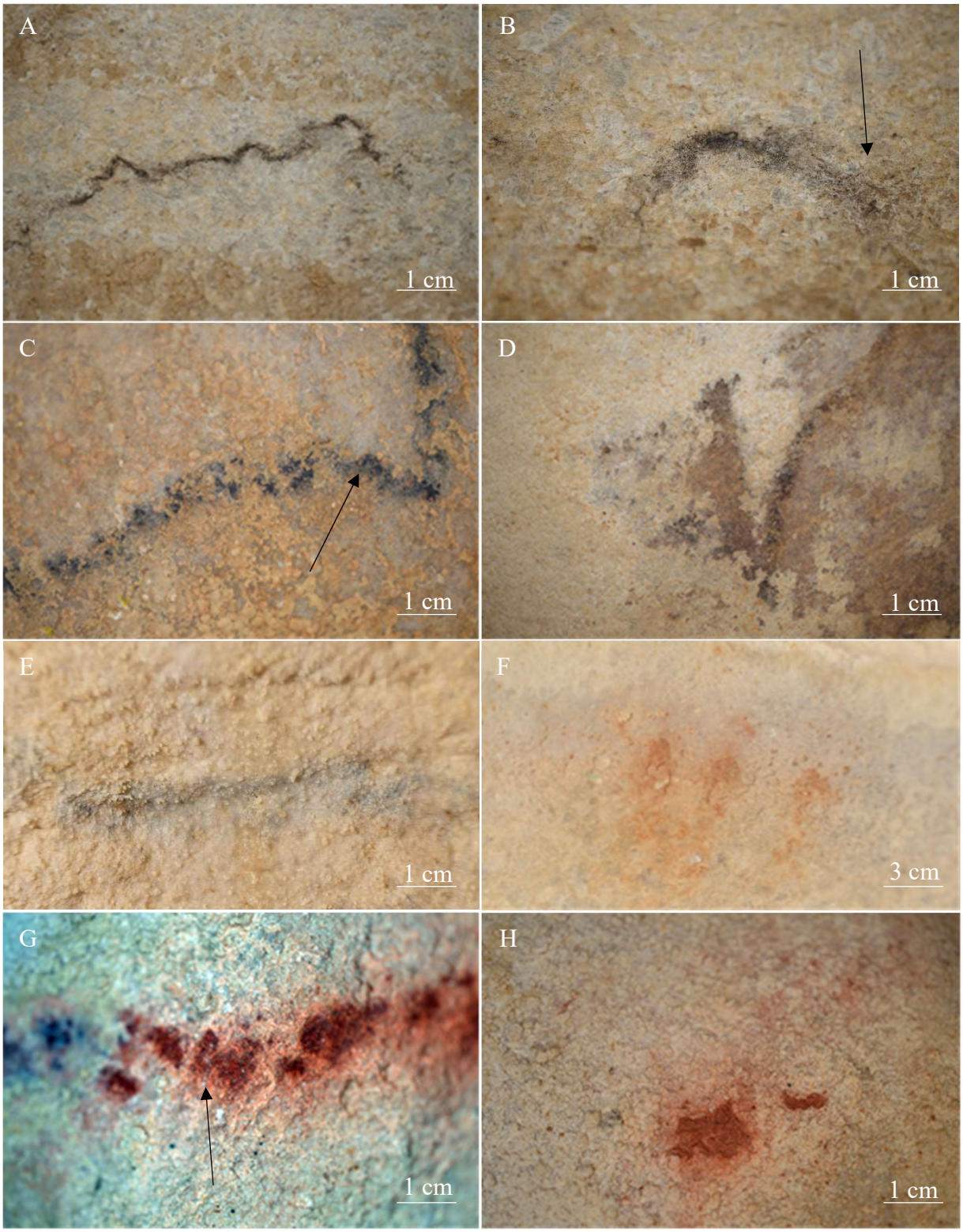

Figure 7: Diversity of the pictorial techniques used to perform Escoural's cave art. Pictorial layers' macro-photos of different figures found inside the cave. A: Figure 61: thin line with ridges (distinct from the ones of the substrate) characteristic of pencil painting. B: Figure 61: thin line with ridges and smoothing, possibly with fingerprints (arrow). C: Figure 44: line of irregular thickness with the presence of ridges, and possible finger shape (arrow). D: Figure 30: superficial charcoal drawing performed with a low pressure of the charcoal. E: Figure 24: charcoal drawing performed with "high" pressure on the charcoal. F: Figure 28: red traces shape and size like fingers. G: Figure 29: red line of irregular thickness with some ridges (arrow). H: Figure 36: red paste like pigment, with traces of black charcoal particles.

All the previous observations highlighted different pictorial techniques, pointing out the existence of numerous occupation phases inside the cavity. Therefore, Escoural Cave study appears to be more complex than initially thought, possibly due to the existence of numerous occupation phases during the Upper Palaeolithic.

C. Pigments' identification

The analyses permitted to confirm that all representations identified in the cave are of anthropic origins. Although, as observed with the Dino-Lite digital microscope, Figure 6.A, most of them were covered by calcite, microscopic observations of the samples collected allowed to observe the pigments with a reduced calcite layers.

Despite the overwhelming signal of calcium due to the support and the over calcite layer, the *in situ* XRF analyses permitted to determine clearly that all red figures analysed contained a high level of iron, and that black figures distinguish in two main type of pigments: the manganese oxides and the carbonaceous material, Appendix 6. Since the measures were performed without any filter improving the signal of the lower elements, it was not possible to distinguish bone black from charcoal since calcium could not be used as a criterion to split the two due to the support and phosphorus was not detected precisely enough to allow the distinction.

Three samples, three black (E1, E4, E6) and one red (E2), presented both red and black pigments. In all of them, although the stratigraphy was not cleared the black seemed to cover the red, differing from the observations made by Lejeune et al. on a figure not sampled in this work (Araujo et al., 1995).

i. Black pigments

The different techniques provided complementary information, allowing the identification of the pigment and their characterisation.

As expected, in the conditions of measure, infrared appeared to be the less efficient to identify the various black pigments. Due to the wavenumbers' range used to perform the infrared spectroscopy, the characteristic bands of manganese oxides were out of range and therefore, could not be detected with this technique.

The infrared spectrum of the sample containing bone black highly defers from all the other ones. The signal was strong but few bands appeared, Figure 8.A. The signal collected from 3500 cm^{-1} to 2000 cm^{-1}, could correspond to the characteristic bands of aliphatic C-H and O-H of an altered bone black pigment (van Loon and Boon, 2004), while the few bands identifiable all correspond to bands found in the mineral part of bones: 1565 cm^{-1} to amide II, 1402 cm^{-1} to carbonate groups stretch, 1024 cm^{-1} to PO_4^{3-} asymmetric stretch, 870 cm^{-1} to carbonate groups bend, 600 cm^{-1} to PO_4^{3-} bend (Alvarez-Lloret et al., 2006; Figueiredo et al., 2012). Comparing this spectrum with the spectra of whitened bone black pigment acquired by van Loon and Boon, Figure 8.B , it seems that the present pigment is rather quite altered but of similar composition (van Loon and Boon, 2004). For other samples infrared only provided information on the substrate and mainly detected calcite, Appendix 7.

Raman spectroscopy revealed the existence of at least two different kinds of black pigments: one containing manganese oxides and another one of a carbonaceous composition. Indeed, the presence of amorphous carbon was spotted thanks to the two broad peaks around 1550 and 1350 cm^{-1}. It did not permit to distinguish charcoal from bone black, since the 961 cm^{-1} was not spotted in the sample containing bone black, despite numerous attempts to spot it. As reported by Coccato et al. this criterion was not taken into account to distinguish the different carbonaceous pigments (Coccato et al., 2015). Raman spectrometry permitted to detect manganese oxides thanks to the following characteristic bands: 580 and 650 cm^{-1}, Appendix 2. Calcite was spotted on all samples as a substrate for the pigment layer.

Scanning electron microscopy of the black pigments' cross sections collected inside the cave of Escoural revealed the existence of at least three different paintings pots: one made of manganese oxides, one of wood charcoal and the last one made of bone black covering a clay layer containing some siliceous features identified as marine fossils. Point analysis performed on particle recognised as pigments during optical microscopy, permitted to complete the

identification of the different black pigments. The EDS analysis confirmed the previous results obtained with Infrared and Raman spectroscopies, providing a clear distinction between manganese oxides, bone black and wood charcoal as can be seen in Figure 9.A and 9.C. While manganese oxides are easily identified since they contain a high level of manganese, bone black is spotted thanks to the simultaneous detection of calcium and phosphorus on the particles of pigment.

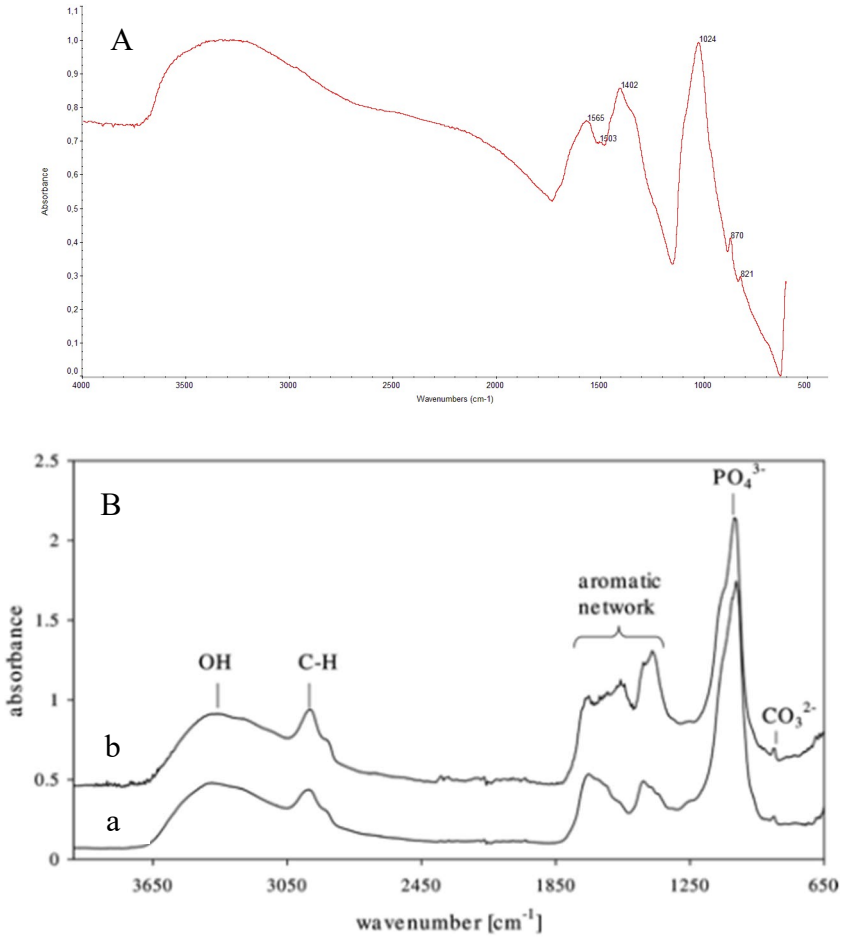

Figure 8: Bone black Infrared spectra. A: Infrared spectrum of sample GdE 13. B: Infrared spectra of bone black in oil paintings (van Loon and Boon, 2004): a: White deteriorated bone black, b: healthy bone black.

Finally, since analysis were carried out on cross sections embedded in epoxy resin, wood charcoal was identified when no other element than carbon was spotted on the EDS spectra and particles' morphology.

Concerning the preparation of the black pigments to perform the different figures found in Escoural, only the manganese oxides presented traces of potassic feldspar, as visible in Appendix 2, possibly corresponding to a filler added by Palaeolithic populations as referenced in numerous French Palaeolithic caves (Clottes et al., 1990a). The manganese oxide presents an acicular structure as discernible in Figure 9.B. SEM-EDS analysed performed on the manganese needles' structures revealed relatively high-level of potassium and traces of barium, see Figure 9.A. These seem to point out the presence of cryptomelane, (K, Ba)Mn_8O_{16}·xH_2O, the only manganese oxide with high content of potassium, having an acicular structure, and with possible traces of barium. The XRD experiments did not allow to confirm the presence of cryptomelane but only revealed the presence of an amorphous phase. However, for a mineral to be spotted with the XRD, it has to represent more than 3% of the total sample analysed. As observed with the SEM, the manganese oxide phase is very small and was most probably not detected with the XRD. TEM analyses of the sample should permit to provide a clear identification of the manganese oxide. If to be confirmed, the presence of cryptomelane, a common natural manganese oxide, proves that the pigment used by the Palaeolithic was not heated or at temperatures lower than 400 °C. Indeed, at higher temperatures the cryptomelane starts to alter and loses its tunnel-shape structure and turn into another manganese oxide, known as bixbyite, Mn_2O_3 (Chalmin et al., 2004).

The three black paintings including bone black, GdE 13, E6 and E8, also contain clay that might have been used as a filler or an extender. The traces element identified with the SEM-EDS analysis tend to prove that those clays are of natural detritic origin. Palaeolithic might have added the clay to obtain a more malleable substance, easier to apply on the walls' surface, without changing significantly the black hue (Clottes et al., 1990a, 1990b). However, the clay might be just a secondary deposit due to water leaking on the walls' surface. Analyses of the clay found inside the cave, should permit to determine if those clays should be considered as parts of pigment's manufacture or as secondary deposits over existing bone black drawings.

Sample GdE 13 slightly differs from the other two samples containing bone black. While these last two also presents charcoal particles, GdE 13 only contains bone black mixed with siliceous marine fossils, as illustrated in Figures 9.C and 9.D. The presence of these materials seems to point out the use of clays of distinct origins, and therefore, of different painting pots. As detailed in Table 3, it is also confirmed by the dimensions of bone shards observed. Indeed,

GdE 13 exhibits larger bone shards than the two other samples having similar bone shards' dimensions.

Figures made with charcoal do not exhibit any traces of any filler. The only samples with traces of clays and other compounds correspond to the only two samples presenting both red and black particles. Therefore, it is here considered that the traces of clay and other traces are to be attributed to the red painting and not the black drawings. It seems that for all charcoal representations, the coloured material was directly applied on the wall without any anthropic action to modify its mechanical and aesthetical properties. Consequently, they are all to be considered as drawings and not paintings.

All charcoal's samples do not present similar charcoal's particles' size and aspect. Indeed, two major groups, A and B, can be distinguished by the size of the charcoal's particles and their aspect. The group A, including GdE A, E1 and E12, corresponds to charcoal's sample of large dimensions (average length higher than 15 μm), it has a lamellar aspect, which can make it look like graphite in some samples as depicted in Figure 9.E. The group B, containing E4, E6 and E8, exhibits smaller charcoal particles with no special structure's features, see Appendix 2. Due to those differences, it is thought that at least two distinct charcoals were used to perform the black drawings of Escoural.

To put it in a nutshell, although the vast majority of the black representations of Escoural corresponds to charcoal drawings, the palette is rather broad with the use of manganese oxide, bone black and distinct charcoals. The black paintings can be divide into three main groups: the paintings made of either manganese (GdE 7) or bone black pigments (GdE 13), the charcoal drawings performed with charcoals (GdE A and E12) and the paintings that might have been reused as charcoal drawings (E1, E4, E6 and E8). Among this last groups, two subgroups should be differentiated: the reuse of black painting (E 6 and E8) and the reuse of red ones (E1 and E4). These wide variety of the representations leads to conclude that numerous distinct painting pots were used. Among the black representations, three distinct painting pots can be distinguished: the manganese oxide (GdE 7), the bone black with large shards (GdE 13) and the bone black with small shards (E6 and E8); and two different kind of charcoal drawings: one leaving large charcoal particles (GdE A, E1 and E12) and one leaving smaller ones (E4, E6 and E8).

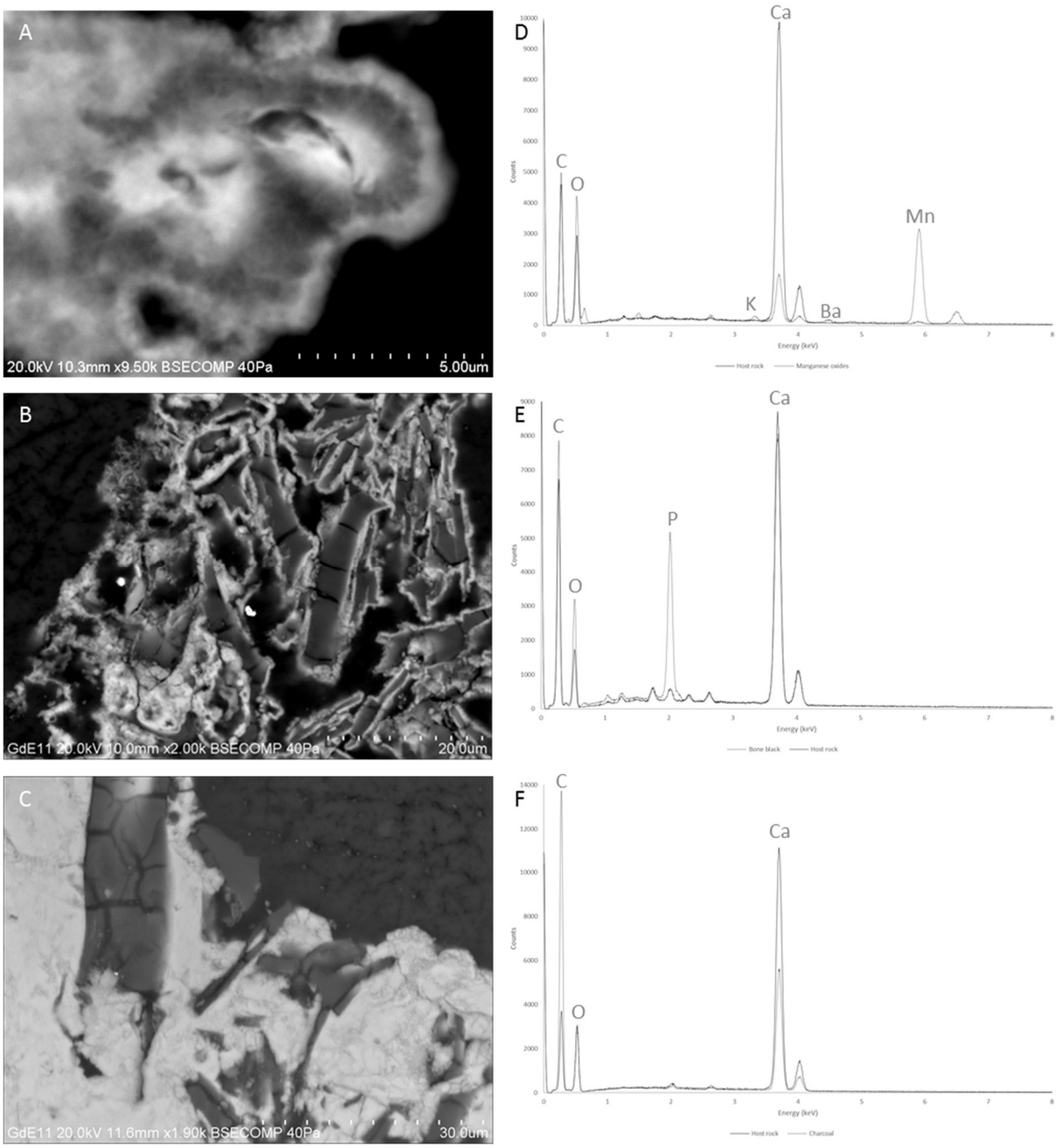

Figure 9: SEM-EDS observations and analyses of black pigments' cross-sections. A: SEM observation of the acicular structure of the manganese oxide pigment; B: SEM observation of the bone black structure. Calcium phosphate appears in white, carbonaceous material in grey and barium sulphate in white; C: SEM observation of the charcoal particles of group A (medium grey) embedded in calcium carbonate substrate (white). D: SEM-EDS spectrum of the manganese oxide black pigment; E: SEM- EDS spectra of bone black; F: SEM-EDS spectrum of the charcoal particles.

Table 4 sums up the three different kind of black pigments identified: bone black, manganese oxide and charcoal. Since among these three main groups, some clear distinct features were identified, the groups were divided into sub-groups indicating possible different preparation of

the pigments. For further details of the black pigments characteristic behaviours, the reader is referred to Appendix 2.

Table 4: The different black pigments identified in the cave of Escoural.

SAMPLE	LOCATION	FIGURE	DESCRIPTION	PIGMENTS	
				Group	Sub-group
GDE 7	Gallery 2	61	Non identifiable vestige between ochre lines	Mn oxide	/
GDE 13	Gallery 1	44	Vestige of a right horse head	Bone black	Large shards
GDE A	Room 1	26	Right hybride head	Charcoal	Large particles
E1	Gallery 1	30	Lower left horseback legs	Charcoal	Small particles
				Hematite	Ti-oxide
E4	Gallery 2	59	Right horse head	Charcoal	Small particles
				Hematite	Ti-oxide
E6	Room 1	19	Left horse back legs	Charcoal	Mixed with bone black
				Bone black	Small shards
E8	Room 1	22	Geometric symbols	Charcoal	Mixed with bone black
				Bone black	Small shards
E12	Gallery 6	66	Geometric symbols	Charcoal	Large particles

ii. Red pigments

As it is previously detailed for black pigments, the different analysis performed on the red pigments provided complementary information allowing to understand their composition.

Infrared and Raman spectra of the red pigments highlighted the presence of traces of clay, hematite and gypsum in some samples over a calcite substrate overwhelming most of the other components' signal. Weak signals of hematite were spotted with Raman on most of the samples containing red pigments. Appendix 3 sums up the various bands spotted and compounds identified with infrared and Raman analyses. Due to the low signal of the pigment, infrared and

Raman were not sufficient to characterize and distinguish the different red pictorial materials. Therefore, further analyses were carried out with SEM-EDS and XRD.

XRD analyses permitted to confirm the results obtained with infrared and Raman, assessing the presence of calcite and hematite for all the red samples analysed. Several issues were encountered with the micro-XRD analyses: orientation issues, and detection limit of the mineral phases. Those two issues led to poor quality diffractograms from which only few pieces of information could be collected. Due to mineral's orientation issue, the spectra collected presented a strong dissymmetry with the large increase of particular orientation. The detection limit of the mineral phases was the most problematic issue since most pigments analysed here are minor phases of very low relative quantity when compared to the calcite. It resulted in the low signal of the pictorial material making the identification of the crystalline phases it contained almost the impossible.

SEM observations coupled with EDS analyses permitted to distinguish five distinct types of pigments among the eight analysed. The various groups may be the results of distinct manufacturing process of the pigments, though it could for some of them also be due to distinct alteration state. Further discussion on the influence of the degradation of the artworks on the composition of the pictorial layer will be done after presenting the five kinds of pigments identified.

Among the red representations of the cave of Escoural, two distinct kinds of artworks must be distinguished: paintings made up of manufactured pigments and a possible drawing performed with a natural ochre crayon. The labels given to the five different preparations identified are referring to the specificities which permitted to distinguish them, they are four paintings: potassic feldspar with biotite, gypsum with potassic feldspar and biotite, highly heterogeneous mixture of numerous phases containing marine fossils, and a preparation of talc, albite, calcium phosphate and hematite; one sample presented a pigment's composition which could be of natural origin with no anthropic manufacturing and should therefore be referred to as part of a drawing.

Different elements allowed to define distinct groups of red pigments: the iron mineral identified thanks to their colour and XRD patterns, the size of these particles and the other mineral phases with which the iron minerals were found to be associated with.

The only sample considered as a pigment from a red drawing (E5) presented a very thin pictorial layer with tiny iron particles in a thin layer (4 to 5 μm) of Si-Al clay. The scarcity, as visible in Figure 10.A, and the size of the particles, smaller than 15 μm, Figure 10.F, support the idea that the representation 72 corresponds to a drawing performed with a natural ochre. Indeed, such a size of the iron particles could not be obtained by grinding hematite, therefore the iron particles found in this sample are considered to be from natural origin.

Among the other groups of red pigments, the biotite (GdE 11 and GdE 12) and Ti-oxides (GdE B and E2) subgroups might correspond to two natural ochres, though the presence of biotite and potassium feldspar could probably indicate the existence of two distinct manufacturing processes. Indeed, the presence of potassium feldspar and biotite has been considered as an evidence of manufacturing of Palaeolithic pigments by adding them to coloured material such as ochre as fillers. Naturally, these can also be found in clay without any anthropic actions. In non-anthropic mixed ochres, the minerals such as biotite and potassium feldspar are usually of small size (less than 3 μm), while anthropic admixtures are usually of higher dimensions, between 10 to 50 μm, with possibly higher sizes if the minerals were not grinded (Clottes et al., 1990a).

Considering the size of the mineral parts, the two sub-groups can be further differentiated. Indeed, the Ti-oxides sub-group presents mineral phases of micrometric size, while the biotites of the biotite sub-group have sizes ranging from 10 to 100 μm, see Figures 10.G and 10.H. Therefore, the first group should be considered as natural ochre, while the second one corresponds to a manufactured mixture. This trend is confirmed by the size of the iron particles. Indeed, the Ti-oxides subgroup has iron particles of small size, attributable to natural ochre formation, while the biotite subgroup has iron oxide which sizes range from 0.9 to 50 μm. It is thought that Palaeolithic might have added micrometric hematite to strengthen the red of their pigment.

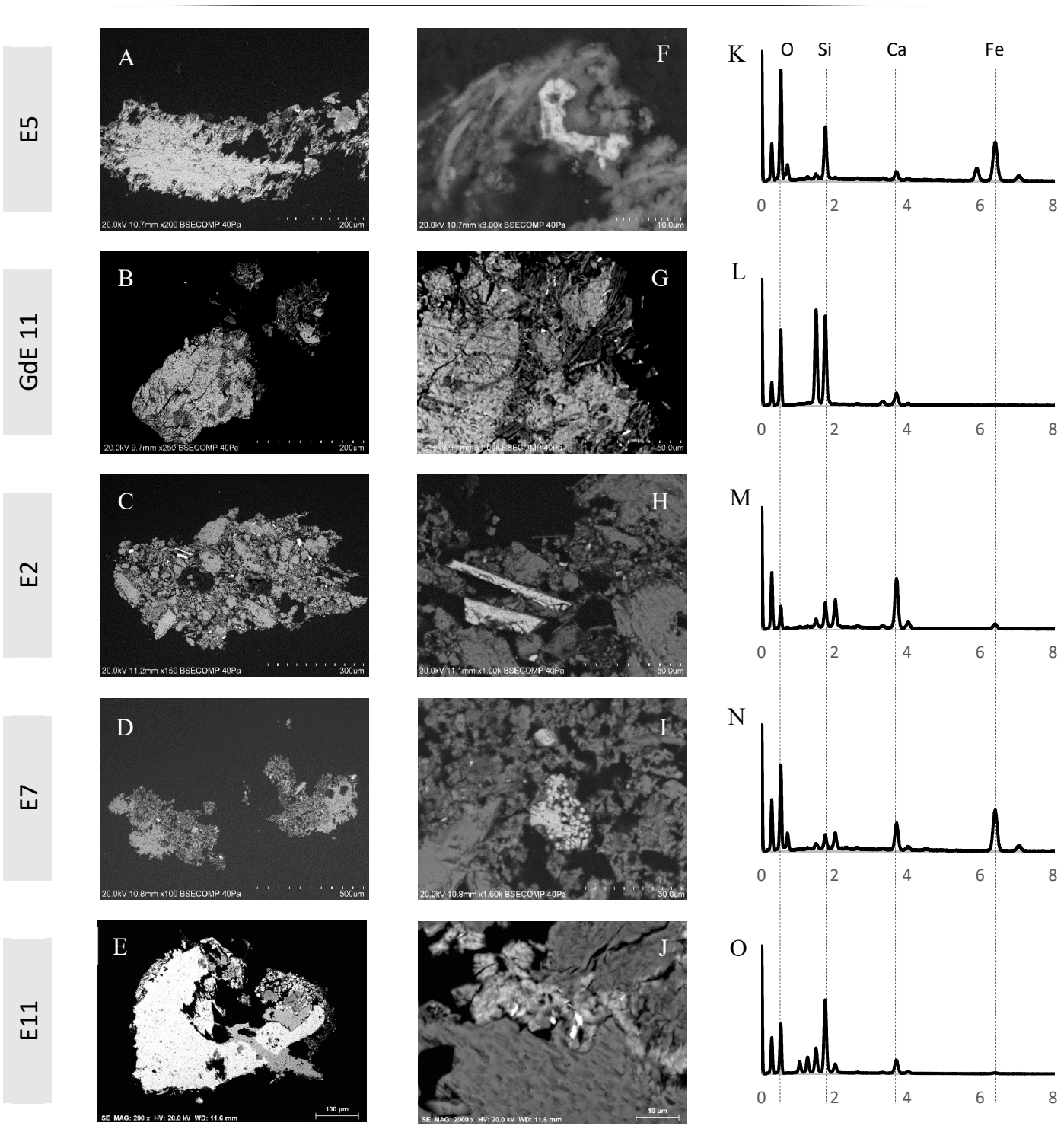

Figure 10: SEM-EDS observations and analyses of red pigments. A-E: General SEM observations of the samples. F-J: Observations of the iron-rich particles found in the different samples. The iron particles are in white, clay and biotite in grey, the calcite substrate is in greyish white. K-O: SEM-EDS spectra of the clays in which the iron-rich particles were found. The spectra show the counts (arbitrary unit) in function of the energy in keV. The energies are shown between 0 and 8 keV because no peak was present above 8 keV. The four elements indicated help to understand the diversity of the red samples.

One other subgroup containing hematite can be identified as an anthropic mixture. Only one sample was attributed to a mixture of hematite, gypsum and feldspar with some scarce traces of apatite. Analyses with SEM-EDS clearly identified the presence of gypsum and feldspar, and detected traces of calcium phosphate, as seen in Figure 10.N. The apatite was then identified thanks to XRD analysis. Such traces of apatite have already been registered in other cases. They were attributed to the preparation of the pigments with bone tools (Clot et al., 1995; Clottes et al., 1990a; Garate et al., 2004), assessing the existence of a manufacturing process of the materials used to perform cave art. This coloured material's processing is confirmed by the presence of gypsum which is usually considered as an extender when detected in prehistoric pigments' preparations (Lorblanchet, 2010; Salomon, 2009).

However, some differences exist between the two samples. Although they both correspond to ochre, the sample E11 presents a very particular structure. Indeed, the pictorial layer containing the iron particles is very thin (around 2 μm) and corresponds to iron particles embedded in a calcium phosphate matrix surrounded by two different clays one of the albite family, and one close to talc, as depicted in Figure 10. The Palaeolithic could have used some wet and malleable part of the wall to perform a kind of coloured paste they then applied on the wall's surface (Lorblanchet, 2010) without preparing the surface, therefore leaving the clay layer on which the pictorial layer lies. A possible explanation of the talc could be a later appropriation of the drawing or, as the talc and clay connected to it seem to cover it, an attempt to remove completely the drawing. Further investigations should provide more understanding of the figure 22 and its composition, allowing to confirm or not the previous hypothesis.

Although the sample E11 presents some major differences with the sample E7, both present traces of apatite and therefore are being considered to be part of the same manufacturing group. The sample E 7 might have suffered further alterations than the sample E 11 explaining the differences between the two samples.

Finally, one last group of red pigments was identified and corresponded to the sample E13. Contrary to the other groups, this last one did not contain hematite but lepidocrocite. The presence of this iron oxide-hydroxide FeO(OH) is confirmed by the hue of the sample, more orange than the other samples containing hematite. The lepidocrocite was detected thanks to XRD anaylisis of sample E13.

Table 5 sums up the different kind of red pigments identified. Since among these main groups, some clear distinct features were identified, the groups were divided into sub-groups indicating possible different preparations of the pigments. For further details of the red pigments characteristic behaviours, the reader is referred to Appendix 3.

Table 5: The distinct red preparations identified in Escoural

SAMPLE	LOCATION	FIGURE	DESCRIPTION	PIGMENTS	
				Group	Sub-group
GDE 11	Gallery 1	29	Geometric	Hematite	Ti-oxides
GDE 12	Gallery 1	36	Geometric	Hematite	Ti-oxides
GDE B	Room 1	23	Geometric	Hematite	Biotite
E2	Gallery 1	30	Red trace on black left horse	Hematite	Biotite
E5	Gallery 11	72	Right horse head	Hematite	Drawing
E7	Room 1	Next 22	Non identifiable	Hematite	Apatite
E11	Room 1	64	Geometric	Hematite	Apatite
E13	Gallery 6	New	Right ox head	Lepidocrocite	Drawing

D. Conclusion for the parietal art's corpus

Although the present work did not provide a full understanding of the pigments used by the Palaeolithic in Escoural, it proved that the cave presents more complexities than what was thought until now. Indeed, it was thought that all the figures had been registered, that their composition should be of similar ochres for the red or charcoal for the black. The present thesis highlighted the presence of figures never recorded before, clarified the interpretation of some recorded but not understood and clearly demonstrated the use of numerous distinct pigment's preparation inside the cave of Escoural.

The investigations carried out permitted to revise the corpus of the parietal art of Escoural Cave, Tables 6.A and 6.B. Figures that were not recorded or confused with other representations in previous studies were identified thanks to the various imaging techniques used.

Despite the fact that their discoveries prove that much still has to be performed on the site to ensure its understanding, they provide new insights on the parietal art corpus of the cave. Indeed, the belgo-lusitanian team recorded 27 paintings inside of Escoural. Adding 35 figures to this corpus considerably changes its distribution and the trend it presents. It is especially true in the present case, since the figures added to the corpus mostly correspond to horses' heads. It considerably reduces the marginality of the cave in the thematic of the representations when compared to other caves. Indeed, as described by Pigeaud (Pigeaud, 2002), until this work, archaeologists considered that most paintings inside the cave correspond to geometric figures. Their amount - 37 % - in the cave of Escoural was exceptional compared to the number of figurative representations, and tend to be used to present Escoural as a "marginal" cave of Western Europe cave art phenomenon.

With the present study, 21 horses and 6 bovides are added to Escoural's cave art. It considerably changes the proportion between the distinct categories of paintings. As for most Western European cave art, horses seem to be the predominant theme of the representations found in Escoural. Therefore, the cave fully integrates this phenomenon in the thematic of the representations and could be compared to other sites in Spain and France. Though oxen figures have been found in other caves such as Chauvet (Ariège, France) (Clottes and Arnold, 2001) and Lascaux (Dordogne, France) (Aujoulat, 2004) , the discovery of 6 of them inside Escoural is crucial in the further interpretation of its corpus. Compared to the 7.4% of the Palaeolithic representations figuring oxen in French caves discovered in 1995, the 9.6 % of the oxen figures of Escoural is relatively high (Sauvet and Wlodarczyk, 1995). The ratio between the horses and the secondary animal that constitutes ox reminds what can be found in other caves in France. Some of them host numerous representations of a same animal with some few representations of another species. It is for example the case in Rouffignac (Dordogne, France) with numerous mammoths and few caprine, or Font-de-Gaume (Dordogne, France) with bisons and some rare lions. The present revision of the corpus mainly underlines the importance of the horse and

the ox for the populations who occupied the site. It also links more the thematic of Escoural Cave to what can be found in Upper Palaeolithic caves of the French-Cantabrian region.

Table 6: Revision of the parietal art corpus of Escoural Cave.

6.A: The corpus of Escoural Cave's paintings and drawings as recorded by M. Lejeune

	Animals					*Geometric*	*Unknown*	*Total*
		Horse	Bovide	Unknown	Hybrid			
Black	9	4	1	3	1	1	3	*13*
Red	2	2	0	0	0	6	2	*10*
Red and black	0	0	0	0	0	3	1	*4*
Total	*11*	*6*	*1*	*3*	*1*	*10*	*6*	*27*

6.B: The revised corpus of Escoural Cave's paintings and drawings

	Animals					*Geometric*	*Unknown*	*Total*
		Horse	Bovide	Unknown	Hybrid			
Black	32	23	3	5	1	2	4	*38*
Red	9	4	2	2	0	9	3	*21*
Red and black	0	0	0	0	0	3	0	*3*
Total	*41*	*27*	*7*	*7*	*1*	*14*	*7*	*62*

The sampling procedure that was performed allowed to study the spatial distribution of the black and red pigments inside the cave. The main results obtained from the performed analyses were that numerous distinct preparations were used to perform the artwork found in the cave. This large diversity tends to point out that numerous Palaeolithic performed the paintings/drawings over distinct occupation phases of the site.

As it can be seen in Appendix 8, it appears that the most remote galleries present the original pigment's preparation such as bone black and manganese oxides. The large part of the cave seems to have been used with no specific trend. The difficulty to understand the distinct phases of realisation would tend to reinforce the idea that the cave was visited numerous times by diverse individuals who performed various representations all over the walls of the cave.

Further analyses should be carried out to date the distinct figures, and especially the carbon based black drawings of Escoural's parietal art. Carbon dates obtained should then be

compared to the ones obtained with Uranium-Thorium from the dating of the calcite layers. Doing so would not only provide a clear context of the painting but it might also provide a better knowledge of the different areas detected in this study. Such dates would allow to understand if all the charcoal paintings were performed in a same period or not and if the bone black painting is “contemporary” to them. Thanks to the calcite dating, even inorganic paintings could be indirectly dated to better understand the Upper Palaeolithic occupations of the cave.

Similarly, provenance studies of the inorganic pigments both red and black would provide better insight of the communities who performed Escoural’s cave art. Such studies would allow to reposition Escoural inside the Upper Palaeolithic Iberian Peninsula. It might also help to understand the existence of parietal art in such a “marginal” location. The provenance studies should be performed with LA-ICP-MS to identify the traces. Naturally possible sources should also be sampled. It is important to note that an old iron mine lies nearby the cave of Escoural. Perhaps the Palaeolithic already knew this outcrop as a site where they could collect red coloured material. Due to the presence of distinct ochre in the representations of Escoural, distinct outcrops should be sampled to understand the different sources for raw pictorial material.

Part III Microbial populations of Escoural Cave

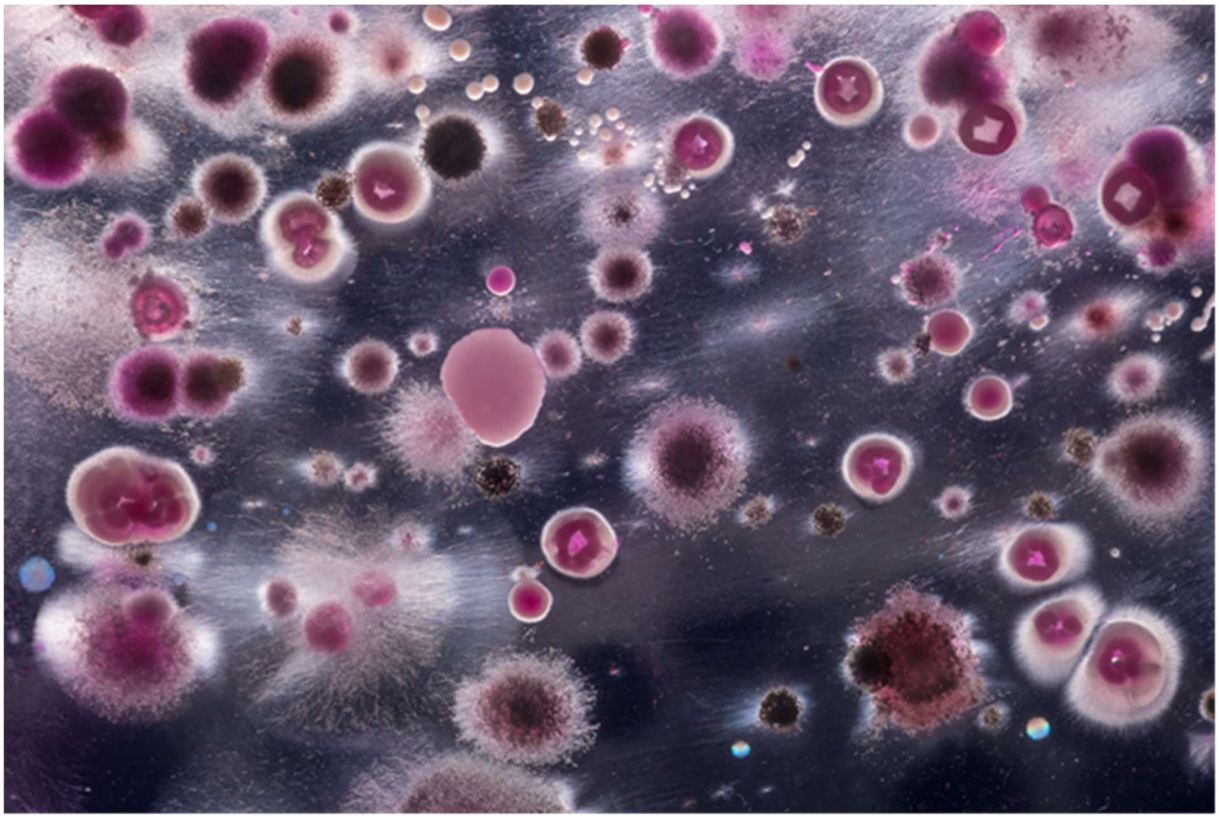

CRB culture's plate of microorganisms from Escoural Cave, © A.L. Campos

Among the main issues CH, and more precisely cave art, is facing are biocolonisation and biodegradation. Both lead, as described in Part I Chapter 2.A, to the alteration of the artworks through aesthetical and mechanical damages, and the development of microbial biofilms.

The cave of Escoural, as in other hypogean environments should host some particular biofilms, characteristic of underground cavities as it was explained in Part I Chapter 2. B. However, as it is the cave for some other caves such as Pech-Merle (Quercy, France), numerous biological contamination has been observed inside the cave of Escoural. Some of them are shown in Figure 11, larger examples of the biota and microbiota thriving in the cave are show in Appendix 9.

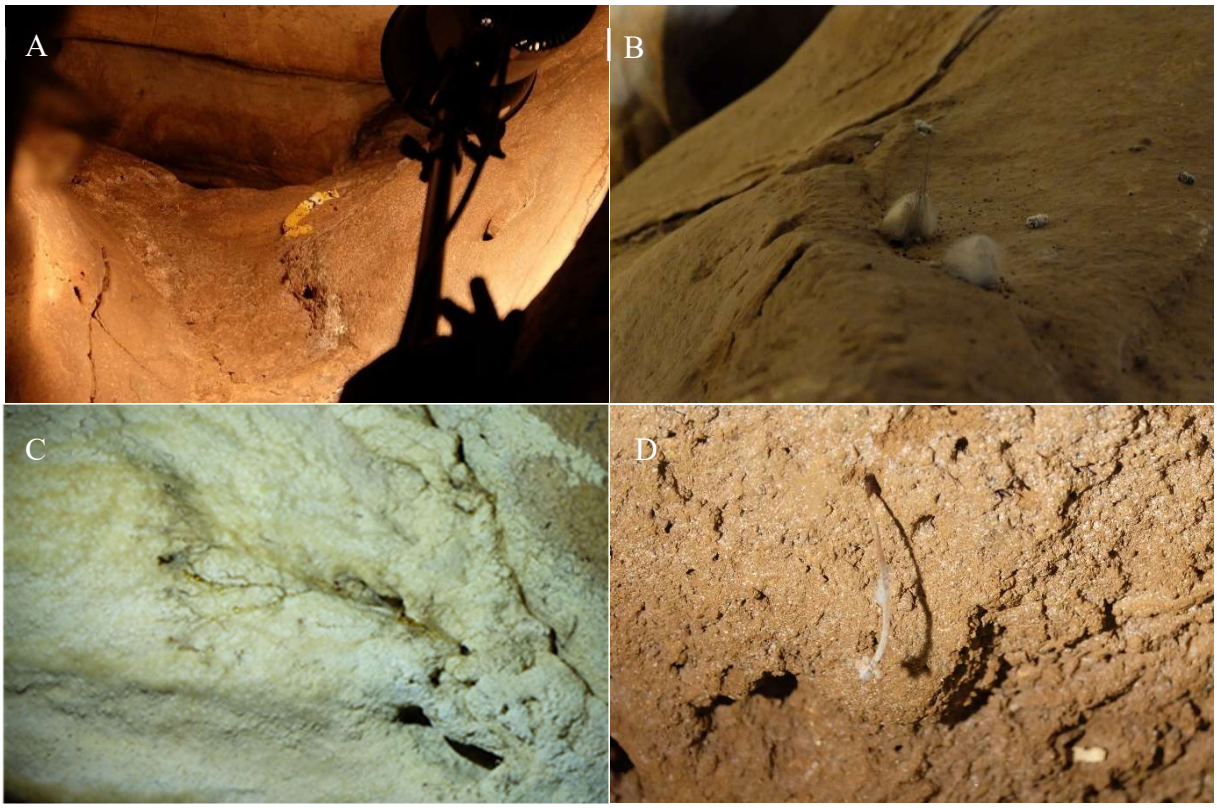

Figure 11: Observations of biological contamination inside the cave of Escoural. A: Yellow and white mushroom's growth spotted at two different periods in the gallery 1. B: Temporary fungal contamination largely spread on the diverse materials (wood, rock and soil) present in the cave during one of the visit of the cave. C: Roots penetrating inside the cave and releasing some yellow-orange fluid inside the cave. D: Plants' development inside the cave.

In studies focusing on the microbial contamination of CH's artefacts, the observation of the biodeteiogenic activity and the assessment of the microbial metabolic activity both provide crucial information to comprehend the extent of the contamination.

Chapter 1. Biocontamination's assessment

A. Methods

i. Sampling

Samples were collected with a sterile scalpel or swap by scratching the walls' surface. Each sample was collected with a blade cleaned with ethanol to ensure the non-contamination of the diverse samples and then stored in sterile tubes with sterile MRD. The different sampled areas covered a large diversity of speleothems and locations according to apparent biological contaminations or specific speleothems features thought to be of microbial origin, Appendix 10. The location of each sample was precisely documented through various photographs taken during the sampling procedure. The samples were then stored in the fridge before being analysed during the following week of the sampling procedure.

ii. Scanning electron microscopy

For assessing the microbial contamination of the samples and observing the microbiota thriving in the cavity, its extent and activity on the host-rock, microsamples were observed by Scanning Electron Microscopy (SEM).

Microsamples were coated with Au-Pd (Quorum Q150R ES) during 300 s, at 25 mA, and observed in a HITACHI S-3700N variable pressure scanning electron microscope (VP-SEM) with accelerating voltage of 9-10 kV.

iii. Raman

Raman spectrometry was used to assess the presence of microbial contamination in the different samples, and to detect some of their biodeteriogenic activity such as the production of oxalatic compounds. Measurements were performed without any preparation of the samples by Raman microspectrometry using a HORIBA Xplora Raman microscope (Tokyo,

Japan), with capacity increased to one hundred times, and a charge coupled device detector. Analysis were carried out with two different lasers of 638 and 785 nm with a 1-50% filter to avoid samples' destruction. The spectra were acquired in scanning mode after 5 to 10 scans with an acquisition of 10-20 s and spectral resolution of 5cm^{-1}.

iv. Culture dependent method

All biological samples, Appendix 10, (10 mg) were diluted in MRD and inoculated (100 µL) in selective media: nutrient agar (NA, HIMEDIA—peptic digest animals of 5 g/ L, beef extract 1.5 g/L, yeast extract 1.5 g/L, sodium chloride 5 g/L and agar 15 g/L) for bacteria isolation and yeast development, malt extract agar (MEA, HIMEDIA—malt extract 30 g/L, peptone mycologic 5 g/L and agar 15 g/L), Cooke's Rose Bengal (CRB, Microbiology—peptone 5 g/L, glucose 10 g/L, dipotassium hydrogen phosphate 1 g/L, magnesium sulphate 0.5 g/L, Rose Bengal 0.05 g/L, chloramphenicol 0.1 g/L and agar 15.5 g/L) to isolate filamentous fungi, and ASM1 (ASM-1, $NaNO_3$ 2000 µmol/L, $MgSO_4$ 200 µmol/L, $CaCl_2$ 200 µmol/L, K_2HPO_4 100 µmol/L, Na_2HPO_4 100 µmol/L, $FeCl_3$ 4 µmol/L, H_3BO_3 40 µmol/L, $MnCl_2$ 7 µmol/L, $ZnCl_2$ 3.2 µmol/L, $CoCl_2$ 0.08 µmol/L, $CuCl_2$ 0.0008 µmol/L, Na_2.EDTA 20 µmol/L) for algae and cyanobacteria developments.

The cultures were incubated at 30 °C for 24–48 h for the development of bacteria, and for 4–5 days at 28 °C for fungal growth. To detect slow microbial growing the inoculated Petri dishes stayed in incubation up more time (up to 30 days). Each different colony observed was picked up to obtain pure cultures, stored at 4 °C and periodically peaked to maintain the cultures active.

Macroscopic and microscopic features of each fungal isolates permitted to carry out the identification and characterisation of the different communities isolated in the laboratory. Microscopic observations of the fungal strains were performed on a biological microscope BA410E Motic coupled to a camera MoticamPRO 282B and the Motic Images Plus 2.0LM software, with tape and Lactophenol Blue solution (PanReac AppliChem).

The identification of the fungal strains isolated was performed at the genus level. It was performed on 5 days old cultures. The strains were all observed with the tape. If observations from the plate obtained with tape method did not permit a clear observation of the

reproductive structures and characteristic features of the genus, a new plate was performed picking the fungal strain with a loop.

v. Culture independent methods

Next generation sequencing (NGS)

Three samples, GdE 3, GdE 17 and GdE 16, were used to perform next generation sequencing. The procedure is presented in Appendix 11 together with a summary of the results they obtained.

NGS is a fairly recent technique, which started to be used in 2005. It relies on the possibility to amplify simultaneously a large amount of DNA to later identify the various sequences due to their unique layout from one species to another. It is of great interest since it allows to identify microbial species which could not be cultured in the laboratory, allowing to have a better insight of the microbial diversity thriving in a site.

Fluorescence in situ hybridisation (FISH)

Two samples, GdE 17'' and GdE 5''''', were used to perform some *ex situ* tests of the fluorescence *in situ* hybridisation. The method and results are subject of an article (August 2016). The general outlines are presented in Appendix 12.

B. Biocontamination and biodegradation

i. Biocontamination's assessment

The SEM observations carried out on the gold coated samples highlighted the existence of a large span of biological contaminations in the samples from inside the cavity. The samples observed ranged from no observed microbial contamination to very high and diverse biocontamination.

Sample GdE 4 presented no microbial traces at all, presenting a very clean rock's surface, Figure 12.A, evidencing the absence or the extremely low extent of microbial communities in this sample.

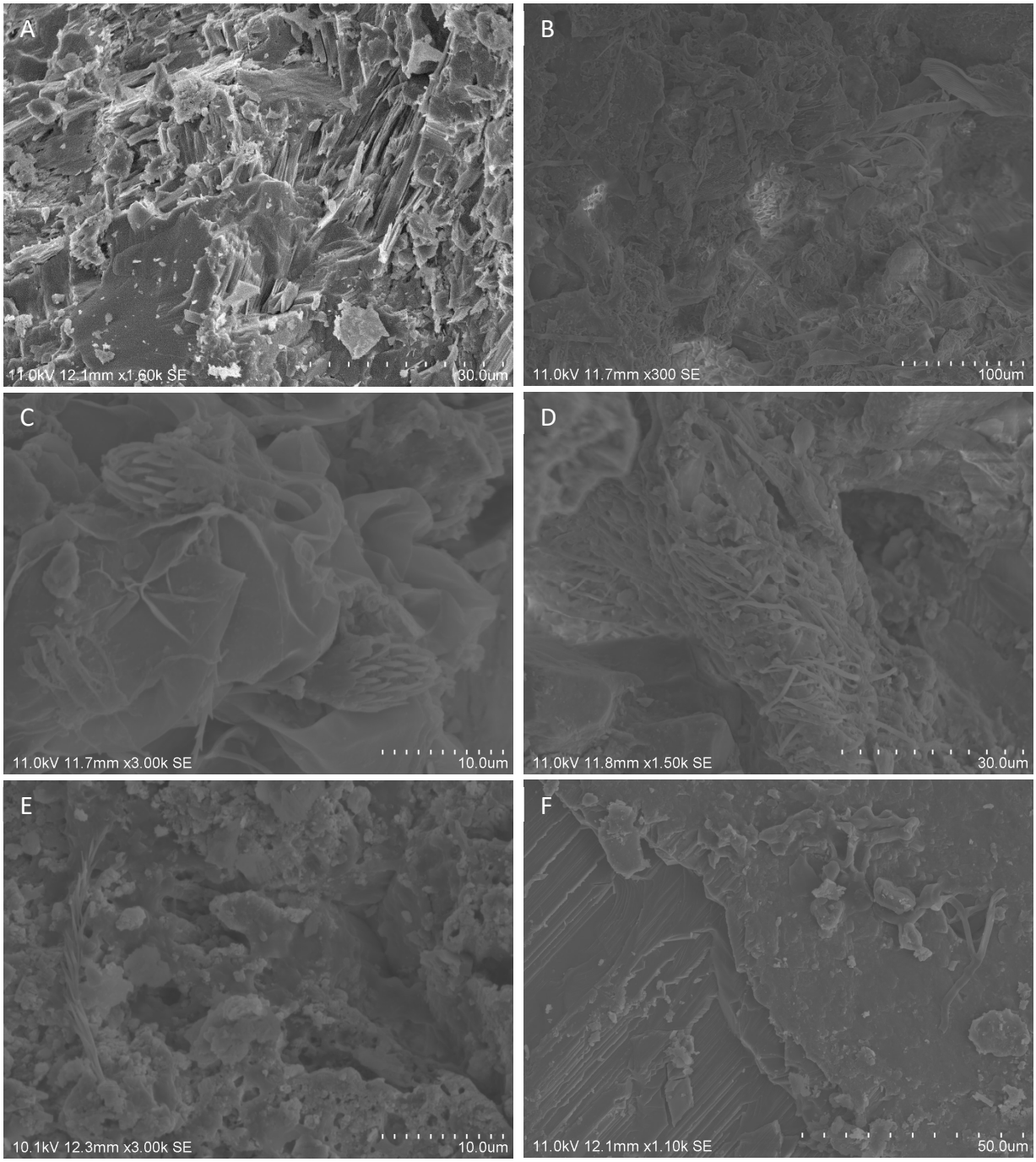

Figure 12: SEM observations to assess the microbial contamination of Escoural cave. A: Clean surface of GdE 4, B to D: High organic content and heterogeneity of GdE 3, E: Typical fungal structures and biofilm spotted on samples from inside the cave (GdE 17'''), F: Polymeric extracellular substance of GdE 23.

For most of the samples from inside the cave, SEM observations permitted to spot small fungal colonisation, through the detection of hyphal structures, Figure 12.E, but no bacterial communities. However, most of them also exhibited traces of microbial biofilms, with EPS' detection, Figure 12.F and Appendix 9.

Two sample from inside the cave, GdE 3 and GdE 5'''', and the only sample from outside the cave which was analysed, GdE 23, presented evidences of fungal contamination with hyphal structures, Figure 12.D and Appendix 9, most of the time embedded in EPS, Figure 12.F, and spores, Appendix 9. They also exhibited cells with reduced dimension were detected, which can be indicative of the presence of bacterial cells, Figure 1.H of Appendix 11.
The two previous samples from inside the cavity also presented high biological contaminations with micro-plants, Figure 12.B-C, and dead microfauna, possibly arthropods, Appendix 9. Both of these biological contaminations were used as nutrients' sources by the microbial populations thriving in the samples, explaining their high microbial contaminations compared to the other samples of Escoural Cave.

ii. Biodeteriogenic activity of the microbial populations of Escoural Cave

The SEM observations carried out on the gold coated samples did not evidence any biodeteriogenic activity of the microbial communities observed on the rock, Figure 13. None of the reported characteristic microbial destructive nor constructive fabrics in hypogean environment were spotted (Cañaveras et al., 2001).

The Raman spectra performed on the samples from inside the cave, pigments and host-rock with microbial contamination confirmed the SEM observations. None of them exhibited any trace of microbial induced alterations such as oxalates. Two of the most important oxalates in limestone's environments are whewellite ($Ca(C_2O_4).H_2O$). and the weddelite ($Ca(C_2O_4).2H_2O$). None of their characteristics bands (1489, 1462, 900 and 500 cm^{-1} for whewellite (Tournié et al., 2011), 1472, 900 and 500 cm^{-1} for weddelite (Edwards et al., 2000)). Similarly, the samples analysed with Raman spectroscopy did not exhibit any of the bands of carotenoidal compounds (1503, 1283, 1193, 1148, and 1002 cm^{-1}).

Assays to assess the biodeteriogenic activity of diverse microbial strains from inside the cave are currently in progress. Due to the large number of fungal strains isolated, only one strain of each most important genus: *Penicilium*, *Aspergillus*, *Mucor*, *Cladosporium* and one unknown were chosen to perform this study for the fungal strains. For the bacterial strain, the selection was performed according to the colour of the colonies. Three strains were selected to cover different colour: white translucent, yellow and orange. It should provide a better insight of the microbial threat that the Escoural Cave's artwork might be endangered by in the coming months or years. The results from this experiment are expected in September 2016 and will be included in a communication[5] and publication for the ECBMS 2016 congress.

C. Microbial population's diversity

The study of the microbial diversity with culture-dependent method relied on 32 samples from inside and outside of the cavity. Among 32 samples, 5 were collected outside of the cave to provide some insights of the microbial populations thriving just outside of the hypogean site. Appendix 10 locates the different samples used to carry out the microbial diversity of the cave and details the organisms isolated for each one of them.

In total, it permitted to isolate 62 fungal strains and 22 bacterial strains from the CRB, MEA and NA media. The ASM1 medium presented numerous microbial growths, though most of them were imputable to organism already isolated with another media and did not correspond to algae nor cyanobacteria. However, 3 green strains, most probably algae, were spotted in two distinct samples: one outside of the cave – GdE 23, with 3 strains – and one inside the cave – GdE 2, with 1 strain -. One other coloured strain was observed on the ASM1's culture of GdE 23, presenting a brown coloration. Due to their slow growth, approximately a month, and the large microbial contamination of the ASM1 plate hosting them, the isolation of these strains was still being performed at the time of the thesis' writing.

[5] Oral communication accepted. The congress will be held on Novermber 17-18th 2016.

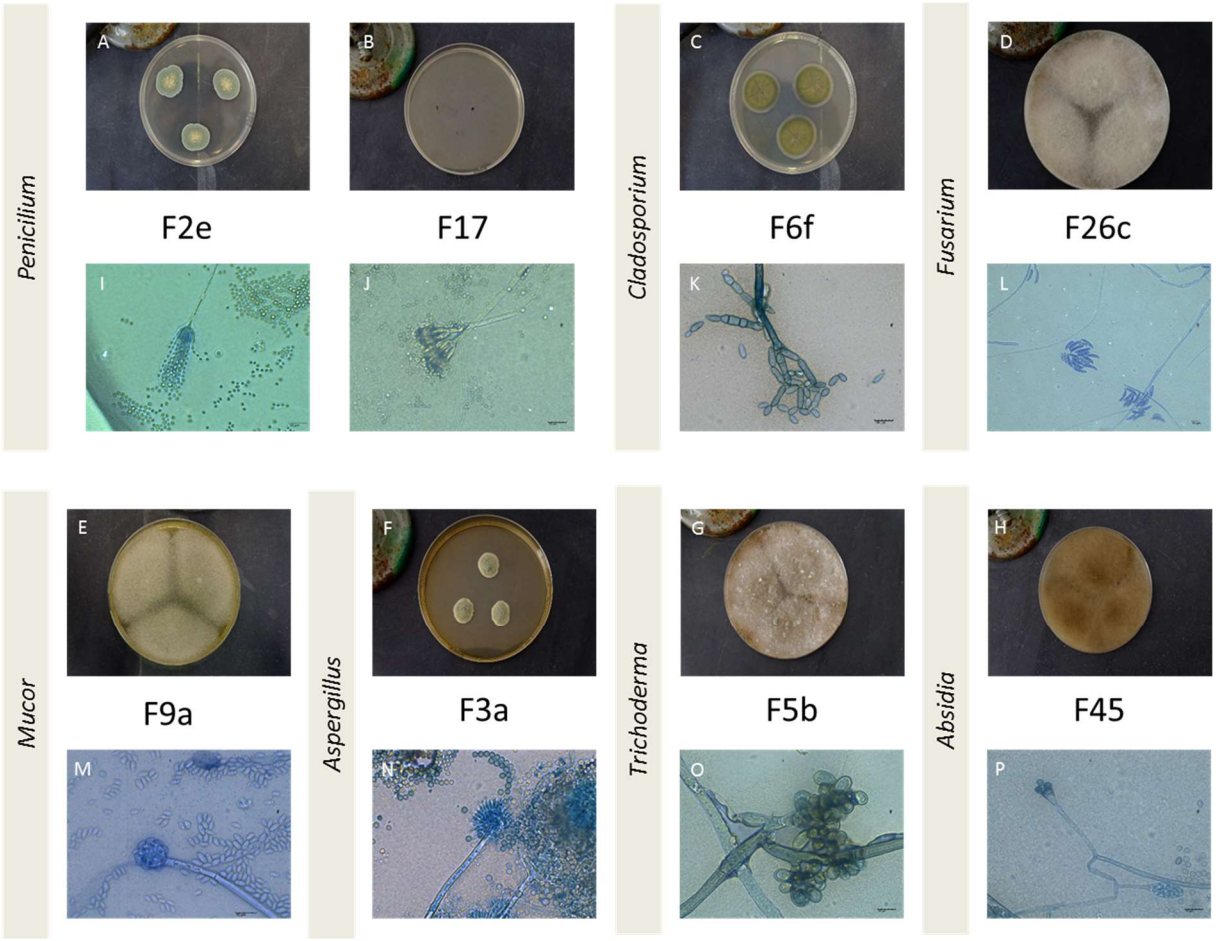

Figure 13: Diversity of the isolated fungal strains of the cavity. A -H: MEA cultures of distinct fungal trains. I-J: Two different microscopic features of the Penicilium genus. K-P: Microscopic observations of the fungal strains.

Figure 14 presents some of the characteristic features of the genus identified among the fungal strains isolated inside the natural hypogea. Strains of a same genus, but of distinct species present similar characteristic structure, though they also exhibit slight variations in their microscopic features, as exemplified with *Penicilium* in Figures 13.A-B, and 13.I-J.

Among the 62 isolated fungal strains, 13 – representing 7% of the fungal population – could not be identified during the time of the thesis. Those fungi might correspond to strains with no similarities with commonly encountered genus such as *Penicilium*, Figures 13.-B and13.I-J, *Aspergillus,* Figures 13.F and 13.N, *Cladosporium* , Figures 13.C and 13.K, *Mucor*, Figures 13.E and 13.M, *Trichoderma*, Figures 13.G and 13.O and *Fusarium*, Figures 13.D and 13.L. Distinction was made between the 7 unidentified species, for which no characteristic features were observed, and the 6 unknown ones, for which characteristics features were observed but could not be attributed to any specific genus. However, the unidentified species could possibly be

close to *Hypomeces*, while the unknown ones could probably be identified with access to known fungal strains isolated from cave's samples. Indeed, some of them presented some features that could resemble the ones of *Tolypocladium*, *Geomyces* or *Engyondotium* isolated in Lascaux (Bastian et al., 2010). Their study through DNA extraction and amplification should permit to characterize them.

Since most of the microorganisms cannot be isolated in laboratory's conditions, and that one sample could not provide a complete insight of the microbial diversity, it was decided to group the different samples according to the part of the cave there were collected from. Five distinct groups corresponding to five locations were created: the gallery 1, the gallery 2, the room 1, the outside of the cave and the inside of the cave. The last group (inside of the cave) corresponds to the sum of the three first groups (gallery 1, gallery 2 and room 1) and the sample GdE 19 that could not be included in any of these groups due to its location near the nowadays entrance of the cavity.

As only three samples were analysed with NGS, it was decided to group them and only provide a general microbial diversity of the cave. The results obtain from the NGS were then only compare to the results from the culture-dependent method from the total microbial population of the inside of the cavity.

Figure 14 and Appendix 10 present the microbial, fungal and bacterial populations determined thanks to the distinct methods and the various groups previously defined. Although numerous strains could not be isolated in the laboratory and therefore inducing a bias in the relative proportion of the strains, the results obtained from the different techniques and for the various groups tend to present similar results. Indeed, the bacterial communities are the most important, representing more than 92 %, Figure 14, of the microbial population. It was confirmed by NGS and FISH techniques. FISH showed the predominance of the bacteria in the biofilms of the two samples studied, only detecting prokaryotic cells, Appendix 12.

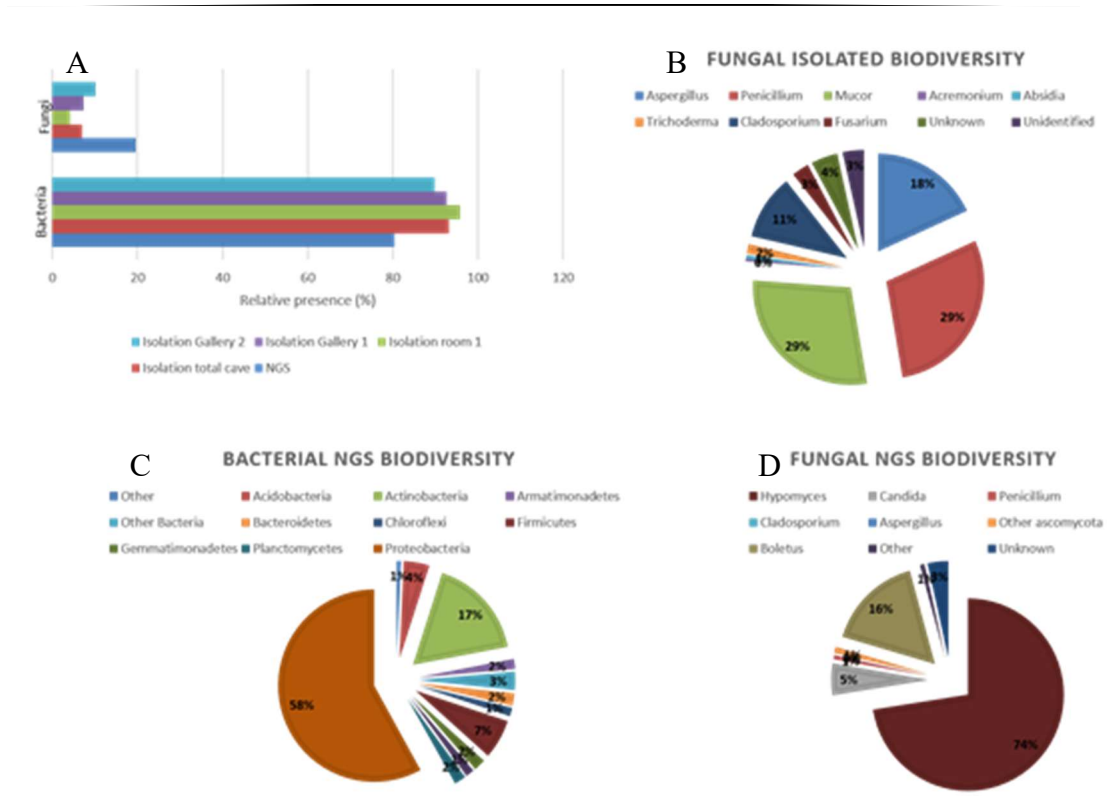

Figure 14: The microbial diversity of Escoural's cave. A: The proportion of fungal/bacterial strains according to the different techniques and locations inside the cave. B: The fungal biodiversity inside the whole cave according to the culture dependent technique. C: The bacterial diversity according to NGS. D: The fungal diversity according to NGS.

The NGS results point out that the cave hosts a very diverse microbial population with 2250 distinct bacterial strains (22 isolated), and 550 fungal strains (62 isolated). These results are coherent since it is usually than less than 1 % of the bacterial strains can be culture, but that more fungal strains can be cultured in laboratory. NGS has enabled to confirm the presence of some micro-organisms already identified by culture-dependent methods, but rather provided a vast contribution to the identification of several genera and species not previously identified in these environments, Appendix 11. It also evidenced the presence of numerous unknown species.

Figures 14.B and 14.D show that the fungal strains isolated and cultured in the laboratory do not correspond to the most spread ones inside the cave of Escoural. Indeed, the isolated fungal strains correspond to a minority of species almost no discernible in Figure 14.D.

The *Hypomeces* and *Boletus* correspond to the two major genus of fungi contaminating the cave. They are known to be usually found in deep soils. Therefore, their presence in the Escoural Cave is not a surprise.

None of the species known for their harmfulness toward cave art, such as *Bracteacoccus minor* (Lefèvre, 1974), *Fusarium solani* (Dupont et al., 2007), and *Ochroconis lascauxensis* (Pedro Maria Martin-Sanchez et al., 2012), have been reported inside Escoural Cave through isolation nor NGS. Fungal species isolated and identified in the cavity are known as common species and were already reported in other sites (Bastian et al., 2010; Pedro M. Martin-Sanchez et al., 2012).

Although the culture dependent method appears to be very limited, extremely biased when studying the microbial diversity of such a site, it allows to comprehend better some of the strains present and more importantly perform tests on these strains to understand biodegradation and consequently find some appropriate solutions to preserve the artworks contaminated.

In any case, assessing the microbial diversity of a site is not sufficient to comprehend its biocontamination. Indeed, microorganism can be present at various stage of growth, from dormant, then having no activity, to the exponential growth when the microbial activity is the most important. Naturally, microorganisms at different stage of growth do not have the same influence on the material it colonized, therefore it is necessary to analyse the microbial activity and viability.

Chapter 2. Viability assessment

Since it is essential to understand the activity of the microbiota thriving in biocolonised samples, numerous tests exist to assess the viability of the biocontamination (Li et al., 2007; Martín-Navarro et al., 2014; Mosmann, 1983). DNA quantification together with biomarkers analyses, such as desidrogenase enzymatic activity provide complementary information allowing the understanding of the biological and microbial contaminations (Martín-Navarro et al., 2014; Rinta-Kanto et al., 2005).

During this work, three of those microbial assessment's experiments were carried out together with DNA's quantification. The three methods to assess the microbial contamination viability, are the ergosterol's quantification, the MTT and Presto Blue analyses. They complete each other and permit to have a broad overview of the biocontamination in the samples collected. Indeed DNA's quantification provides an overview of the biological contamination of the samples, while MTT and Presto Blue rely on the respiration of the microorganisms, therefore can be applied to all species, and the investigation on ergosterol focuses on quantifying the sterol's content found in fungi, some cyanobacteria and green algae cell walls.

Although the ergosterol's extraction and quantification exists to assess the biocontamination of samples such as soils and modern building material, it has never been used to asses CH's microbial colonisation (de S Saad et al., 2003). The method had first to be optimized for CH's field. Therefore, it is detailed in a separate chapter, Part III Chapter 3 p. 90.

A. The methods

i. MTT Assay

MTT 3-(4,5-dimethylthiazol-2-yl)-2,5-diphenyltetrazolium bromide assay is a screening method implemented in 1983 (Mosmann, 1983) to measure cell viability. It relies on the reduction of tetrazolium salt by cells' respiration's process (through dehydrogenase enzyme activity) to purple formazan crystals (Boncler et al., 2014; Mosmann, 1983). The method is rather economic, though toxic for the cells since crystals must be solubilized into DMSO, therefore allowing only measure at a specific time.

The procedure followed the one developed by Rosado et al. (Rosado et al., 2013). Weighted microsamples were mixed with 300 µL of MTT, solution prepared with 1M Tris-HCl buffer (pH 7.5) and 0.5% 2-(p-iodophenyl)-3-(p-nitrophenyl)-5-phenyltetrazolium chloride, and incubated 4 hours at 37°C in the dark. The samples were then centrifuged during 10 minutes at 10 000 rpm and the supernatant phase was removed to leave only the purple crystals, which were

dissolved in 350 µL of DMSO/ethanol (1:1). Tubes were then mixed during 30 seconds with a Vortex mixer to ensure proper dissolution of the crystals. The solutions were then kept for 10 minutes in the dark at room temperature and centrifuged again during 10 minutes at 10 000 rpm. The amount of iodonitrotetrazolium formazan (INTF) released was measured spectrophotometrically (U-3010; Hitachi, Tokyo, Japan) with 200 µL of the supernatant in 96-wells plates at 570 nm.

ii. Presto blue

Presto Blue is a reagent based on the same process than the almar blue reaction. Cell's respiration reduces the blue resazurin into red resofurin (Mariscal et al., 2009). Since it is a quite new reagent, only few studies already used it. The few found in the literature focused on comparing its performance with other tests such as Almar Blue an MTT (Boncler et al., 2014 ; Martín-Navarro et al., 2014 ; Xu et al., 2015). Those few studies demonstrated that the Presto Blue have comparable results with other methods when used with absorbance but better detection limit and sensitivity when used with fluorescence (Martín-Navarro et al., 2014; Xu et al., 2015).

Presto Blue assays were carried out in 96-wells plates, each well containing 90 µL of a prepared solution to be tested and 10 µL of the Presto Blue reagent. Plates were then incubated at 37°C for a specific time, determined after kinetic studies of the reaction of Presto Blue with solutions of known number of microbial cells. The change of absorbance at 570 and 600 nm permitted to quantify the viable cells present in the prepared solutions.

Each experiment was carried out in triplicate, with blanks containing only physiological serum and Presto Blue but no cell and control containing physiological serum and cells only. The activity of the solutions evaluated was thence determine by subtracting the absorbance at 600 nm to the one at 570 nm. The result from the blank containing the Presto Blue was thence subtracted to all over result to ensure the normalisation of the results.

iii. DNA quantification

DNA Extraction from Natural Samples (adapted from (Rinta-Kanto et al., 2005)*)*

For DNA extraction small pieces of the samples collected in Escoural suspended in 100 µL lysis buffer (TE buffer: 1M Tris, 0.5M EDTA, pH=8). The cells were disrupted by lysozyme (15 µL of 2 mg/mL) with 20 mg of micro glass beads. The solutions were vortexed and incubated at 37°C for 40 minutes. 15 µL of α-Chymotrypsin solution (4 mg/mL, in 10% SDS) were added. Solutions were then incubated at 50°C for 60 minutes. 100 µL of a solution of Phenol/Chloroform/Isoamyl alcohol (25:24:1) freshly prepared were added. The tubes were agitated and centrifuged (1 min, 1000 rpm, 4°C). The supernatant (aqueous phase) was transferred to a different tube. A volume of Chloroform isoamyl alcohol (24:1) freshly prepared equal to the supernatant volume was added to it. The solution was once again mixed and centrifuged (1 min, 1000 rpm, 4°C). The aqueous phase was transferred again and 100% ethanol was added to it (twice the volume of the aqueous phase, around 200 µL) with 3M Sodium acetate (0.3 times the aqueous phase, approximately 30 µL). The solutions were stored in a freezer at -20 °C overnight to ensure the precipitation of DNA. The DNA was then shaped into pellets by centrifuging the samples at 11900g for 25 minutes. The supernatant contained in the tube was removed and the DNA pellets air-dried. The pellets were suspended in sterile buffer (1X TE buffer, pH=8). The solutions obtained were then stored in a freezer at -20°C for further analyses.

Quantification of DNA

The quantity of DNA present in the samples was quantified by photometric analysis. The measures were performed with the Thermo Scientific µDrop plate on the MultiskanGo apparatus (MultiskanGo, Thermoscientific). The DNA concentration was then calculated from the absorbance at 260 nm according to the following equation: DNA concentration (µg/ml) = Abs260 x 50 µg/mL. The purity of the DNA was estimated thanks to two ratios: Abs260/Abs280 and Abs260/Abs230. The first ratio corresponds to index indicating the presence of proteins and consequently of contaminants in the sample. The second one indicates the presence of organic compounds. All the results presented here are the mean of four measures performed in the same conditions. To accurately quantify DNA, the blank was made with the buffer used in the extraction step (TE buffer: 1M Tris, 0.5M EDTA, pH=8). Although estimated the purity of

the DNA is not presented here, since no particular care was taken to purify it, since it was only used to quantify the DNA and not to perform further analyses.

B. Real sample analyses

The microbial contamination of six samples from inside the Escoural Cave and the outside environment surrounding it were studied, Appendix 13 details their location and description. For each experiment, each sample was only analysed in duplicate due to the limitation induced by the samples' sizes.

Table 7 presents the average of the duplicates of each experiment, for all the samples analysed. For DNA quantification, the results presented correspond to the concentration of DNA quantified in a given amount of sample, while the PB and MTT results just present the mean of the absorbance. Each duplicate having the same weigh (20 mg), it is possible to directly compare them, without having to convert to any equivalent activity of pure cultures of any microbial strain.

A first important remark that has to be done, is that the different techniques provided coherent results between them. The following paragraphs discuss about the different pieces of information provided by the distinct techniques. The correlation and coherence of the different results are discussed in Part III Chapter 4 p.100.

The DNA's quantification provides a general estimation of the organic content containing DNA present in the samples analysed. Indeed, the procedure used to perform the DNA's quantification would extract DNA from all types of organisms. Therefore, micro-plants, dead organisms, would also be taken into account in the final DNA concentration. Although SEM observations showed the presence of such contaminations, the extracted DNA should be analysed with selective primers PCR amplification to distinguish the microbial DNA from all other biological contamination. Therefore, the DNA quantification corresponds to a biological contamination's index. As depicted in Figure 11, p. 75, numerous biological outbreaks were spotted inside the cave with the presence of mushrooms, plants' roots, and bats' faeces.

*Table 7: Microbial contamination assessment of Escoural's samples. Values presented in the table are the average of the duplicates. * The absorbance presented here were measured on diluted solutions and then multiplied by the factor of dilutions.*

Sample	*Location*	*DNA concentration (mg/g)*	A_{PB}	A_{MTT}
GdE 3	Room 1	211.5	1.8*	0.40*
GdE 4	Gallery 2	2.4	0	0
GdE 5''''	Gallery 2	2.5	0	0
GdE 8	Gallery 1	10,0	6.0*	0.50*
GdE 17	Room 1	2.8	0	0
GdE 17'''	Room 1	2.4	0	0
GdE 23	Outside	3.43	0.49	0.02

As seen in Table 7, the biological contamination of the samples from inside Escoural's cave is in general relatively low (less than 3 mg/g), as it is often reported in such environments (Culver and Pipan, 2009). The scarce amounts of nutrients and of light are usually seen as limiting factors for the development of biological contaminations. When spotted inside the cave these outbreaks such as micro-plants and bats' faeces presented, as expected, higher amount of DNA. According to the present results, the biological contaminations spotted inside the cave seem to be rather local and do not influence the general conditions of the cave. Further studies monitoring the biological and microbial contaminations of the cave should provide better insights on this point.

As expected from the calibration curves of MTT and PB, the MTT exhibited lower signal and therefore sensitivity than the PB. Such behaviour is expected since studies have shown that MTT's signal strongly depends on the metabolism of the microbial strain analysed with MTT (Berridge et al., 2005; Berridge and Tan, 1993). Indeed, according to those studies MTT is reduced by enzymes which activities rely on the reduced pyridine NADH. There conclusions lead them to question the use of MTT due to the high dependence of the cytoplasmic metabolism of different strains. These studies performed on pure microbial cultures, also prove that it is necessary to consider that various organisms provide distinct activity results. Since the

metabolic activity of a microbial strain changes during the distinct stages it goes through, it is important to consider that according to the stage it is a microbial colony will exhibit distinct activity.

Despite the difference of sensitivity of the two methods, the MTT and PB 's assays correlate each other well, confirming that only three samples hosted enough viable microbial cells to obtain a signal.

The results tend to show that the cave presents a low viable microbial contamination, confirming the results obtained with the ergosterol's quantification. Only locations with major biological contaminations present a viable microbial activity, confirming that nutrients' supply is severely limiting the microbial development. Beyond this first observation, it also implies that the microbial diversity observed in the cave, could easily develop if nutrients are provided inside the cave. Therefore, it is necessary to ensure that as low as possible nutrients' sources should be left in the cave.

As fungi are considered to be the most damageable microorganisms for CH, assessing the extent of their presence in the cave would provide a crucial knowledge of the possible fungal threat for the artworks. For reaching this goal, it is necessary to use a method that will not be influenced by the large bacterial populations. Ergosterol's extraction and quantification is one of them.

Chapter 3. Fungal biocontamination's assessment

A. The method

Quantification of fungal biomass in soil samples rest on the use of different methods, which fall into four main distinct categories (Joergensen and Wichern, 2008): microscopic techniques, selective respiration inhibition, quantification of cell membrane components (ergosterol assays), and quantification of cell wall components (glucosamine). Microscopic techniques present high variations, while selective respiration inhibition exhibits the inconvenient of being

arduous to implement for numerous samples. In this work, ergosterol assays were considered to be better suited to evaluate fungal contamination of the walls of Escoural Cave.

Ergosterol is the predominant sterol present in fungi and some higher plants. As demonstrated by Seitz et al., ergosterol assays by high-pressure liquid chromatography (HPLC) detect smaller amounts of fungal contamination than chitin's quantification or direct quantification of fungal growth through microscope observations (Seitz et al., 1979, 1977). Since then, the method has widely spread out, and further developments were carried out on various materials for distinct application. As sum up by Young and Games (Young and Games, 1993), they include a wide variety of materials: food contamination during the different steps of cereals processing from growth to milling (Cahagnier et al., 1983; Hamilton et al., 1988; Jambunathan et al., 1991; Miller et al., 1983; Naewbanij et al., 1986; Seitz et al., 1979; Seitz and Bechtel, 1985; Young et al., 1984; YOUNG and MILLER, 1985); in other plants such as broad beans (Al-Shabibi and Al-Mashikhi, 1987), malt (Mueller et al., 1991), tobacco (Bindler et al., 1988), grapes (Porep et al., 2014), and spruce needles (Osswald et al., 1986; Simmleit and Schulten, 1989); oil contamination (Abramson and Smith, 2003; Mohd As'wad et al., 2011; Muniroh et al., 2014); to study the decay of plant material (Newell et al., 1988; Nilsson et al., 1990); to study soil fungal biomass (Baldrian et al., 2013; Beni et al., 2014; Gong et al., 2001; Montgomery et al., 2000; Ruzicka et al., 2000; West et al., 1987) and ergosterol's content of some microbial species such as fungi (Newell et al., 1987), mushrooms (Huang et al., 1985), and yeast (Arnezeder et al., 1989; He et al., 2000); and to study fungal contamination of building materials (de S Saad et al., 2003; Görs et al., 2007; Hippelein and Rügamer, 2004).

Although numerous studies were carried out on the topic, the method used to perform such analyses rests on the initial procedure set up by Seitz (Seitz et al. 1977, 1979), based on C18 reversed phase HPLC separation and UV detection at 282 nm. Only a few studies tried to improve the sensitivity of the procedure by modifying some steps of the initial process, such as methanolic extraction under saponifying conditions (Griffiths et al., 1985; Schwadorf and Müller, 1988), the use of Si-60 normal-phase HPLC columns (Schwadorf and Müller, 1988; Zill et al., 1988), and photoionization detection with Gas chromatography separations (Krull et al., 1985; Varga et al., 2006).

Extraction and quantification of ergosterol were performed according to the procedure described by Young and adapted by de Saad (de S Saad et al., 2003; Young, 1995). To properly quantify the amount of the sterol contained in each sample, a calibration curve was established with standard solutions. The different standards solutions were prepared by the dilution of a mother solution of ergosterol (commercial solution, Sigma-Aldrich) in methanol for HPLC analysis (methanol 99,99% grade, Sigma-Aldrich). The extraction rate of different procedures was thence quantified to optimise the technique to the sample used in this study, Part III Chapter 3.B.

Each sample was weighed in sterile conditions to ensure the absence of contaminations of the aliquots used to perform the ergosterol assays. Aliquots were suspended in 2.0 mL of methanol (commercial solution, Sigma-Aldrich) and 0.5 mL of 2M aqueous sodium (prepared in the laboratory) in sterilised tubes. Tubes were sealed with kitchen film and a screw cap, and mixed for 20 seconds using a Vortex mixer. The tubes were then microwaved together in a domestic microwave oven, operating at a medium high power and heated 4 times for 10 seconds to avoid any explosion of the tubes. After 2 hours of cooling, samples came back to room temperature and liquid extraction of extraction of ergosterol began. Extraction of the sterol was performed three times by adding 2 mL of petroleum ether (60/80) inside the tubes and after agitation, the supernatant phase was collected and dried. After drying, around 5 hours at 70°C, the crust formed in the Eppendorf was dissolved in 200 µL of methanol for HPLC analysis. Detection and quantification thence were carried out through C18 reverse-phase high-performance chromatography with UV detection at 280 nm. Analyses were performed on a Hitachi Pump L-2100 ELITE LaChrom HPLC apparatus with a Purospher Star Merck (LiChro CART 250-4.6 RP-18 endcapped) column coupled with a Hitachi UV Detector 2400 ELITE LaChrom and the EZ ChromElite software.

B. Optimisation of the method

Although the method used to quantify ergosterol was based on the one developed by Saad and Young, it had to be optimised for Cultural Heritage field. Indeed, while Young focused on soils' fungal contamination, Saad studied building material's contamination (Frostegard and Baath,

1996; Young, 1995). Therefore, both did not have to face the crucial issue of Cultural Heritage's artefact: the impossibility to perform large sampling actions. The optimisation of the ergosterol's quantification rested on 3 different parts: checking the viability of the method to quantify it, the realisation of a calibration curve to quantify the extraction rate of the procedure, the miniaturisation of the sample, and the optimisation of the extraction rate.

i. Viability of the HPLC's detection of ergosterol

Since all the process of optimisation of the method relied on the quantification of ergosterol by HPLC, the first step consisted in checking the possibility to detect the sterol with HPLC. To do so, standards of pure ergosterol solutions prepared in the laboratory were injected in the HPLC. The UV detector at 280 nm permitted to detect and quantify the sterol thanks to the area of detection peak. Due to the absence of control over the temperature of the column, the retention time of ergosterol could vary between 16 and 19 min, for the methanol as a mobile phase. As expected, higher temperatures of the room in which the experiments were carried out lead to a lower retention time.

Due to the previous issue of room temperature's dependence, it was decided to inject a standard solution every 3 samples (every 1h30), since the temperature of the room could change quite a lot in a day.

ii. Calibration curve and viability of the method to quantify ergosterol

The calibration curve of the area of the HPLC's detection peak of ergosterol as a function of the sterol concentration injected was established thanks to ergosterol's standard solutions, which were prepared in the laboratory with a mother solution of 500 µg/mL of ergosterol diluted in methanol. Nine standard solutions of distinct concentration were prepared by dilution of the mother solutions. The concentrations covered by those standards ranged from 0.5 µg/mL to 50 µg/mL. The area of the HPLC's detection peak of ergosterol was calculated thanks to a manual detection of the peak with the EZChrom Elite software. Each measure was performed in triplicate. The mean, and standard deviation of the three measurements were used to build the calibration curve shown in Figure 15.

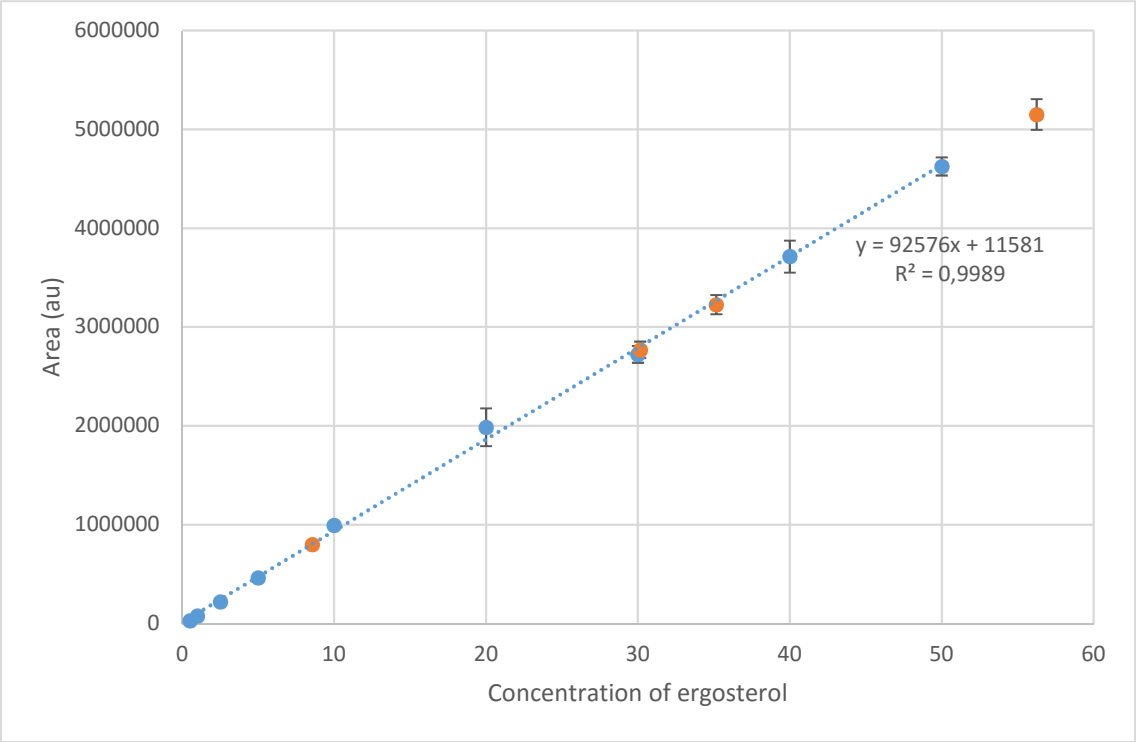

Figure 15: Calibration curve of the ergosterol's quantification through the HPLC-UV detector

Once the calibration curve was built, it was necessary to check the viability of the method developed by de Saad (de S Saad et al., 2003) to extract and quantify the sterol from real samples. The first step consisted in assessing the possibility to extract and quantify ergosterol from pure fungal cultures. Two different fungal strains were used one of *Aspergillus niger* and one of *Coriolus versicolor*. For both, two samples of different weight were realised to check the possibility to detect distinct quantities of fungal mass through the area of the HPLC's detection peak of ergosterol. Since this step was performed just to check the viability of the procedure developed in the literature, measures were only performed on a single sample. As seen in Figure 15, extraction of ergosterol was possible for both strains and gave comparable results for similar weight, Table 8.A. The concentration determined permitted to validate the range of the concentrations used in the calibration curve since in real samples, fungal strains would not be pure and their concentration would tend to be lower than in the case of pure fungal strains' analysis. It also confirmed that different fungal strains do not have the same content of ergosterol, Table 8.A.

Slight changes of the procedure written by de Saad et al. were experimented to see if they could improve the extraction of ergosterol from pure fungal cultures. Counting the original

procedure, four distinct extraction's process were compared with pure fungal cultures. Table 8.B presents the distinct procedures and the areas of the ergosterol's peak for each of them. Each procedure was performed in duplicate to assess the variability of the procedure of extraction with distinct amounts of pure fungal structure for each replicate. As seen on Table 8.B, the first results obtained pointed out that the procedure with nitrogen permitted to have a high extraction of ergosterol. Though the value obtained seems to be way too high when compared to the other values. It is possible that the flask used to perform the experiments was contaminated. Therefore, a new set of experiments was set up with new and clean flask.

The two procedures with ultrasonication steps presented lower ergosterol's area than the other two procedures. This could be due to the fact that the ultrasonication could lead to the alteration of some of the ergosterol molecules by breaking some of the weak chemical bounds of the molecule, resulting in the production of another molecule of a different retention time, and therefore not detected.

The two procedures involving nitrogen show a large variability of the ergosterol's area detection. This is mostly due to the fact that during those procedures, the collection of the crushed fungal structures is relatively arduous. Due to this variability, it was preferred to use the original procedure used by de Saad et al.

iii. Miniaturisation of the sample

Since the procedure developed by de Saad et al. permitted to extract ergosterol from pure fungal culture but was initially used to analyse bio-contamination of building materials, it was necessary to adapt it to the specificity of Cultural Heritage's material by minimising the amount of sample used to quantify the ergosterol, and therefore the fungal contamination of the walls of Escoural's cave.

Table 8: Optimisation of the ergosterol's extraction for Cultural Heritage samples. A: Variability of the ergosterol content in different fungal strains.B: Optimisation of the procedure according to the area of the ergosterol detection peak. C:

Miniaturisation of the samples through the optimisation of the extraction rate with different amounts of mortar and of ergosterol. D: Optimisation of the liquid-liquid extraction of ergosterol.

Table 8A: Variability of the ergosterol content in different fungal strains

Strain	*Weigh (mg)*	*Estimated concentration (µg/mL)*	*Massic concentration*
C. versicolor	34	8,55	5,03E-05
C. versicolor	102	35,16	6,89E-05
A. niger	195	30,15	3,09E-05
A. niger	314	56,25	3,58E-05

Table 8B: Optimisation of the procedure according to the area of the ergosterol detection peak

Procedure	*Fungal weight sampled*	*Nitrogen*	*Ultra-sonication*	*Estimated concentration (µg/mL)*
A1	4,5 mg	No	No	3,13
A2	8,2 mg	No	No	6,86
B1	4,5 mg	No	Yes	0,97
B2	8,1 mg	No	Yes	8,13
C1	4,5 mg	Yes	No	11,08
C2	8 mg	Yes	No	2,30
D1	4,5 mg	Yes	Yes	1,29
D2	8,5 mg	Yes	Yes	6,88

Table 8C: Miniaturisation of the samples through the optimisation of the extraction rate with different amounts of mortar and of ergosterol.

Sample	*Matrix*	*Matrix weight (mg)*	*Amount of ergosterol injected*	*Corrected extraction rate*
Mortar 1	Mortar	5,1	32 µL (125 µg/mL) – 4 g	70
Mortar 2	Mortar	10,0	32 µL (125 µg/mL) – 4 g	74
Mortar 3	Mortar	19,9	32 µL (125 µg/mL) – 4 g	83
Mortar 4	Mortar	10,1	8 µL (125 µg/mL) – 1 g	63
Mortar 5	Mortar	10,1	16 µL (125 µg/mL) – 2 g	67
Mortar 6	Mortar	10,0	24 µL (125 µg/mL) – 3 g	76
Rock	Rock	15	32 µL (125 µg/mL) – 4 g	83

Table 8D: Optimisation of the liquid-liquid extraction.

Solvent for the liquid-liquid extraction	*Matrix*	*Matrix weight (mg)*	*Amount of ergosterol injected*	*Extraction rate*
Petroleum ether (60/80)	Mortar	20	32 µL (125 µg/mL) – 4 g	80
Dichloromethane	Mortar	20	32 µL (125 µg/mL) – 4 g	66

The miniaturisation of the samples was performed thanks to the use of mock up samples consisting in sterilized mortar in which were injected different amounts of pure ergosterol. For this optimisation, the amount of ergosterol injected being different for some of the experiments, the parameter used to compare the different extraction was the calculated ergosterol's extraction rate. It determines the percentage of ergosterol injected in the mortar recovered thanks to the extraction procedure. To calculate it, it was necessary to determine the weight of ergosterol injected and the weight of ergosterol recovered. This was made possible thanks to the calibration curve which allowed the determination of the ergosterol's concentration of a solution and the knowledge of the volume of each of the solutions. Table 8.B presents the different experiments and the extraction rate of ergosterol for each one of them. All experiments were performed in triplicates.

Influence of the amount of mortar

To study the influence of the amount of mortar on the extraction rate, three different amount of mortars were used: 5, 10 and 20 mg, all with the same amount of sterol: 32 µL of a solution of 125 µg/mL of ergosterol (equivalent of 4 g of ergosterol).

Compared to what is found in literature, this extraction rate is in the average (de S Saad et al., 2003; Hippelein and Rügamer, 2004; Mille-Lindblom et al., 2004; Mueller et al., 1991; Porep et al., 2014; Schwadorf and Müller, 1988; Seitz et al., 1979, 1977, 1977).

The behaviour shows that the miniaturisation of the samples could result in a major decrease of the effectiveness of the procedure usually used. A possible explanation for this trend could rely on the decrease of the solubility of the ergosterol in the discarded methanol phase due to the mortar. In this case, as the amount of mortar increases, the solubility of the ergosterol in the methanol phase decreases and more are extracted thanks to ether petroleum (60/80). This explanation seems to make sense when compared with the influence of the amount of ergosterol on the extraction rate.

Influence of the amount of ergosterol

Similarly, the influence of the amount of ergosterol injected was analysed through the analysis of four different amounts (32 µL, 24 µL, 16 µL, and 8 µL of a solution of 125 µg/mL of ergosterol, corresponding respectively to 4, 3, 2 and 1 g of ergosterol) injected in a same amount of mortar (10 mg).

As presented in Table 8.C, the extraction rate improves significantly when the amount of ergosterol injected increases, reaching 83 % for 32 µL of the solution of ergosterol. This trend also tends to confirm that the miniaturisation of the samples to perform this quantification presents a major limit. As evoked earlier and as it will be detailed a bit later, the decrease of the extraction rate with the decrease of the ergosterol's amount injected could be due to a solubility of the ergosterol in methanol too close to the one in petroleum ether (60/80). In this case, few quantities of ergosterol would stay in the discarded methanol phase during the liquid-liquid extraction phase of the ergosterol's extraction.

Consequences on the miniaturisation of the samples

Both, the influence of the mortar and ergosterol's amount, lead to consider that although possible, it was necessary to minimise as much as possible the miniaturisation of the sample. Therefore, all samples were weighted to obtain 20 mg of samples or if it was not possible due to the size of the sample the closest weight to it allowing the experiments to be done in triplicates.

iv. Optimisation of the extraction rate

As evoked in the previous part, the extraction rate obtained using the procedure developed by de Saad et al. lead to an extraction rate of 85 %. Numerous articles mentioned lower or similar extraction rate with n-pentane or petroleum ether as solvents to perform the liquid-liquid extraction of ergosterol, such as Abramson and Smith with 65 to 70 % (Abramson and Smith, 2003), Bermingham with 85 % (Bermingham et al., 1995), Murinoh with 62% (Muniroh et al., 2014) and Ruzicka with 70 to 90 % (Ruzicka et al., 2000). Few publications indicate better extraction rates between 80 and 104 % with n-pentane (Görs et al., 2007; Grant and West,

1986; Hippelein and Rügamer, 2004; Montgomery et al., 2000). Attempting to improve the extraction rate, triplicates made of 20 mg of mortars with known amount of ergosterol injected in it were used to extract ergosterol using either petroleum ether or dichloromethane to perform the liquid-liquid extraction. The experiments were performed with dichloromethane due to the theoretical solubility of ergosterol in it, which is much higher than the one in ether petroleum and n-pentane. Since ergosterol has similar solubility in n-pentane and ether petroleum, it was decided for logistical issues to only perform the experiments with petroleum ether.

As presented in Table 8.D, extraction performed with the petroleum ether provided results than the one performed with the dichloromethane. Therefore, it was decided to perform the extraction of ergosterol from real samples with petroleum ether (60:80) as the solvent to perform the liquid-liquid extraction.

C. Real samples analyses

i. Extraction rate on rock

All the previous extraction rates were calculated with a substrate of mortar, though the real samples from the cave have a matrix slightly different: limestone. In order to improve the results obtained from the ergosterol's quantification as much as possible, the extraction rate was calculated with a sterile matrix limestone from the cave of Escoural. To do so, rock from outside the cave was collected, crushed, cleaned and sterilized to ensure to have no contamination from any microorganisms. Then samples of 20 mg of the sterilized rock were weight and 4 g of ergosterol was injected in them. The extraction of ergosterol was then performed following the optimal procedure of de Saad et al. (de S Saad et al., 2003). The experiments were performed in triplicate and results are presented in Table 8.C.

It appears that the extraction slightly improves compared to the one obtained with mortar. This could be explained by the partial dissolution in the petroleum ether (60/80) of some

compounds contained in the mortar used to perform the previous experiments. It would then lead to a reduction of the solubility of the ergosterol in this same phase and decrease slightly the final extraction rate. The previous results from the miniaturisation of the samples comfort the possible partial dissolution of compounds contained in mortar. To better understand the different trends observed, it would be necessary to identify all the distinct compounds detected by the HPLC-UV detector, through coupling those analyses with a mass spectrometer.

The calculated extraction rate on rock permitted to correct the different concentrations of ergosterol for the real samples. The correction, due to the non-total recovery of the ergosterol due to the extraction procedure, was performed after the determination of the concentration of ergostrol contained in the samples.

ii. Quantification of ergosterol of Escoural's sample

The quantification of the ergosterol was performed on seven samples of the site of Escoural, according to the procedure developed in Part III Chapter 3.B. Six (GdE 3, GdE 4, GdE 5''''', GdE 8, GdE 17 and GdE 17''') from inside the cave and one from outside the cave (GdE 23). Table 9 presents the different samples, their location in the cave, and the results of the ergosterol's quantification. Appendix 10 presents a map detailing the location of each of the sample used for the ergosterol's quantification. Each sample was carefully crushed in sterile conditions, homogenized and analysed in triplicates. All replicates were weighted and clearly identified during the whole duration of the analyses.

The results, presented in Table 9, show a relatively small concentration of ergosterol in most of the samples of Escoural. One (GdE 4) even did not present enough ergosterol to detect it with the HPLC procedure. Only three samples (GdE 3, GdE 8 and GdE 23) had concentrations higher than 2 mg/g. Those samples are all of different natures, confirming that ergosterol, and therefore fungi, could be found on every substrate.

Table 9: Quantification of ergosterol of Escoural's samples

Sample	*Location*	*Average ergosterol concentration (mg/g)*	*Standard deviation of the ergosterol concentration*
GdE 3	Room 1	18,6	18,41
GdE 4	Gallery 2	/	/
GdE 5’’’’’	Gallery 2	1,8	0,11
GdE 8	Gallery 1	4771,1	41,90
GdE 17	Room 1	1,7	0,24
GdE 17’’’	Room 1	1,1	0,69
GdE 23	Outside	4,9	0,40

The highest concentration of ergosterol was found in the sample GdE 8, located near bats' faeces. Due to high nutrients' content, it largely favours the fungal growth, explaining the high ergosterol content found in this sample.

Further discussions on the microbial and fungal contaminations of the cave according to those results are made in the following chapter.

Chapter 4. Escoural's microbial contamination

The four different techniques used to analyse the biological and microbial contamination of the cavity correlated well between each other. Only the DNA's quantification appeared to diverge from the other techniques, Figure16. As it does not assess the microbial contamination but the biological ones, taking into account other organisms, viable or not, it confirms the complementarity of these techniques and highlights that the high DNA's content does not imply a large viable microbial contamination, confirming the necessity to assess both biological and microbial content.

As it was evidenced by the SEM observations and the analyses of the microbial diversity, Escoural Cave exhibits a large diversity of the microbial populations thriving in it. According to the different techniques used to study the microbial diversity, the bacterial communities represented most of the microbial communities with minor fungal contaminations. Ergosterol's quantification confirmed these results by highlighting a rather low ergosterol's content.

There are three major issues when trying to quantify the fungal biomass through the quantification of the ergosterol's content: the possible contamination by micro-plants, the difference of the sterol's concentration from one species to another, as already seen in Table 9.A, and the alteration of it after the death of the organism which produced it.

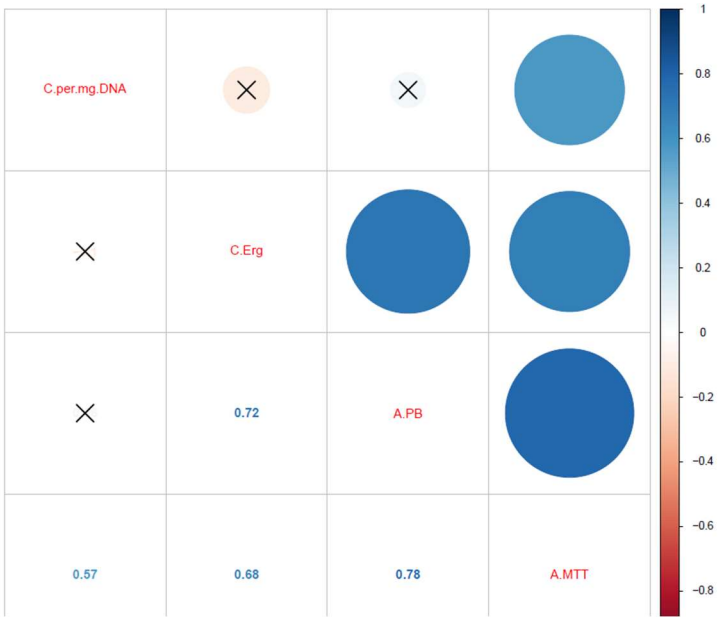

Figure 16: Correlation profile of the microbial contamination's data. Software: R. The figure represents the coefficient of the correlation matrix of the different techniques performed to assess the biological and microbial contaminations of Escoural Cave. The circles show a graphic representation of the value indicated in the lower part of the plot. A blue hue indicates a positive correlation, while a red one corresponds to a negative one. The non-significant correlation's coefficients are crossed out. The statistics were performed with the corrplot function of the R software with a 95% level for the significance test.

It is well known that some plants also produce sterol and could therefore contaminate the samples, making impossible to evaluate the fungal biomass present on the sample. During the sampling procedure, great care was made to avoid collection of samples contaminated by roots and plants which could have contaminated the sample with non-fungal ergosterol. But micro-plants, not visible bare-eyed, could also be present and falsify the quantification of the fungal biomass. SEM observations of a gold-coated aliquot of sample GdE 3 indicated the presence of micro-leaves and parts of micro-plants, see Figures 12.B and 12.C. Although, this sample was carefully crushed and homogenised, the quantification of the ergosterol content presented a high ergosterol content with a large variability which could be due to the presence of these micro-plants. Indeed, few papers focusing on the production of ergosterol by plants, pointed out the fact that different plants and different part of a same plant have distinct ergosterol's amount (Mueller et al., 1991). In any case, this sample should be removed from the study of

the quantification of the fungal biomass inside the cave since non-fungal ergosterol could falsify the results.

Another major aspect to have in mind when trying to estimate the fungal biomass present in a sample is that not all fungal strains produce and store the same amount of ergosterol (Bindler et al., 1988; Miller et al., 1983; Wallander et al., 1997; Zill et al., 1988). Indeed, two species with distinct metabolisms could produce two very distinct amount of ergosterol. In this case, the estimation of the fungal biomass has to be performed carefully since, for a similar amount of the two fungal strains, the biomass quantification of the two strains will provide two distinct results. It was confirmed in the present thesis, Table 8.A.

Another issue, which is often debated in ergosterol's literature, is its subsistence in the environment after the death of the organisms who produced it. Although, numerous studies highlighted that ergosterol is extremely sensitive to light and alter relatively fast (Ruzicka et al., 2000; Zhao et al., 2005), other tend to prove that it can subsist for some time after the death of the organism who produced it (Mille-Lindblom et al., 2004). In any case, for the present studies, even if ergosterol subsists for a long time after the death of the fungi, it indicates the existence of a fungal colonisation in the sample.

Having all of this in mind, it is possible to compare the ergosterol results with the SEM observations of the samples' biocontamination. As predicted from the few fungal structures observed with SEM, most samples from inside the cave had low ergosterol's content (less than 2000 μg per g of sample), or no detectable ergosterol at all, Table 10. Their sterol's levels were even lower to the one of the only sample from outside of the cavity.

Among the samples analysed, GdE 8 presented a high content of ergosterol. Although it was not observed with SEM, these results seem coherent with the microbial isolation performed on the sample and its nature. Indeed, this sample corresponds to a dark brown black fluid matter which could correspond to a highly hydrated bat faeces (guano). Indeed, the sample was collected on a highly hydrated wall, near where a bat was spotted during the first expedition to the cave. The microbial cultures performed on this sample permitted to isolate numerous fungal and bacterial organisms. Together with the MTT and PB results, Part III Chapter 2.B, this

sample appears to have a very high microbial activity, which is unusual for cave and even for natural non-faecal sample. Therefore, it is thought to correspond to faecal colonies, which should be removed carefully to prevent further development of microbial colonies which could damage the host rock and propagate to panels hosting artwork.

Comparing the results of the distinct samples between them permits to have a better knowledge of the fungal biocontamination of the cave of Escoural. It seems that fungi are present but rather low developed in most of the cave. Only some very specific locations with high organic and water content present a high fungal biomass which could if not monitored properly endanger the limestone support and the artwork found in Escoural.

The study of the microbial diversity of Escoural Cave highlighted the presence of numerous distinct strains, mostly typical from deep soils communities. Although the large panel of species that are present in the cave, the microbial viability activity is rather low in most of the cave. None of the species known for their harmfulness toward cave art have been reported inside Escoural Cave through isolation nor NGS. However, great care should be taken, since the well-known *Bracteacoccus minor* (Lefèvre, 1974), *Fusarium solani* (Dupont et al., 2007), and *Ochroconis lascauxensis* (Pedro Maria Martin-Sanchez et al., 2012) who colonized Lascaux' paintings and started to alter them, were initially not present in the cave and develop first due to important anthropic presence and then poor management of the microbial outbreaks. The famous case of Lascaux should help to understand the importance of monitoring the dynamic of the microbial communities inside the cave of Escoural, even if these communities do not seem to play any role in the degradation of the artworks.

Only few locations, with obvious high biological contaminations such as bat's faeces, mushroom's growth, and roots provide the sufficient nutrients allowing the development of a viable microbial niche. Therefore, the large diversity that was observed through culture dependent technique and NGS, should be present at a dormant stage. In such conditions, the microorganisms can survive in poor-nutrient context and develop again when they get sufficient nutrients to survive and grow. Although it implies that the microbial biodegradation is rather low, it is important to monitor their growth dynamic and action on the rock. Indeed, a small nutrient supply can be enough for some of the dormant microorganisms to develop and

colonize the artwork, more particularly for damageable fungi (Jurado et al., 2008). During the different visits of the cave (approximately one every month during months), various sources of nutrients for the microbial species were spotted: bat's faeces, roots, mushroom's growth, butterfly's corpse, and the wooden structure build for visiting the cave. From one visit to another, some microbial developments appeared and disappeared due to the lack of sustainable nutrients' source, though proving the presence of an important dynamic in the microbial communities of Escoural Cave. As once the artwork is colonised, it is arduous to remove the microbial communities without damaging the representations, it is necessary to monitor this microbial dynamic and prevent any stagnation of nutrients inside the cave.

Conclusion

The Room 1 hosting most of the parietal art and numerous biological outbreaks.

© A.L. Campos

The present study of Escoural Cave aimed at providing new insights on the pigments used to perform the Palaeolithic paintings and drawings and on the microbial diversity possibly threatening them.

The analyses, which covered a very large corpus from various parts of the cavity, highlighted a large diversity of the materials and techniques used to perform Escoural's representations. It also clarified the interpretation of some of the Palaeolithic paintings and drawings and evidenced numerous distinct phases during which numerous artworks were performed on top of each other. These numerous phases lead to a nowadays complex situation due to the superposition of the figures and their alteration. Further studies would clarify the chronological sequence of the different phases and the possibly bring further insights on some of the habits of the communities who performed the parietal representations of Escoural.

The analyses of the microbial communities evidenced that the microbial populations do not constitute the main threat endangering the parietal art's corpus of Escoural. Nonetheless, as the biological contaminations evolved rather drastically from one visit to another during the present thesis, it is primordial to monitor the microbial communities present in the cave, their dynamic of proliferation, and their possible deteriogenic action on both the support and the paintings and drawings.

As the microbial activity appeared to be less concerning than the weathering of the walls for the conservation of the artwork, it is also necessary to monitor at the same time the climatic conditions of the cave. In reality the two are complementary and should provide a general overview of the dynamic that could endangered the artworks present in the cave of Escoural.

The main issue altering the parietal art of Escoural is leaking water due to alternative condensation/evaporation cycles. Condensation phases induce major diffusion of the pictorial layers, leading to the appearance of pigment's drip on the walls' surface, altering the artwork by fading the shape of the representations and depleting the pictorial layers. On the contrary, evaporation phase favoured the formation of mineral phases over the various Palaeolithic representations. Developing such monitoring to ensure the conservation of the exceptional artwork of Escoural is crucial to permit further investigations and comprehend the complex parietal art's corpus of the cavity.

Bibliography

Abadía, O.M., 2006. Art, crafts and Paleolithic art. J. Soc. Archaeol. 6, 119–141. doi:10.1177/1469605306060571

Abramson, D., Smith, D.M., 2003. Determination of ergosterol in canola (Brassica napus L.) by liquid chromatography. J. Stored Prod. Res. 39, 185–191.

Aksu, Z., Eren, A.T., 2005. Carotenoids production by the yeast Rhodotorula mucilaginosa: Use of agricultural wastes as a carbon source. Process Biochem. 40, 2985–2991. doi:10.1016/j.procbio.2005.01.011

Al-Shabibi, M.M.A., Al-Mashikhi, S.A.E., 1987. Ergosterol content in relation to fungal spoilage of broad bean in storage. Can. Inst. Food Sci. Technol. J. 20, 50–52.

Altenburgera, P., Kämpferb, P., Makristathisc, A., Lubitza, W., Bussea, H.-J., 1996. Classification of bacteria isolated from a medieval wall painting. J. Biotechnol. 47, 39–52. doi:10.1016/0168-1656(96)01376-4

Alvarez-Lloret, P., Rodriguez-Navarro, A.B., Romanek, C.S., Gaines, K.S., Congdon, J., 2006. Quantitative analysis of bone mineral using FTIR. Macla 6, 45–47.

Araujo, A.C., Lejeune, M., Santos, A.I., 1995. Gruta do Escoural: necropole neolitica e arte rupestre paleolitica. Instituto Portugues do Patrimonio Arquitectonico e Arqueologico.

Ariño, X., Saiz-Jimenez, C., 1996. Colonisation and deterioration processes in Roman mortars by cyanobacteria, algae and lichens. Aerobiologia 12, 9–18. doi:10.1007/BF02248118

Arnezeder, C.H., Koliander, W., Hampel, W.A., 1989. Rapid determination of ergosterol in yeast cells. Anal. Chim. Acta 225, 129–136.

Arroyo, G., Arroyo, I., Arroyo, E., 1997. Microbiological analysis of Maltravieso cave (Caceres), Spain. Int. Biodeterior. Biodegrad. 40, 131–139.

Aujoulat, N., 2004. Le geste, l'espace et le temps, 1ere ed, Arts rupestres. Seuil, Paris.

Aujoulat, N., 2002. Lascaux. Le rôle du déterminisme naturel: des modalités d'élection du site aux protocoles de constitution des édifices graphiques pariétaux. Université Bordeaux 1, Bordeaux.

Baffier, D., Girard, M., Menu, M., Vignaud, C., 1999. La couleur à la Grande Grotte d'Arcy-sur-Cure (Yonne). Anthropol. 103, 1–21.

Baldrian, P., Větrovský, T., Cajthaml, T., Dobiášová, P., Petránková, M., Šnajdr, J., Eichlerová, I., 2013. Estimation of fungal biomass in forest litter and soil. Fungal Ecol. 6, 1–11. doi:10.1016/j.funeco.2012.10.002

Barquin, R.M., 2013. Estudio ambiental y medidas de conservacion preventiva de las manifestaciones rupestres de la gruta de Escoural (Alentejo, Portugal). Actuaciones 2010-2012.

Bastian, F., Alabouvette, C., Jurado, V., Saiz-Jimenez, C., 2009a. Impact of biocide treatments on the bacterial communities of the Lascaux Cave. Naturwissenschaften 96, 863–868.

Bastian, F., Alabouvette, C., Saiz-Jimenez, C., 2009b. Bacteria and free-living amoeba in the Lascaux Cave. Res. Microbiol. 160, 38–40. doi:10.1016/j.resmic.2008.10.001

Bastian, F., Jurado, V., Nováková, A., Alabouvette, C., Sáiz-Jiménez, C., 2010. The microbiology of Lascaux cave. Microbiology 156, 644–652.

Beck, L., Lebon, M., Lahlil, S., Grégoire, S., Odin, G.P., Rousselière, H., Castaing, J., Duran, A., Vignaud, C., Reiche, I., others, 2014a. Analyse non destructive des pigments préhistoriques: du laboratoire à la grotte. Paléo 63–74.

Beck, L., Rousselière, H., Castaing, J., Duran, A., Lebon, M., Lahlil, S., Plassard, F., 2013. Analyse in situ des dessins préhistoriques de la grotte de Rouffignac par fluorescence X et diffraction X portable. ArchéoSciences 139–152.

Beck, L., Rousselière, H., Castaing, J., Duran, A., Lebon, M., Moignard, B., Plassard, F., 2014b. First use of portable system coupling X-ray diffraction and X-ray fluorescence for in-situ analysis of prehistoric rock art. Talanta 129, 459–464. doi:10.1016/j.talanta.2014.04.043

Beni, A., Soki, E., Lajtha, K., Fekete, I., 2014. An optimized HPLC method for soil fungal biomass determination and its application to a detritus manipulation study. J. Microbiol. Methods 103, 124–130. doi:10.1016/j.mimet.2014.05.022

Bermingham, S., Maltby, L., Cooke, R.C., 1995. A critical assessment of the validity of ergosterol as an indicator of fungal biomass. Mycol. Res. 99, 479–484.

Berridge, M.V., Herst, P.M., Tan, A.S., 2005. Tetrazolium dyes as tools in cell biology: new insights into their cellular reduction. Biotechnol. Annu. Rev. 11, 127–152.

Berridge, M.V., Tan, A.S., 1993. Characterisation of the Cellular Reduction of 3-(4,5-dimethylthiazol-2-yl)-2,5-diphenyltetrazolium bromide (MTT): Subcellular Localisation, Substrate Dependence, and Involvement of Mitochondrial Electron Transport in MTT Reduction. Arch. Biochem. Biophys. 303, 474–482. doi:10.1006/abbi.1993.1311

Berrouet, F., 2009. Les altérations d'origine biologique dans l'art pariétal : exemple des relations structurales et conceptuelles entre le mondmilch et les représentations paléolithiques : cas particulier de la grotte de Lascaux et enjeux conservatoires. Bordeaux 1, Bordeaux.

Bindler, G.N., Piade, J.J., Schulthess, D., 1988. Evaluation of selected steroids as chemical markers of past or presently occurring fungal infections on tobacco. Beitr. Zur Tab. Tob. Res. 14, 127–134.

Boncler, M., Różalski, M., Krajewska, U., Podsędek, A., Watala, C., 2014. Comparison of PrestoBlue and MTT assays of cellular viability in the assessment of anti-proliferative effects of plant extracts on human endothelial cells. J. Pharmacol. Toxicol. Methods 69, 9–16. doi:10.1016/j.vascn.2013.09.003

Brunet, J., Vouvé, J., 1996. Contexte géologique et supports des oeuvres, in: La conservation des grottes ornées, Conservation du Patrimoine. CNRS Editions, Paris, pp. 53–68.

Cahagnier, B., Richard-Molard, D., Poisson, J., 1983. Evolution of the ergosterol content of cereal grains during storage. A possibility for a rapid test of fungal development in grains. Sci. Aliments 3, 219–244.

Cañaveras, J.C., Cuezva, S., Sanchez-Moral, S., Lario, J., Laiz, L., Gonzalez, J.M., Saiz-Jimenez, C., 2006. On the origin of fiber calcite crystals in moonmilk deposits. Naturwissenschaften 93, 27–32. doi:10.1007/s00114-005-0052-3

Cañaveras, J.C., Hoyos, M., Sanchez-Moral, S., Sanz-Rubio, E., Bedoya, J., Soler, V., Groth, I., Schumann, P., Laiz, L., Gonzalez, I., Saiz-Jimenez, C., 1999. Microbial Communities Associated With Hydromagnesite and

Needle-Fiber Aragonite Deposits in a Karstic Cave (Altamira, Northern Spain). Geomicrobiol. J. 16, 9–25. doi:10.1080/014904599270712

Cañaveras, J.C., Sanchez-Moral, S., Saiz-Jimenez, C., 2001. Microorganisms and Microbially Induced Fabrics in Cave Walls. Geomicrobiol. J. 18, 223–240. doi:10.1080/01490450152467769

Capodicasa, S., Fedi, S., Porcelli, A.M., Zannoni, D., 2010. The microbial community dwelling on a biodeteriorated 16th century painting. Int. Biodeterior. Biodegrad. 64, 727–733. doi:10.1016/j.ibiod.2010.08.006

Cappitelli, F., Abbruscato, P., Foladori, P., Zanardini, E., Ranalli, G., Principi, P., Villa, F., Polo, A., Sorlini, C., 2009. Detection and elimination of cyanobacteria from frescoes: the case of the St. Brizio Chapel (Orvieto Cathedral, Italy). Microb. Ecol. 57, 633–639. doi:10.1007/s00248-008-9441-4

Cappitelli, F., Toniolo, L., Sansonetti, A., Gulotta, D., Ranalli, G., Zanardini, E., Sorlini, C., 2007. Advantages of using microbial technology over traditional chemical technology in removal of black crusts from stone surfaces of historical monuments. Appl. Environ. Microbiol. 73, 5671–5675. doi:10.1128/AEM.00394-07

Cartailhac, E., Breuil, H., 1908. Les peintures et gravures murales des cavernes pyrénéennes, III-Niaux (Ariége). L'anthropologie 19, 15–46.

Carvalhosa, A.B., 1989. Sobre a Faixa Vulcano-Sedimentar de Monfurado (Escoural). Serviços Geologicos de Portugal.

Chadefaux, C., Vignaud, C., Menu, M., Reiche, I., 2008. Multianalytical study of Palaeolithic reindeer antler. Discovery of antler traces in Lascaux pigments by TEM. Archaeometry 50, 516–534. doi:10.1111/j.1475-4754.2008.00373.x

Chalmin, E., Menu, M., Altuna, J., 2002. Les matières picturales de la grotte d'Ekain (Pays Basque). Munibe 54, 35–51.

Chalmin, E., Menu, M., Vignaud, C., 2003. Analysis of rock art painting and technology of Palaeolithic painters. Meas. Sci. Technol. 14, 1590.

Chalmin, E., Vignaud, C., Menu, M., 2004. Palaeolithic painting matter: natural or heat-treated pigment? Appl. Phys. A 79, 187–191. doi:10.1007/s00339-004-2542-0

Chalmin, E., Vignaud, C., Salomon, H., Farges, F., Susini, J., Menu, M., 2006. Minerals discovered in paleolithic black pigments by transmission electron microscopy and micro-X-ray absorption near-edge structure. Appl. Phys. A 83, 213–218. doi:10.1007/s00339-006-3510-7

Cigna, A.A., 2002. Modern trend in cave monitoring. Acta Carsologica 31, 35–54.

Clot, A., Menu, M., Walter, P., 1995. Manières de peindre des mains à Gargas et Tibiran (Hautes-Pyrénées). L'Anthropologie 99, 221–235.

Clottes, J., 2008a. L'art des Cavernes. Phaidon, Paris.

Clottes, J., 2008b. Introduction, in: L'art Des Cavernes. Phaidon, Paris.

Clottes, J., Arnold, M., 2001. La grotte Chauvet: l'art des origines. Seuil Paris.

Clottes, J., Courtin, J., Vanrell, L., 2005. Cosquer redécouvert. Seuil.

Clottes, J., Menu, M., Walter, P., 1990a. La préparation des peintures magdaléniennes des cavernes ariégeoises. Bull. Société Préhistorique Fr. 87, 170–192. doi:10.3406/bspf.1990.10434

Clottes, J., Menu, M., Walter, P., 1990b. New light on the Niaux paintings. Rock Art Res. 7, 21–26.

Coccato, A., Jehlicka, J., Moens, L., Vandenabeele, P., 2015. Raman spectroscopy for the investigation of carbon-based black pigments: Investigation of carbon-based black pigments. J. Raman Spectrosc. 46, 1003–1015. doi:10.1002/jrs.4715

Couraud, C., 1991. Les pigments des grottes d'Arcy-sur-Cure (Yonne). Gall. Préhistoire 33, 17–52. doi:10.3406/galip.1991.2284

Cuezva, S., Fernandez-Cortes, A., Porca, E., Pašić, L., Jurado, V., Hernandez-Marine, M., Serrano-Ortiz, P., Hermosin, B., Cañaveras, J.C., Sanchez-Moral, S., Saiz-Jimenez, C., 2012. The biogeochemical role of Actinobacteria in Altamira Cave, Spain. FEMS Microbiol. Ecol. 81, 281–290. doi:10.1111/j.1574-6941.2012.01391.x

Cuezva, S., Sánchez-Moral, S., Sáiz-Jiménez, C., Cañaveras, J.C., 2009. Microbial communities and associated mineral fabrics in Altamira Cave, Spain.

Culver, D.C., Pipan, T., 2009. The biology of caves and other subterranean habitats. Oxford University Press, USA.

d'Errico, F., Dayet Bouillot, L., García-Diez, M., Pitarch Martí, A., Garrido Pimentel, D., Zilhão, J., 2016. The technology of the earliest European cave paintings: El Castillo Cave, Spain. J. Archaeol. Sci. 70, 48–65. doi:10.1016/j.jas.2016.03.007

Davies, B.H., 2009. Carotenoid metabolism as a preparation for function. Pure Appl. Chem. 63, 131–140. doi:10.1351/pac199163010131

Dayet, L., d'Errico, F., Garcia-Moreno, R., 2014. Searching for consistencies in Châtelperronian pigment use. J. Archaeol. Sci. 44, 180–193. doi:10.1016/j.jas.2014.01.032

De Mortillet, G., 1883. Le Préhistorique, antiquité de l'homme. Ch. Ferdinand Reinwald.

de SANOIT, J., CHAMBELLAN, D., PLASSARD, F., 2005. Caractérisatîon in situdu pigment noir de quelques oeuvres pariétales de la Grotte de Rouffignac à l'aide d'un système portable d'analyse par fluorescence X (XRF). ArchéoSciences 29, 61–68.

de S Saad, D., Kinsey, G.C., Paterson, R., Gaylarde, C., 2003. Ergosterol analysis for the quantification of fungal growth on paint films. Proposal for a standard method. Surf. Coat. Int. Part B Coat. Trans. 86, 131–134.

Delluc, B., Delluc, G., Bazile-Robert, E., Galinat, B., Guichard, F., Ozanne, M., 1983. Les grottes ornées de Domme (Dordogne) : La Martine, Le Mammouth et le Pigeonnier. Gall. Préhistoire 26, 7–80. doi:10.3406/galip.1983.1709

dos Santos, F., 1964. Vestigios de pinturas rupestres descobertos na gruta do Escoural. O Arqueol. Port. 2, 5–47.

Dupont, J., Jacquet, C., Dennetière, B., Lacoste, S., Bousta, F., Orial, G., Cruaud, C., Couloux, A., Roquebert, M.-F., 2007. Invasion of the French Paleolithic painted cave of Lascaux by members of the Fusarium solani species complex. Mycologia 99, 526–533.

Edwards, H.G.M., Newton, E.M., Russ, J., 2000. Raman spectroscopic analysis of pigments and substrata in prehistoric rock art. J. Mol. Struct. 550, 245–256.

Engel, A.S., 2012. Chemoautotrophy A2 - White, William B., in: Culver, D.C. (Ed.), Encyclopedia of Caves (Second Edition). Academic Press, Amsterdam, pp. 125–134.

Figueiredo, M.M., Martins, A.G., Gamelas, J.A.F., 2012. Characterisation of bone and bone-based graft materials using FTIR spectroscopy. INTECH Open Access Publisher.

Flood, J., 1999. The Riches of Ancient Australia: An Indispensable Guide for Exploring Prehistoric Australia. University of Queensland Press.

Frostegard, A., Baath, E., 1996. The use of phospholipid fatty acid analysis to estimate bacterial and fungal biomass in soil. Biol. Fertil. Soils 22, 59–65.

Garate, D., Laval, É., Menu, M., 2004. Étude de la matière colorante de la grotte d'Arenaza (Galdames, Pays Basque, Espagne). L'Anthropologie 108, 251–289. doi:10.1016/j.anthro.2004.06.001

Garcia-Vallès, M., Vendrell-Saz, M., Krumbein, W.E., Urzì, C., 1997. Coloured mineral coatings on monument surfaces as a result of biomineralisation: the case of the Tarragona cathedral (Catalonia). Appl. Geochem. 12, 255–266.

Geneste, J.-M., Menu, M., Julien, M., David, F., 2008. Les matières colorantes au début du Paléolithique supérieur: caractérisation chimique et structurale, transformation et valeur symbolique. Techné 15–21.

Gong, P., Guan, X., Witter, E., 2001. A rapid method to extract ergosterol from soil by physical disruption. Appl. Soil Ecol. 17, 285–289.

Görs, S., Schumann, R., Häubner, N., Karsten, U., 2007. Fungal and algal biomass in biofilms on artificial surfaces quantified by ergosterol and chlorophyll a as biomarkers. Int. Biodeterior. Biodegrad. 60, 50–59. doi:10.1016/j.ibiod.2006.10.003

Grant, W.D., West, A.W., 1986. Measurement of ergosterol, diaminopimelic acid and glucosamine in soil: evaluation as indicators of microbial biomass. J. Microbiol. Methods 6, 47–53.

Griffin, P.S., Indictor, N., Koestler, R.J., 1991. The biodeterioration of stone: a review of deterioration mechanisms, conservation case histories, and treatment. Int. Biodeterior. 28, 187–207.

Griffiths, H.M., Jones, D.G., Akers, A., 1985. A bioassay for predicting the resistance of wheat leaves to Septoria nodorum. Ann. Appl. Biol. 107, 293–300.

Gurtner, C., Heyrman, J., Piñar, G., Lubitz, W., Swings, J., Rölleke, S., 2000. Comparative analyses of the bacterial diversity on two different biodeteriorated wall paintings by DGGE and 16S rDNA sequence analysis. Int. Biodeterior. Biodegrad. 46, 229–239.

Hamilton, R.M., Trenholm, H.L., Thompson, B.K., 1988. Chemical, nutritive, deoxynivalenol and zearalenone content of corn relative to the site of inoculation with different isolates of Fusarium graminearum. J. Sci. Food Agric. 43, 37–47.

He, X., Huai, W., Tie, C., Liu, Y., Zhang, B., 2000. Breeding of high ergosterol-producing yeast strains. J. Ind. Microbiol. Biotechnol. 25, 39–44.

Henshilwood, C.S., d'Errico, F., Watts, I., 2009. Engraved ochres from the middle stone age levels at Blombos Cave, South Africa. J. Hum. Evol. 57, 27–47.

Herrera, L.K., Videla, H.A., 2009. Surface analysis and materials characterisation for the study of biodeterioration and weathering effects on cultural property. Int. Biodeterior. Biodegrad. 63, 813–822. doi:10.1016/j.ibiod.2009.05.002

Hippelein, M., Rügamer, M., 2004. Ergosterol as an indicator of mould growth on building materials. Int. J. Hyg. Environ. Health 207, 379–385.

Huang, B.-H., Yung, K.-H., Chang, S.-T., 1985. The sterol composition of Volvariella volvacea and other edible mushrooms. Mycologia 959–963.

Hughes, J.C., Solomon, A., 2000. A preliminary study of ochres and pigmentaceous materials from KwaZulu-Natal, South Africa: towards an understanding of San pigment and paint use. Natal Mus. J. Humanit. 12, 15–31.

Huyghe, R., 1962. Larousse encyclopedia of prehistoric and ancient art: art and mankind. Prometheus Press.

Jambunathan, R., Kherdekar, M.S., Vaidya, P., 1991. Ergosterol concentration in mold-susceptible and mold-resistant sorghum at different stages of grain development and its relationship to flavan-4-ols. J. Agric. Food Chem. 39, 1866–1870.

Jaubert, J., 2008. L'« art » pariétal gravettien en France : éléments pour un bilan chronologique. PALEO Rev. Archéologie Préhistorique 439–474.

Jaubert, J., Verheyden, S., Genty, D., Soulier, M., Cheng, H., Blamart, D., Burlet, C., Camus, H., Delaby, S., Deldicque, D., others, 2016. Early Neanderthal constructions deep in Bruniquel Cave in southwestern France. Nature 534, 111–114.

Jezequel, P., Wille, G., Bény, C., Delorme, F., Jean-Prost, V., Cottier, R., Breton, J., Duré, F., Despriee, J., 2011. Characterisation and origin of black and red Magdalenian pigments from Grottes de la Garenne (Vallée moyenne de la Creuse-France): a mineralogical and geochemical approach of the study of prehistorical paintings. J. Archaeol. Sci. 38, 1165–1172.

Joergensen, R.G., Wichern, F., 2008. Quantitative assessment of the fungal contribution to microbial tissue in soil. Soil Biol. Biochem. 40, 2977–2991.

Jurado, V., Sanchez-Moral, S., Saiz-Jimenez, C., 2008. Entomogenous fungi and the conservation of the cultural heritage: A review. Int. Biodeterior. Biodegrad. 62, 325–330. doi:10.1016/j.ibiod.2008.05.002

Krull, I.S., Swartz, M., Driscoll, J.N., 1985. Derivatisation of Drugs and Bioorganics for Improved Detection by Gas Chromatography and Photoionisation Detection (GC-PID). Anal. Lett. 18, 2619–2632.

Kusumi, A., Li, X., Osuga, Y., Kawashima, A., Gu, J.-D., Nasu, M., Katayama, Y., 2013. Bacterial Communities in Pigmented Biofilms Formed on the Sandstone Bas-Relief Walls of the Bayon Temple, Angkor Thom, Cambodia. Microbes Environ. 28, 422–431. doi:10.1264/jsme2.ME13033

Lefèvre, M., 1974. La "maladie verte"de Lascaux. Stud. Conserv. 19, 126–156.

Leroi-Gourhan, A., 1982. The dawn of European art: An introduction to Palaeolithic cave painting. CUP Archive.

Li, Y., Wadsö, L., Larsson, L., Bjurman, J., 2007. Correlating two methods of quantifying fungal activity: Heat production by isothermal calorimetry and ergosterol amount by gas chromatography–tandem mass spectrometry. Thermochim. Acta 458, 77–83. doi:10.1016/j.tca.2007.01.005

López-Montalvo, E., Villaverde, V., Roldán, C., Murcia, S., Badal, E., 2014. An approximation to the study of black pigments in Cova Remigia (Castellón, Spain). Technical and cultural assessments of the use of carbon-based black pigments in Spanish Levantine Rock Art. J. Archaeol. Sci. 52, 535–545. doi:10.1016/j.jas.2014.09.017

Lorblanchet, M., 2010. Art pariétal: grottes ornées du Quercy. Ed. du Rouergue.

Lorblanchet, M., Delpech, F., Renault, P., Andrieux, C., 1973. La grotte de Sainte-Eulalie à Espagnac (Lot). Gall. Préhistoire 16, 3–62. doi:10.3406/galip.1973.1436

Lotze, F., 1945. Zur Gliederung der Variszíden in der Iberischen Meseta. Geotekt Forsch 6, 78–92.

Malaurent, P., Huneau, F., Lastennet, R., Fabre, R., 2004. Etudes pour la conservation des parois de la grotte d'Escoural-Portugal (Conservation grottes ornées No. 2004–24). Centre de Développement des Géosciences Appliquées - CDGA, Bordeaux.

Mariscal, A., Lopez-Gigosos, R.M., Carnero-Varo, M., Fernandez-Crehuet, J., 2009. Fluorescent assay based on resazurin for detection of activity of disinfectants against bacterial biofilm. Appl. Microbiol. Biotechnol. 82, 773–783. doi:10.1007/s00253-009-1879-x

Martín-Navarro, C.M., López-Arencibia, A., Sifaoui, I., Reyes-Batlle, M., Cabello-Vílchez, A.M., Maciver, S., Valladares, B., Piñero, J.E., Lorenzo-Morales, J., 2014. PrestoBlue® and AlamarBlue® are equally useful as agents to determine the viability of Acanthamoeba trophozoites. Exp. Parasitol. 145, S69–S72. doi:10.1016/j.exppara.2014.03.024

Martin-Sanchez, P.M., Nováková, A., Bastian, F., Alabouvette, C., Saiz-Jimenez, C., 2012. Two new species of the genus Ochroconis, O. lascauxensis and O. anomala isolated from black stains in Lascaux Cave, France. Fungal Biol. 116, 574–589.

Martin-Sanchez, P.M., Nováková, A., Bastian, F., Alabouvette, C., Saiz-Jimenez, C., 2012. Use of biocides for the control of fungal outbreaks in subterranean environments: The case of the Lascaux Cave in France. Environ. Sci. Technol. 46, 3762–3770.

Menu, M., Walter, P., 1996. Les rythmes de l'art préhistorique. Techne 3, 11–23.

Menu, M., Walter, P., Vigears, D., Clottes, J., 1993. Façons de peindre au Magdalénien. Bull. Société Préhistorique Fr. 90, 426–432. doi:10.3406/bspf.1993.9672

Mille-Lindblom, C., von Wachenfeldt, E., Tranvik, L.J., 2004. Ergosterol as a measure of living fungal biomass: persistence in environmental samples after fungal death. J. Microbiol. Methods 59, 253–262. doi:10.1016/j.mimet.2004.07.010

Miller, J.D., Young, J.C., Trenholm, H.L., 1983. Fusarium toxins in field corn. I. Time course of fungal growth and production of deoxynivalenol and other mycotoxins. Can. J. Bot. 61, 3080–3087.

Mohd As'wad, A.W., Sariah, M., Paterson, R.R.M., Zainal Abidin, M.A., Lima, N., 2011. Ergosterol analyses of oil palm seedlings and plants infected with Ganoderma. Crop Prot. 30, 1438–1442. doi:10.1016/j.cropro.2011.07.004

Moissan, H., 1903. Sur une matière colorante des figures de la grotte de la Mouthe. Comptes Rendus Hebd. Séances Académie Sci. 144–145.

Moissan, H., 1902. Sur les matières colorantes des figures de la grotte de Font-de-Gaume. Comptes Rendus Hebd. Séances Académie Sci. 134, 1539–1540.

Montgomery, H.J., Monreal, C.M., Young, J.C., Seifert, K.A., 2000. Determinination of soil fungal biomass from soil ergosterol analyses. Soil Biol. Biochem. 32, 1207–1217.

Mosmann, T., 1983. Rapid colorimetric assay for cellular growth and survival: Application to proliferation and cytotoxicity assays. J. Immunol. Methods 65, 55–63. doi:10.1016/0022-1759(83)90303-4

Moyo, S., Mphuthi, D., Cukrowska, E., Henshilwood, C.S., van Niekerk, K., Chimuka, L., 2016. Blombos Cave: Middle Stone Age ochre differentiation through FTIR, ICP OES, ED XRF and XRD. Quat. Int. 404, 20–29. doi:10.1016/j.quaint.2015.09.041

Mueller, H.-M., Schwadorf, K., Modi, R., Reimann, J., 1991. [Ergosterol and fungal count in malt sprouts and grass meal]. Agribiol. Res. Ger. FR.

Mulec, J., 2008. MICROORGANISMS IN HyPOGEON: EXAMPLES FROM SLOVENIAN KARST CAVES MIKROORGANIZMI PODZEMLJA: PRIMERI IZ SLOVENSKIH KRAŠKIH JAM. Acta Carsologica 1, 37.

Muniroh, M.S., Sariah, M., Zainal Abidin, M.A., Lima, N., Paterson, R.R.M., 2014. Rapid detection of Ganoderma-infected oil palms by microwave ergosterol extraction with HPLC and TLC. J. Microbiol. Methods 100, 143–147. doi:10.1016/j.mimet.2014.03.005

Naewbanij, M., Seib, P.A., Chung, D.S., Seitz, L.M., Deyoe, C.W., 1986. Erosterol versus dry matter loss as quality indicator for high-moisture rough rice during holding. Cereal Chem.

Newell, S.Y., Arsuffi, T.L., Fallon, R.D., 1988. Fundamental procedures for determining ergosterol content of decaying plant material by liquid chromatography. Appl. Environ. Microbiol. 54, 1876–1879.

Newell, S.Y., Miller, J.D., Fallon, R.D., 1987. Ergosterol content of salt-marsh fungi: effect of growth conditions and mycelial age. Mycologia 688–695.

Nilsson, K., Bjurman, J., others, 1990. Estimation of mycelial biomass by determination of the ergosterol content of wood decayed by Coniophora puteana and Fomes fomentarius. Mater. Org. 25, 275–283.

Northup, D.E., Lavoie, K., 2001. Geomicrobiology of Caves: A Review. Geomicrobiol. J. 18, 199–222. doi:10.1080/01490450152467750

Nuevo, M.J., Martín Sánchez, A., Oliveira, C., Oliveira, J., 2012. In situ energy dispersive X-ray fluorescence analysis of rock art pigments from the “Abrigo dos Gaivões” and “Igreja dos Mouros” caves (Portugal): In situ EDXRF analysis of rock art pigments. X-Ray Spectrom. 41, 1–5. doi:10.1002/xrs.1373

Nugari, M.P., Pietrini, A.M., Caneva, G., Imperi, F., Visca, P., 2009. Biodeterioration of mural paintings in a rocky habitat: The Crypt of the Original Sin (Matera, Italy). Int. Biodeterior. Biodegrad. 63, 705–711. doi:10.1016/j.ibiod.2009.03.013

Olivares, M., Castro, K., Corchón, M.S., Gárate, D., Murelaga, X., Sarmiento, A., Etxebarria, N., 2013. Non-invasive portable instrumentation to study Palaeolithic rock paintings: the case of La Peña Cave in San Roman de Candamo (Asturias, Spain). J. Archaeol. Sci. 40, 1354–1360. doi:10.1016/j.jas.2012.10.008

Osswald, W.F., Höll, W., Elstner, E.F., 1986. Ergosterol as a biochemical indicator of fungal infection in spruce and fir needles from different sources. Z. Für Naturforschung C 41, 542–546.

Pepe, O., Sannino, L., Palomba, S., Anastasio, M., Blaiotta, G., Villani, F., Moschetti, G., 2010. Heterotrophic microorganisms in deteriorated medieval wall paintings in southern Italian churches. Microbiol. Res. 165, 21–32. doi:10.1016/j.micres.2008.03.005

Pigeaud, R., 2002. The decorated cave of Mayenne-Sciences (Thorigne-en-Charnie, Mayenne): border-cave at the boundary of ante-magdalenian world. L’Anthropologie 106, 445–489.

Pigeaud, R., Plagnes, V., Bouchard, M., Bahain, J.-J., Causse, C., Demailly, S., Falguères, C., Laval, É., Noël, F., Rodet, J., Valladas, H., Walter, P., 2010. Analyses archéométriques dans la grotte ornée Mayenne-

Sciences (Thorigné-en-Charnie, Mayenne). L'Anthropologie 114, 97–112. doi:10.1016/j.anthro.2010.01.004

Polo, A., Cappitelli, F., Brusetti, L., Principi, P., Villa, F., Giacomucci, L., Ranalli, G., Sorlini, C., 2010. Feasibility of removing surface deposits on stone using biological and chemical remediation methods. Microb. Ecol. 60, 1–14. doi:10.1007/s00248-009-9633-6

Pomies, M.-P., Morin, G., Vignaud, C., 1998. XRD study of the goethite-hematite transformation: application to the identification of heated prehistoric pigments. Eur. J. Solid State Inorg. Chem. 35, 9–25.

Porep, J.U., Walter, R., Kortekamp, A., Carle, R., 2014. Ergosterol as an objective indicator for grape rot and fungal biomass in grapes. Food Control 37, 77–84. doi:10.1016/j.foodcont.2013.09.012

Portillo, M.C., Gonzalez, J.M., 2009. Comparing bacterial community fingerprints from white colonisations in Altamira Cave (Spain). World J. Microbiol. Biotechnol. 25, 1347–1352. doi:10.1007/s11274-009-0021-7

Ranalli, G., Zanardini, E., Sorlini, C., 2009. Biodeterioration - Including Cultural Heritage. Encycl. Microbiol., Academic Press.

Reichnach, S., 1900. Le totémisme animal. Comptes Rendus Séances Académie Inscr. B.-lett. 44, 442.

Renault, P., 1983. Etudes récentes sur le karst de Niaux-Lombrives-Sabart (Ariège). Karstologia 2, 17–22.

Rinta-Kanto, J.M., Ouellette, A.J.A., Boyer, G.L., Twiss, M.R., Bridgeman, T.B., Wilhelm, S.W., 2005. Quantification of toxic Microcystis spp. during the 2003 and 2004 blooms in western Lake Erie using quantitative real-time PCR. Environ. Sci. Technol. 39, 4198–4205.

Rodriguez-Navarro, C., Rodriguez-Gallego, M., Ben Chekroun, K., Gonzalez-Muñoz, M.T., 2003. Conservation of ornamental stone by Myxococcus xanthus-induced carbonate biomineralisation. Appl. Environ. Microbiol. 69, 2182–2193.

Roldán, C., Murcia-Mascarós, S., Ferrero, J., Villaverde, V., López, E., Domingo, I., Martínez, R., Guillem, P.M., 2010. Application of field portable EDXRF spectrometry to analysis of pigments of Levantine rock art. X-Ray Spectrom. 39, 243–250. doi:10.1002/xrs.1254

Roldán, C., Villaverde, V., Ródenas, I., Novelli, F., Murcia, S., 2013. Preliminary analysis of Palaeolithic black pigments in plaquettes from the Parpalló cave (Gandía, Spain) carried out by means of non-destructive techniques. J. Archaeol. Sci. 40, 744–754. doi:10.1016/j.jas.2012.07.015

Rölleke, S., Muyzer, G., Wawer, C., Wanner, G., Lubitz, W., 1996. Identification of bacteria in a biodegraded wall painting by denaturing gradient gel electrophoresis of PCR-amplified gene fragments coding for 16S rRNA. Appl. Environ. Microbiol. 62, 2059–2065.

Román, R.S., Bañón, C.B., Landete Ruiz, M.D., 2015. Analysis of the red ochre of the El Mirón burial (Ramales de la Victoria, Cantabria, Spain). J. Archaeol. Sci. 60, 84–98. doi:10.1016/j.jas.2015.03.033

Rosado, T., MARTINS, M.R., Pires, M., Mirão, J., CANDEIAS, A., CALDEIRA, A.T., 2013. Enzymatic monitorisation of mural paintings biodegradation and biodeterioration. Int. J. Conserv. Sci.

Rosado, T., Mirão, J., Candeias, A., Caldeira, A.T., 2015. Characterizing Microbial Diversity and Damage in Mural Paintings. Microsc. Microanal. 21, 78–83. doi:10.1017/S1431927614013439

Ruzicka, S., Edgerton, D., Norman, M., Hill, T., 2000. The utility of ergosterol as a bioindicator of fungi in temperate soils. Soil Biol. Biochem. 32, 989–1005.

Salomon, H., 2009. Les matières colorantes au début du Paléolithique supérieur: sources, transformations et fonctions. Bordeaux 1.

Sanchez-Moral, S., Canaveras, J.C., Laiz, L., Saiz-Jimenez, C., Bedoya, J., Luque, L., 2003. Biomediated Precipitation of Calcium Carbonate Metastable Phases in Hypogean Environments: A Short Review. Geomicrobiol. J. 20, 491–500. doi:10.1080/713851131

Sanchez-Moral, S., Portillo, M.C., Janices, I., Cuezva, S., Fernández-Cortés, A., Cañaveras, J.C., Gonzalez, J.M., 2012. The role of microorganisms in the formation of calcitic moonmilk deposits and speleothems in Altamira Cave. Geomorphology 139–140, 285–292. doi:10.1016/j.geomorph.2011.10.030

Sánchez-Moral, S., Soler, V., Cañaveras, J.C., Sanz-Rubio, E., Van Grieken, R., Gysels, K., 1999. Inorganic deterioration affecting the Altamira Cave, N Spain: quantitative approach to wall-corrosion (solutional etching) processes induced by visitors. Sci. Total Environ. 243–244, 67–84. doi:10.1016/S0048-9697(99)00348-4

Sandmann, G., Albrecht, M., Schnurr, G., Knörzer, O., Böger, P., 1999. The biotechnological potential and design of novel carotenoids by gene combination in Escherichia coli. Trends Biotechnol. 17, 233–237.

Sauvet, G., Wlodarczyk, A., 1995. Eléments d'une grammaire formelle de l'art pariétal paléolithique. L'Anthropologie 2/3, 193–211.

Schwadorf, K., Müller, H.M., 1988. Determination of ergosterol in cereals, mixed feed components, and mixed feeds by liquid chromatography. J.-Assoc. Off. Anal. Chem. 72, 457–462.

Seitz, L.M., Bechtel, D.B., 1985. Chemical, physical, and microscopical studies of scab-infected hard red winter wheat. J. Agric. Food Chem. 33, 373–377.

Seitz, L.M., Mohr, H.E., Burroughs, R., Sauer, D.B., 1977. Ergosterol as an indicator of fungal invasion in grains. Cereal Chem.

Seitz, L.M., Sauer, 0D B., Burroughs, R., Mohr, H.E., Hubbard, J.D., 1979. Ergosterol as a measure of fungal growth [Alternaria and Aspergillus, in cereal grains]. Phytopathol. USA.

Silva, A.C., 2011. Escoural: uma gruta pré-histórica no Alentejo.

Simmleit, N., Schulten, H.-R., 1989. Thermal degradation of spruce needles studied by time-resolved mass spectrometry and multivariate data analysis. Anal. Chim. Acta 223, 371–385.

Soleilhavoup, F., 1986. Les surfaces de l'art rupestre en plein air : relations avec le milieu biophysique et méthodes d'étude. Anthropol. 90, 743–782.

Strzelczyk, A.B., 2004. Observations on aesthetic and structural changes induced in Polish historic objects by microorganisms. Int. Biodeterior. Biodegrad. 53, 151–156. doi:10.1016/S0964-8305(03)00088-X

Šubrt, J., Pérez-Maqueda, L.A., Criado, J.M., Real, C., Boháček, J., Večerníková, E., 2000. Preparation of nanosized hematite particles by mechanical activation of goethite samples. J. Am. Ceram. Soc. 83, 294–298.

Tinoi, J., Rakariyatham, N., Deming, R.L., 2005. Simplex optimisation of carotenoid production by Rhodotorula glutinis using hydrolyzed mung bean waste flour as substrate. Process Biochem. 40, 2551–2557. doi:10.1016/j.procbio.2004.11.005

Tournié, A., Prinsloo, L.C., Paris, C., Colomban, P., Smith, B., 2011. The first in situ Raman spectroscopic study of San rock art in South Africa: procedures and preliminary results. J. Raman Spectrosc. 42, 399–406. doi:10.1002/jrs.2682

Tran, T.H., Govin, A., Guyonnet, R., Grosseau, P., Lors, C., Garcia-Diaz, E., Damidot, D., Devès, O., Ruot, B., 2012. Influence of the intrinsic characteristics of mortars on biofouling by Klebsormidium flaccidum. Int. Biodeterior. Biodegrad. 70, 31–39. doi:10.1016/j.ibiod.2011.10.017

Tsatskin, A., Gendler, T.S., 2016. Identification of "red ochre" in soil at Kfar HaHoresh Neolithic site, Israel: Magnetic measurements coupled with materials characterisation. J. Archaeol. Sci. Rep. 6, 284–292. doi:10.1016/j.jasrep.2016.02.027

van Loon, A., Boon, J.J., 2004. Characterisation of the deterioration of bone black in the 17 th century Oranjezaal paintings using electron-microscopic and micro-spectroscopic imaging techniques. Spectrochim. Acta Part B At. Spectrosc. 59, 1601–1609.

Varga, M., Bartók, T., Mesterházy, Á., 2006. Determination of ergosterol in Fusarium-infected wheat by liquid chromatography–atmospheric pressure photoionisation mass spectrometry. J. Chromatogr. A 1103, 278–283. doi:10.1016/j.chroma.2005.11.051

Vaultier, M., dos Santos, F., Glory, A., 1965. La grotte ornée d'Escoural (Portugal). Bull. Société Préhistorique Fr. 62, 110–117. doi:10.3406/bspf.1965.4017

Vegas, R., 1968. Sobre la Existencia de Precambrio en la Baja Extremadura. Estud. Geol. 24, 85–89.

Vignaud, C., Salomon, H., Chalmin, E., Geneste, J.-M., Menu, M., 2006. Le groupe des « bisons adossés » de Lascaux. Étude de la technique de l'artiste par analyse des pigments. L'Anthropologie 110, 482–499. doi:10.1016/j.anthro.2006.07.008

Vlasceanu, L., Popa, R., Kinkle, B.K., 1997. Characterisation of Thiobacillus thioparus LV43 and its distribution in a chemoautotrophically based groundwater ecosystem. Appl. Environ. Microbiol. 63, 3123–3127.

Vouvé, J., 1987. Essais sur les risques touristiques et la société face à la surconsosommation culturelle. Cas de Lascaux - Lascaux II. Presented at the Actes des troisièmes rencontres internationales pour la protection du Patrimoine Culturelle, Avignon.

Wallander, H. akan, Massicotte, H.B., Nylund, J.-E., 1997. Seasonal variation in protein, ergosterol and chitin in five morphotypes of Pinus sylvestris L. ectomycorrhizae in a mature Swedish forest. Soil Biol. Biochem. 29, 45–53.

Warscheid, T., Braams, J., 2000. Biodeterioration of stone a review. Int. Biodeterior. Biodegrad. 46, 343–368.

West, A.W., Grant, W.D., Sparling, G.P., 1987. Use of ergosterol, diaminopimelic acid and glucosamine contents of soils to monitor changes in microbial populations. Soil Biol. Biochem. 19, 607–612.

White, W.B.W.B., 1988. Geomorphology and hydrology of karst terrains.

Xu, M., McCanna, D.J., Sivak, J.G., 2015. Use of the viability reagent PrestoBlue in comparison with alamarBlue and MTT to assess the viability of human corneal epithelial cells. J. Pharmacol. Toxicol. Methods 71, 1–7. doi:10.1016/j.vascn.2014.11.003

Young, J.C., 1995. Microwave-assisted extraction of the fungal metabolite ergosterol and total fatty acids. J. Agric. Food Chem. 43, 2904–2910.

Young, J.C., Fulcher, R.G., Hayhoe, J.H., Scott, P.M., Dexter, J.E., 1984. Effect of milling and baking on deoxynivalenol (vomitoxin) content of eastern Canadian wheats. J. Agric. Food Chem. 32, 659–664.

Young, J.C., Games, D.E., 1993. Supercritical fluid extraction and supercritical fluid chromatography of the fungal metabolite ergosterol. J. Agric. Food Chem. 41, 577–581.

YOUNG, J.C., MILLER, J.D., 1985. Appearance of fungus, ergosterol and Fusarium mycotoxins in the husk, axial stem and stalk after ear inoculation of field corn. Can. J. Plant Sci. 65, 47–53.

Zhao, X.R., Lin, Q., Brookes, P.C., 2005. Does soil ergosterol concentration provide a reliable estimate of soil fungal biomass? Soil Biol. Biochem. 37, 311–317. doi:10.1016/j.soilbio.2004.07.041

Zill, G., Engelhardt, G., Wallnöfer, P.R., 1988. Determination of ergosterol as a measure of fungal growth using Si 60 HPLC. Z. Für Lebensm.-Unters. Forsch. 187, 246–249.

Index

E

F

H

I

M

N

O

P

S

U

V

W

Appendix

Imaging session of the parietal representations of Escoural Cave

© S. Costa

Appendix 1: The climate of Escoural Cave (Malaurent et al., 2004)

The following part entirely relies on the work performed by Malaurent et al. in 2004. It aims at presenting some of the most important results about the climatic variations inside the cave. The results and interpretations were all performed by Malaurent et al. The following pages constitute a very synthetic summary to help the reader the extent of the climatic variations and their possible influences on the Palaeolithic representations of Escoural Cave.

To perform their climatic study inside the cave, they implemented different probes in various parts of the cavity, Figure 1. It permitted them to highlight the differences of variations existing in this particular environment.

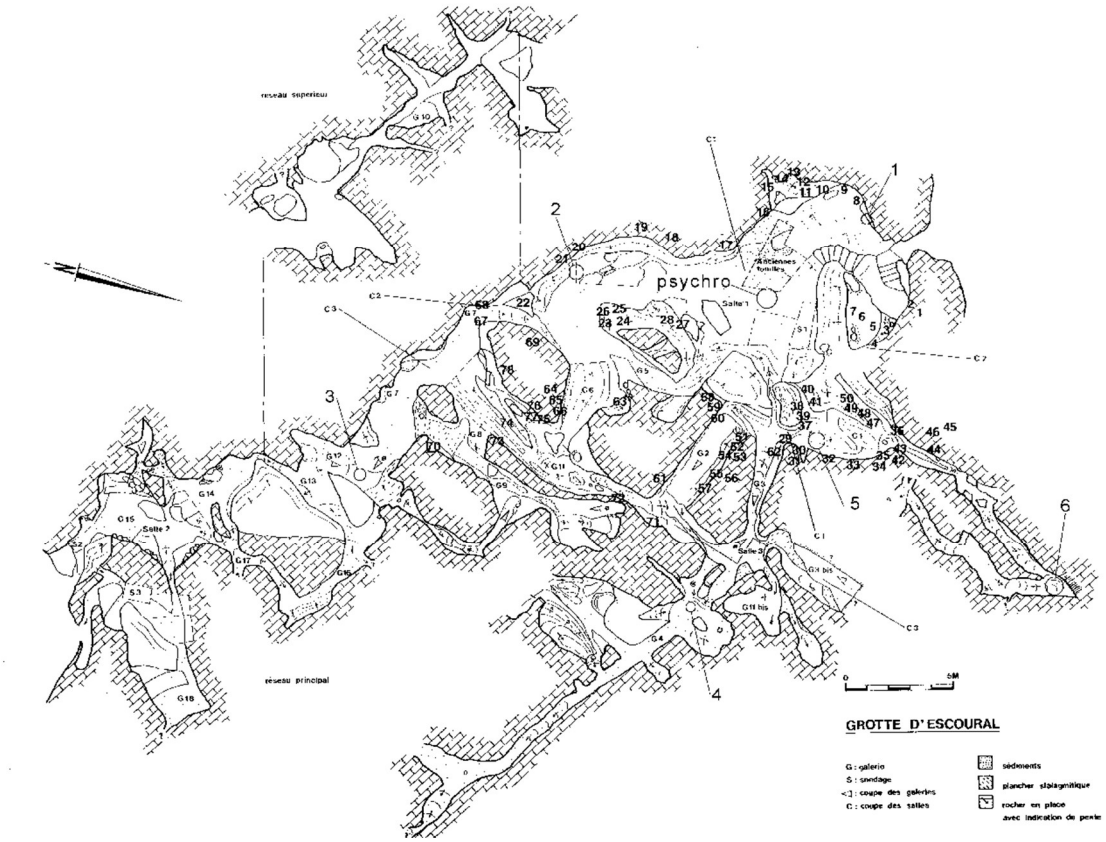

Figure 1: Location of the climatic probes inside the cave of Escoural (large number with lines).

Although they measured numerous parameters, only the variations of the temperatures of the rock and the air are presented in this appendix. Both are largely sufficient to provide a first insight on the influence of the climatic conditions on the conservation of parietal art. Naturally, they should be complemented with other measures to confirm the results and provide a full comprehension of the climatic variations. They distinguish two damageable situations briefly presented here.

During their study, it appeared that three locations, 1 (Room 1- Entrance), 3 (Room 2) and 6 (Gallery 1- remote gallery) were subject to high temperatures' variations greatly endangering the artworks hosted

in those parts of the site. Indeed, they all encounter numerous evaporation/condensation cycles, Figure 2.A, threatening the integrity of the representations as mentioned in the thesis.

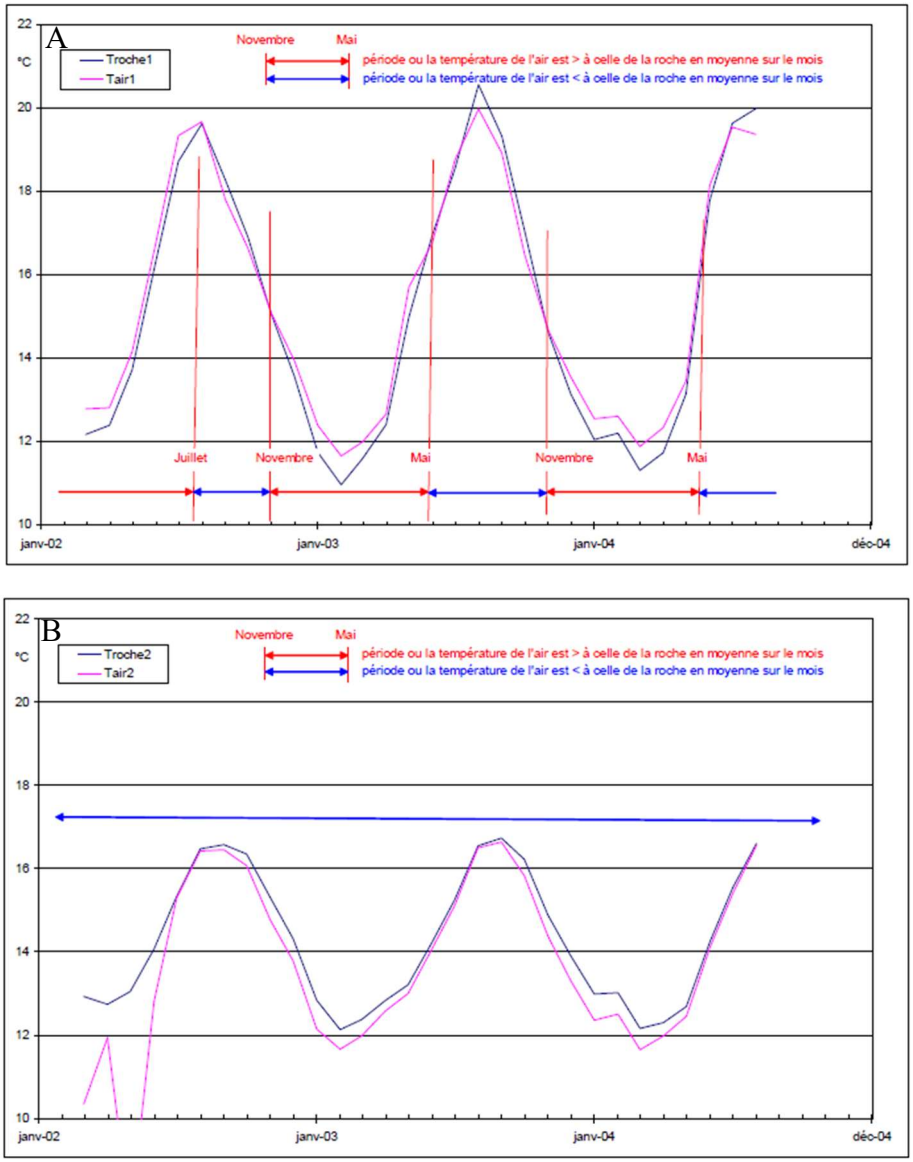

Figure 2: Comparison of the variations of the rock and air temperatures presenting the different situations of the evaporation/condensation cycles found in Escoural Cave. A: High number of evaporation/condensation cycles. Probe 1, 3 and 6. B: No evaporation/condensation cycles with permanent evaporation conditions. Probe 2 and 4.

Locations of probes 2 (Room 1) and 4 (remote room) appeared to be in constant evaporation conditions, Figure 2.B. However, they received water from water leaking on the walls of the cave, observations made by Milene Gil Duarte Casal (Malaurent et al. 2004). The water evaporates quickly due to the specific climatic conditions of these locations, though damaging the artwork it leaks on before evaporating.

Appendix 2: Black pigments' samples

The present appendix does not aim at developing more the discussion about the black pigments' characterisation and diversity, but just to present the results that were not included in the thesis.

Location of the samples

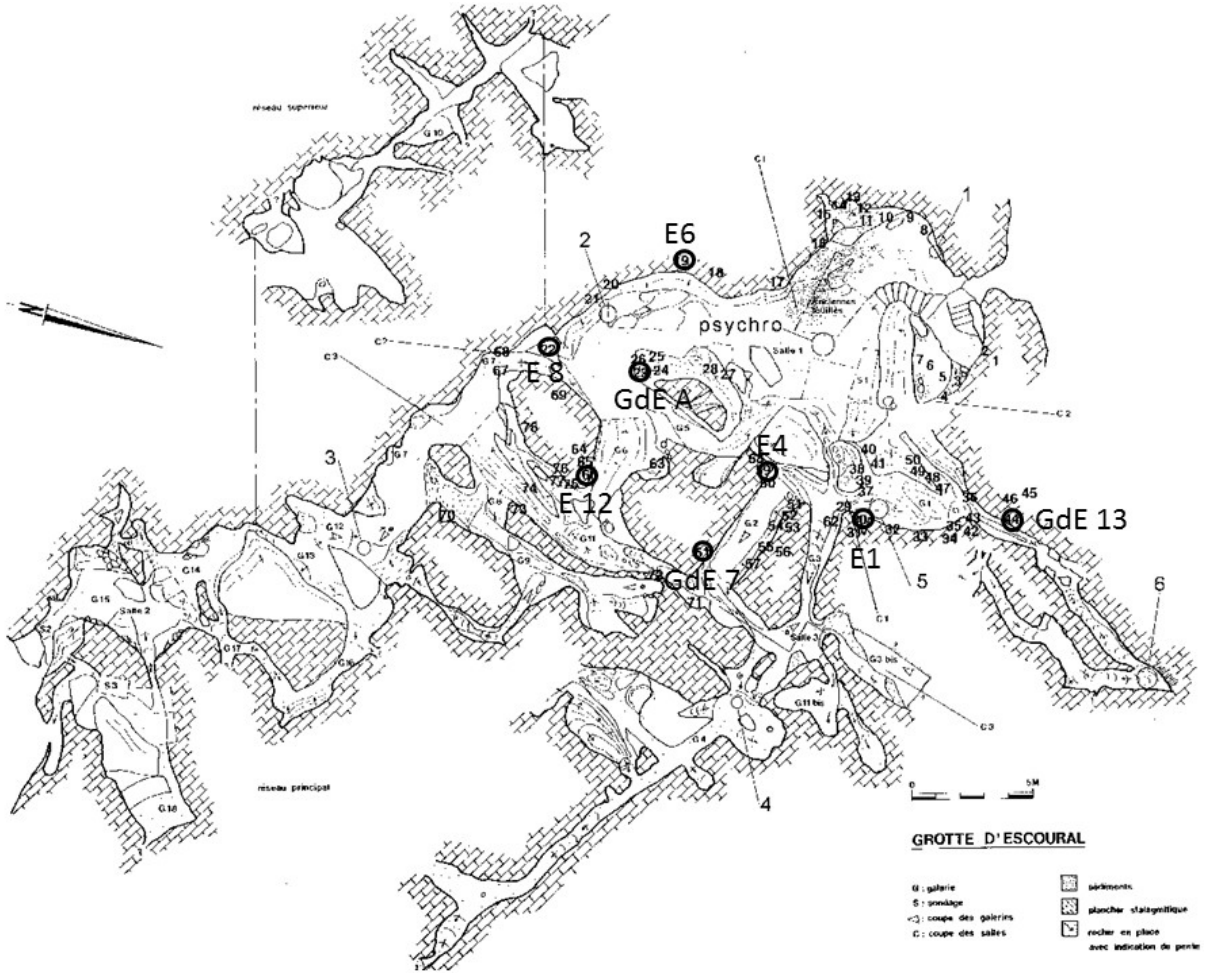

Figure 1: Location of the black pigments' samples inside the cave of Escoural.

The sampling procedure covered most of the black representations recorded by M. Lejeune (Araujo et al., 1995). Only two were not studied, one due to accessibility issues and another by lack of pigments sampled during the sampling campaign. Therefore, the large majority of the panels hosting recorded black representations were analysed. However imaging techniques revealed the existence of numerous black representations not recorded before and therefore not studied here, Appendix 4.

Samples' analyses

The following pages present complementary results to support the conclusions developed in the thesis (Part II Chapter 3). The reader is referred to Figure 9 of the thesis (Part II Chapter 3.C, p.57) and the Table 1 of the present appendix for the identification of the coloured material used to perform the black

representations. In a matter of conciseness, only sample of each group of the black pigments is shown here.

Sample GdE 7: Manganese oxide, painting 61

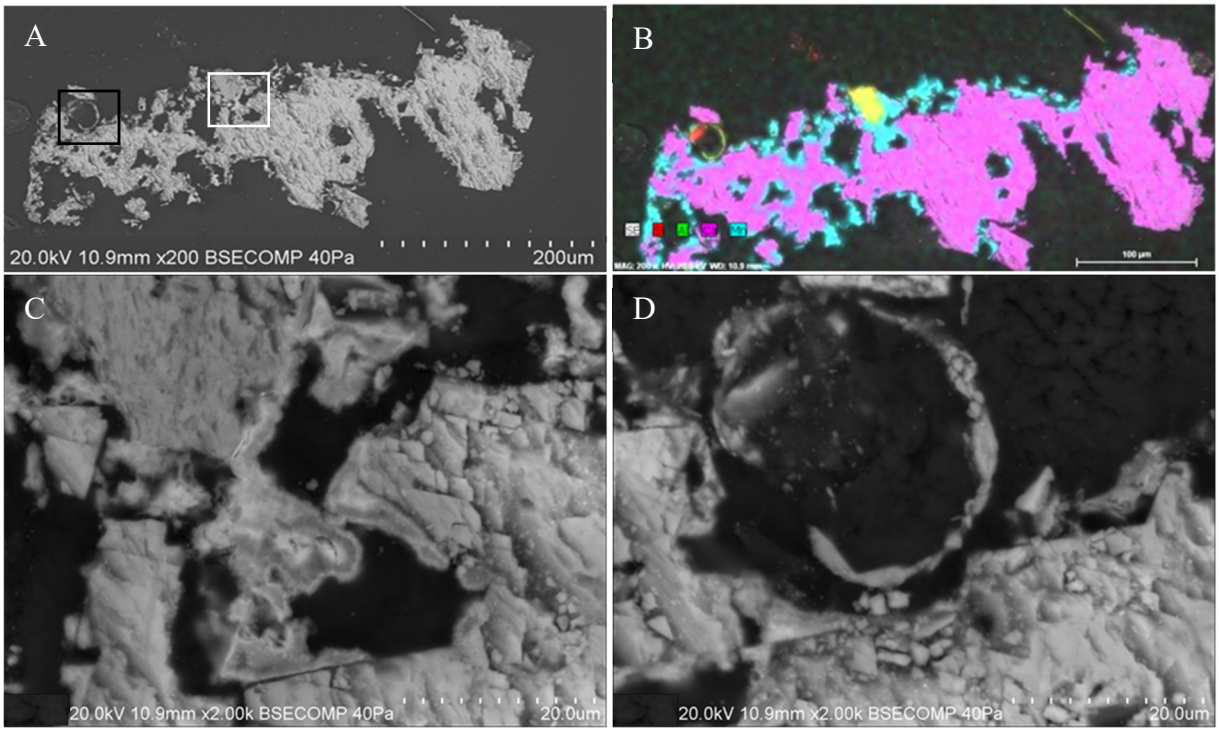

Figure 2: SEM-EDS observations and analyses of sample GdE 7. A: General view of the sample's cross section. The white rectangle shows the area observed in Figure 2.C, the black one the one in Figure 2.D; B: General mapping of the sample's cross section; C: Detailed observations of the manganese oxide layer and of the potassium feldspar; D: Unidentified feature rich in aluminium and calcium, possibly a gastropod's shell.

The sample GdE 7, the only one containing manganese oxide, presented a complex distribution of the coloured material in the cross section analysed, Figure 2.B. As it was not possible to ensure that the stratigraphy's orientation of the pictorial layer was preserved during the realisation of the cross section, it is possibly due to the cross section.

Two specific features were detected in the cross section analysed: the presence of a large potassium feldspar particle, Figure 2.C, and an unidentified structure attributed to a possible gastropod shell, Figure 2.D. The potassium feldspar was identified thanks to its shape and the EDS analysis evidencing the simultaneous presence of potassium, aluminium and silica.

Sample GdE 13: Bone black, painting 44

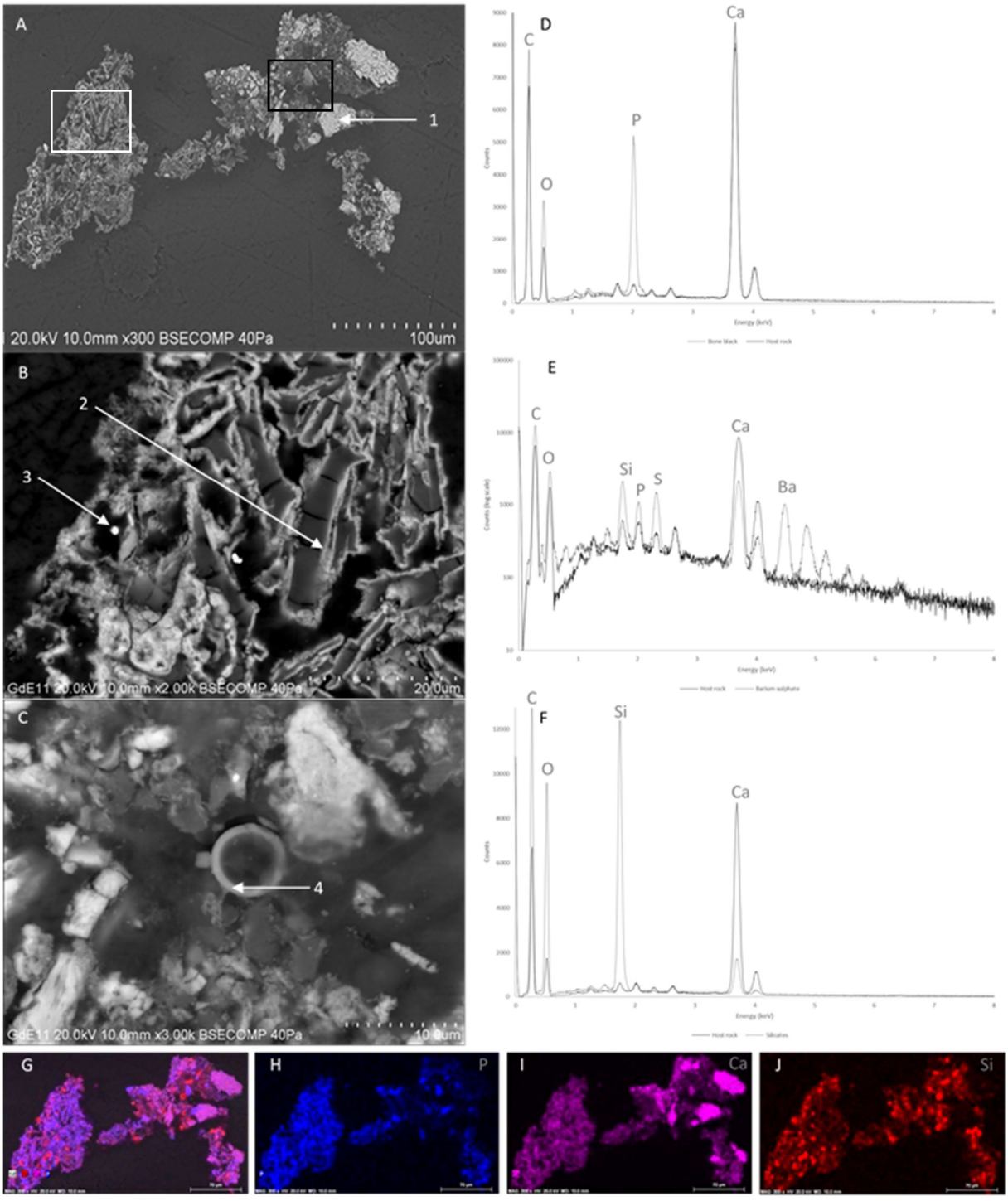

Figure 3: SEM-EDS observations and analyses of sample GdE 13. A: General view of the sample's cross section. The white rectangle shows the area observed in Figure 3.B, the black one the one in Figure 3.C. The substrate of calcium carbonate appears in white on the right, the calcium phosphates are in a darker white, and the silicates are in grey. Number 1: spot of the SEM-EDS analysis of the host rock; B: Detailed observations of the bone black layer with some barium sulphate particles (white particles). Number 2: spot of the bone black's SEM-EDS analysis, Number 3: spot of the barium sulphate's SEM-EDS analysis; C: Unidentified annular feature rich in silica surrounded by clay (dark grey) and calcium phosphate particles (white). Number 4: spot of the SEM-EDS analysis of the unidentified feature; D: SEM-EDS spectra of spots 1 and 2; E: SEM-EDS spectra spots 1 and 3. F: SEM-EDS spectra of the spots 1 and 4; G: General mapping of the sample GdE 13 with P, Ca and Si. H: General mapping of P; I: General mapping of Ca; J: General mapping of Si.

The sample GdE 13, the only one containing manganese oxide, presented a clear stratigraphy with two distinct layers: outermost layer containing bone black, Figure 3.B and 3.D, and barium sulphates' particles, Figure 3.B and 3.E, containing clay mixed with calcium phosphate particles and silicates, Figure 3.C and 3.F, and the calcium carbonate host rock, Figures 3.A, G-J.

The identification of bone black was clear thanks to the morphology of the micro-shards observed, Figure 3.B, and the SEM-EDS spectrum, Figure 3.D revealing a high content of phosphorus and carbon compared to the host rock.

Sample GdE A: Charcoal with large particles, drawing 23 (similar to E 12, drawing 66)

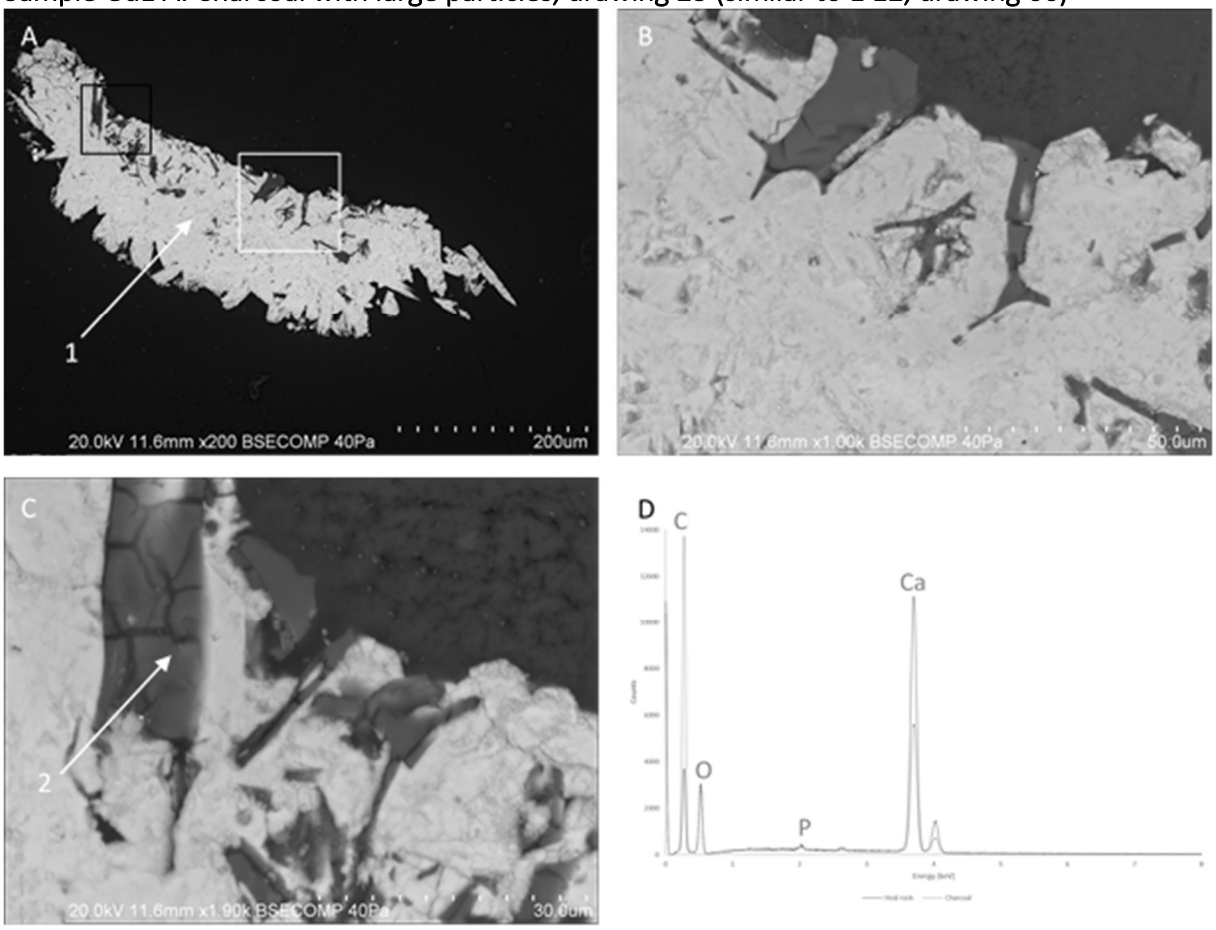

Figure 4: SEM-EDS observations and analyses of sample GdE A. A: General view of the sample's cross section. The white rectangle shows the area observed in Figure 4.B, the black one the one in Figure 4.C. The substrate of calcium carbonate appears in white on the right, and the carbonaceous material in grey. Number 1: spot of the SEM-EDS analysis of the host rock; B: Detailed observations of charcoal particles. The host rock appears in white and the carbonaceous material in grey; C: Detailed observations of charcoal particles. The host rock appears in white and the carbonaceous material in grey. Number 2: spot of the SEM-EDS analysis of the charcoal particles; D: SEM-EDS spectra of spots 1 and 2.

The sample GdE A, one of the two samples – with the sample E12 collected on the representation 66 in the gallery 6 – containing large charcoal particles, presented a clear stratigraphy with a layer of approximately 60 µm containing charcoal particles, Figures 4.B-C, and a second layer corresponding to the host rock, Figure 4.A, composed of calcium carbonate with traces of phosphorus, Figure 4.D. The

clear differences of carbon and calcium content between the black particles and the host rock, Figure 4.D, permitted to identify charcoal.

Sample E4: Charcoal with small particles, drawing 59 (similar to E1, drawing 30)

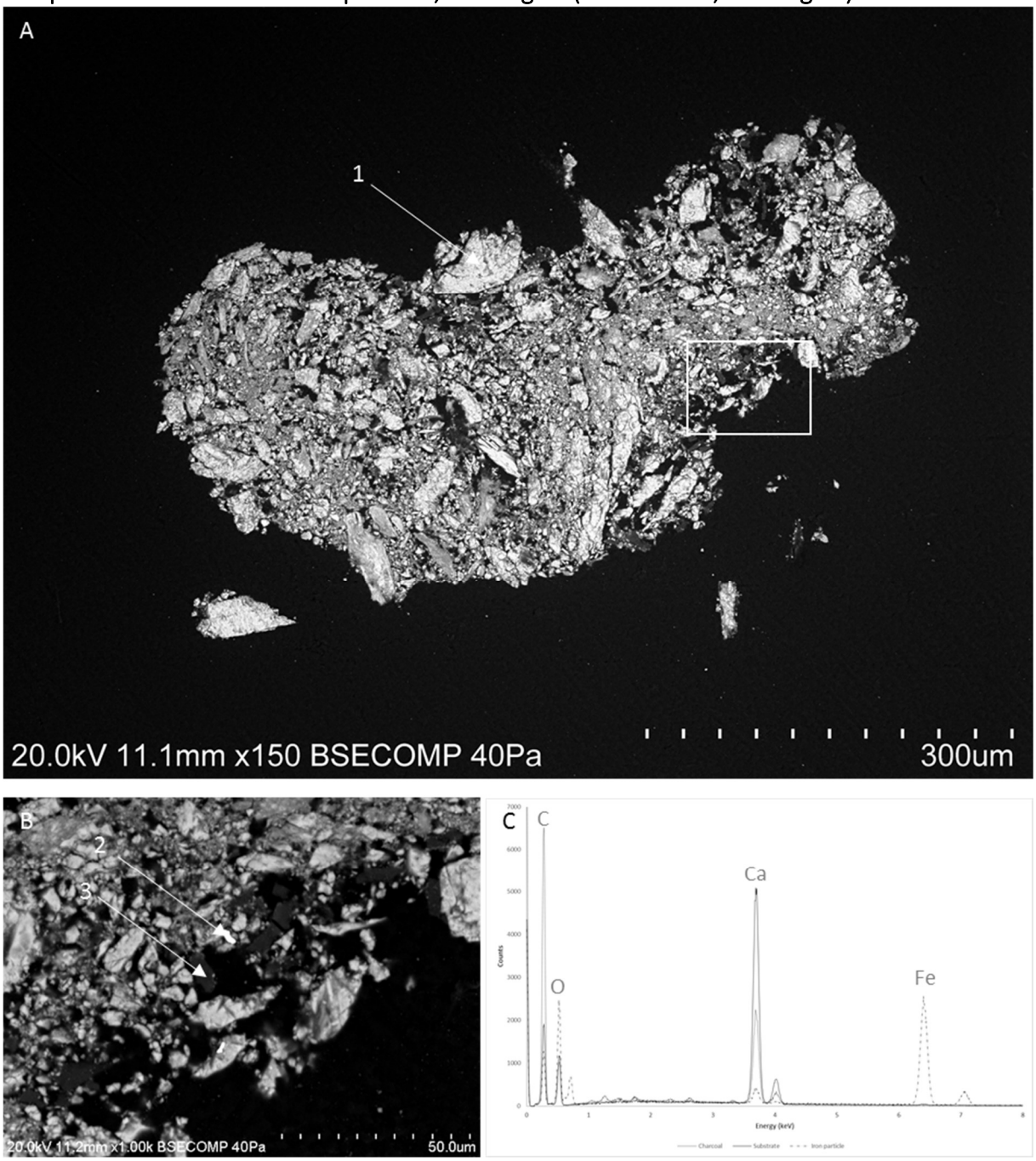

Figure 5: SEM-EDS observations and analyses of sample E4. A: General view of the sample's cross section. The white rectangle shows the area observed in Figure 5.B. Number 1: spot of the SEM-EDS analysis of the host rock; B: Detailed observations of charcoal particles. Iron particle appears in white, carbonaceous material in dark grey, calcium carbonate in grey. Number 2: spot of the SEM-EDS analysis of the charcoal particles. Number 3: spot of the SEM-EDS analysis of the iron-rich particle; C: SEM-EDS spectra of spots 1, 2, and 3.

The sample E4, one of the two samples – with the sample E1 collected on the representation 30 in the gallery 1 – containing small charcoal particles with iron-rich particles, did not present a clear

stratigraphy. The host rock seemed to be covered by a layer composed of clay mixed with a calcium carbonate matrix. Furthermore, tiny iron-rich particles were spotted in different parts of the sample containing the small charcoal particles, Figure 5.B-C. Charcoal and iron particles were clearly identified by comparison with the substrate signal, Figure 5.C.

Sample E8: Charcoal with small particles and bone black, drawing 22 (similar to E6, drawing 19)

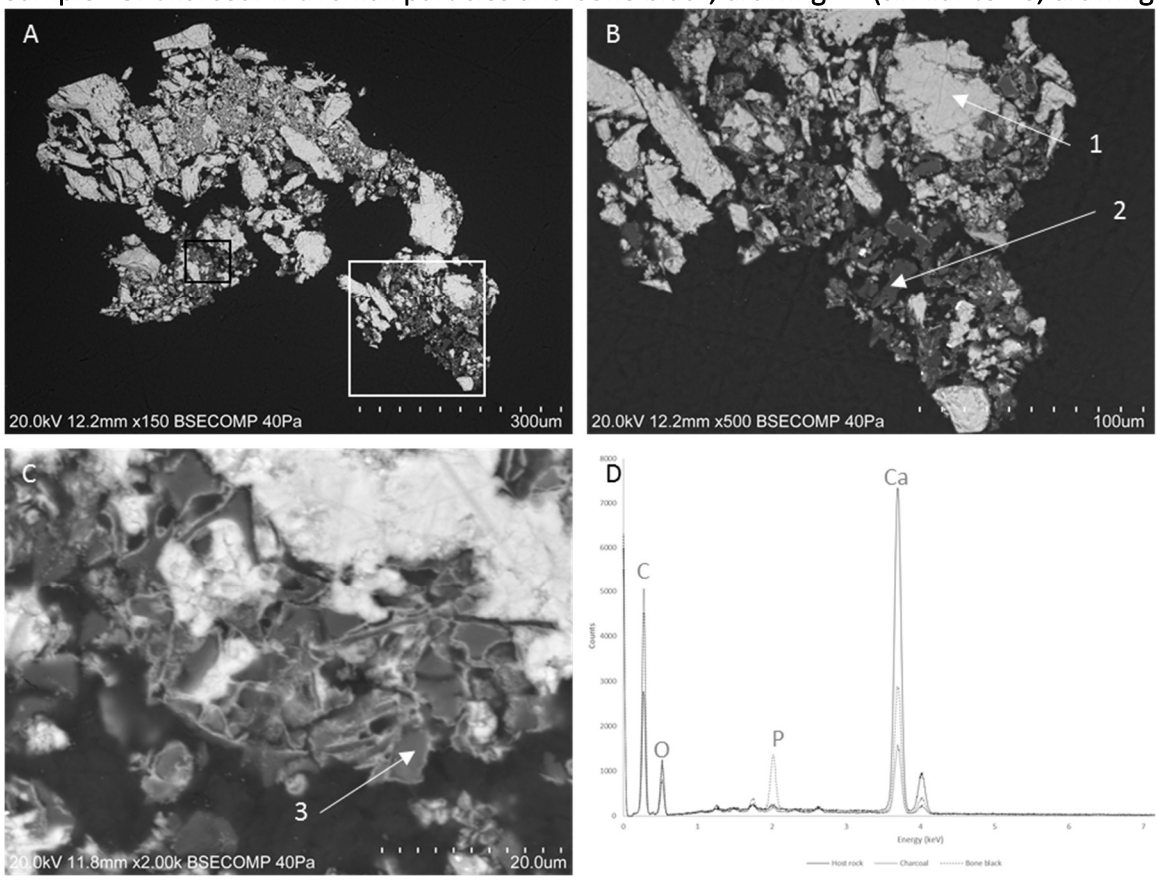

Figure 6: SEM-EDS observations and analyses of sample E8. A: General view of the sample's cross section. The white rectangle shows the area observed in Figure 6.B, the black one the one detailed in Figure 6.C; B: Detailed observations of charcoal particles. Barium sulphate appears in white, carbonaceous material in dark grey, calcium carbonate in white grey. Number 1: spot of the SEM-EDS analysis of the host rock. Number 2: spot of the SEM-EDS analysis of the charcoal particles; C: Detailed observations of bone black particles. Calcium carbonate appears in white, calcium phosphate in grey. Number 3: spot of the SEM-EDS analysis of the bone black particles; D: SEM-EDS spectra of spots 1, 2, and 3.

The sample E8, one of the two samples – with the sample E6 collected on the representation 19 in the room 1 – containing small charcoal particles with bone black particles, did not present a clear stratigraphy. The host rock seemed to be covered by a layer composed of calcium carbonate and sulphate. Furthermore, distinct black pigments were spotted: charcoal, Figure 6.B, and bone black, Figure 6.C. Charcoal and bone black particles were clearly identified by comparison with the substrate signal, Figure 6.D.

Table 1: Black pigments' samples from Escoural. Cal: calcite ; Hm : Hematite ; Q : quartz ; Kao : kaolinite; C: C-matter; Gy: gypsum; CaP: calcium phosphate; AC: amorphous carbon, A : amorphous phase

Sample	Location	Figure	Interpretation	Pictorial technique	Raman	FTIR	SEM							XRD	Pigments		Habits
							EDS	Structure	Size range	Mean size	Std dev	Filler	Traces		Group	Sub-group	
GdE 7	Gallery 2	61	Unidentified	Painting (S)	Cal + Mn	Cal + Mn	Mn, K, Ba	Acicular	Layer: 2µm Needle: 0,5*0,1µm	/	/	K-feldspar	Gastropod shell?	A	Mn oxide	/	Painting (S)
GdE 13	Gallery 1	44	Right horse head	Painting (F)	Cal + AC	Cal + bone (altered)	Ca + P	Bone shards	/	L: 16,7 l: 5,0	L: 5,1 l: 0,1	Clay	Fe-oxide, siliceous structures, BaS	/	Bone black	Large shards	Painting (F)
GdE A	Room 1	23	Right hybrid head	Drawing (H)	Cal + AC	Cal	No	Charcoal particles	9,6 – 44,1	25	10,9	/	/	/	Charcoal	Large particles	Drawing (H)
E1	Gallery 1	30	Left horse body*	Drawing (L)	AC	Cal	No	Layered	11,7 – 37,7	19,6	7,9	/	Fe and Ti, BaS, clay	/	Charcoal	Small particles	Reuse Drawing (L)
															Hematite	Ti-oxide	
E4	Gallery 2	59	Right horses	Drawing (H)	Cal + AC	Cal	No Fe oxides	Charcoal particles	6,2 – 12,1	9,3	2,1	/	Clay, feldspar, Fe oxides	/	Charcoal	Small particles	Reuse Drawing (H)
															Hematite	Ti-oxide	
E6	Room 1	19	Left horse body *	Drawing (H)	Cal + AC	Cal + Kao	No Ca + P	Charcoal and bone shards	C: 5 - 15,1	C: 7,5 B: L: 14,8 l: 2,4	C: 3,8 B: L: 5,1 l: 0,2	Clay	Fe, Ti, Zn, diagenetic CaP	/	Charcoal	Small particles	Reuse Drawing (H)
															Bone black	Small shards	
E8	Room 1	22	Unidentified	Drawing (H)	AC	Cal + bone ?	No Ca + P	Charcoal and bone shards	C: 7,9 – 23,5	C: 13,8 B: L: 5,2 l: 2,6	C: 5,6 B: L: 0,8 l: 1,0	Clay	Fe oxides, BaS	Cal	Charcoal	Small particles	Reuse Drawing (H)
															Bone black	Small shards	
E12	Gallery 6	66	Geometric	?	AC	Cal + bone ?	No	Charcoal particles	9,4 – 33,1	15,7	9,0	/	/	/	Charcoal	Large particles	Drawing

Appendix 3: Red pigments' samples

The present appendix does not aim at developing more the discussion about the red pigments' characterisation and diversity, but just to present the results that were not included in the thesis.

Location of the samples

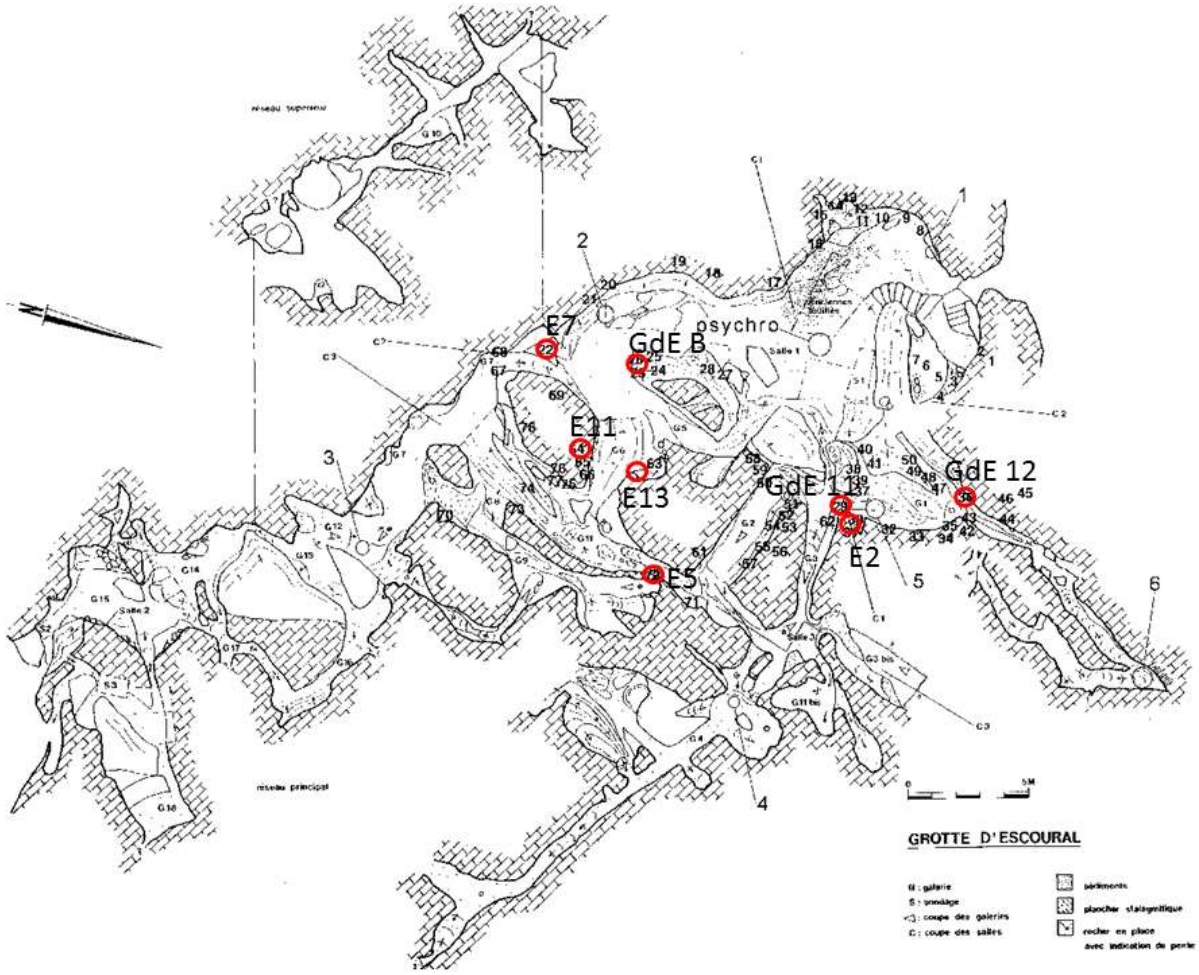

Figure 1: Location of the red pigments' samples inside the cave of Escoural.

The sampling procedure covered most of the red representations recorded by M. Lejeune (Araujo et al., 1995). A coupled of red representations were not studied, due to accessibility issues, lack of visibility of the figures recorded by M. Lejeune or lack of pigments sampled during the sampling campaign. However, the large majority of the panels hosting recorded red representations were analysed. However imaging techniques revealed the existence of numerous red representations not recorded before and therefore not studied here, Appendix 4.

Samples' analyses

The following pages present complementary results to support the conclusions developed in the thesis (Part II Chapter 3). The reader is referred to Figure 10 of the thesis (Part II Chapter 3.C, p.63) and the

Table 1 of the present appendix for the identification of the coloured material used to perform the red representations. In a matter of conciseness, only sample of each group of the black pigments is shown here.

Sample GdE 11: Ochre with Ti oxides, painting 29 (similar to GdE 12, painting 36)

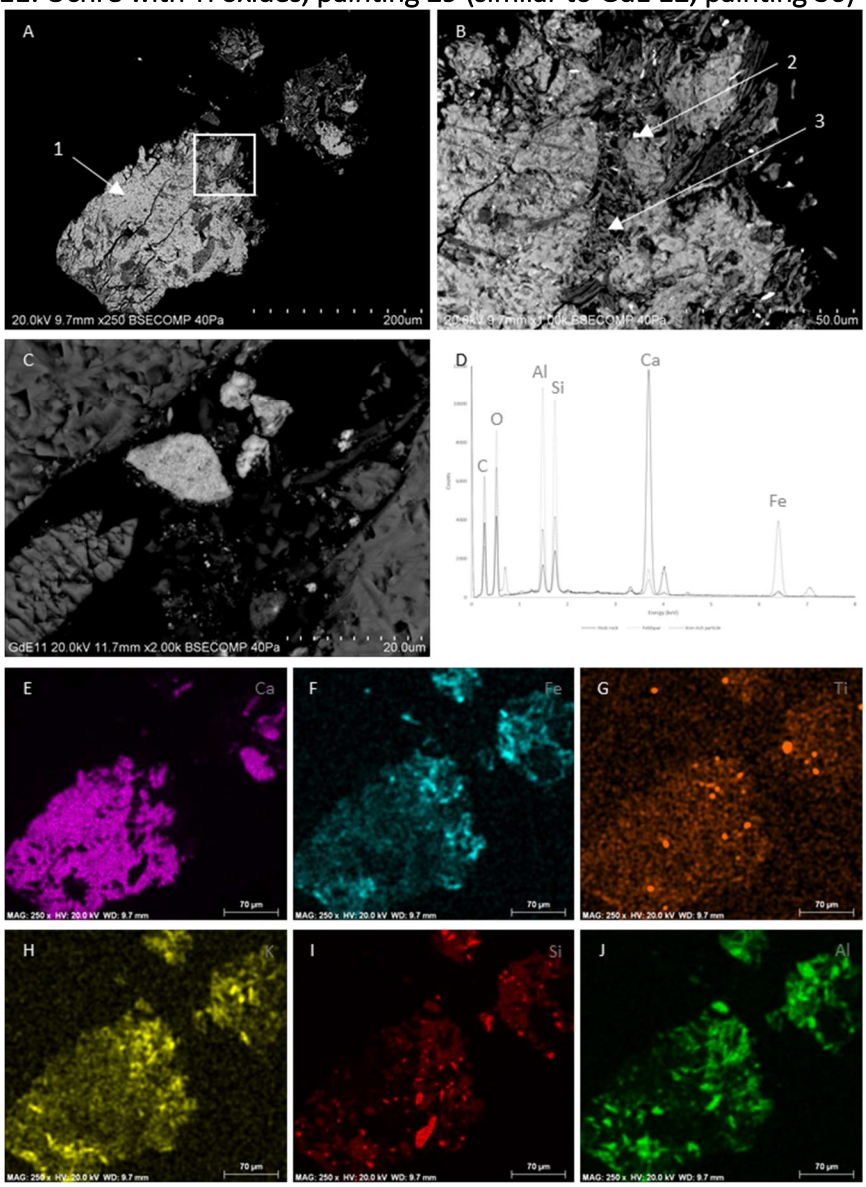

Figure 2: SEM-EDS observations and analyses of sample GdE 11. A: General view of the sample's cross section. The white rectangle shows the area observed in Figure 2.B. The substrate of calcium carbonate appears in white, and the alumina silicates are in grey. Number 1: spot of the SEM-EDS analysis of the host rock; B: Detailed observations of the pigment layer with iron-rich particles (in white). Number 2: spot of the iron particles' SEM-EDS analysis, Number 3: spot of the feldspar's SEM-EDS analysis; C: Detail observation of the iron particle.; D: SEM-EDS spectra of spots 1, 2, and 3; E: General mapping of Ca. F: General mapping of Fe; G: General mapping of Ti; H: General mapping of K; I: General mapping of Si; J: General mapping of Al.

The sample GdE 11, one of the two samples – with the sample GdE 12 collected on the representation 36 in the gallery 1 – containing ochre with Ti oxides, presented a clear stratigraphy with a pictorial layer composed of iron and titanium oxides mixed with alumina silicates, Figures 2.A-B, 2.F-J, and a second

layer corresponding to the host rock, Figure 2.A and 2.E, composed of calcium carbonate, Figure 2.D. The clear differences of carbon and calcium content between the pictorial layer and the host rock, Figure 2.D, permitted to identify iron and feldspars (Al-Si) in the pictorial preparation.

Sample GdE B: Ochre with biotites, painting 23 (similar to E2, painting 30)

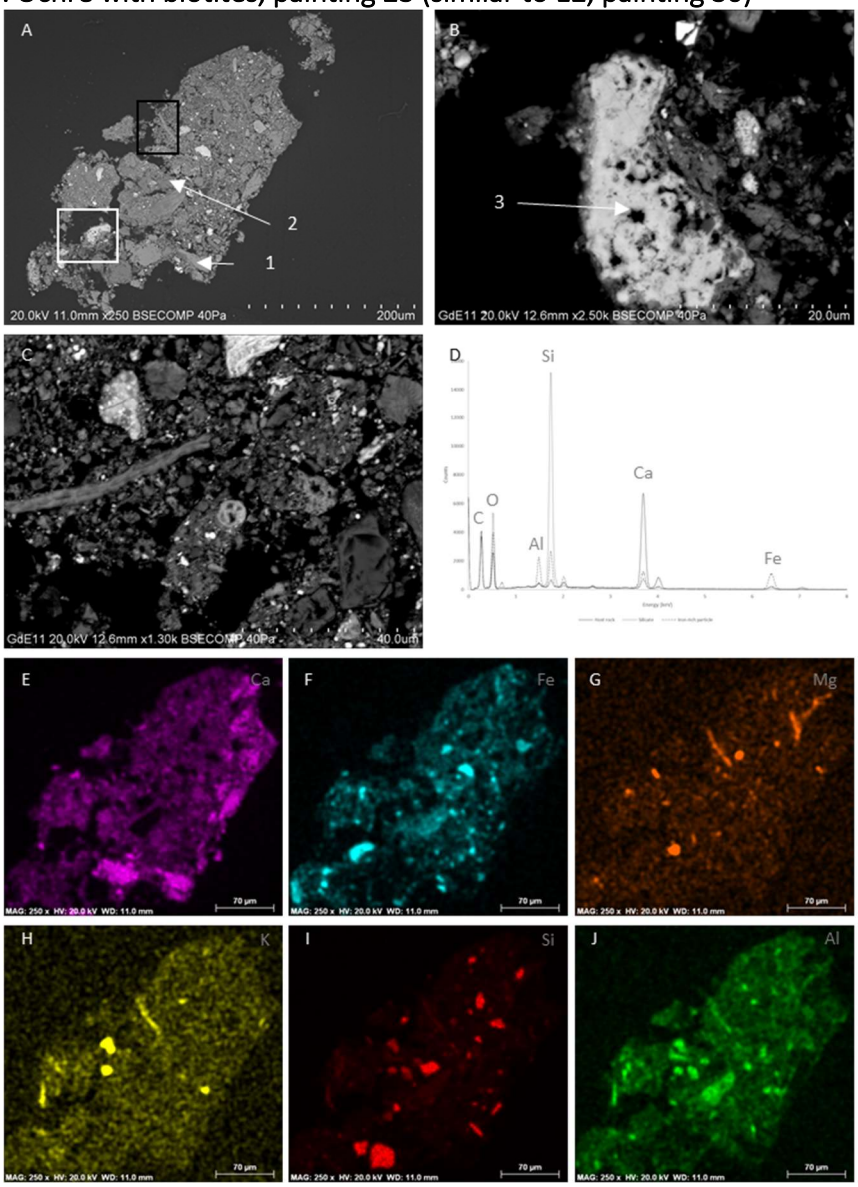

Figure 3: SEM-EDS observations and analyses of sample GdE B. A: General view of the sample's cross section. The white rectangle shows the area observed in Figure 3.B, the black one the one in Figure 3.C. The substrate of calcium carbonate appears in grey on the right, and the iron-rich particles are in white. Number 1: spot of the SEM-EDS analysis of the host rock. Number 2: spot of the SEM-EDS analysis of the silicate; B: Detailed observations of the iron-rich particle (white particle). Number 3: spot of the iron-rich particle SEM-EDS analysis; C: Unidentified features rich in manganese (grey) surrounded by clay (dark grey) and iron-rich particles (white); D: SEM-EDS spectra of spots 1, 2, and 3; E: General mapping of Ca; F: General mapping of Fe; G: General mapping of Mg; H: General mapping of K; I: General mapping of Si; J: General mapping of Al.

The sample GdE B, one of the two samples – with the sample E2 collected on the representation 30 in the gallery 1 – containing ochre with biotite, presented a clear stratigraphy with a heterogeneous pictorial layer composed of iron oxides mixed with feldspar, biotite and silicates, Figures 3.A, 3.B, 3.F-J,

and a second layer corresponding to the host rock, Figure 3.A and 3.E, composed of calcium carbonate, Figure 3.D. The feldspars were identified thanks to the combined composition of K-Al-Si, Figure 3.D, while biotite were identified thanks to their morphology and high content in Mg.

Sample E5: Ochre, drawing 72 (similar to E13, new drawing)

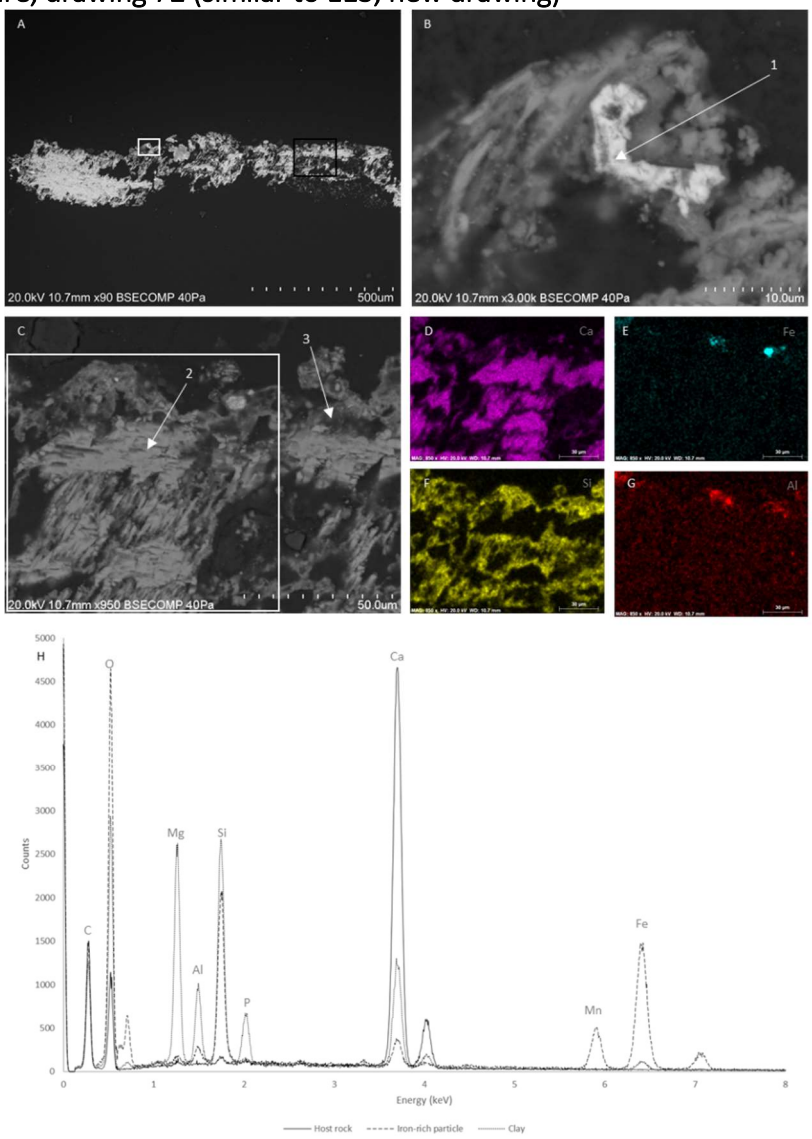

Figure 4: SEM-EDS observations and analyses of sample E5. A: General view of the sample's cross section. The white rectangle shows the area observed in Figure 5.B, the black one the one in Figure 5.B. The substrate of calcium carbonate appears in white, and the silicates are in grey; B: Detailed observations of the iron-rich particles (white)embedded in clay (grey). Number 1: spot of the iron particle's SEM-EDS analysis; C: Observation of the layer supporting the pigment. Calcium carbonate are in light grey, silicates in dark grey and iron particles in white. Number 2: spot of host rock's SEM-EDS analysis. Number 3: spot of the SEM-EDS analysis of the clay; D: General mapping of Ca; E: General mapping of Fe; F: General mapping of Si; G: General mapping of Al; H: SEM-EDS spectra of spots 1, 2, and 3.

The sample E5, one of the two samples – with the sample E13 collected on the representation recently discovered in the gallery 11 – composed of ochre with scarce iron particles, presented a clear stratigraphy with a very thin pictorial layer composed of iron oxides embedded in an Mg-rich, clay

Figures 4.A-C, 4.E-G, and a second layer corresponding to the host rock, Figure 4.A and 4.E, composed of calcium carbonate mixed with scarce traces of clay, Figure 4.C-H.

Sample E7: Ochre with apatite, painting next to representation 22

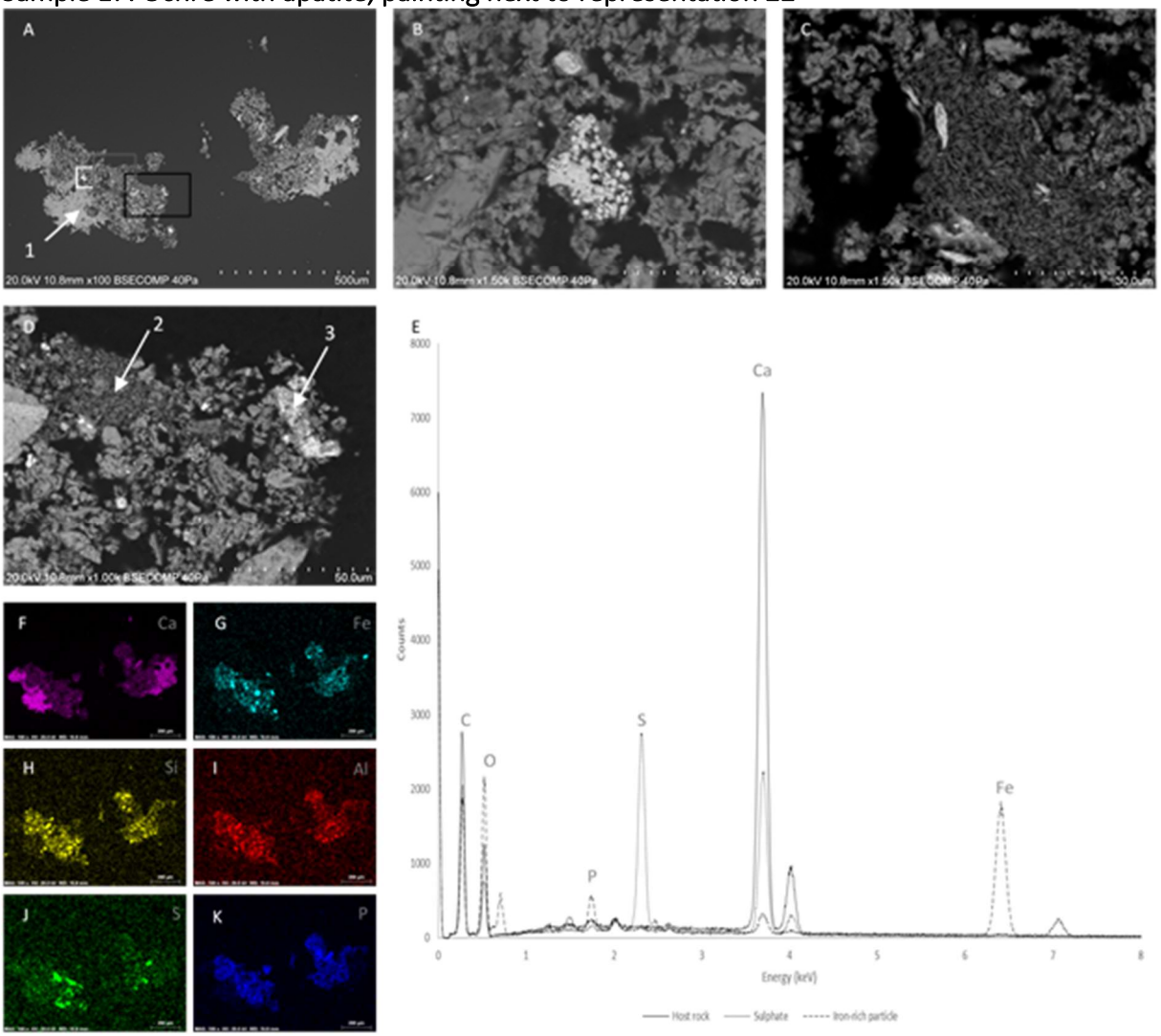

Figure 5: SEM-EDS observations and analyses of sample E7. A: General view of the sample's cross section. The white rectangle shows the area observed in Figure 5.B, the grey one the one in Figure 5.C, and the black area of Figure 5.D. The substrate of calcium carbonate appears in white, the calcium phosphates and sulphates are in a grey, and the iron-rich particles are in white. Number 1: spot of the SEM-EDS analysis of the host rock; B: Detailed observations of an iron particle (white) surrounded by calcium phosphates (grey); C: Detailed observations of an iron particle (white) surrounded by calcium sulphate (grey); D: Detailed observations of an iron particle (white) surrounded by calcium sulphate (grey). Number 2: spot of the SEM-EDS analysis of the calcium sulphate SEM-EDS. Number 3: spot of the SEM-EDS analysis of the iron particle; E: SEM-EDS spectra spots 1, 2, and 3; F: General mapping of Ca; G: General mapping of Fe; H: General mapping of Si; I: General mapping of Al; J: General mapping of S; General mapping of P.

The sample E7 was the only sample with a pictorial layer composed of iron oxides mixed with calcium phosphates and calcium sulphates, Figures 5.A-D, 5.F-K. Both could have been added as fillers to the coloured material corresponding to an altered clay containing lepidocrocite, Table 1.

Sample E11: Ochre with apatite, painting 64

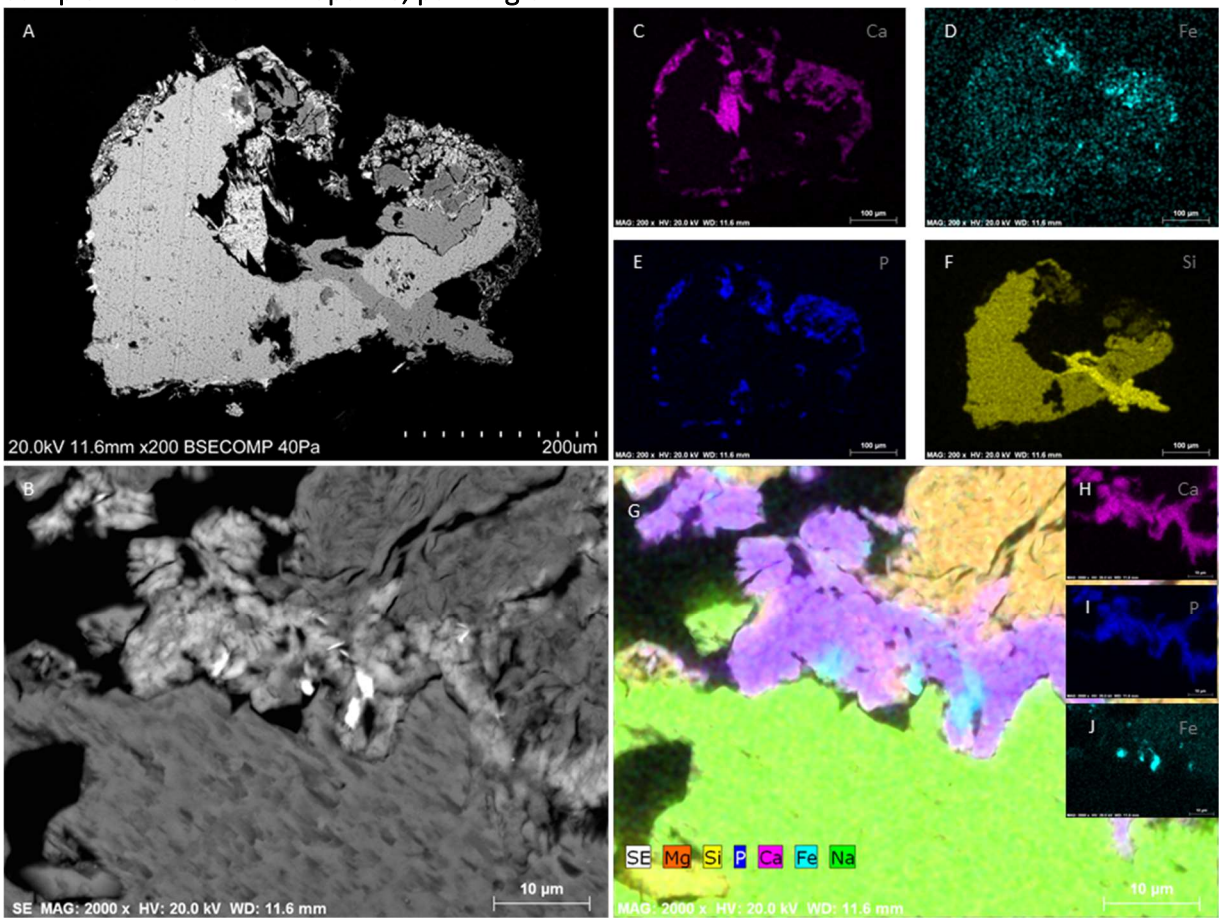

Figure 6: SEM-EDS observations and analyses of sample E11. A: General view of the sample's cross section; B: Detailed observations of the pictorial layer between two distinct clays. Both clays appear in grey, the pictorial layer composed of calcium phosphate (light grey) and iron-rich particles (white).; C General mapping of Ca; D: General mapping of Fe; E: General mapping of P; F: General mapping of Si; G: Mapping of the pictorial layer with Mg, Si, P, Ca, Fe and Na; H: Ca mapping of the pictorial layer; I: P mapping of the pictorial layer; J: Fe mapping of the pictorial layer.

The sample E11, was the only sample mainly composed of silicate support, Figures 5.A and 5.F. The observation and analysis of the pictorial layer revealed that it was embedded between two clays of different composition, Figure 5.B and 5.G-J. The pictorial layer was largely composed of iron particles embedded in a calcium phosphate matrix.

Although they present major differences, E7 and E11 were considered to be part of the same group due to the presence of calcium phosphate in the pictorial layer, indicating that both could have been manufactured in similar ways.

Table 10 Red pigments' samples from Escoural. Cal: calcite ; Hm : Hematite ; Q : quartz ; Kao : kaolinite; C: C-matter; Gy: gypsum; CaP: calcium phosphate; AC: amorphous carbon; Fl: high fluorescence preventing the ay identification; Hd: hydroxyapatite; Lp: lepidocrocite.

Sample	Location	Figure	Interpretation	Pictorial technique	Raman	FTIR	SEM						XRD	Pigments		Habits
							EDS	Size range	Mean size	Std dev	Filler	Traces		Group	Sub-group	
GdE 11	Gallery 1	29	Geometric	Painting (O)	Cal +Hm	Cal + Kao +Q	Fe +Ti	0,5 – 2,8	1,5	0,8	K-feldspar	/	Cal	Helmatite	Ti oxides	Painting (O1)
GdE 12	Gallery 1	36	Geometric	Painting (O)	Cal +Hm	Cal + Kao + C	Fe +Ti	1,4 – 16,3	5,3	3,7	K-feldspar	/	/	Hematite	Ti oxides	Painting (O1)
GdE B	Room 1	23	Geometric	Painting (F)	Cal +Hm	Cal + Kao + Gy	Fe	1,9 – 29,8	13,6	14,2	K-feldspar + biotite	Gy	/	Helmatite	Biotite	Painting (O2)
E2	Gallery 1	30	Left horse*	Painting (O)	Cal +Hm+ AC	Cal + Kao	Fe	2,2 – 56,7	10,6	9,7	K-feldspar + biotite	BaS	Cal + Hm + Q	Hematite	Biotite	Painting (O2)
E5	Gallery 11	72	Right horse head	Painting (O)	Fl	Cal + Kao +Q	Fe	0,9 - 15	4	6,2	Clay ?	CaP traces	/	Lepidocrocite	Drawing	Drawing (O)
E7	Room 1	Next 22	Unidentified	?	Fl	Cal + Kao + Gy + CaP	Fe	0,9 – 30,1	9,2	9,1	Gy + feldspar	CaP traces	Cal + Hd+ Gy	Hematite	Apatite	Painting (O3)
E11	Room 1	64	Geometric	?	Cal +Hm	Cal + Kao +Q	Fe	0,2 – 2,4	1,3	0,9	Talc + albite	CaP traces	/	Hematite	Apatite	Painting (O3)
E13	Gallery 6	New	Right ox head	?	Cal	Cal + Kao + Q	Fe	0,6 – 2,8	1,5	0,7	Clay ?	CaP traces	Cal + clay +Lp	Lepidocrocite	Drawing	Drawing (O)

Appendix 4: Observations with the Dino-Lite microscope

In situ observations carried out with the Dino-Lite digital microscope are briefly presented in this appendix. Since most of them do not provide valuable information, they were not included in the thesis. However, it seemed to be important to include them in the appendix since they provide some insights of the calcite layer covering most of the artwork of Escoural Cave. Moreover, they constitute crucial results in the development of a procedure to study rock art sites. Since the results evidence that the pieces of information collected are not valuable and that the system require to touch the wall hosting the artwork, endangering the representations, it is strongly advised to not include this system in the procedure to study rock art sites. Although some observations provided valuable information, macro-photographs proved to be less invasive and of higher value to study the pictorial technique and the homogeneity of the pictorial layers.

Furthermore, the low accessibility of some of the figures considerably reduce the interest of this technique, since it greatly endangered either the experimenter or the representation. The reader should compare the photographs presented in this appendix with the one presented in Figure 7 of the thesis (Part II Chapter 3.B, p.51) to forge his own opinion on the interest of the technique.

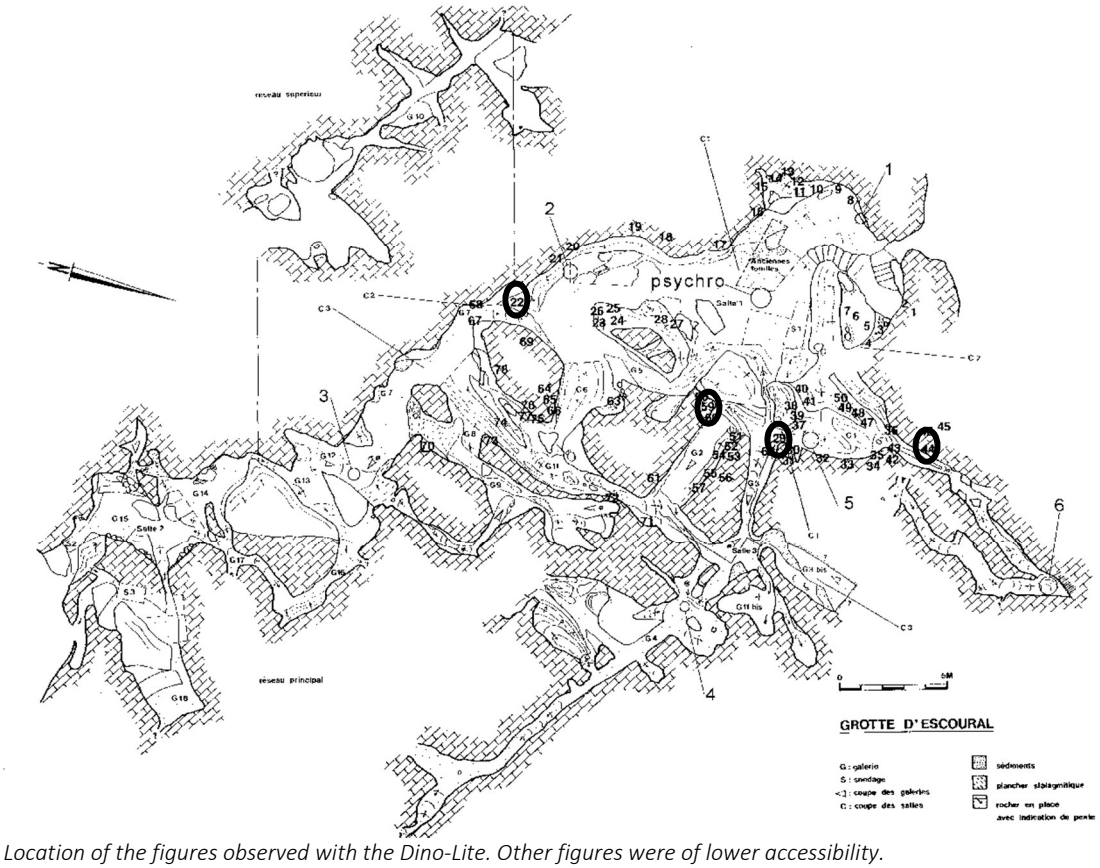

Figure 1: Location of the figures observed with the Dino-Lite. Other figures were of lower accessibility.

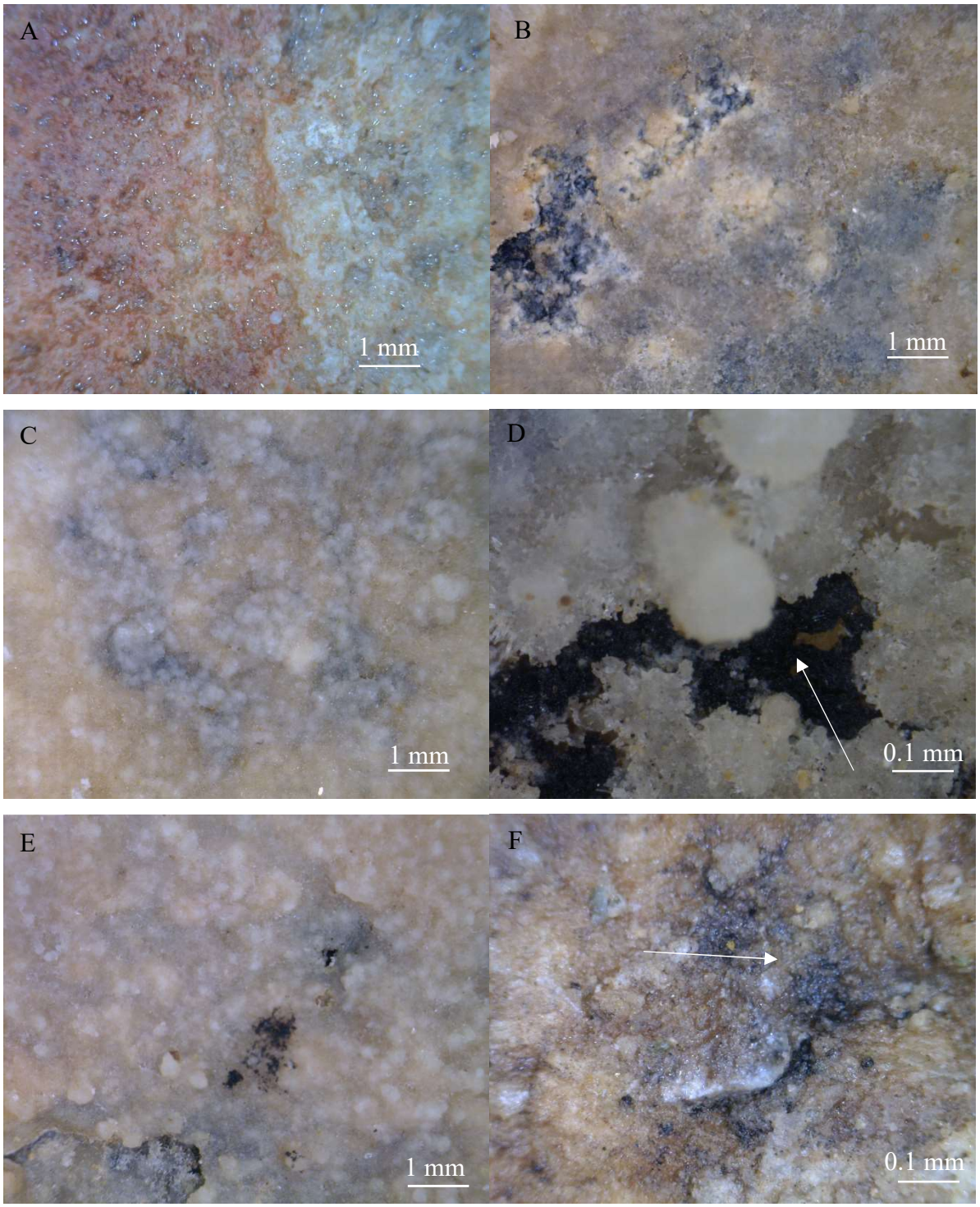

Figure 2: Observations of the pictorial techniques and state of conservation with the digital microscope. A: Observation of the clear-cut edges of figure 29. B: Observation of the figure 60 covered with a heterogeneous calcite layer, the figure might have been engraved due to the pictorial techniques. C and D: Observations of figure 22 with a calcite layer fading the pigment layer and the presence of tiny ridges (see arrow) possibly due to charcoal particles. E and F: Observations of figure 30 with different layers of pigments, some covering earlier ones, and possible ridges (see arrow) due to charcoal particles.

Appendix 5: Revision of the parietal corpus of Escoural Cave

Imaging techniques used during the thesis, infrared reflectography and visible enhancing treatment with DStretch, permitted to understand better the various panels hosting parietal art, by providing new insights about the interpretation of the figures recorded by M. Lejeune (Araujo et al., 1995).

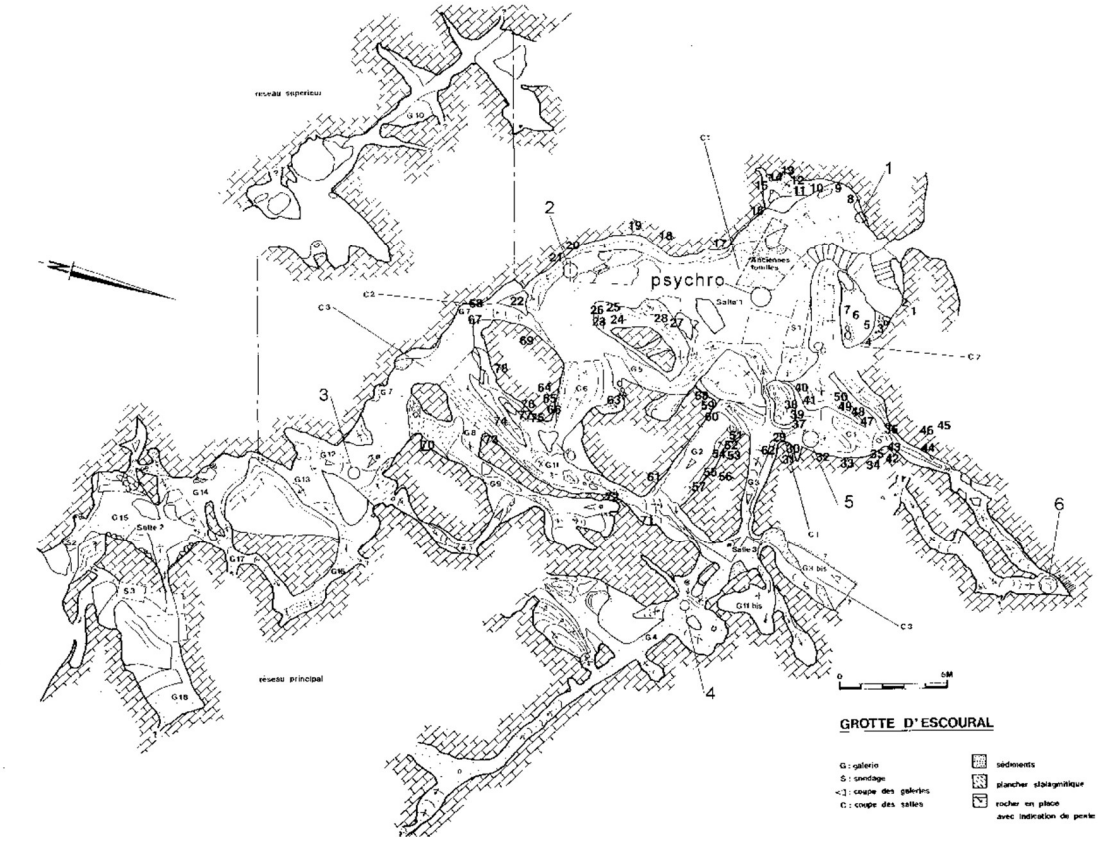

Figure1: Map of the cave with the location of the different figures recorded by M. Lejeune

Table 1 of this appendix presents the inventory of the paintings and drawings of Escoural Cave with the new interpretations performed thanks to the work carried out during the thesis. Tables 7 presented in the thesis relies on the following table. When the representations were not studied during the present study, most of the time because they could not be spotted in the cave, no interpretation of them is given.

*Table 1: Revised inventory of the parietal art figures of Escoural Cave. Localisation: S: room; G: gallery; Colour: R: red; B: black; Category: P: painting; D: drawing; Interpretations: Ge: geometric; Tc: tectiforme; P: point; D: oriented to the right; G: oriented to the left; TD: head oriented to the right; TG: head oriented to the left; J:/leg; NR: not recorded. * The interpretation of these figures is complex and need to be confirmed with other techniques. ** The ox was recorded by Farinha dos Santos but removed by M. Lejeune.*

Old reference	*New reference*	*Localisation*	*Anthropic*	*Colour*	*Category*	*Previous interpretation*	*New interpretation*
8	8	S 1 (East)	Yes	B/ R	P	Ge (Tc)	Unidentified
11	11.A	S 1 (East)	Yes	R	P	Horse (D)	Horse (D)
	11.B		Yes	R	P		Ge (P)
	11.C		Yes	R	P		Ge (P)
	11.D		Yes	R	P	NR	Horse (TD)
17	17	S 1 (East)	Yes	R	P	?	Animals?
19	19.A*	S 1 (East)	Yes	B	D	Horse (G)	Horse (G)?
	19.B*		Yes	B	D		Horse (TD)?
	19.C*		Yes	B	D		Horse (TD)?
	19.D*		?	B	D		Horse (J)?
22	22.A*	S 1 (South)	Yes	B	D	Gé	Animal (D)
	22.B*		Yes	B	D		Animal (D)
	22.C*		Yes	B	D		Unidentified
	22.D*		Yes	R	P		Animal?
	22.E*		Yes	R	P		Unidentified
23	23.A*	S 1 (North)	Yes	B	D	Hybrid (D)	Hybrid (D)
	23.B*		Yes	B	D		Horse (TG)
	23.C*		Yes	B	D		Animal (G)
	23.D*		Yes	B	D		Cheval (TD)
24	24	S 1 (North)	Yes	B	D	Bovid (G)	Bovid (G)
25	25.A	S 1 (North)	Yes	B	D	Horse (G)	Horse (G)
	25.B		Yes	R	P	Cf 28	Animal?
26	26	S 1 (North)	Yes	B/ R	P	Geometric	Bovid (F)?/Ge
28	28	S 1 (North)	Yes	R	P	Ge	Ge
29	29	G 1 (West)	Yes	R	P	Ge	Ge
30	30.A	G 1 (West)	Yes	B	D	Horse (JG)	Horse (JG)
	30.B		Yes	B	D	Unidentified	Horse (G)
	30.C		Yes	B	D	NR **	Unidentified
	30.D		Yes	R	P		Ox (TD)
	30.E		Yes	R	P	Unidentified	Horse (TG)
33	33	G 1 (West)	?	B	?	Vestiges	/
35	35.A	G 1 (West)	Yes	B	?	Unidentified	Unidentified
	35.B		Yes	R	P	Unidentified	Horse?
36	36	G 1 (North)	Yes	R	P	Ge	Ge
44	44	G 1 (East)	Yes	B	P	Horse	Horse (TD)
45	45	G 1 (East)	Yes	B	?	Unidentified	/

48	48	G 1 (East)	?	R	?	Ge	/
	56.A		Yes	R	P	Ge	Animal?
56	56.B	G 2 (North)	Yes	R	P	NR	Horse (D)
	56.C		Yes	R	P		Unidentified
	58.A		Yes	B	D	Animal	Horse (TD)
58	58.B	G 2 (South)	Yes	B	D		Unidentified
	58.C		Yes	R	P	NR	G (P)?
	59.A		Yes	B	D		Horse (TD)
	59.B		Yes	B	D		Horse (D)
59	59.C	G 2 (South)	Yes	B	D	Unidentified	Horse (D)
	59.D		Yes	B	D	animal	Horse (D)
	59.E		Yes	B	D		Ox?
	59.F		Yes	B	D		Animal
60	60.A	G 2 (South)	Yes	B	D	Animal with	Horse (D)
	60.B		Yes	B	D	horns	Horse (D)
61	61.A	G 2 (South)	Yes	B	P	G	Unidentified
	61.B		?	B	?		Horse (D)
64	64	G 6 (South)	Yes	R	P	Vestiges	/
66	66	G 6 (South)	Yes	B	D	Vestiges	/
68	68	G 7 (East)	?	R	?	G (P)	/
70	70	G 9 (West)	?	R	?	Vestiges	/
72	72.A	G 11 (West)	Yes	R	D ?	Horse (TD)?	Horse (TD)
	72.B		Yes	B	?	NR	Horse (TD)?
76	76	G 11 (East)	?	R	?	G (P)	/
77	77	G 11 (East)	?	B	?	G(P)	/
NR	79	G 6 (North)	Yes	R	P	NR	Ox (TG)
NR	80	G 1 (West)	?	B	?	NR	Humanoid?
NR	81	G 1 (West)	?	B	?	NR	Caprine?

To support the previous table, some of the images which helped to build Table 1 are presented in the following figures. For the figure 59, the reader is referred to the Figure 5 of the thesis (Part II Chapter 3.A, p. 46). Only some of the most striking figures are presented here.

Figure 8

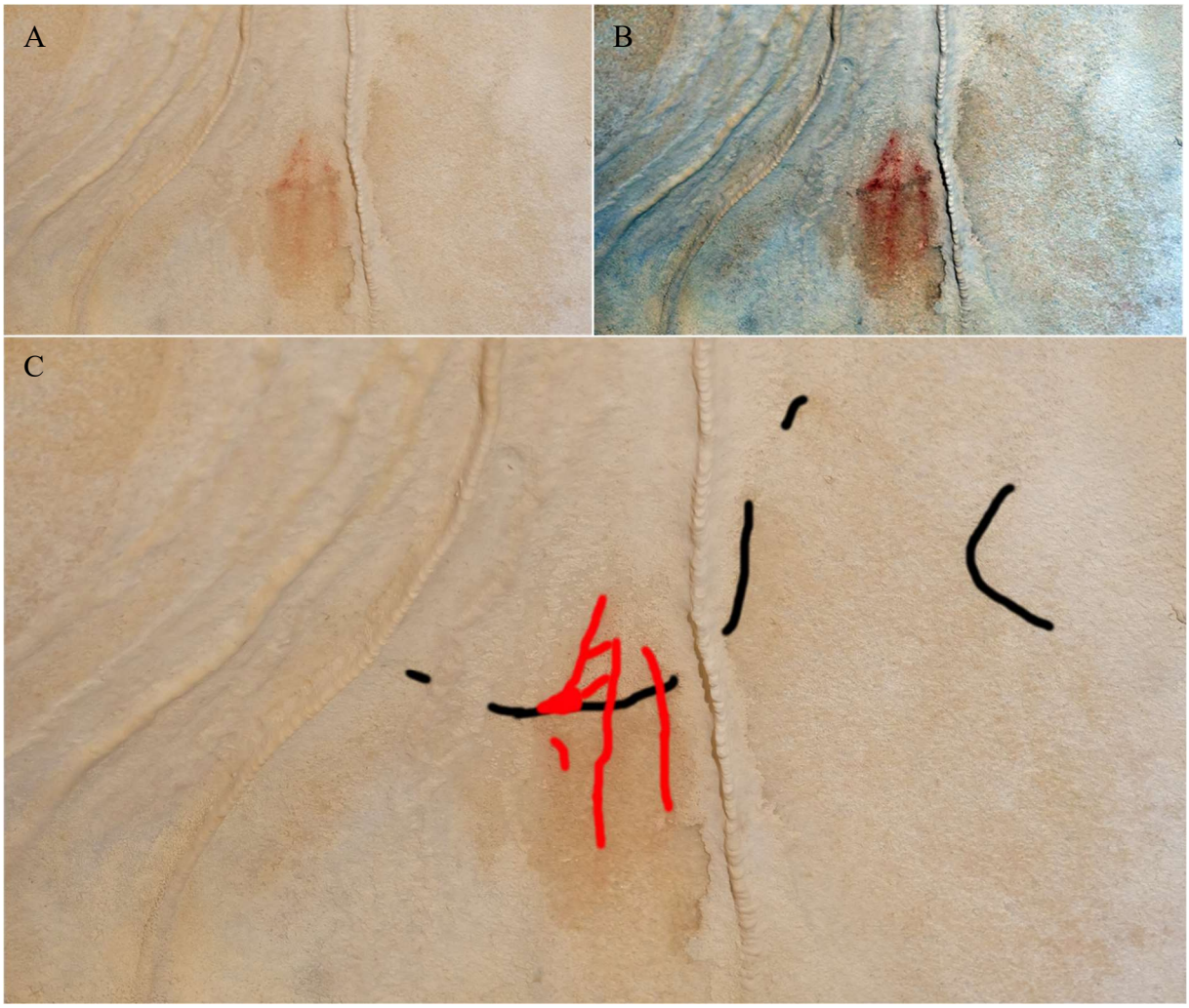

Figure 2: Attempt to provide a new interpretation of figure 8. A: Visible light photo of the figure 8 as it can be seen in the cave. B: Visible light photo of the figure 8 after treatment with DStretch (CB: colour balance). C: Interpretation of the figure 8 performed based on numerous Dstretch treatments comparison.

The figure 8 was recorded as a black and red tectiform (roof-like) geometric representations. The DStretch treatments of the visible photo tend to show the presence of black pigments the calcite veil surrounding the figure recorded. The black figure seems to form the back and neck of what could be horse. The red might corresponds to later addition in a narrative appropriation by later populations. Further investigations are needed to confirm these hypotheses.

Figure 11

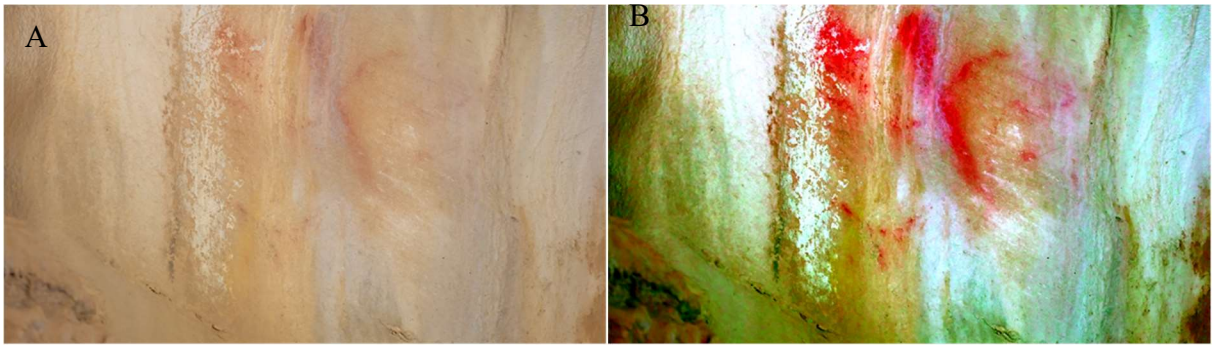

Figure 3: Interpretation of figure 11. A: Visible light photo of the figure 11. B: Visible light photo of the figure 11 after treatment with DStretch (CB: colour balance).

The figure 11 was recorded as a red horse oriented to the right. The DStretch treatments eased the reading of the figure and clearly distinguish the horse male from the two geometric figures located above the horse. As the DStretch provided a rather clear reading of the figure, it was preferred not to add some personal interpretation to not bias later reading. Some red pigments also appeared to be trapped in the calcite layer located under its head. Since no clear shape could be distinguished among these traces, it is thought that they could be imputable to the weathering of the figure.

It is here important to note that the figure 11 greatly suffered from water leaking on the wall from a crack in the ceiling. During the recent arrangement of the cave to open it to the public, a small shelter was implemented near the ceiling to avoid the water to leak on the figure.

Figure 17

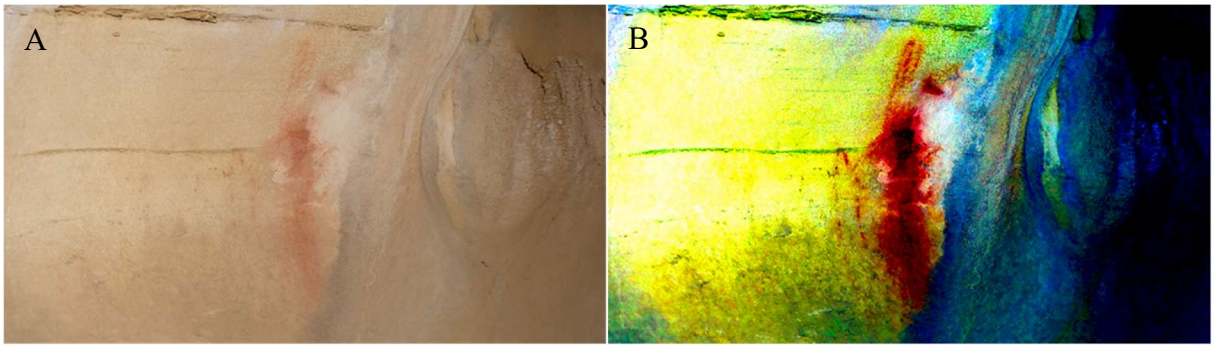

Figure 4: Interpretation of figure 17. A: Visible light photo of the figure 17. B: Visible light photo of the figure 17 after treatment with DStretch (LDS: red pigments appear in red, black ones in black blue).

The figure 17 was recorded as a red stain of unidentifiable shape. The DStretch treatments did not permit to ease the reading of the figure due to the large colour drip that altered the representation. Although two possible heads of herbivores – one on the left oriented to the left, and the other oriented at the top of the figure oriented to the right – can be spotted on the LDS Dstretch image, Figure 4.B, it

was preferred not to show any personal interpretation as the figure could easily be interpreted differently.

Figure 19

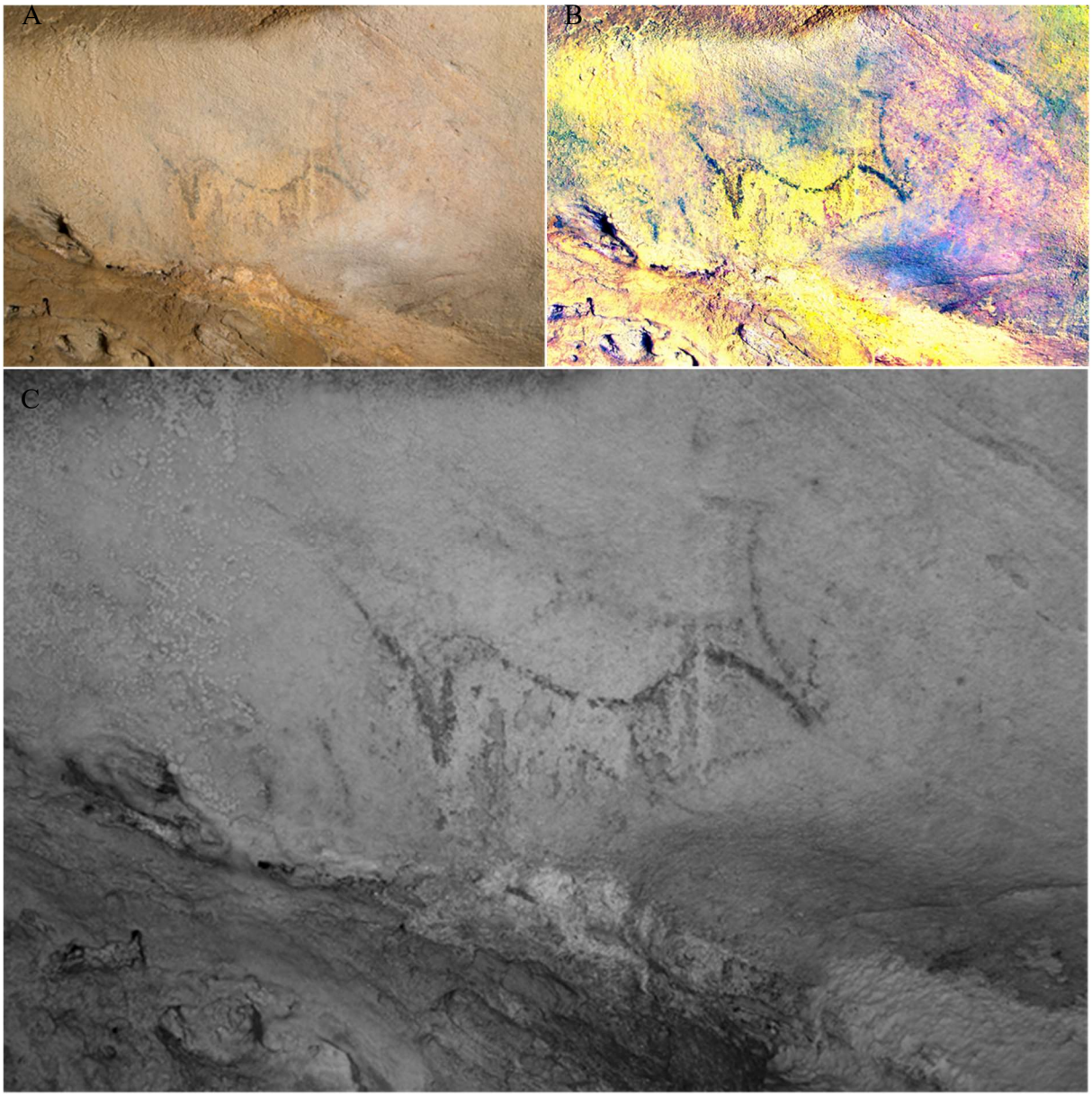

Figure 5: Interpretation of figure 19. A: Visible light photo of the figure 19. B: Visible light photo of the figure 19 after treatment with DStretch (LDS: red pigments appear in red, black ones in black blue). C: Infrared imaging of the figure 19. Different altered figures can be spotted behind the most obvious drawing.

The figure 19 was recorded as a left black horse, possibly a mare in foal. The DStretch treatments demonstrated the existence of altered former drawings. However, it was not possible to properly interpret them. The infrared imaging confirmed this conclusion and provided a better view of those altered drawings. Despite the improvement obtained with this technique, the interpretations

performed are still unsure and question to inner debates. Consequently, it is left to the reader to perform his own interpretation of the drawings spotted on this panel.

Figure 28

Figure 6: Figure 28. A: General context of figure 28. The figure 28 of M. Lejeune corresponds to all the red traces visible traces of the panel of the hybrid. B: Macrophotography of the red traces, presenting some characteristics of finger-painting.

The figure 28 registered by M. Lejeune corresponds to several unidentifiable red traces.

Figure 30

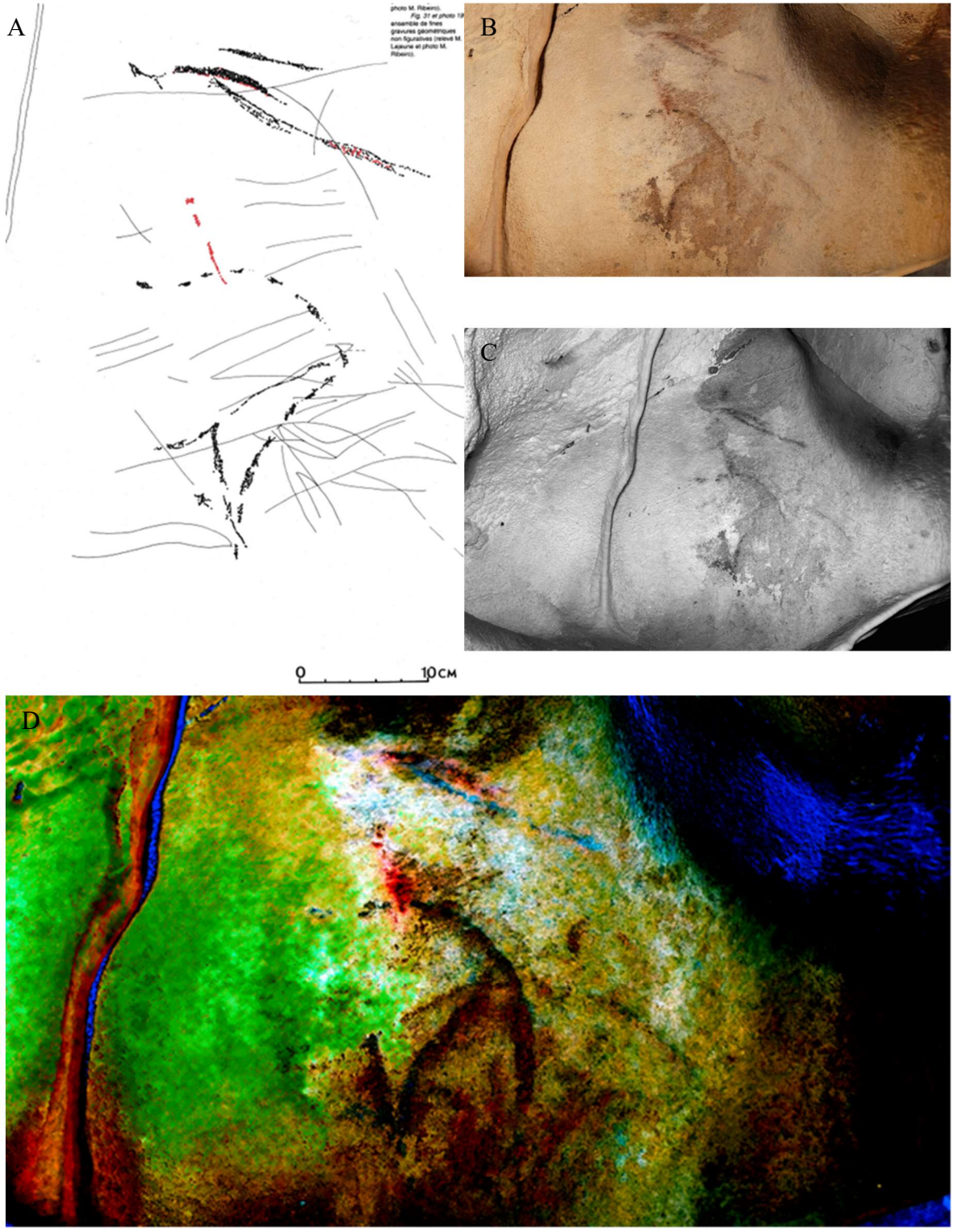

Figure 7: Interpretation of figure 30. A: The figure 30 as it was recorded by the belgo-lusitanian team lead by M. Lejeune. B: Visible light photo of the figure 30. C: Infrared imaging of the figure 30. D: Visible light photo of the figure 30 after treatment with DStretch (combination of several treated layers).

The figure 30 was recorded as being made of different parts: the back legs of a black left horse, and unidentified red and black traces. The DStretch treatments were the most efficient to understand the panel. Indeed, the upper traces were interpreted as a black left horse and a red left horse. It also

permitted to highlight the presence of a red-blackish ox in the lower part of the panel, Figure 6.D Other traces were spotted in the lower part of the panel but could not be interpreted, therefore they are not shown here.

Figure 44

Figure 8: Interpretation of figure 44. A: Visible light photo of the figure 44. B: Visible light photo of the figure 44 after treatment with DStretch (combination of several treated layers). C: Infrared imaging of the figure 44.

The interpretation of the figure 44 has for long been subject to debate. Indeed, it has been seen as a right black horse's head or right black ox' head. Both IR and DStretch treatments confirmed the hypothesis of a right black horse's head. They even confirmed the presence of the neck. This last appears to be extremely altered and seems to remain mostly as an engraving, Figure 8.C.

Figure 56

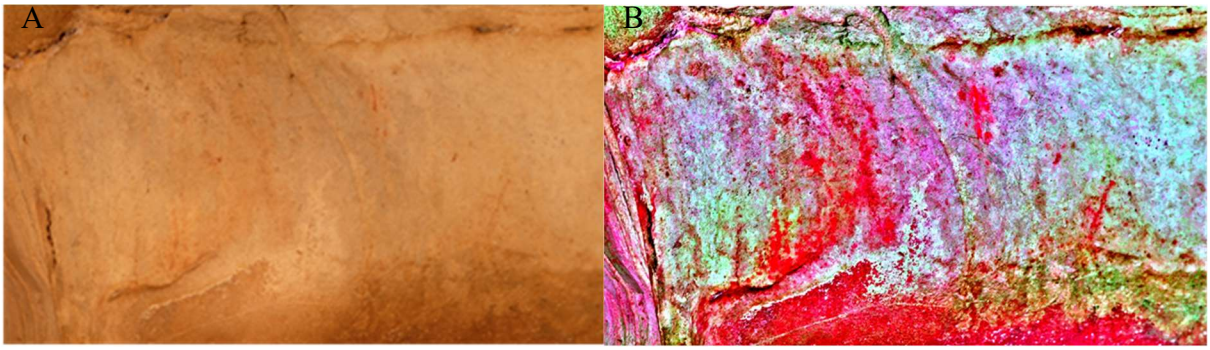

Figure 9: Interpretation of figure 56. A: Visible light photo of the panel the traces recorded as being figure 56. B: Visible light photo of the figure 56 after treatment with DStretch (combination of several treated layers).

The figure 56 was recorded as red unidentifiable traces over the left panel of the gallery 2. The DStretch treatment permitted to spot the presence of a red right horse, right lower part of the panel, Figure 9.B. Other traces were also spotted over the panel but could not be identified due to their scarce amount.

Figure 60

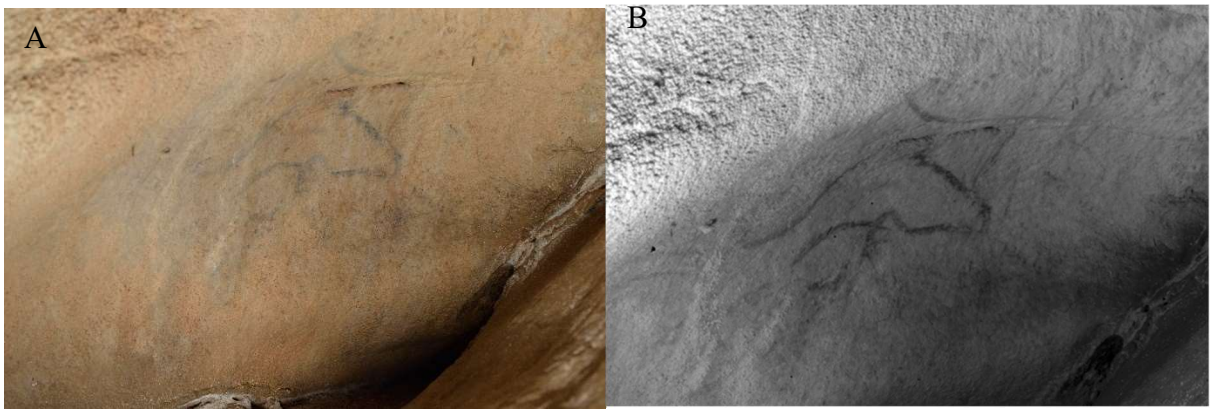

Figure 10: Interpretation of figure 60. A: Visible light photo of the panel the traces recorded as being figure 30. B: Infrared imaging of the figure 60.

The figure 60 was recorded as a right black horse. Although the DStretch treatments did not permit to improve the interpretations of the figure, the IR images provided some crucial new insights. Indeed, it appeared that the figure was composed of at least two distinct complete right black horses, Figure 10.B. It is even thought that the figure actually hosts fours right black horses.

Figure 61

Figure 11: The figure 61. A: General context of the figure 61, two sets of black lines can be spotted one on the left (see B) and one on the right, extremely scarce. The second line could not be identified and is here considered to be of natural origin. B: Close up on figure 61. C: Visible light photo of the figure 61 after treatment with DStretch (combination of several treated layers).

The figure 61 was recorded by M. Lejeune as black traces possibly corresponding to a right animal, possibly some herbivores. The observations performed in the cave and the treatments of the visible pictures did not permit to clarify the reading of this representation. However, it is thought to be the combination of several extremely altered small animals heading to the right.

Figure 79

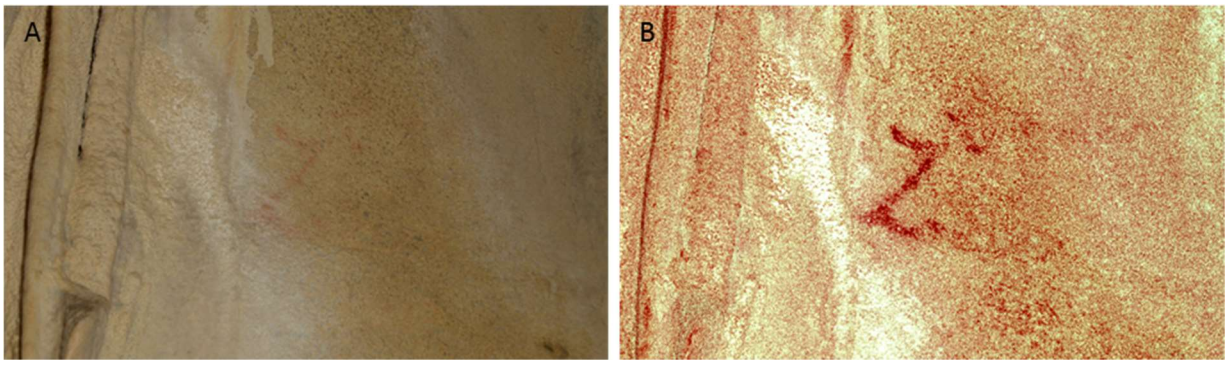

Figure 12: Interpretation of figure 79. A: Visible light photo of the panel the traces recorded as being figure 79. B: D-Stretch treatment of the visible light photo.

The figure 79 was not recorded by the belgo-lusitanian team. It was spotted rather recently and was analysed during this thesis. Although, it faints behind a thin layer of calcite, making its observation arduous and explaining that it was not recorded before, DStretch treatments permitted to provide a clear view of the representation. It corresponds to a red left ox, Figure 12.B.

Figure 80

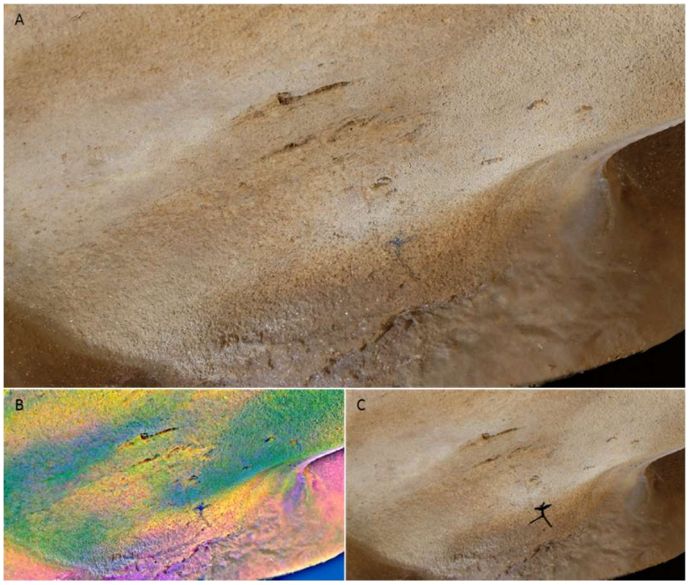

Figure 13: Possible detection of a figure 80. A: Visible light photo of the panel the traces recorded as being figure 80. B: D-Stretch treatment of the visible light photo.C: Interpretation reported on the visible light photo.

As for the figure 81, the real existence of figure 80 is still to be confirmed. Therefore, the reader is kindly asked to build up his own mind on the figures 80 and 81. Both should be further investigated to confirm the presence or not of a small anthropic representation, Figure 13.C, and a kneeling caprine, Figure 14.C

Figure 81

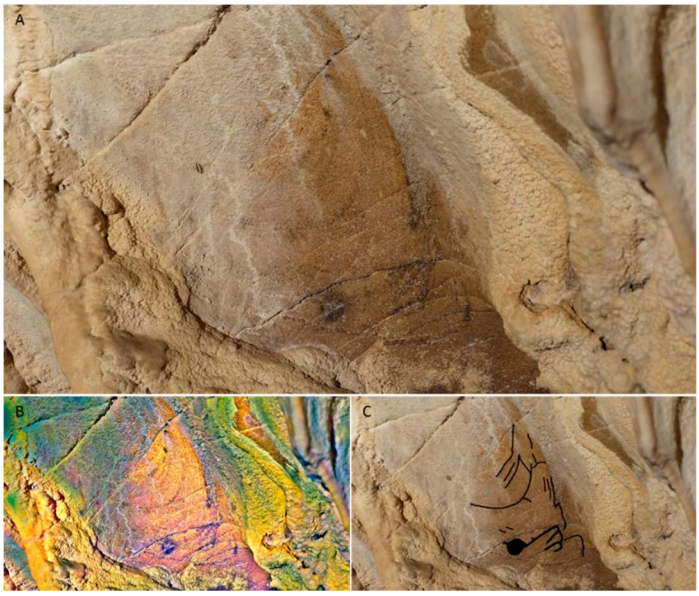

Figure 14: Possible detection of a figure 81. A: Visible light photo of the panel the traces recorded as being figure 81. B: D-Stretch treatment of the visible light photo.C: Interpretation reported on the visible light photo.

Appendix 6: *In situ* XRF analyses

The following figure and table, Figure 1 and Table 1 of this appendix, present the results obtained with the *in situ* XRD analyses on the most accessible artworks of the cave. Once recorded the spectra were all compared to the spectrum of the host rock and the elements identified in each spectrum were quantified in a semi-quantitative way. As the following results did not permit to properly distinguish the pigments, it was decided to not perform XRF analysis on all the representations of the site. As it can be seen the signal from the host-rock is strong and probably prevents the detection of trace elements.

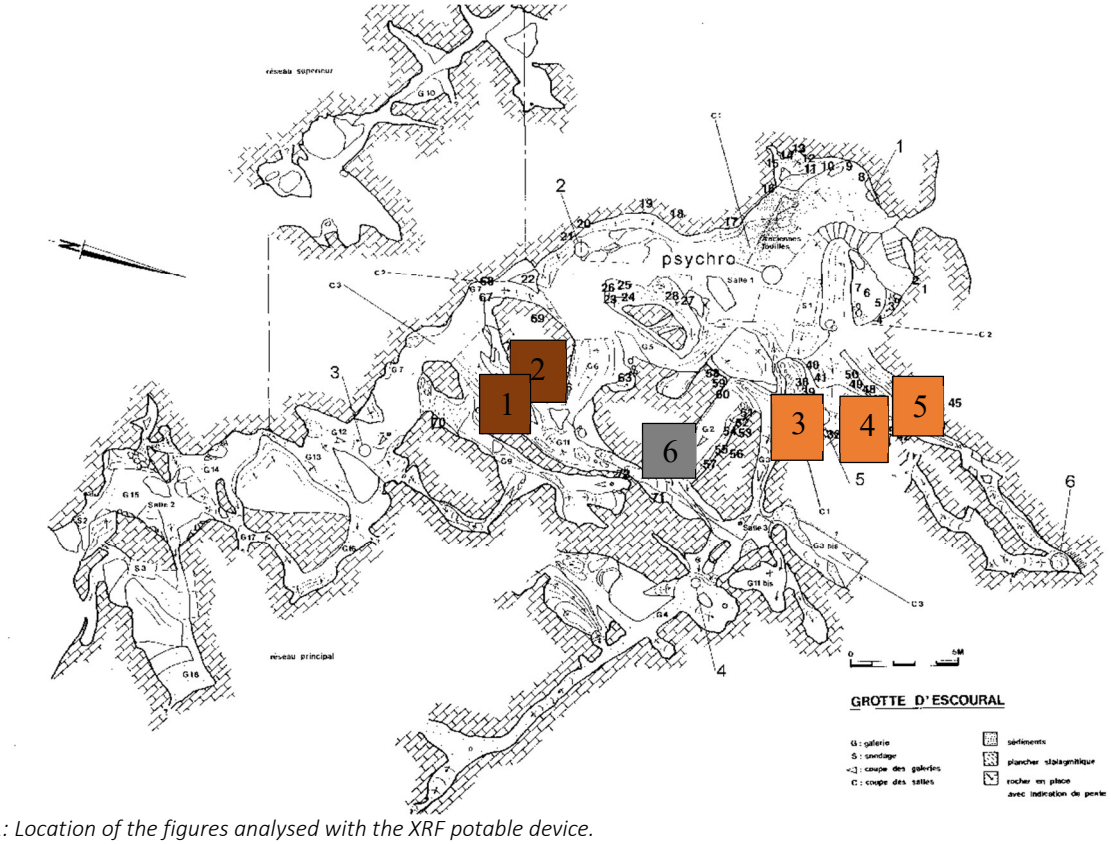

Figure 1: Location of the figures analysed with the XRF potable device.

Table 1: Semi-quantitative XRF analyses of the figures mentioned above.

Analysis	*Colour*	*Location*	*Al*	*Si*	*P*	*S*	*K*	*Ca*	*Ti*	*Mn*	*Fe*	*Sr*	*Cu*	*Zn*	*Zr*
Test 1	Background	1	T	T	T	T	-	5	T	-	1	T	T	T	-
Pint1 preto	Black	1	-	T	T	T	-	5	T	-	T	T	T	-	-
Ibrido preto	Black	2	T	T	T	T	-	5	T	-	T	T-	T	-	-
Ibrido red	Red	2	-	T	T	T	T	5	1	1	3	T	T	-	T
Geometric 1	Red	3	-	-	T	T	T	5	T	T	3	T	T	-	-
Geometric 3	Red	3	-	-	-	T	T	5	T	-	1	T	T+	-	-
Escada bck	Background	4	-	-	T	T	-	5	T	T	1	T	-	-	-
Escada 1	Red	4	-	-	T	T	-	5	T	T+	2	T	T	T	T
Diverticulo	Red	5	T	T	T	T	-	5	T+	T	2	T	T	T	T
Gallery	Black	6	-	-	T	T-	-	5	T	2	2	T	T	T	-

Appendix 7: Spectroscopic analyses of the pigments' samples of Escoural.

The different compounds that were identified with the Raman and Infrared techniques are listed in the two tables below. Table 1 presents the Raman characteristic bands identifies and Table 2 the infrared ones.

Table 1: Raman bands of the different compounds detected on the pigments' samples of Escoural.

Raman (cm^{-1})		Attribution	References
References	Present work		
1300-1390	1360	Amorphous carbon: D1 band (A_{1g})	Coccato et al. 2015
1550-1620	1550	Amorphous carbon: G (E_{2g2}, E_{2g}) and D2 band (oxidised sp^2 carbon, imperfect graphite)	Coccato et al. 2015
961 but not always detected	-	Bone black: phosphate	Edwards et al. 2000 Coccato et al. 2015
225, 245, 292, 409, 497, 608, 658, 1314	297, 415, 609	Hematite	Pigeaud et al. 2011 Tournié et al. 2010 Edwards et al. 2000 Prinsloo et al. 2008
152, 280, 712, 1086	154, 282, 712, 1086	Calcite	Pigeaud et al. 2011 Edwards et al. 1998 Edwards et al. 2000
580, 650	650-680	Manganese oxides	Lahlil et al. 2012

Table 2: Infrared bands of the different compounds detected on the pigments' samples of Escoural.

Infrared (cm^{-1})		Attribution	References
References	Present work		
600, 1024	600, 1024	PO_4^{3-} hydroxyapatite	Alvarez-Lloret et al. 2006 Figueiredo et al. 2012
870, 1401	870,1401	CO_3^{2-} hydroxyapatite	Alvarez-Lloret et al. 2006 Figueiredo et al. 2012
712, 870, 1410, 1795, 2550, 2860, 2960	712, 870, 1410, 1795, 2550, 2860, 2960	Calcite	Chukanov
799	796	Quartz	Chukanov
3697, 3669, 3652, 3620	3653, 3686, 3698	Kaolinite	Chukanov
> 600	-	Manganese oxides	Chukanov

Appendix 8: Spatial Repartition of the pigments' preparation in Escoural Cave

The apparent scarcity of the parietal artwork could have supposed the existence of few occupation phases with few distinct preparations supported by a specific spatial distribution of the pictorial material used to perform the paintings and drawings of the site. The following figures, Figures 1 and 2 of this appendix, present the spatial distribution of the distinct materials and preparations identified and detailed in Table 1 of Appendix 2 and 3. Conclusions are included in Part II Chapter3.C of the thesis.
Although some particularities seem to appear for the black pigments, with four to five distinct visits of the cave, it seems that there is no evident spatial distribution of the materials used to perform the various representations. It tends to support the hypothesis of long and discontinuous occupation phases of the site leading to a complex corpus.

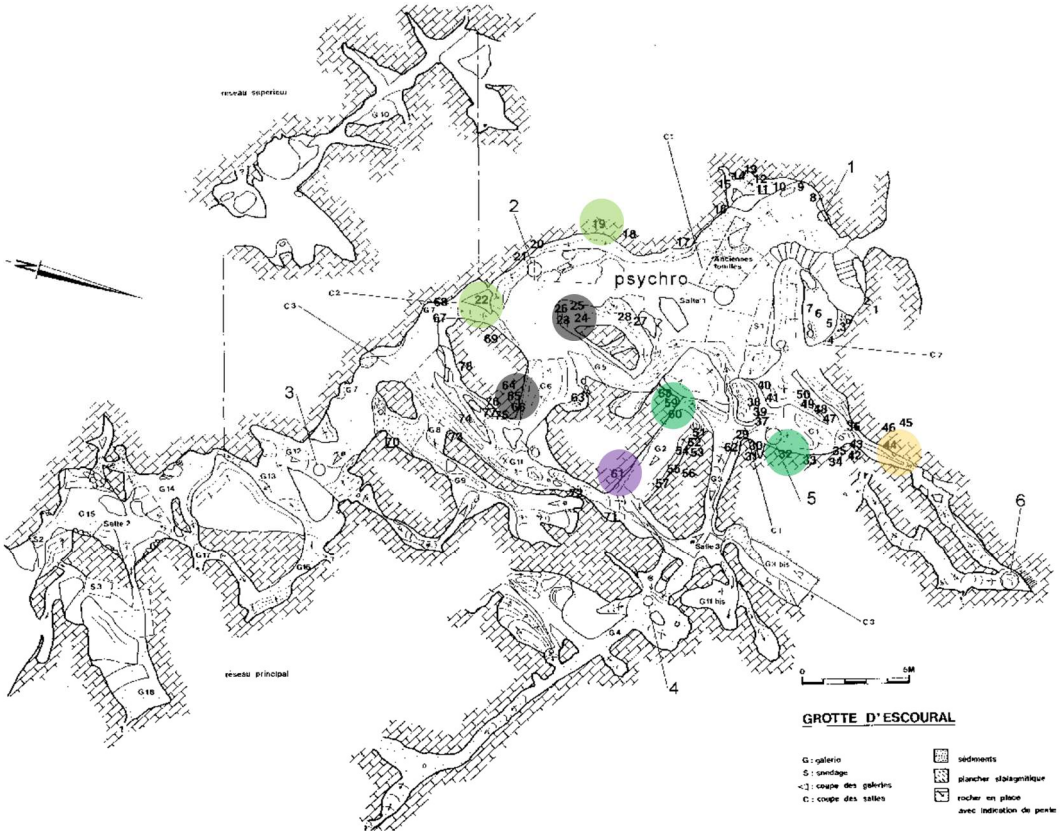

Figure 1: Spatial distribution of the distinct pictorial materials used to perform the black representations. Purple: Manganese oxides; Yellow: Bone black only; Black: charcoals with large particles, Light green: charcoals with small particles and traces of bone black; Green: charcoals with small particles and traces of iron oxides.

The spatial distribution of the black pigments, Figure 1, highlights the presence of "marginal" pigments for the cave in the most remote parts of the cavity, supporting their occasional use. Due to the relative spatial coherence of the groups of charcoals' drawings, it seems that each of these three groups can be distinguished and correspond to drawings performed during a same period. Therefore, between four

and five phases can be distinguished among the black pigments. Two of the black pigments' groups, the ones of charcoal's small particles, correspond to a reuse of pre-existing figures, making possible to identify two distinct phases: the one of the earlier figures and the one of the charcoal drawings. Indeed, the two groups were identified thanks to traces attributed to previous figures, therefore they might have been performed at the same time. Therefore, four distinct materials were spotted, leading to a minimum number of four distinct individuals and probably visits.

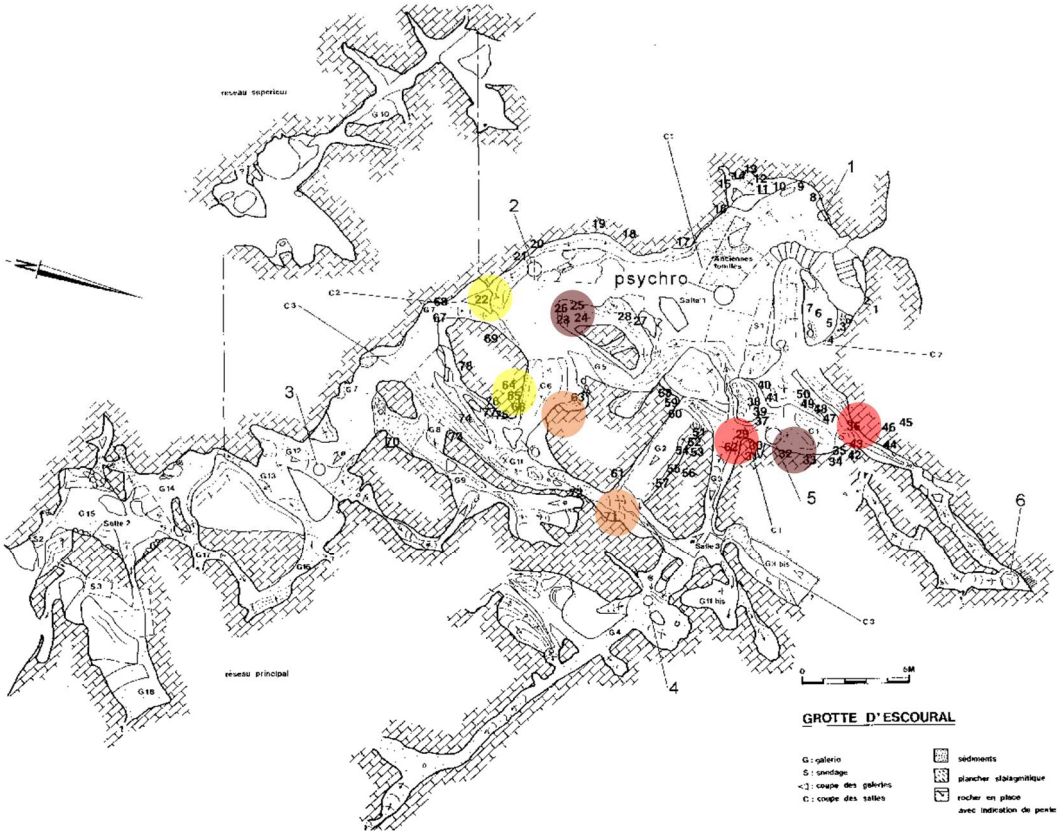

Figure 2: Spatial distribution of the distinct black pictorial materials used to perform the red representations. Light red: ochre with biotite; Dark red: ochre with Ti-oxides; Yellow: Ochre with traces of calcium phosphate and apatite; Orange: ochre drawings.

The spatial distribution of the red pigments, Figure 2, highlights the presence of ochres were used in various locations with no direct link between the panels they were found on. Indeed, only the ochres with traces of calcium phosphate and apatite was found to be attributable to a coherent work area for an individual. The other groups do not present this coherence and are found in diverse parts of the cave. It tends to support the idea that the cave was visited several time by diverse communities.

Stylistic considerations and dating of the calcite layers should provide valuable information to comprehend the spatial distributions presented in this appendix. Both are currently being performed and compared to the results presented in the thesis.

It has to be noted that the present study does not include the figures that were detected in the present study. It also does not ensure the homogeneity of the materials used on a same panel. Further studies

will have to focus on these two points to provide a better comprehension of the various occupation phases and their impact on the parietal corpus of Escoural Cave.

Appendix 9: Diversity of the communities thriving in Escoural

As a large diversity of organisms, living and thriving inside the cave, were spotted during the different visits of the cave, the present appendix sums up all of them. The reader is referred to the Figure 13 of the thesis (Part IV Chapter 1, p. 88) to see some of the organisms described in Table 1. It also presents some complementary SEM observations of the samples from the cave to illustrate the large diversity of the communities thriving in Escoural, Figure 1.

Table 1: Organisms spotted inside the cave of Escoural.

Organism	Date	Number	Location	Observation
Bat	01/04/2016	1	Gallery 1	Disturb by the visit the bat moved to another part of the cave.
	27/05/2016	1	Gallery 1	
Butterfly	20/07/2016	1	Room 1	Corpse of a dead butterfly was discovered in Room 1 just before entering the gallery 1.
Roots	Every visit	Numerous	All the cave	The extent of the roots changed from one visit to another in the Room 1, in other location they remain the same at every visit.
Plants	Every visit	Numerous	Room 1	The extent of the plants changed from one visit to another.
Fungi	27/05/2016	Numerous	All the cave	A large fungal contamination spread all over the cave and colonised all king of support but rapidly disappeared leaving no trace of it a month later.
Mushroom	01/04/2016	1	Gallery 1	The two first mushrooms were spotted almost on the same spot. The last three ones observed during the last visit were located on the opposite wall than the other two. All of them looked similar.
	27/05/2016	1	Gallery 1	
	20/07/2016	3	Gallery 1	

All of these organisms described in Table 1 provide nutrients for the development of microorganisms which cannot be observed on the site, though can be observed with SEM. The images presented in the Figure 1 of this appendix complement the ones of Figure 12 of the thesis (Part III Chapter 1.C, p.81) and Figure 1 of Appendix 13.

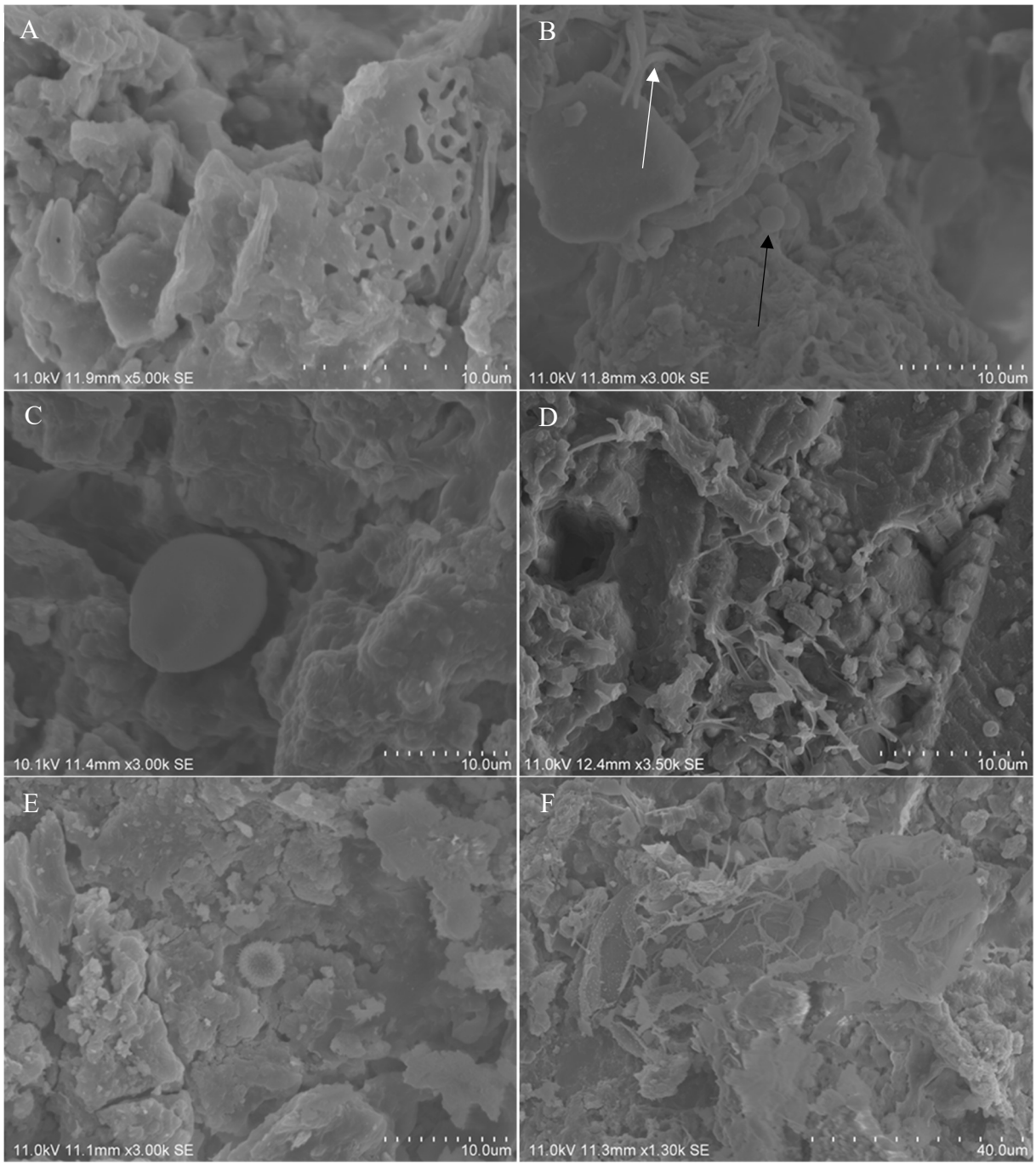

Figure 1: SEM observations of gold-coated samples from the cave of Escoural evidencing the presence of a large diversity of the communities thriving inside the cave. A: Biofilm covering the rock evidencing the presence of microbial populations, sample GdE 3; B: Bacterial (black arrow) and fungal (white arrow) populations, sample GdE 3; C: Spore, probably of a fungal strain, sample GdE 5''''; D: Fungal mycelia and biofilm colonising the rock, sample GdE 14; E: Unidentified microorganism sharing some common characteristics with some Archae, sample GdE 5''''; F: Corpse of a micro-insect used as a source of nutrient by fungal populations, sample GdE 5''''.

Appendix 10: The microbial diversity of Escoural: a culture-dependent technique

The study of the microbial diversity of Escoural Cave relied on 32 samples from inside and outside of the cavity. From these samples, 5 were collected outside of the cave to provide some insights of the microbial populations thriving just outside of the hypogean site, and 27 inside the cavity.

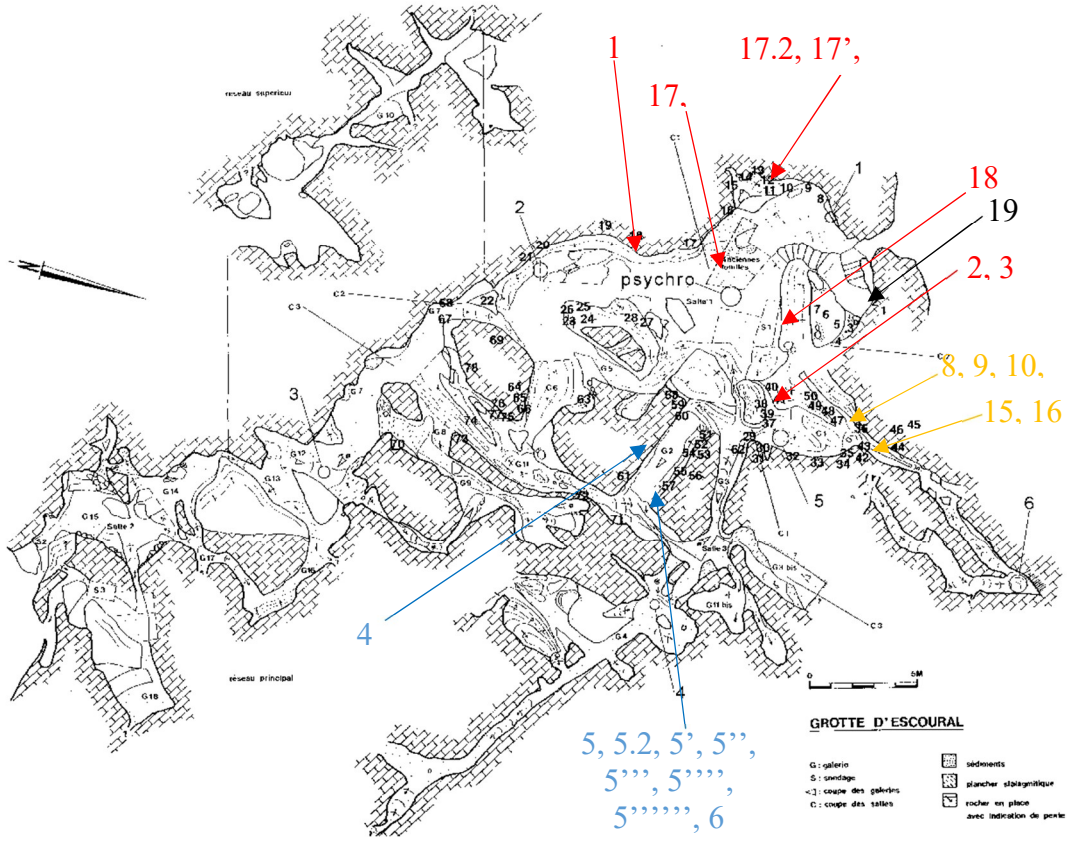

Figure 1: Location of the samples collected to study the microbial diversity of the site. Red: samples from the group room 1; Yellow: samples from the group gallery 1; Blue: samples from the group gallery 2; Black: sample located near the entrance.

Due to the number of samples collected and to their distribution in the cave, it was considered that comparing the samples between them was not really valuable. Therefore, the different samples were grouped in five different groups according to their location (Figure 1): outside of the cave, gallery 1, gallery 2, room 1 and near the entrance.

The different strains isolated were then counted for each sample and permitted to dress the two tables presenting the abundance of the different microbial strains according to the different parts of the site, Tables 1 and 2. A column containing the total number of different strains isolated from the inside was

include, summarizing the sum of the different strains from the four sampling groups. To facilitate the comparison between the microbial contamination from the inside and the outside of the cave. The two tables presented here permitted to build the Figure 16 of the thesis (Part IV Chapter 1.C, p. 93).

Table 1: Abundance of the bacterial strains isolated in the cave.

			Inside			**Outside**	**Total**
							inside+outside
Strain	Room 1	Gallery 1	Gallery 2	Entrance	$Total_{inside}$	$Total_{outside}$	
b1a	12	7	0	0	19	0	**19**
b1d	0	106	0	0	106	0	**106**
b2b	800	326	600	0	1726	100	**1826**
b2c	200	200	0	0	400	0	**400**
b2d	0	22	0	0	22	0	**22**
b3c	0	82	104	0	186	6	**192**
b4a	600	500	1000	100	2200	500	**2700**
b4b	205	104	100	100	509	0	**509**
b5a	100	0	0	0	100	0	**100**
b5b	0	0	100	0	100	0	**100**
b6a	100	0	100	0	200	0	**200**
b6b	0	0	5	0	5	0	**5**
b6d	23	23	100	0	146	4	**150**
b6e	0	200	7	0	207	0	**207**
b8a	0	100	0	100	200	400	**600**
b10	102	300	0	0	402	100	**502**
b12	0	100	0	0	100	0	**100**
b13b	0	0	100	0	100	100	**200**
b14	7	0	0	100	107	0	**107**
b15	5	0	120	100	128	100	**228**
b16b	2	0	0	0	2	0	**2**
b18	119	0	0	0	119	0	**119**
Total	**2275**	**2070**	**2336**	**500**	**7084**	**1310**	**8394**

*Table 2: Abundance of the fungal strains isolated in the cave. * Strains with no genus were not successfully identified.*

Strain	Genus	Room 1	Gallery 1	Gallery 2	Outside	Inside	Total
F1a	*Mucor*	10	1	131	0	142	**142**
F1b	*Trichoderma*	2	0	1	1	3	**4**
F1c	*Aspergillus*	1	0	4	0	5	**5**
F2a	*Penicillium*	27	22	7	0	56	**56**
F2d	*Penicillium*	5	0	20	1	25	**26**
F2e	*Aspergillus*	3	62	1	0	66	**66**
F2f	*Penicillium*	1	8	4	0	13	**13**
F3a	*Aspergillus*	9	0	1	0	10	**10**
F3b	*Aspergillus*	1	4	1	0	6	**6**
F3c	*	0	0	21	0	21	**21**
F4	*	1	0	0	0	1	**1**
F5a	*Mucor*	1	0	0	0	1	**1**
F5b	*Trichoderma*	4	0	0	0	4	**4**
F6b	*	0	2	0	0	2	**2**

F6f	*Cladosporium*	0	39	9	1	48	**49**
F6g	*Aspergillus*	0	0	1	0	1	**1**
F7	*Penicillium*	0	0	17	0	17	**17**
F8	*Aspergillus*	0	3	0	3	3	**6**
F9a	*Mucor*	0	5	0	0	5	**5**
F9b	*Acremonium*	0	1	0	0	1	**1**
F9c	*	0	1	0	0	1	**1**
F10	*Penicillium*	1	0	0	0	1	**1**
F11	*Penicillium*	1	0	0	0	1	**1**
F12a	*	0	0	0	2	0	**2**
F12b	*	0	0	0	6	0	**6**
F13	*Mucor*	0	0	0	2	0	**2**
F14	*Cladosporium*	0	0	2	2	2	**4**
F15	*Mucor*	1	0	5	1	6	**7**
F17	*Penicillium*	0	0	2	12	2	**14**
F18	*Cladosporium*	0	0	0	4	0	**4**
F19	*Mucor*	0	0	0	1	0	**1**
F20a	*Acremonium*	0	1	0	0	1	**1**
F20b	*Mucor*	0	0	0	2	0	**2**
F21a	*	0	5	0	0	5	**5**
F21b	*	0	0	2	2	2	**4**
F22	*	0	0	0	1	0	**1**
F23	*Penicillium*	3	0	1	0	4	**4**
F24a	*Fusarium*	1	0	1	0	2	**2**
F24b	*	5	0	1	0	6	**6**
F25	*Fusarium*	3	0	0	0	3	**3**
F26a	*Penicillium*	3	6	0	0	9	**9**
F26b	*Penicillium*	1	0	0	0	1	**1**
F26c	*Fusarium*	0	0	1	0	1	**1**
F27a	*Penicillium*	1	0	0	0	1	**1**
F27c	*Penicillium*	0	0	1	0	1	**1**
F28a	*Unknown*	1	0	0	0	1	**1**
F28b	*Mucor*	1	0	1	0	2	**2**
F29	*Mucor*	1	0	0	0	1	**1**
F31	*Fusarium*	1	0	3	0	4	**4**
F32	*Penicillium*	1	0	11	0	12	**12**
F33	*Cladosporium*	7	0	0	0	7	**7**
F34	*Penicillium*	2	0	0	0	2	**2**
F35	*Penicillium*	1	0	0	0	1	**1**
F36	*	0	0	1	0	1	**1**
F37	*Penicillium*	0	0	1	0	1	**1**
F38	*Penicillium*	0	0	1	0	1	**1**
F39	*Penicillium*	1	0	0	0	1	**1**
F43	*Aspergillus*	0	0	5	0	5	**5**
F44	*Unknown*	0	1	0	0	1	**1**
F45	*Absidia*	0	2	1	0	3	**3**
F46	*Penicillium*	0	0	1	0	1	**1**
F48	*Penicillium*	0	0	4	0	4	**4**
	Total	**101**	**163**	**263**	**41**	**527**	**568**

Appendix 11: NGS analysis of microbial communities in Escoural Cave

To study the biodiversity and have a full overview of the microbial populations thriving inside the cave of Escoural, Next Generation Sequencing (NGS) analyses were performed. The present appendix describes the methods and results of that procedure.

The three samples, GdE 3, GdE 16, and GdE 17 were collected as described in the thesis with a sterile scalpel and stored at 4°C in a sterile micro-tube. They were chosen for their high potential diversity of microbial contamination, reported in Table 1 of the present appendix. The location of the samples inside the cave can be seen on Figure 1 of appendix 10.

Table 1: Brief description of the samples sent for NGS analysis

Sample	*Location*	*Microbial activity (MTT assay)*
GdE 3	Room 1 (North)	High
GdE 16	Gallery 1	Not detected
GdE 17	Room 1 (East)	Low

Methodology

16S rRNA Gene and ITS region Analysis of Microbial Communities

Sample Preparation and Sequencing

DNA was extracted from samples using QIAmp DNA Stool Mini Kit (Qiagen, Limburg, Netherlands), with minor modifications to manufacturer's instructions.

Bacterial and Fungal Communities were characterised by Illumina Sequencing for the 16S rRNA V3-V4 region and Internal Transcribed Spacer 2. DNA was amplified for the hypervariable regions with specific primers and further reamplified in a limited-cycle PCR reaction to add sequencing adaptor and dual indexes. First, PCR reactions were performed for each sample using 2X KAPA HiFi HotStart Ready Mix. In a total volume of 25 µL, 12.5 ng of template DNA and0.2 µM of each PCR primer. For bacteria the following primers were used:forward primer Bakt_341F 5′-CCTACGGGNGGCWGCAG-3′ and reverse primer Bakt_805R 5′-GACTACHVGGGTATCTAATCC-3′ (Herlemann et al., 2011 and Klindworth et al., 2013). For fungi, a pool of forward primers was used: ITS3NGS1_F 5′-CATCGATGAAGAACGCAG-3′, ITS3NGS2_F 5′-CAACGATGAAGAACGCAG-3′, ITS3NGS3_F 5′-CACCGATGAAGAACGCAG-3′, ITS3NGS4_F 5′-CATCGATGAAGAACGTAG-3′, ITS3NGS5_F 5′-CATCGATGAAGAACGTGG-3′, and ITS3NGS10_F 5′-CATCGATGAAGAACGCTG-3′ with the reverse primer ITS3NGS001_R 5′-TCCTSCGCTTATTGATATGC-3′ (Tedersoo et al., 2014). The PCR conditions involved a 3 min denaturation at 95ºC, followed by 25 cycles

of 98ºC for 20 s, 55ºC for 30 s and 72ºC for 30 s and a final extension at 72ºC for 5 min. Negative controls were included for all amplification reactions. Electrophoresis of the PCR products was undertaken on a 1% (w/v) agarose gel and the ~490 bp V3-V4 and ~390 bp ITS2 amplified fragments were purified using AMPure XP beads (Agencourt, Beckman Coulter, USA) according to manufacturer's instructions. Second PCR reactions added indexes and sequencing adaptors to both ends of the amplified target region by the use of 2X KAPA HotStart Ready Mix, 5µL of each index (i7 and i5) (Nextera XT Index Kit, Illumina, San Diego, CA) and 5µL of the first PCR product in a total volume of 50µL. The PCR conditions involved a 3 min denaturation at 95ºC, followed by 8 cycles of 95ºC for 30s, 55ºC for 30s and 72ºC for 30s and a final extension at 72ºC for 5 min. Electrophoresis of the PCR products was undertaken on a 1% (w/v) agarose gel and the amplified fragments were purified using AMPure XP beads (Agencourt, Beckman Coulter, USA) according to manufacturer's instructions. The amplicons were quantified by fluorimetry with PicoGreen dsDNA quantitation kit (Invitrogen, Life Technologies, Carlsbad, California, USA), pooled at equimolar concentrations and paired-end sequenced with the V3 chemistry in the MiSeq® according to manufacturer's instructions (Illumina, San Diego, CA, USA) at Genoinseq (Cantanhede, Portugal). They were multiplexed automatically by the Miseq® sequencer using the CASAVA package (Illumina, San Diego, CA, USA) and quality-filtered with PRINSEQ software (Schmieder and Edwards, 2011) using the following parameters: 1) bases with average quality lower than Q25 in a window of 5 bases were trimmed, and 2) reads with less than 220 bases were discarded for V3-V4 samples and less than 100 bases for ITS2 samples.

The forward and reverse reads were then merged by overlapping paired-end reads using the AdapterRemoval v2.1.5 (Schubert et al., 2016) software with default parameters.

The QIIME package v1.8.0 (Caporaso et al., 2010) was used for Operational Taxonomic Units (OTU) generation, taxonomic identification and sample diversity and richness indexes calculation.

Sample IDs were assigned to the merged reads and converted to fasta format (split_libraries_fastq.py, QIIME). Chimeric merged reads were detected and removed using UCHIME (Edgar et al., 2011) against the Greengenes v13.8 databases (DeSantis et al., 2006) for V3-V4 samples and UNITE/QIIME ITS v12.11 databases (Abarenkov et al., 2010) for IST2 samples (script identify_chimeric_seqs.py, QIIME).

OTUs were selected at 97% similarity threshold using the open reference strategy. First, merged reads were pre-filtered by removing sequences with a similarity lower than 60% against Greengenes v13.8 databases for V3-V4 samples and UNITE/QIIME ITS v12.11 databases for ITS2 samples. The remaining merged reads were then clustered at 97% similarity against the same databases listed above. Merged reads that did not cluster in the previous step were again clustered into OTU at 97% similarity. OTUs with less than two reads were removed from the OTU table. A representative sequence of each OTU was then selected for taxonomy assignment (pick_rep_set.py, assign_taxonomy.py; QIIME).

Results

The analysis of microbial communities was made using a new molecular approach, used here for the first time in hypogean context.

This Metagenomics approach with NGS (Next-Generation Sequencing) has enabled to confirm the presence of some microorganisms already identified by culture-dependent methods, but rather provided a vast contribution to the identification of several genera and species not previously identified in these environments.

In relation to the bacterial communities it was possible to get around 2300 OTU whose distribution is mostly *Proteobacteria* (43%); *Actinobacteria* (14%); *Firmicutes* (6%), *Acidobacteria* (3%), *Bacteroidetes* (1.6%); *Gemmatimonadetes* (1.5%); *Nitrospirae* (1.1%); *Planctomycetes* (1.5%) and *Chloroflexi* (1%). The majority were genera *Pseudomonas* and *Bacillus* but also *Lysinibacillus*; *Staphylococcus*; *Streptococcus*, *Sphingobacterium*; *Nitrospira*; *Ochrobactrum*; *Agrobacterium*; *Sphingomonas*; *Acinetobacter*; *Enhydrobacter*; *Photobacterium* and *Macromonas*.

In the case of fungi, it was obtained approximately 550 OUT, mostly *Ascomycota* (80%) and *Basidiomycota* (11%). The most abundants was *Hypomyces* (48%) and *Boletus* (10%) but also *Agaricus*; *Penicillium*; *Cladosporium*; *Candida*; *Kluyveromyces*; *Sporobolomyces* and *Gongronella*.

List of the microorganisms identified

Bacteria:

Mainly: *Proteobacteria* (43%); *Actinobacteria* (14%); *Firmicutes* (6%), *Acidobacteria* (3%), *Bacteroidetes* (1,6%); *Gemmatimonadetes* (1,5%); *Nitrospirae* (1,1%); *Planctomycetes* (1,5%) and *Chloroflexi* (1%).

The main genus were *Pseudomonas* and *Bacillus*, but the following genus were also detected: *Lysinibacillus*; *Staphylococcus*; *Streptococcus*, *Sphingobacterium*; *Nitrospira*; *Ochrobactrum*; *Agrobacterium*; *Sphingomonas*; *Acinetobacter*; *Enhydrobacter*; *Photobacterium*. Table 2 presents the list of the species identified among the diverse genus.

Table 2: List of the bacterial strains identified to the species level with NGS.

Genus	Species
Acinetobacter	*johnsonii*
	rhizosphaerae
Actinomadura	*vinacea*
Aggregatibacter	*segnis*
Agrococcus	*jenensis*
Bacillus	*cereus*
	muralis
	humi
	firmus
	coagulans
Brevundimonas	*diminuta*
Corynebacterium	*durum*
Haemophilus	*parainfluenzae*
Hyphomicrobium	*sulfonivorans*
Kocuria	*palustris*
	rhizophila
Lysinibacillus	*boronitolerans*
Methylotenera	*mobilis*
Neisseria	*cinerea*
Nitrosovibrio	*tenuis*
Paenibacillus	*lautus*
	macerans
	lautus
Paracoccus	*aminovorans*
	marcusii
Photobacterium	*angustum*
	intermedia
Prevotella	*melaninogenica*
	nanceiensis
	tannerae
Propionibacterium	*acnes*
Pseudomonas	*fragi*
	nitroreducens
Rhizobium	*leguminosarum*
Rhodococcus	*fascians*
Rhodoplanes	*elegans*
Rothia	*aeria*
Sphingobacterium	*mizutaii*
	faecium
	multivorum
Sphingomonas	*yabuuchiae*
Staphylococcus	*epidermidis*
	equorum
Tetrathiobacter	*kashmirensis*
Variovorax	*paradoxus*
Veillonella	*dispar*
	chondroitinus

Fungi:

Mainly: Ascomycota (80%) e Basidiomycota (11%).

The main genus were *Hypomyces* (48%) and *Boletus* (10%) but the following genus were also identified: *Agaricus*; *Penicillium* (1%); *Cladosporium* (0,1%); *Candida*; *Kluyveromyces*; *Sporobolomyces* and *Gongronella.*Table 3 presents the list of the fungal genus and species identified with NGS.

Table 3: List of the fungal strains identified to the genus or species level with NGS

Genus	Species
Candida	*tropicalis*
Kluyveromyces	*marxianus*
Penicillium	*fellutanum*
	brevicompactum
	chrysogenum
	spinulosum
Cladosporium	*cladosporioides*
Gongronella	*butleri*
Schizophyllum	*commune*
Pezizomycotina	*sp.*
Tylospora	*sp.*
Boletus	*dryophilus*
Betamyces	*americaemeridionalis*

References

Abarenkov K, Nilsson RH, Larsson K, Alexander IJ, Eberhardt U, Erland, S, Høiland K, Kjøller R, Larsson E, Pennanen T, Sen R, Taylor AFS, Tedersoo L, Ursing BM, Vrålstad T, Liimatainen K, Peintner U, Kõljalg U. 2010. The UNITE database for molecular identification of fungi – recent updates and future perspectives. New Phytologist, 186(2), 281-285.

Caporaso JG, Kuczynski J, Stombaugh J, Bittinger K, Bushman FD, Costello EK, Fierer N, Pena AG, Goodrich JK, Gordon JI, Huttley GA, Kelley ST, Knights D, Koenig JE, Ley RE, Lozupone CA, McDonald D, Muegge BD, Pirrung M, Reeder J, Sevinsky JR, Turnbaugh PJ, Walters WA, Widmann J, Yatsunenko T, Zaneveld J, Knight R. 2010. QIIME allows analysis of high-throughput community sequencing data. Nature Methods 7(5): 335-336.

DeSantis TZ, Hugenholtz P, Larsen N, Rojas M, Brodie EL, Keller K, Huber T, Dalevi D, Hu P, Andersen GL. 2006. Greengenes, a chimera-checked 16S rRNA gene database and workbench compatible with ARB. Appl Environ Microbiol 72(7):5069–5072.

Edgar RC, Haas BJ, Clemente JC, Quince C, Knight R. 2011. UCHIME improves sensitivity and speed of chimera detection. Bioinformatics. 27(16):2194-200.

Herlemann DPR, Labrenz M, Juergens K, Bertilsson S, Waniek JJ and Anderrson AF 2011. Transition in bacterial communities along the 2000 km salinity gradient of the Baltic Sea. ISME J 5:1571-1579.

Klindworth, A, Pruesse, E, Schweer, T, Peplies, J, Quast, C, Horn, M, & Glöckner, F O. 2013. Evaluation of general 16S ribosomal RNA gene PCR primers for classical and next-generation sequencing-based diversity studies. Nucleic Acids Research, 41(1), e1.

Schmieder, R, Edwards, R. 2011. Quality control and preprocessing of metagenomic datasets. Bioinformatics. 27:863-864

Schubert M, Lindgreen S, Orlando L. 2016. AdapterRemoval v2: rapid adapter trimming, identification, and read merging. BMC Res Notes. 9: 88.

Tedersoo L, Bahram M, Põlme S, Kõljalg U, Yorou NS, Wijesundera R, Villarreal Ruiz L, Vasco-Palacios AM, Thu PQ, Suija A, Smith ME, Sharp C, Saluveer E, Saitta A, Rosas M, Riit T, Ratkowsky D, Pritsch K, Põldmaa K, Piepenbring M, Phosri C, Peterson M, Parts K, Pärtel K,Otsing E, Nouhra E, Njouonkou AL, Nilsson RH, Morgado LN, Mayor J, May TW, Majuakim L, Lodge DJ, Lee SS, Larsson KH, Kohout P, Hosaka K, Hiiesalu I, Henkel TW, Harend H, Guo LD, Greslebin A, Grelet G, Geml J, Gates G, Dunstan W, Dunk C, Drenkhan R, Dearnaley J, De Kesel A, Dang T, Chen X, Buegger F, Brearley FQ, Bonito G, Anslan S, Abell S, Abarenkov K. 2014. Global diversity and geography of soil fungi. Science 346(6213):1256688

Appendix 12: FISH analysis of the microbial communities of Escoural Cave

Two samples from the cave of Escoural were used to perform some Fluorescence *In Sit*u Hybridisation (FISH) *ex situ* assays. It permitted to observe some of the microbial communities' organisation and perform some tests with methodologies in development in the HERCULES biotechnology laboratory. The present correspond to selected arranged extracts from an article submitted to Applied Physics A (Marina González-Pérez, Catarina Brinco, Ricardo Vieira, Tânia Rosado, Guilhem Mauran, António Pereira, António Candeias, Ana Teresa Caldeira (2016). An innovative in-suspension RNA-FISH protocol fro simultaneous analysis of yeast and bacteria thriving in artworks Applied Physics A -submitted).

RNA-Fluorescence *In Situ* Hybridisation (RNA-FISH) is a promising tool to identify the microorganisms potentially responsible for Cultural Heritage (CH) biodeterioration (Otlewska et al., 2014). It can provide information about the target metabolically active microorganisms present in a sample (presence, number and spatial distribution) (Amann and Fuchs, 2008; Levsky and Singer, 2003; Moter and Göbel, 2000). The RNA-FISH technique is based on the detection and localisation of target RNA sequences within fixed cells by the hybridisation of nucleic acid probes labelled with fluorochromes (Amann et al., 1990). Variousdifferent target organisms can be simultaneously detected by applying probes labelled with dyes with distinct excitation/emission spectra.

Two microsamples, GdE 5'''' and GdE 17''' (Fig 1a and 1b, respectively), were analysed by RNA-FISH. The microbial cells were recovered from them by transferring the samples to 50 mL screw-cap centrifuge tubes, adding 2,0 ml of Maximum Recovery Diluent (MRD, Sigma-Aldrichand maintaining overnight at 30.0ºC with continuous shaking (140 rpm).

Fluorescence images were taken with an MoticamPRO 282B camera mounted on a BA410E Motic microscope coupled to a 100W Quartz Halogen Koehler illumination with intensity control and to an epi-attachment (EF-UPR-III) and a Power Supply Unit (MOTIC MXH-100). It was equipped with the Motic filter sets Cy3, (excitation (ex) D540/25x, dichroic mirror (dm) 565DCLP, and emission (em) D605/55m), FITC (ex D480/30x, dm 505DCLP, em D535/40m) and Cy5 (ex D436/20x, dm 455DCLP, em D480/40m). Images were recorded and analysed with the Motic Images Plus 2.0LM.

The autofluorescence of the microbial suspensions from the unfixed and fixed samples were tested by microscopic inspection of the cellular suspensions by epifluorescence microscopy using the Cy3, FITC and Cy5 filter sets before the analysis by RNA-FISH. None FISH signals were observed.

The microbial cells extracted from the two microfragments from the Escoural Cave, GdE 5'''' and GdE 17''', were analysed by the RNA-FISH method as described in the methodology. The blanks shown none

autofluorescence signals which notably facilitated the analysis of the results obtained by RNA-FISH (Fig 1c and 1e). By applying the EUB338-Cy3/EUK516-6-FAM mix, the RNA-FISH after the analysis under the Cy3 (orange) and FTIC (6-FAM- green) filters revealed that only intense orange signals were obtained. Thus, RNA-FISH resulted in the detection of a large concentration of active eubacteria living in the sampled areas of Escoural Cave (Fig 1d and 1f).

GdE 5'''' and GdE 17''' microsamples were also analysed by Scanning Electron Microscopy (SEM). The microscopical inspection evidenced the presence of biofilms covering a significant area of the microfragments as well as of microbial contaminants (Fig 1g-j). Among others, cells with reduced dimension were detected, which can be indicative of the presence of bacterial cells (Fig 1h). This corroborated the results obtained by FISH analysis. Besides that, other microorganisms were also identified in the Escoural Cave giving the indication of the presence of a wide diversity of communities since filamentous fungi, cyanobacteria, microalgae and insects. The NGS technique enabled to confirm that, whereas different types of microorganisms are thriving in the Escoural Cave, it was predominantly colonised by prokaryote cells, Appendix 12. This also support the findings obtained by RNA-FISH.

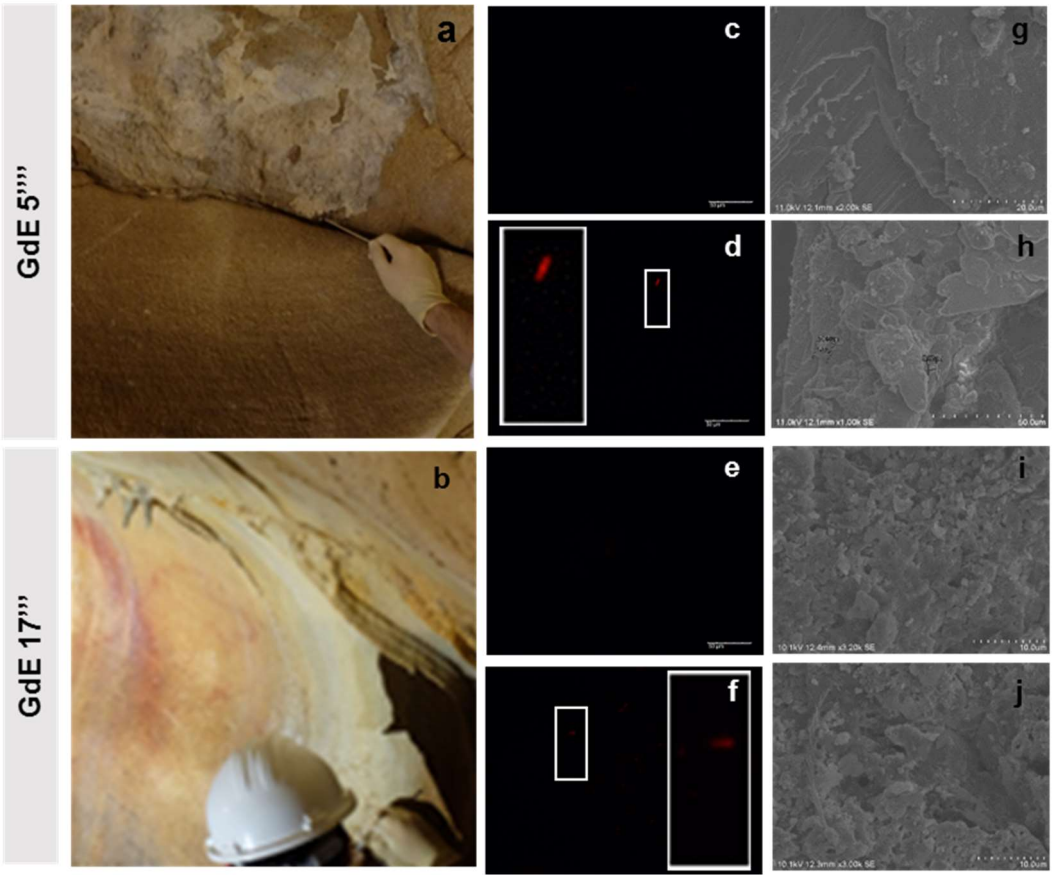

Figure 1: Analysis of rock microfragments GdE 5'''' and GdE 17''' from Escoural Cave (a, b), by: i) the RNA-FISH protocol developed in this work for the blanks -without probe addition- (c, e) and for the FISH samples -using the EUB338-Cy3/EUK516-6-FAM mix- (d, f); ii) SEM inspection (g-j).

References from the article

A. Otlewska, J. Adamiak, and B. Gutarowska, Acta Biochim. Pol. 61, 217 (2014).

J. M. Levsky and R. H. Singer, J. Cell Sci. 116, 2833 (2003).

R. Amann and B. M. Fuchs, Nat. Rev. Microbiol. 6, 339 (2008).

A. Moter and U. B. Göbel, J. Microbiol. Methods 41, 85 (2000).

R. I. Amann, L. Krumholz, and D. A. Stahl, J. Bacteriol. 172, 762 (1990).

Appendix 13: Location of the microbial contamination's assessment' s samples.

The present appendix aims at providing the location of the samples used to assess the microbial activity. A brief description of the sample is then provided.

Location of the samples

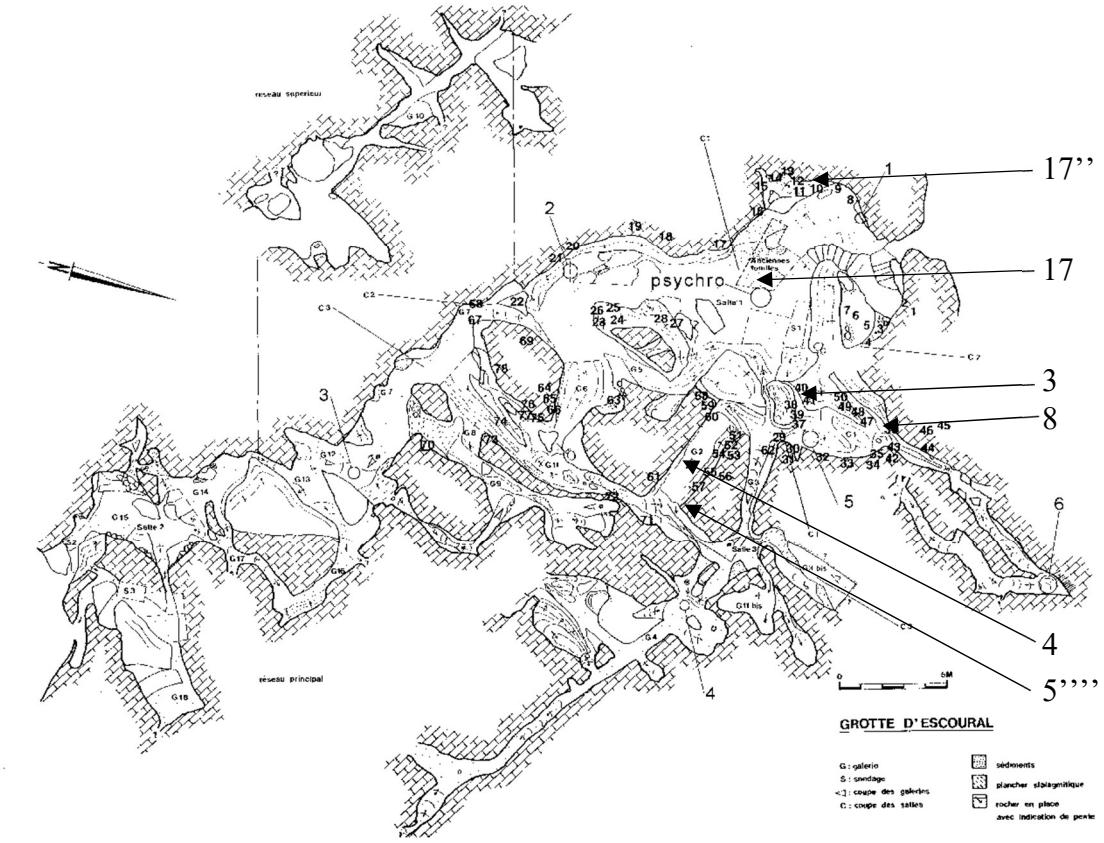

Figure 1: Location of samples used to carry out the assays of the microbial activity in Part III of the thesis. The sample GdE 23 came from the outside of the cave, therefore is not present on this map.

Description of the samples

Sample GdE 3

On the left (North) wall of corridor between room 1 and the galleries 1 to 3, in the end of the corridor next to the entrance to gallery 1. Wall presents particular speleothems with a bubonic aspect and a very humidity of the substrate. The upper part of the wall hosts the bubonic calcite while its lower part present earth, probably clay, that could have felt from the ceiling.

The wall has a very translucent aspect, due to a very high humidity level of the wall. The lower part of the wall has a muddy aspect, due to a very high humidity level of the wall and possible clay felt from the

ceiling. The wall is subject to light during visits and to water runoff, as indicated by the earth particles distribution. Bubonic calcite speleothems appear over wet light-brown calcite layer with some earth connected to them, Figure 2.A. Some of the bubonic speleothems present in the upper light brown part of the wall are also present in the lower dark brown part where mud is important.
Sampling was performed on the upper part of the wall by collecting the clay/earth attached to the bubonic speleothems.

Sample GdE 4

On the right (South) wall of gallery 2, in its beginning, probably next to figure 60 from M. Lejeune. The wall presents in its upper part some naturally ocre-coloured lines on the beige substrate. It tends to form minor cracks on the substrate.
The wall presents in its upper part ocre brown crust forming some cracks in the substrate, Figure 2.B. The beige substrate seems to have laminar morphology, with acicular crystals, while the crust presents paralepipedic crystals of brown to black appearance.
Sampling was performed on the brown crust.

Sample GdE 5''''

On the left (North) wall of the gallery 2, near the end of the gallery, just under a white speleothem development in a crack of the substrate, Figure 2.C. The wall presents a small white development surrounded by numerous cracks in which different minerals can be seen.
Sampling was performed on dark brown minerals located just under the white speleothem, in an accessible and visible part of the crack of the substrate.

Sample GdE 8

On the left (West) wall of gallery 1, in its end, next to figure 36 from M. Lejeune. The wall presents an overhang and a small gallery probably connecting the cave to the outside world. Traces of water runoff are important, so are the traces of interactions with outside world (mushroom, bat…), Figure 2.D.
Covering some of the water runoff traces, under bat location, two black stains coupled with a yellow upper one can be found on the overhang. Those are guano from the bat, not dry but nor fresh.
Sampling was performed on the black part of the guano.

Sample GdE 17

Near the right (West) wall of the room 1, where excavations have been carried out to remove the Neolithic remains, the cave present some loose earth/ clay.

Sample GdE 17’’’

On the right (east) wall of the great room, near the nowadays entrance and the red horse head painting. The wall presents few white drips with obvious watering actions leaking all along the wall from ceiling to floor in very localized bands, Figure 2.E.
The wall presents a white speleothem with apparent high homogeneity.
Sampling was performed on light brown mineral located in the centre part of the watering effect bands.

Sample GdE 23

Outside of the cave, just in front of the entrance, the rock presents a clear and clean layer aspect with some obvious microbial contamination, Figure 2.F.

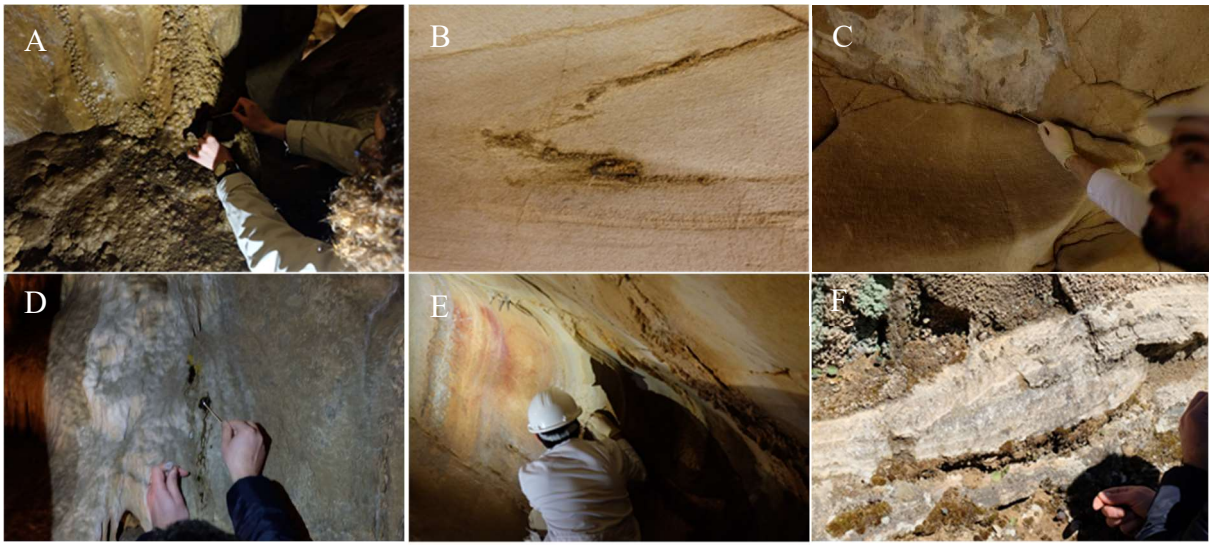

Figure 2: Areas sampled to assess the microbial activity of the communities contaminating the different spots. A: Sample GdE3 located in Room1; B: Sample GdE 4 located in Gallery 2; C: Sample GdE 5’’’’ located in Gallery 2; D: Sample GdE 8 located in Gallery 1; E: Sample GdE 17’’’ located in Room 1; F: Sample GdE 23 located outside of the cave on the rock.

Rock art and microorganism – a new insight on Escoural Cave

Abstract

European cave art is of tremendous importance to understand the cultural traditions of the Upper Palaeolithic (35 000 – 10 000 BP) populations. Indeed, Prehistoric communities performed numerous cave paintings all over Western Europe. Understanding these artworks should provide a better knowledge of these early cultural aspects. Although numerous studies have been carried out to analyse the materials used by those communities, nothing has been done on the techniques' palette of Escoural Cave's representations. The present work aims at providing the very first data about the techniques and materials used by the Prehistoric to perform the cave paintings of Escoural (Alentejo, Portugal), and the microorganisms possibly endangering this unique parietal art.
In situ observations coupled with an extensive micro-sampling and micro-destructive analyses allowed to characterize the coloured material and the way they were applied on the walls of the cave. Both red and black pigments present major composition's disparities among the different paintings and drawings, supporting a more complex occupations' chronology than what was earlier thought.
The Palaeolithic paintings have suffered deterioration from environmental conditions and include chemical, mechanical and aesthetic alterations, possibly as a result of fungal activity. The standard techniques for biological assessments used in these contexts provided important insights on the diversity of the microbial population, though they have accuracy limitations. To understand the extent and viability of the existing microbiota, DNA quantification and biomarkers analyses, such as desidrogenase activity were performed and correlated with ergosterol amounts.

Arte rupestre e microorganismos – uma nova abordagem na Gruta do Escoural

Resumo

A Arte Rupestre Europeia é de grande importância para compreender as tradições culturais da população do Paleolítico Superior (35 000 - 10 000 BP). De fato, as comunidades Pré-históricas realizaram inúmeras pinturas rupestres em toda a Europa Ocidental, sendo crucial compreender estas obras de forma a proporcionar um melhor conhecimento destes ancestrais aspectos culturais. Embora vários estudos tenham sido realizados para analisar os materiais utilizados por estas comunidades, nada foi efetuado sobre a técnica de execução das representações presentes na Gruta do Escoural. O presente trabalho visa fornecer os primeiros dados sobre as técnicas e materiais utilizados na Pré-História para executar as pinturas rupestres de Escoural (Alentejo, Portugal) bem como caracterização dos microorganismos possivelmente associados aos danos deste bem único.
Observações *in situ*, juntamente com uma extensa micro-amostragem e análises micro-destrutivas permitiu caracterizar os pigmentos utilizados e a forma como eles foram aplicados nas paredes da caverna. Tanto os pigmentos vermelhos como os pretos apresentam composição distinta nas diversas pinturas e desenhos aí representados, apoiando a presença de diferentes ocupações contrariamente ao que se pensava até então.
As pinturas Paleolíticas têm sofrido deterioração, devido às condições ambientais, nomeadamente alterações químicas, mecânicas e, possivelmente como resultado da atividade fúngica. As técnicas usualmente utilizadas para a avaliação de contaminação biológica fornecem informação importante sobre a diversidade da população microbiana, embora apresentem algumas limitações. Para entender a extensão e a viabilidade da microbiota existente, a quantificação de DNA e análise de biomarcadores como actividade de desidrogenases foram realizadas e correlacionadas com o conteúdo em ergosterol.

Cofinanciado por: